

# **COMSAT**

Technical Review

Volume 22 Number 1, Spring 1992

*Advisory Board* Joel R. Alper  
Joseph V. Charyk  
John V. Evans  
John. S. Hannon

*Editorial Board* Richard A. Arndt, *Chairman*  
S. Joseph Campanella  
Dattakumar M. Chitre  
Calvin B. Cotner  
Allen D. Dayton  
Russell J. Fang  
Ramesh K. Gupta  
Michael A. Hulley  
Edmund Jurkiewicz  
Lewis R. Karl  
Ivor N. Knight  
George M. Metze  
Hans J. Weiss  
Amir I. Zaghoul

*Past Editors* Pier L. Bargellini, 1971–1983  
Geoffrey Hyde, 1984–1988

*Editorial Staff* MANAGING EDITOR  
Margaret B. Jacocks  
TECHNICAL EDITOR  
Barbara J. Wassell  
PRODUCTION  
Barbara J. Wassell  
N. Kay Flesher  
Virginia M. Ingram  
Nancy K. McKeithen  
Margarite R. del Rio  
CIRCULATION  
Merilee J. Worsey

COMSAT TECHNICAL REVIEW is published by the Communications Satellite Corporation (COMSAT). Subscriptions, which include the two issues published for a calendar year, are: one year, \$20 U.S.; two years, \$35; three years, \$50; single copies, \$12; article reprints, \$3. Overseas airmail delivery is available at an additional cost of \$18 per year. Make checks payable to COMSAT and address to: Records Department, Communications Satellite Corporation, 22300 COMSAT Drive, Clarksburg, MD 20871-9475, U.S.A.

ISSN 0095-9669

© COMMUNICATIONS SATELLITE CORPORATION 1992  
COMSAT IS A TRADE MARK AND SERVICE MARK  
OF THE COMMUNICATIONS SATELLITE CORPORATION

## COMSAT TECHNICAL REVIEW

Volume 22 Number 1, Spring 1992

- 1 EDITORIAL NOTE  
**G. Hyde AND S. B. Bennett**

### *INTELSAT VI: System and Applications*

- 5 EARTH STATION CONSIDERATIONS FOR INTELSAT VI  
**M. P. Brown, Jr., F. A. S. Loureiro AND M. Stojkovic**
- 19 DCME IN THE INTELSAT VI ERA  
**M. Onufry, G-P. Forcina, W. S. Oei, T. Oishi, J. F. Phiel  
AND J. H. Rieser**
- 57 VIDEO TRANSMISSION AND PROCESSING IN THE INTELSAT VI ERA  
**L-N. Lee AND A. K. Sinha**

### *INTELSAT 603 Reboost*

- 73 INTELSAT 603 "REBOOSTED" TO SYNCHRONOUS ORBIT  
**S. B. Bennett**

### *Non-INTELSAT VI Papers*

- 93 THE IM MICROSCOPE: A NEW APPROACH TO NONLINEAR ANALYSIS OF SIGNALS IN SATELLITE COMMUNICATIONS SYSTEMS  
**D. S. Arnstein, X. T. Vuong, C. B. Cotner AND H. M Daryanani**
- 125 REAL-TIME TRANSMISSION OF GROUP 3 FACSIMILE OVER INTERCONNECTED PUBLIC SWITCHED DIGITAL MOBILE SATELLITE NETWORKS  
**S. Dimolitsas, J. H. Rieser AND H. Feldman**
- 149 A DIGITALLY IMPLEMENTED MODEM: THEORY AND EMULATION RESULTS  
**J. J. Poklemba AND F. R. Faris**
- 197 TRANSLATIONS OF ABSTRACTS  
FRENCH 197 SPANISH 201
- 205 AUTHOR INDEX, CTR 1991
- 207 INDEX OF 1991 PUBLICATIONS BY COMSAT AUTHORS
- 217 PAPERS SCHEDULED FOR PUBLICATION IN THE CTR INTELSAT VI SERIES

## **Editorial Note**

G. HYDE, Guest Editor, COMSAT

S. B. BENNETT, Associate Guest Editor, INTELSAT

This is the fourth issue of the *COMSAT Technical Review* (CTR) dedicated to the INTELSAT VI satellite and system. Because of the importance and complexity of the INTELSAT VI satellite and its associated system operation, three issues of CTR were needed to fully document the process leading to its very successful implementation. These issues cover the subject from concept, through design and test, to in-orbit operation. Related fourth and fifth issues address system applications and the implementation of satellite-switched time-division multiple access (SS-TDMA). Compilation of this series is a joint effort of COMSAT and INTELSAT, including co-editors from each organization.

The first issue in the CTR INTELSAT VI series\* described the overall development process, as well as system planning, specification of the spacecraft bus and communications payload, and the design for SS-TDMA and frequency-division multiple access (FDMA) services. The second issue focused on the design of the INTELSAT VI spacecraft and its communications payload, dealing with the design of the spacecraft bus; the attitude and payload control system; a design overview and description of the communications payload; the design, implementation, and testing of the antenna system; and the design and implementation of the on-board SS-TDMA package. The third issue in the series covered a wide range of topics, including measures taken to ensure a reliable satellite; the launch, deployment, and in-orbit testing phases; and the operation of the satellite in orbit.

This fourth issue in the INTELSAT VI series addresses a variety of topics of concern to the system user, including earth station considerations and the advantages obtained through use of digital circuit multiplication equipment (DCME) and video signal processing. In addition, a summary coverage of the successful mission to reboost INTELSAT 603 is included. The first paper deals with the considerations that formed the basis for the INTELSAT VI transmission systems design, to minimize impact on the earth segment and reduce costs. These factors included compatibility with INTELSAT V/V-A, stationkeeping/tracking tolerances, downsizing of the Standard A and C antenna diameters, and introduction of new 6/4-GHz allocations. The second paper discusses the

---

\*Refer to pages 217 through 221 of this issue for a listing of the papers scheduled for publication in this series. Papers on other topics may also be included.

possible evolution of TV signal processing in the INTELSAT VI era, including analog TV signals (HTTV, FTTV, and TMTV), as well as digitized TV signals for standard TV formats, HDTV, and teleconferencing, using a variety of services which will eventually include ISDN and BISDN. DCME is the subject of the third paper, which traces its evolution, details current technology and design considerations, and discusses future directions. The fourth paper summarizes the recent successful experience in reboosting the INTELSAT 603 satellite from the low-earth orbit, where it had been stranded, to geostationary orbit where it now functions. Included is an overview of the preparatory work and the development of supersynchronous insertion, as well as the actual mission.

The fifth issue in the INTELSAT VI series will be devoted to describing all aspects of the SS-TDMA system, which was first used for commercial purposes on INTELSAT VI.

The editors trust that this comprehensive treatment of the INTELSAT VI system will prove useful to future system planners. The papers in the CTR INTELSAT VI series are the result of a major effort by a large group of authors from COMSAT, INTELSAT, and Hughes Aircraft Corporation, and we congratulate them on their substantial achievement.



*Geoffrey Hyde received a B.A.Sc. in engineering physics and an M.A.Sc. in electrical engineering from the University of Toronto in 1953 and 1959, respectively, and a Ph.D. in electrical engineering from the University of Pennsylvania, Philadelphia, in 1967. Prior to joining COMSAT Laboratories in July 1968, he worked on antennas, microwaves, and propagation at RCA, Moorestown, NJ, and at Avro Aircraft Company and Sinclair Radio Labs in Canada.*

*At COMSAT prior to 1974, Dr. Hyde was concerned with the development of the torus antenna, a general antenna analysis computer program (GAP), and related areas of endeavor. In February 1974 he became Manager of the Propagation Studies Department, where his work included a wide variety of efforts in propagation measurement and analysis. In 1980 he joined the staff of the Director, COMSAT Laboratories, and in 1984 became Assistant to the Director. His duties included coordination of the COMSAT R&D programs, coordination of ITU activities at COMSAT Laboratories, and editorship of the COMSAT Technical Review. In June 1989 he retired, and is currently a consultant to COMSAT Laboratories.*

*Dr. Hyde is a member of URSI Commissions B and F, and the AIAA, and is a Registered Professional Engineer in Ontario, Canada. His honors include David Sarnoff Fellowships (1965 and 1966), Fellow of the IEEE (1987), and the IEEE G-AP award for best paper, 1968 (jointly with Dr. Roy C. Spencer).*

*Simon B. Bennett received a B.E.E. from City College of New York in 1959 and an M.E.E. from New York University in 1961. His career, which spans the entire history of communications satellites, began with work on the first TELSTAR satellite program at Bell Telephone Laboratories from 1959 to 1963. He continued in this field from 1961 to 1974 at COMSAT, where he contributed to the success of satellite programs from Early Bird to INTELSAT IV.*



*In 1974, Mr. Bennett joined INTELSAT as Manager of Engineering, where he was engaged in the formulation and application of INTELSAT's intersystem coordination process. Subsequently, as Manager of Space Segment Programs, he was responsible for all technical and programmatic aspects of satellites and launch vehicles encompassing the INTELSAT V and VI series of satellites. This was followed by 1 year as Director of System Planning. From 1986 to 1990, he was in charge of the operation of INTELSAT's fleet of 15 to 18 satellites and associated tracking, telemetry, command, and monitoring facilities. From early 1990 until his retirement from INTELSAT in July 1992, he was assistant to the Vice President for Engineering and Research. He is currently President of Bennett Consultancy, Alexandria, Virginia.*

## ***Earth station considerations for INTELSAT VI***

M. P. BROWN, JR., F. A. S. LOUREIRO, AND M. STOJKOVIC

(Manuscript received January 7, 1991)

### ***Abstract***

When transitioning from one satellite series to the next, INTELSAT makes every attempt to minimize the impact on the earth segment and to reduce earth station costs. This paper describes how such a transition was accomplished for the INTELSAT VI series with respect to the INTELSAT V/V-A compatibility mode, earth station tracking requirements, and operation with new C-band frequencies for transponder (1'-2'). Also discussed is the decisionmaking process that was involved in downsizing the 30- to 32-m Standard A (C-band) earth stations to 15-17 m, and the 15- to 18-m Standard C (Ku-band) earth stations to 11-13 m.

### ***Introduction***

INTELSAT VI has played a key role in INTELSAT's continued efforts to minimize the impact on the earth segment, and to reduce costs, when transitioning from one satellite series to the next. For example, INTELSAT VI is the first spacecraft series to include a feature such as the "INTELSAT V/V-A compatibility mode" to enable a direct earth station point-over from previous satellite series without loss of traffic. Also, the INTELSAT VI stationkeeping tolerances (N/S and E/W) were tightened from the  $\pm 0.10^\circ$  limits used for INTELSAT V/V-A, to  $\pm 0.05^\circ$  in an effort to reduce the tracking requirements for smaller earth stations. The decision to extend hemispheric beam transponder bank (1'-2') into the new 6/4-GHz frequencies, which were allocated to the Fixed Satellite Service by the 1979 World Administrative Radio Conference

(WARC'79), was based on the assumption that this action would have little impact on existing or new earth stations. Also, the higher down-link equivalent isotropically radiated power (e.i.r.p.) available on INTELSAT VI was a key factor in INTELSAT's decision to significantly downsize its Standard A (6/4-GHz) earth station requirements from 30–32 m to 15–17 m, and its Standard C (14/11-GHz) earth station requirements from 15–18 m to 11–13 m.

### ***INTELSAT V/V-A compatibility mode***

INTELSAT VI is the first INTELSAT spacecraft series that can be configured so that it appears to have the same beam coverage as the preceding spacecraft series. This is necessary in the case of zone beam coverage because INTELSAT VI has four zone beams (NE, SE, NW, and SW), while INTELSAT V and V-A have two zone beams (East and West). In the "INTELSAT V/V-A compatibility mode," two INTELSAT VI zone beam receiver outputs are combined with a hybrid to make it appear as though the NE and SE zone beams function as one East zone beam, and the NW and SW zone beams function as one West zone beam. The output of the hybrid is fed into two zone beam transponder amplifiers so that carriers are broadcast down to the NE and SE beams (or the NW and SW beams). It is also possible to connect the combined zone beam up-links to hemispheric or spot beam down-links. This capability permits the ground segment to point-over directly to INTELSAT VI using an INTELSAT V or V-A frequency plan, without loss of traffic. After point-over, INTELSAT VI is gradually transitioned to its new four-zone-beam configuration by judicious use of the newly acquired transponder bandwidth to make the necessary earth station carrier rearrangements.

### ***INTELSAT VI stationkeeping limits***

In early 1990, after an operational trial period of 6 months with the first INTELSAT VI (602) at 335.5°E, sufficient experience had been gained to determine that it was practical to hold INTELSAT VI stationkeeping to  $\pm 0.05^\circ$  N/S and E/W. Although somewhat tighter stationkeeping tolerances could be maintained,  $\pm 0.05^\circ$  was found to be a reasonable tradeoff between the number of maneuvers (manpower), spacecraft antenna pointing accuracy, and earth station tracking requirements. As indicated in Table 1, with  $\pm 0.05^\circ$  stationkeeping it is possible for C-band earth stations with 9-m-diameter (and smaller) antennas to employ fixed-mount antennas (*i.e.*, no autotracking). At Ku-band, where the antenna beamwidth is less than half the beamwidth at C-band for the same diameter antenna, antennas of 5.5 m and less can use fixed mounts.

TABLE 1. INTELSAT VI EARTH STATION SIZES AND TRACKING REQUIREMENTS (STATIONKEEPING LIMITS =  $\pm 0.05^\circ$  E/W AND N/S)

FREQUENCY (GHz)	EARTH STATION STANDARD	MINIMUM G/T (dB/K)	TYPICAL SIZE (m)	MINIMUM TRACKING REQUIREMENTS
C-Band (6/4)	A (Previous)	40.7	30–32	Auto
	A (Revised)	35.0	15–17	Auto
	B	31.7	10–13	Auto
	D-2	31.7	10–13	Auto
	D-1	22.7	4.5–5.0	Fixed
	F-3	29.0	9–10	Fixed
	F-2	27.0	7.5–8.0	Fixed
	F-1	22.7	4.5–5.0	Fixed
Ku-Band (14/11 and 14/12)	G*	Any	Any	--
	Z*	Any	Any	--
	C (Previous)	39.0	15–18	Auto**
	C (Revised)	37.0	11–13	Auto**
	E-3	34.0	8–10	Auto**
	E-2	29.0	5.5	Fixed
	E-1	25.0	3.5–4.5	Fixed
	G*	Any	Any	--
Z*	Any	Any	--	

\* Standard G earth stations are used with international leases, and Standard Z earth stations are used with domestic leases. Small 1.8-m television satellite newsgathering (SNG) antennas and 0.6-m microterminals using spread spectrum transmission techniques also fall in the Standard G and Z categories.

\*\* Step track operation can experience difficulties in a Ku-band environment due to rain fades. Tracking systems which utilize program track in conjunction with step track are useful during periods of adverse atmosphere conditions.

This can be compared to the stationkeeping limits of  $\pm 0.10^\circ$  used with the INTELSAT V/V-A series, for which the largest antenna feasible with manually operated or fixed mounts is about 7.5 m at C-band and about 3.5 m at Ku-band.

As an example, Figure 1 compares the main beam (on-axis) antenna gain and the effective, off-axis main beam antenna gain as a function of fixed Ku-band antenna size and the stationkeeping limits used with the INTELSAT V/V-A and VI satellites [1]. The figure shows that a  $\pm 0.05^\circ$  stationkeeping tolerance results in substantial improvement in fixed-mount antenna tracking loss. A

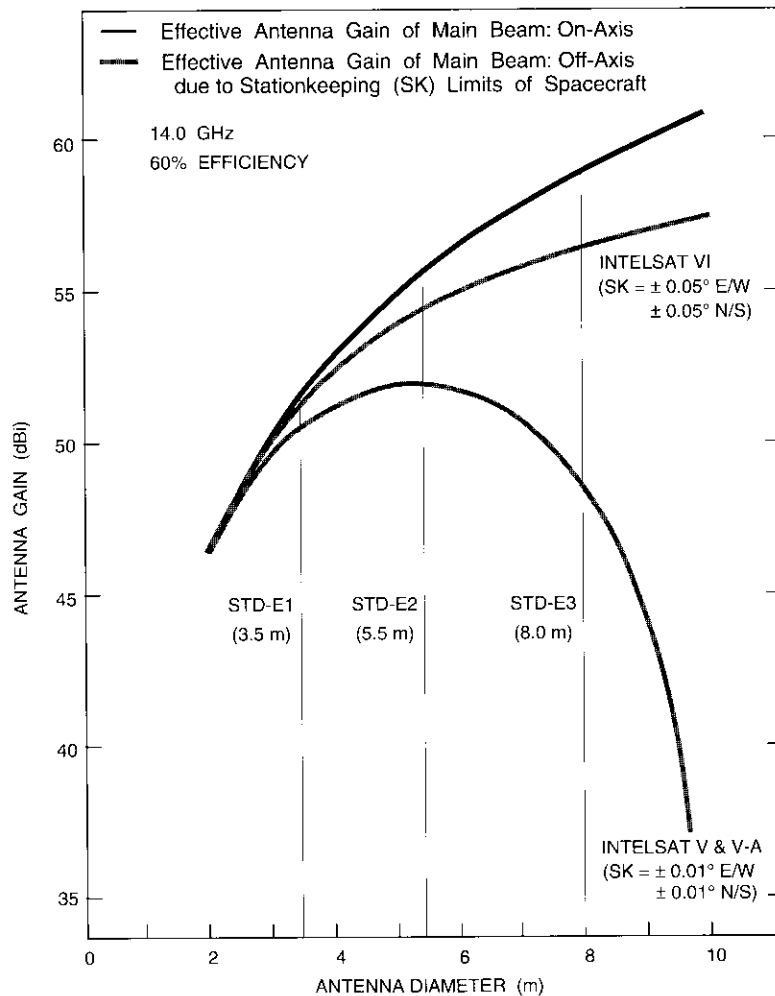


Figure 1. On- and Off-Axis Main Beam Antenna Gain as a Function of Earth Station Antenna Size and Satellite Stationkeeping Tolerance (Ku-band, fixed antennas)

loss of 1.0 to 1.5 dB in on-axis gain was used as the criterion for selecting the size of earth station that could be operated without autotrack.

In addition to eliminating the need for tracking facilities on smaller earth stations, the tighter stationkeeping capability of INTELSAT VI achieved another milestone in INTELSAT's objective of increasing orbital efficiency. All follow-on satellites are being designed for stationkeeping limits of  $\pm 0.05^\circ$  (N/S and E/W).

### Transponder (1'-2')

INTELSAT has introduced part of the new 6/4-GHz frequency band (allocated by WARC'79 to the Fixed Satellite Service) in the INTELSAT VI hemispheric beam transponder bank (1'-2'). This bank of transponders has been assigned a 72-MHz frequency band of 5.854 to 5.926 GHz (up-link) and 3.629 to 3.701 GHz (down-link). A major factor in the decision to use only a small portion (72 MHz) of the new allocation was the need to minimize the hardware impact on existing and new antenna installations. The primary concern lay in the areas of the antenna feed, up- and down-converters, high-power amplifiers (HPAs), and low-noise amplifiers (LNAs). It was known that the useful bandwidth of the antenna feed system could be extended toward 3.6 GHz and 5.8 GHz without approaching waveguide cutoff too closely. It was also believed that operation of the LNAs and HPAs could be extended into this new band without major difficulty. Experience to date has confirmed that use of this transponder has no substantial impact on hardware or performance.

### Standard A and C earth station performance characteristics

When the performance characteristics of the large INTELSAT Standard A (C-band) and Standard C (Ku-band) earth stations were initially developed, the tradeoff between earth and space segment costs favored large earth station antennas because of the high cost of power radiated from satellites, and the expectation that only one or two such earth stations would be established in each country. Since then, higher levels of radiated power and multiple reuse of the frequency bands have been implemented as a result of improved and cost-effective technologies. In this environment, networks using larger antennas become bandwidth- or interference-limited and are unable to fully exploit the increase in satellite radiated power. With the INTELSAT VI series, it was feasible to reduce the size of these antennas to the point where it is economical to build several antennas in each country and (where frequency coordination with terrestrial networks permits) to install them near major cities.

**Cost savings with smaller Standard A and C antennas**

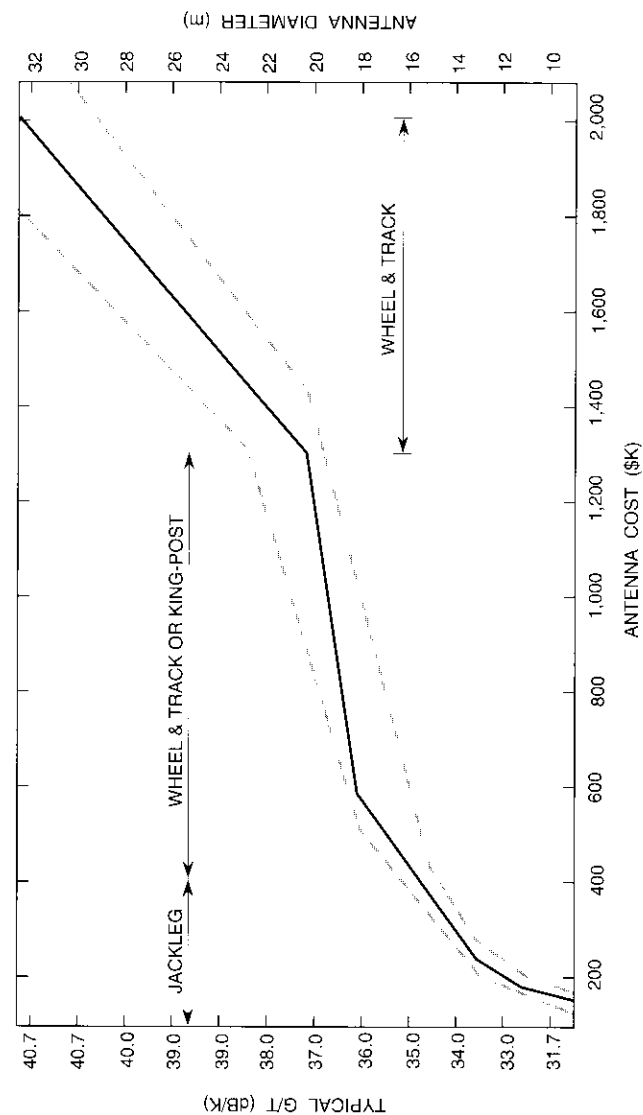
Originally, Standard A antennas (approximately 30 to 32 m in diameter) and Standard C [2] antennas (approximately 15 to 18 m in diameter) were required to meet INTELSAT's established gain-to-noise temperature ratio, *G/T*, standards. On March 12, 1986, in anticipation of the availability of the INTELSAT VI series in the early 1990s, the INTELSAT Board of Governors significantly lowered Standard A and C earth station *G/T* performance requirements to 35 and 37 dB/K, respectively. Prior to this date, Standard A earth stations were required to have a minimum *G/T* of 40.7 dB/K, and Standard C earth stations were required to have a minimum clear-sky *G/T* of 39.0 dB/K. Earth stations built to these *G/T* specifications are called "previous" Standard A or C, while stations built to the new specification are called "revised" Standard A or C.

The cost savings associated with reduction of the *G/T* specification are primarily due to reduction in the size and complexity of the antenna structure. Previous Standard A and C earth stations require complex antenna support structures and massive foundations, which are major contributors to their overall cost. Channel-dependent and RF equipment is expected to consist of basically the same hardware for either the previous or revised earth stations. The reduction in the transmit gain of the smaller earth stations may result in some increase in HPA and combining network costs.

To significantly reduce antenna costs, the diameters must be small enough to permit simpler support structures. The revised INTELSAT standards meet this objective by having *G/T* requirements that are achievable with diameters of 15 to 17 m for C-band, and 11 to 13 m for Ku-band. Figures 2 and 3 present an estimate of the relationship between hardware cost and antenna diameter for both C- and Ku-bands, respectively, in the 1985 time frame when this study was conducted. In general, the revised *G/T* performance requirements are expected to result in about a 50-percent reduction in antenna costs. While current prices are likely to be higher, it is believed that the general cost difference relative to antenna size continues to exist.

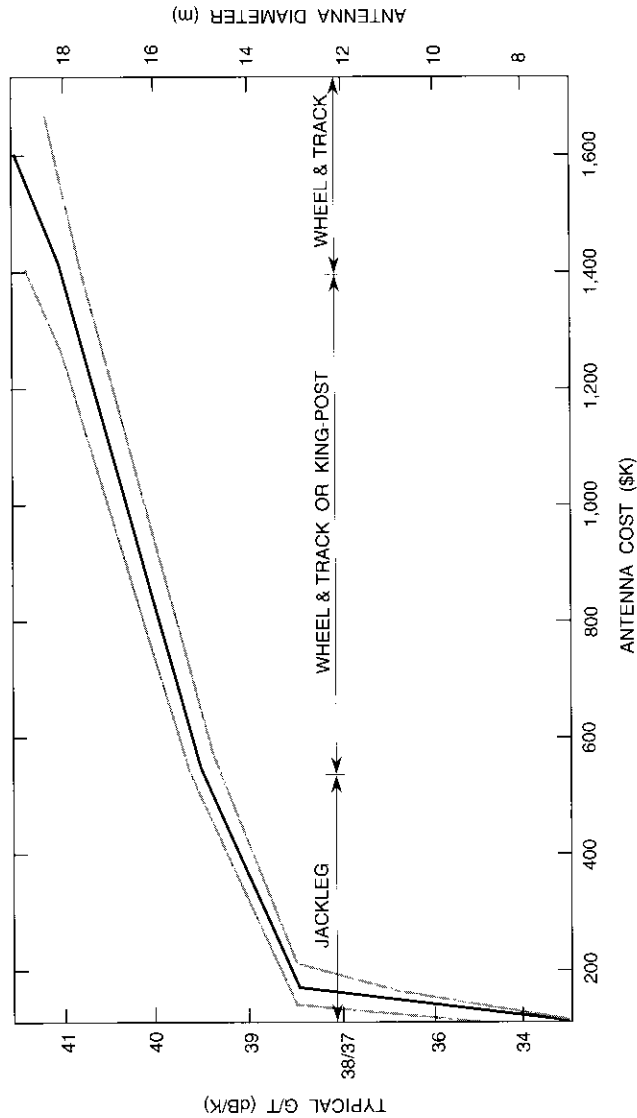
**Impact on transponder capacity**

The use of smaller standard earth stations results in a somewhat lower achievable space segment capacity relative to previous Standard A and C earth stations. Assuming the worst case, in which the system consists solely of revised Standard A earth stations, frequency-division multiplexing (FDM)/FM transponder capacity would be reduced by about 20 percent. In the case of revised Standard C earth stations, FDM/FM transponder capacity would be



- NOTES:
1. Cost includes antenna, dual-polarization feed, and automatic tracking.
  2. A range of antenna diameters is shown for a given *G/T* to cover different LNA noise temperatures.
  3. Region between shaded lines indicates estimated price spread.

Figure 2. Typical Antenna Costs: C-Band (Based on 1985 market conditions)



## NOTES:

1. Cost includes antenna, single-polarization feed, and automatic tracking.
2. Region between shaded lines indicates estimated price range.

Figure 3. Typical Antenna Costs: Ku-Band (Based on 1985 market conditions)

reduced by about 40 percent compared to previous Standard C's. However, the INTELSAT system is now well along in its plan to convert the network from analog to digital transmission, and the impact on transponder capacity is not as great because forward error correction (FEC) is employed to offset the reduction in earth station  $G/T$ . Figure 4 shows the relationship between INTELSAT VI 72-MHz transponder channel capacity and earth station  $G/T$  for both C-band and Ku-band when rate  $3/4$  FEC is applied to digital intermediate data rate (IDR) carriers.\* As indicated in the figure, transponder channel capacity reaches the bandwidth-limited condition of 1,200 channels under the revised standards.

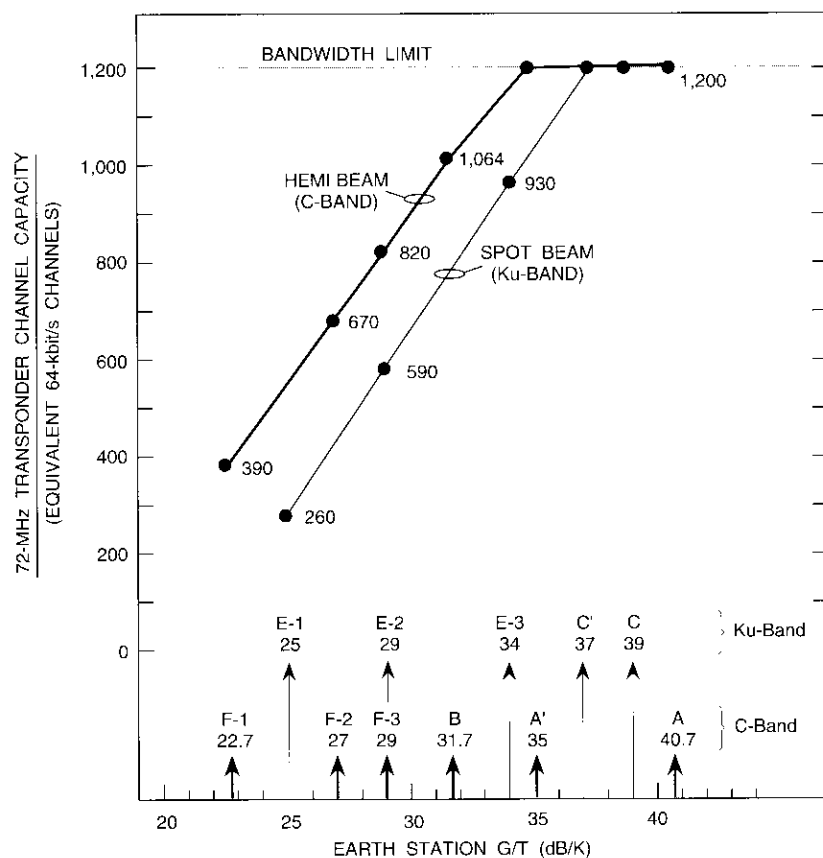
### Quality of service

Earth station  $G/T$  values for revised Standard A and C earth stations have been chosen to ensure that the quality of service provided for previous Standard A and C earth stations continues to be provided to all earth stations meeting the revised standards. A  $G/T$  of 35 dB/K is the lowest figure-of-merit that could be specified for the revised Standard A while maintaining a signal-to-weighted-noise ratio of 49 dB for 20-MHz, open-network, occasional-use TV/FM transmissions into the revised Standard A through the INTELSAT VI global beam transponder with a down-link e.i.r.p. of 26.5 dBW. This is the same signal quality received by a previous Standard A antenna ( $G/T = 40.7$  dB/K) operating with a 17.5-MHz TV signal transmitted from an INTELSAT V or V-A series satellite with a global beam e.i.r.p. of 23.5 dBW. With careful tradeoffs among bandwidth, power, and deviation, the quality of the previous signal has been maintained with a substantially smaller earth station.

For 120-Mbit/s TDMA transmission between previous Standard A earth stations, a rate  $7/8$  FEC code is recommended on certain INTELSAT V/V-A links in order to provide adequate operating margin. The use of this code on all INTELSAT VI links to the revised Standard A earth stations will also provide sufficient operating margin for an earth station  $G/T$  of 35 dB/K. Since time-division multiple access (TDMA) is not expected to be required at Ku-band, it did not influence downsizing decisions for Standard C.

The signal quality for analog FDM/FM transmissions, as well as the error performance for digital transmissions, will be maintained at previous levels through a combination of the higher down-link e.i.r.p. available on

\* These are quadrature phase shift keying/frequency-division multiple access (QPSK/FDMA) carriers ranging from 64 kbit/s to 45 Mbit/s which have been designed to replace FDM/FM/FDMA carriers. These modulation techniques form the backbone of the INTELSAT system for conventional telephony services.



- C = Previous Standard C (G/T = 39 dB/K)  
 C' = Revised Standard C (G/T = 37 dB/K)  
 A = Previous Standard A (G/T = 40.7 dB/K)  
 A' = Revised Standard A (G/T = 35.0 dB/K)

Figure 4. INTELSAT VI 72-MHz Transponder Capacity vs Earth Station G/T (Using digital IDR carriers with rate 3/4 FEC)

INTELSAT VI, changing the transponder gain step to a more sensitive position, and use of FEC on the digital carriers. The performance criterion for FDM/FM carriers is a clear-sky quality of less than or equal to 10,000 pW0p (International Radio Consultative Committee [CCIR] Recommendation 353), and the criterion for digital IDR carriers is a clear-sky bit error rate equal to or better than  $10^{-7}$  (CCIR Rec. 614).

### Conclusions

INTELSAT has designed INTELSAT VI to minimize the impact on the ground segment. The INTELSAT V/V-A compatibility mode on INTELSAT VI is instrumental in accomplishing direct point-over from the INTELSAT V and V-A spacecraft to the new INTELSAT VI spacecraft without traffic loss. In addition, the exceptional stationkeeping performance and high down-link e.i.r.p. of the INTELSAT VI series provide two significant means of lowering antenna costs. First, autotrack equipment is not required with earth station antenna diameters of about 9.0 m and smaller at C-band, and 5.5 m and smaller at Ku-band. Second, the  $G/T$  requirements for larger earth stations have been reduced such that Standard A (C-band) antennas are downsized from 30–32 m to about 15–17 m, and Standard C (Ku-band) antennas are downsized from 15–18 m to about 11–13 m. Transponder (1'-2'), which uses a portion of the new frequency band allocation provided by WARC'79, was also added to the INTELSAT VI satellite series with no impact on existing earth station hardware or performance. These improved ground segment features, made possible with the INTELSAT VI series, are major steps in helping INTELSAT to control costs and remain competitive.

### Acknowledgments

The authors would like to acknowledge guidance received from J. Dicks and the INTELSAT Technical Committee concerning the downsizing of the Standard A and C earth stations, and to thank the INTELSAT Astrodynamics Department for satellite stationkeeping consultations.

### References

- [1] L. M. Buchsbaum, "Pointing Losses in Single-Axis and Fixed-Mount Earth Station Antennas due to Satellite Movement," *International Journal of Satellite Communications*, Vol. 4, No. 2, April–June 1986, pp. 89–96.
- [2] L. F. Gray and M. P. Brown, Jr., "Transmission Planning for the First U.S. Standard C (14/11-GHz) INTELSAT Earth Station," *COMSAT Technical Review*, Vol. 9, No. 1, Spring 1979, pp. 61–89.

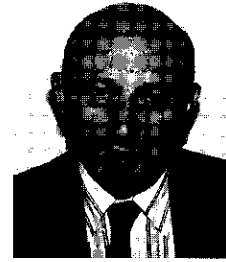


*Martin P. Brown, Jr., received a B.E.E. from the Georgia Institute of Technology in 1966. Prior to entering military service he was employed by IBM at Cape Kennedy, where he was involved in construction of the first Saturn V launch vehicle. From 1967 to 1971, he served as an engineering communications officer with the U.S. Air Force. In 1971 he joined COMSAT Laboratories, where he was primarily involved in transmission design for INTELSAT IV, IV-A, and V. He joined INTELSAT in August 1978 to become Manager of the Satellite Transmission Engineering and Modeling Section, where he has been responsible for*

*FDMA transmission design for the INTELSAT VI, VII, and K satellites, and for preparing the required earth station performance characteristics associated with each of these spacecraft series. He has also been involved in the design of most of the analog and digital modulation techniques employed by INTELSAT, and in the development of computer system models for satellite communications.*

*Mr. Brown is a past Chairman of the IEEE Communications and Broadcast Satellite Systems Committee and a Registered Professional Engineer.*

*Francisco A. Loureiro received a Communications Engineering degree from Universidade Catolica do Rio de Janeiro in 1975, and attended the Master in Communications Systems program at the same university in 1981-1982. From 1977 to 1985, he worked for Embratel, Brazil, at the International Directorate as Manager of the Engineering Division, leading large international telecommunications projects. He had senior engineering responsibilities in both the System Planning and Transmission Engineering divisions of INTELSAT, and in 1990 joined the INTELSAT Assistance and Development Program, where he held the position of Principal Engineer. In 1992, Mr. Loureiro joined Sprint International, where he is currently General Manager of Sprint Brasil.*



*Milenko Stojkovic received the Dipl. Eng. degree in communications and electronics engineering in 1967, the M.Sc. degree in 1977, and the D.Sc. degree in 1983, from the Faculty of Electrical Engineering, University of Belgrade. From 1967 to 1984 he was with PTT Enterprise Belgrade, where he was responsible for planning, installing, and implementing the first Yugoslav earth station. He subsequently served as Chief Engineer for Satellite Systems Development, and then as Head of the Transmission System Development section. He was also associated with the Faculty of EE, University of Belgrade, as Assistant*

*Professor and Docent. Since 1984, he has been with the Communications Engineering Department at INTELSAT.*

## ***DCME in the INTELSAT VI era***

M. ONUFRY, G-P. FORCINA, W. S. OEI, T. OISHI, J. F. PHIEL,  
AND J. H. RIESER

(Manuscript received October 19, 1990)

### ***Abstract***

This paper provides a brief history of the development of digitally implemented circuit multiplication equipment (DCME) within the INTELSAT system. The importance of circuit multiplication in the INTELSAT system is discussed, and an overview of the more significant aspects of the newest INTELSAT circuit multiplication equipment specification (IESS-501) is given. The performance of equipment built in accordance with IESS-501, in a burst error environment, is compared with that of other proprietary circuit multiplication equipment. Potential future enhancements to DCME are also discussed.

### ***Introduction***

Circuit multiplication equipment has been used in the communications field for many years over various transmission media, including cable and satellites. Its function is to concentrate a number of telephone calls onto a smaller number of transmission channels. Analog techniques were employed initially; however, only with the advent of digital technology was it possible to achieve high concentration gain, good transmission performance, and high reliability. The result is referred to as digitally implemented circuit multiplication equipment (DCME).

### ***Specification development***

Interest in the application of digital speech interpolation (DSI) systems within the INTELSAT network began in the late 1960s. COMSAT Laboratories initiated work aimed at improving the performance of speech

interpolation systems by using digital implementation to achieve significant channel multiplication. One objective was to avoid the loss of speech quality resulting from speech spurt freeze-out during short intervals of overload, which tainted the analog time-assigned speech interpolation (TASI) systems of the era. In the laboratory, work was begun on a system using pulse-code modulation (PCM) sample prediction, called Speech-Predictive Encoded Communication (SPEC) [1]. In lieu of the speech spurt freeze-outs that marred TASI, SPEC introduced speech spurts having slightly increased quantizing error. In addition, an effort was initiated under contract with SIT Siemens of Italy to work on a digitally implemented TASI (ATIC in Italian) system [2].

As work progressed, comparative testing of the two approaches strongly favored SPEC because it avoided the occurrence of freeze-outs. SIT Siemens offered to implement a new strategy which modified the digital ATIC to create additional bearer channels during the short-duration overloads that necessarily characterize the random process attending voice channel activity. This was done by "stealing" the least significant bits (LSBs) of normal 8-bit PCM samples to create lower bit rate overload channels. During overload, this approach replaced freeze-outs with spurts of slightly degraded PCM speech. Under testing, the modified ATIC equipment proved to be as effective as SPEC in eliminating freeze-outs. It was also preferred over SPEC because it could easily be extended to low-bit-rate speech encoding techniques such as adaptive differential PCM (ADPCM), subband coders, and linear predictive coders.

These advantages led to the selection of digital TASI with overload channel generation for use in the 60-Mbit/s time-division multiple access (TDMA)/DSI system adopted by INTELSAT in its BG-1-18 system specification, and later in the 120-Mbit/s TDMA/DSI system adopted in the BG-42-65 system specification [3]. This proved to be a wise choice because the compatibility between digital TASI and low-rate encoding has led to DCME with channel multiplication ratios of five and greater.

In 1978, INTELSAT conducted field tests of DSI terminals constructed according to the BG-1-18 TDMA/DSI system specification [4]. The U.S., France, and Italy participated in the trials. Customer traffic was carried over the system, and callback quality assessments proved that the system delivered high-quality, clip-free performance for DSI gains as high as 2.4.

Experience with the BG-1-18 TDMA/DSI provided a basis for development of INTELSAT's 120-Mbit/s TDMA/DSI system specification, which was ultimately approved in 1980 with the release of the BG-42-65 TDMA/DSI systems specification (Revision 2). New features included improved control channel protocols; adaptive threshold speech detection; noise insertion to minimize background noise modulation; voiceband data discrimination; dynamic load

control (DLC), which allows elementary signaling to the switch to prevent severe system overload; and preassigned 64-kbit/s channels. Equipment conforming to the TDMA/DSI specification (BG-42-65, later revised to *INTELSAT Earth Station Standard* [IESS] 307) was built by COMSAT Laboratories [5] and field tested [6]. This led to an operational TDMA/DSI system in the mid-1980s with a nominal circuit multiplication gain of 2.0 to 2.2.

While development of the operational 120-Mbit/s TDMA/DSI equipment was progressing, research efforts were turned to the next generation of DSI, in which additional circuit multiplication was possible through the introduction of lower-rate speech encoding (LRE), in addition to interpolation gain. Interest focused on 32-kbit/s encoding, where the candidate techniques included adaptive delta modulation, subband coding, and ADPCM. Under contract with INTELSAT, COMSAT Laboratories developed a prototype 32-kbit/s DCME system. In the same time frame (1981–1984), the International Telephone and Telegraph Consultative Committee (CCITT) became interested in developing a digital encoding standard for operation at 32 kbit/s [7], and defined an ADPCM algorithm in CCITT Recommendation G.721. Subsequently, CCITT introduced Rec. G.726, which combines the encoding algorithms used in DCME for operation at 16, 24, 32, and 40 kbit/s into a single recommendation. This was adopted by CCITT under the accelerated approval procedures of Resolution 2 in December 1990.

The introduction of 32-kbit/s encoding in DCME created a number of new problems which had to be resolved [8], including the following:

- Potential mistracking between the ADPCM encoder and decoder due to freeze-out.
- Accommodating voiceband data at rates greater than 4,800 bit/s, which may be impaired in bit error ratio (BER) during passage through the ADPCM codec.
- Discriminating the data rate to identify when the voiceband data rate is greater than 4,800 bit/s.
- Modifying the ADPCM encoder to create overload channels by changing the encoding rate from 32 to 24 kbit/s, rather than using simple bit truncation, as was done for PCM-encoded signals.
- Synchronously signaling an encoding rate change to the decoder.

Recognizing that the long-term interests of its users are best served when they can interwork via a network of multdestination and single-destination links, using compatible equipment available from a number of manufacturers, the INTELSAT community undertook to develop an open network DCME

specification. This new specification included special features such as a generic interface to a switch to provide DLC, and new integrated services digital network (ISDN) services such as alternate speech/unrestricted 64-kbit/s service. The use of 40-kbit/s ADPCM was accepted, and a new frame structure involving the concept of a bit bank was adopted. A more efficient control channel was defined, rapid rotation of overload channels was added, and silence elimination for facsimile transmission was introduced. This became the IESS-501 DCME specification [9], which was adopted by the INTELSAT Board of Governors on September 16, 1987. The INTELSAT specification represented a very substantial effort, with contributions by a number of INTELSAT signatories. It was subsequently adopted by EUTELSAT with minor modifications to accommodate R2D signaling, which is widely used in Europe.

The IESS-501 specification was later submitted to the Committee T1 subgroup, TIY1.2, for consideration as the U.S. standard, and to CCITT. In TIY1.2, the basic structure was adopted under COMSAT's leadership and, with changes to accommodate national interests, has evolved into the "American National Standard for Telecommunications, Digital Circuit Multiplication Equipment—Interface, Functional, and Performance Specification." In the CCITT, also under the leadership of COMSAT, revised Rec. G.763 (which was based on IESS-501) was approved in December 1990 under Resolution 2. Thus, a true international standard has evolved and a compatible operational mode exists among the CCITT, Committee T1, INTELSAT, and EUTELSAT DCME specifications which permits interoperability between equipment designed to these specifications.

### **Motivation for using digital circuit multiplication**

INTELSAT has encouraged the conversion of the global network to digital modulation techniques with circuit multiplication largely due to financial incentives. Space segment charges for digital carriers are now computed based on the number of 64-kbit/s channels used, rather than on the number of derived channels. The immediate financial benefit of circuit multiplication systems is therefore given entirely to the users. The global network also benefits, since available capacity is used more efficiently.

Conversion of the INTELSAT system to digital modulation, and the use of digital circuit multiplication with its resulting efficiency and effective reduction of tariffs, is especially timely. Beginning in the late 1980s, the INTELSAT global network has confronted increasing service demands against limited available capacity. To a significant degree, these demands are being met by converting the system from frequency-division multiplexing/frequency

modulation/ frequency-division multiple access (FDM/FM/FDMA) carriers to quadrature phase shift keying (QPSK)/FDMA carriers (intermediate data rate [IDR]) which utilize DCME. Figure 1 shows the growth in the actual number of full-time channels for public switched telephone networks (PSTNs) through 1990, as well as the projected PSTN traffic through the year 2004 (*i.e.*, throughout the INTELSAT VI epoch). This includes FDM/FM, companded frequency-division multiplexing (CFDM)/FM, single channel per carrier (SCPC), IDR, and TDMA. The apparent leveling of the number of satellite channels provided in 1989 and 1990 is the result of the conversion. This dramatically illustrates the effect of DCME on the requirement for 64-kbit/s channels through the first half of the 1990s. The forecast is predicated on a realized DCME gain of 3.2 as conversions are made to IDR, and an underlying annual growth rate of about 13 percent for PSTN traffic. Without DCME, a significant portion of the demand would not be satisfied with the attainable in-orbit satellite capacity.

Depending on traffic loading, channel activity, and the size of the bearer pools, the achievable DCME gain will typically range between 3 and 5 [10]. The impact of bit-borrowing to create the overload channels on the signal-to-quantization noise in the resulting speech signal at the receiver is also discussed in detail in Reference 10, where curves are presented that plot this measure as a function of the number of voice channels interpolated and demonstrate the tradeoff between received signal quality and channel multiplication ratio. With INTELSAT's tariffs now based on the number of 64-kbit/s bearer channels, the cost for utilization of an INTELSAT satellite is reduced by a factor equal to the realized gain. For most users, the cost of implementing DCME is recovered in less than 6 months through savings in space segment costs.

### **Review of IESS-501**

INTELSAT specification IESS-501 was approved for use with both continuous digital (IDR) carriers and burst-mode digital (TDMA) carriers. This section describes the functional characteristics and technical features of the IESS-501 DCME [11],[12].

The circuit multiplication technique adopted in IESS-501 employs a combination of interpolation and encoding. The interpolation process takes advantage of the silence intervals that occur in normal conversation to permit random time-division multiplexing of speech spurts from many conversations onto the bearer transmission channels. Additional signal encoding efficiency is introduced through the use of nominal 32-kbit/s ADPCM encoding, which provides a further doubling of the circuit multiplication gain achieved through interpolation. The DCME also includes a number of important features such as

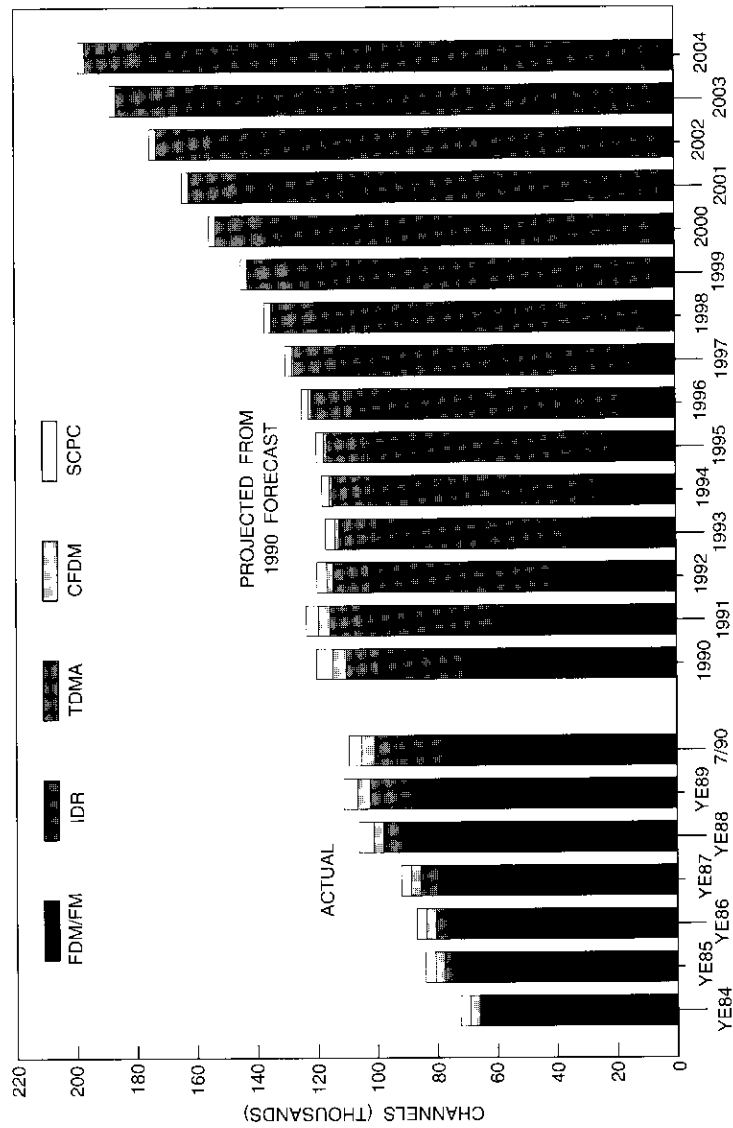


Figure 1. 1990 Forecast of Public Switched Telephony Service

a multiple-destination capability, DLC, and the ability to accommodate a variety of signaling systems.

The multidestination feature capitalizes on the unique ability of a satellite system to deliver a signal to a number of earth stations simultaneously. The DCME specified in IESS-501 can operate with up to four destinations. The bearer can be configured as a single pool of channels, shared by all DCME traffic, or can be segregated into two separate pools. The single-pool case, with more than one destination, constitutes the multidestination mode of operation, while the two-pool case, with one destination per pool, is referred to as the multiclique mode of operation. The case of one single-destination pool and one multidestination pool (two or three destinations) constitutes a mixed mode.

Various applications of these modes are illustrated in Figure 2. Case (a) represents a single-destination DCME located at an international switching center (ISC). A digital terrestrial link (T-link) is required between the ISC and the earth station (E/S). The same circuit multiplication gain available on the satellite link is applicable to the terrestrial link.

Case (b) refers to multiclique DCME located at the switching center. The remarks made for case (a) are also applicable to case (b); however, the bearer capacity is divided into two segregated pools, with a consequent reduction in the circuit multiplication gain due to the use of a smaller interpolation pool. Note that digital cross-connect equipment is necessary at the earth station in order to extract the two cliques destined for the same DCME and generate the DCME received bearer channel.

Case (c) applies to multidestination DCME located at the earth station. The transmitted bearer capacity is shared among all the destinations (four in the example shown), thus providing the maximum circuit multiplication gain by using the largest interpolation pool. Multiplication gain is available only on the satellite link, since the terrestrial link to the ISC carries the uncompressed trunk channels. An analog terrestrial link could be employed, but a transmultiplexer would be required at the DCME interface. Note that the DCME generates one transmitted bearer, but must process four received bearers.

A further feature of the bearer frame is that pool size(s) can be matched to operational need. That is, an entire 2.048-Mbit/s bearer is not used for traffic unless required. When employed in combination with DST/digital non-interpolation (DNI) terrestrial interface modules, TDMA bursts need only be long enough to be compatible with pool size. Similarly, International Business Service (IBS) framing units can be employed to format a baseband for 512-kbit/s IDR carriers for reduced-pool-size DCMEs.

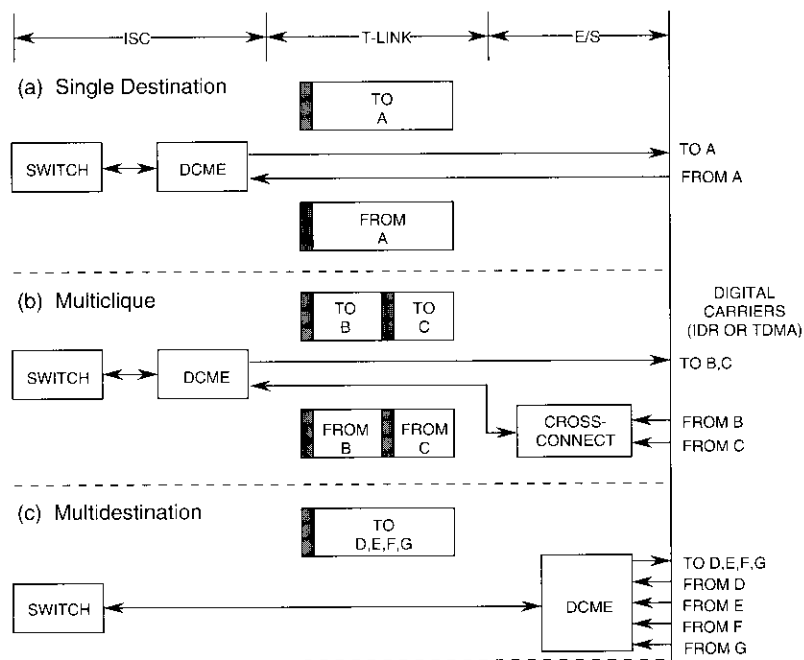


Figure 2. Network Uses of DCME

DLC is an important feature that is used to avoid overloading the DCME. The DCME monitors the average number of bits per sample used to encode speech, and when a preset threshold is reached, a signal is sent to the corresponding switch indicating that no additional traffic should be routed to the DCME. When the load decreases and the average bits per sample rises above a second preset threshold, the DLC signal is removed, indicating that additional new traffic can now be accommodated by the DCME.

A number of signaling systems are in use in the international arena. The DCME must operate with in-band CCITT Signaling System 5, which was specifically designed for interpolation systems. Out-of-band systems such as Signaling Systems 6 or 7 are easily accommodated through the use of preassigned channels that are not subject to DCME processing. For additional flexibility, an option exists for accommodating other signaling systems such as R1 or R2D. The IESS-501 DCME provides a comprehensive set of control signals to a signaling interface. A subset of these signals may then be selected to

coincide with the limitations of the communications link between the ISC and the DCME, as well as any constraints of the corresponding ISC.

Other features include 64-kbit/s unrestricted channel accommodation, silence elimination on facsimile traffic, adaptive noise insertion, and rapid rotation of overload channel assignments. These features are all related to ISDN application of DCME, or to subjective quality improvements.

The IESS-501 DCME can accommodate either preassigned 64-kbit/s unrestricted traffic or alternate speech/64-kbit/s unrestricted traffic. In the latter case, the switch must be able to communicate with the DCME to carry out post-call-setup signaling. CCITT Rec. Q.50 (*Blue Book*, 1988) provides guidance for ISC/DCME communications, as well as for DLC-related signaling, and is also used for proprietary DCME interfaces.

Facsimile transmission is the predominant form of voiceband data transmission over international telephone connections. Typically, pages of text/graphics information are transmitted in one direction, while only short acknowledgment signals are sent in the return direction. The inactive periods in the return direction provide the opportunity to interpolate other active circuits. This feature, called silence elimination, increases the number of bearer channels available to carry speech, thus increasing the average bits per sample used for speech in the return direction.

The voice-gating action that is a natural consequence of interpolation also modulates circuit background noise, which is subjectively annoying. The IESS-501 DCME measures the background noise at the transmitter, quantizes it to seven or eight levels, and conveys this information to the DCME receiver, where the noise is reinserted during silence intervals. This eliminates annoying noise modulation effects.

Increased quantizing noise generated when the DCME operates in the overload mode (when the encoding falls back to 24-kbit/s) must also be considered. To avoid having the same four talkers (the three normal 32-kbit encoded channels which are reduced to 24 kbit/s, plus the one overload channel) continually experience the higher quantization noise, 24-kbit/s encoding is distributed among the full set of bearers carrying speech by randomly selecting a new starting point every DCME frame (2.0 ms).

An automatic channel check procedure has been incorporated in the IESS-501 DCME to detect equipment failures affecting one or more circuits. This procedure is based on the periodic insertion of test signals into individual channels. The receive end is informed of the test signal transmission, and a particular signature is expected at the output of a given ADPCM decoder. If an excessive number of errors are detected, an alarm is raised. An inter-DCME communications channel is used between the corresponding DCMEs to convey



can be stolen, so that an overload SC can be either 3 or 4 bits (see SCs 64 and 65 in Figure 3). Sometimes, an overload SC contains no bits at all because the overload channels are created only when needed.

For preassigned SCs, it is a specification requirement that the bit banks be contiguous, beginning adjacent to the AC. The 4-bit nibble portion of the preassigned data SCs should be contiguous to the bit banks. Spare bits in the banks are available for use by interpolated (*i.e.*, non-preassigned) data channels. Preassigned 64-kbit/s channels should occupy two contiguous nibbles, starting from an even-numbered nibble.

In summary, the SCs are digital channels 3, 4, 5, or 8 bits wide, as shown in Figure 3. As a rule, an SC number does not uniquely define the location of its bits in the bearer frame. Separate procedures map the bits of an SC onto the bits of the bearer structure. Therefore, an SC can be regarded as a logical channel of known capacity (*i.e.*, number of bits).

#### ASSIGNMENT CHANNEL

The main function of the assignment message is to inform the remote DCME of the connections established in the transmit DCME, in order to permit demultiplexing of the compressed primary multiplex bearer. The information provided for this purpose is (SC, IC channel type), where the four types of channels can be identified as voice, data, transparent, and bank.

The AC is an error-protected data channel linking the transmit DCME to its corresponding DCME. The AC delivers an assignment message containing 24 bits of information for every DCME frame that comprises 16 PCM samples (2 ms). A rate 1/2 Golay code capable of correcting up to three errors in a 24-bit block is used. The 48 bits of the assignment message (24 information bits, 22 check bits, and 2 dummy bits) are transmitted over 16 PCM frames, in two blocks, at the rate of 3 bits of encoded AC plus 1 synchronization bit per PCM frame. The AC transmission scheme is shown in Figure 4.

The 24 information bits of the assignment message are divided into three 8-bit segments: the SC word, the IC word, and the data word (as shown in Figure 5). The data word is subdivided into two 4-bit segments: the synchronous data word and the asynchronous data word. The asynchronous data word carries information on alarms, DLC, and channel check procedure. While the entire assignment message is multiplexed over a DCME frame, the information in the asynchronous data word is further multiplexed over a 64-DCME frame multiframe (*i.e.*, the message is available once every 128 ms). The asynchronous data multiframe is synchronized by complementing the synchronization word in DCME frame 0, as indicated in Figure 4.

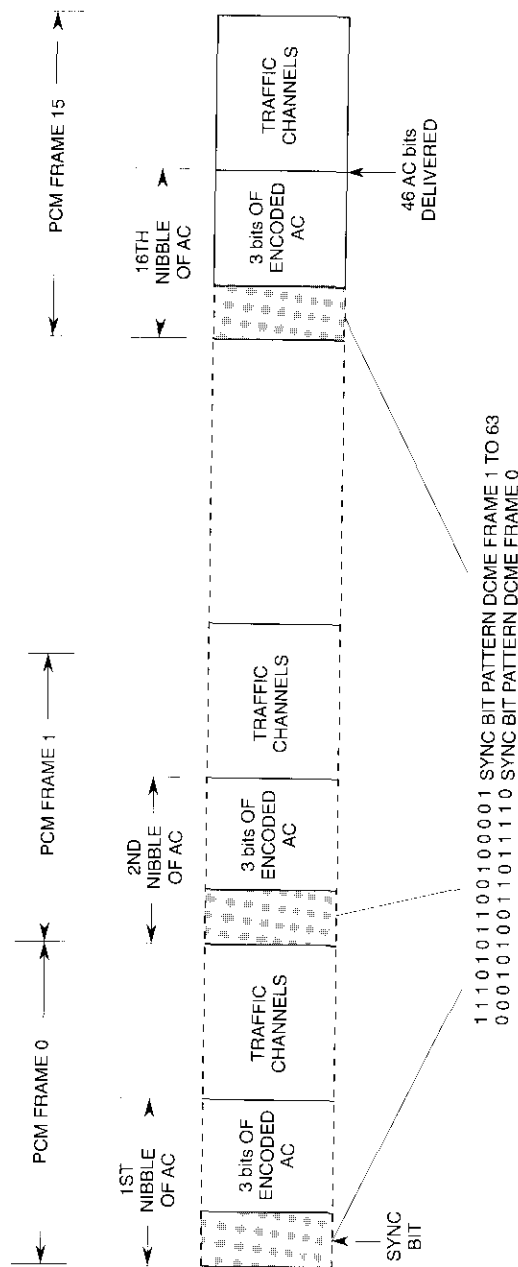


Figure 4. Assignment Channel Transmission Scheme

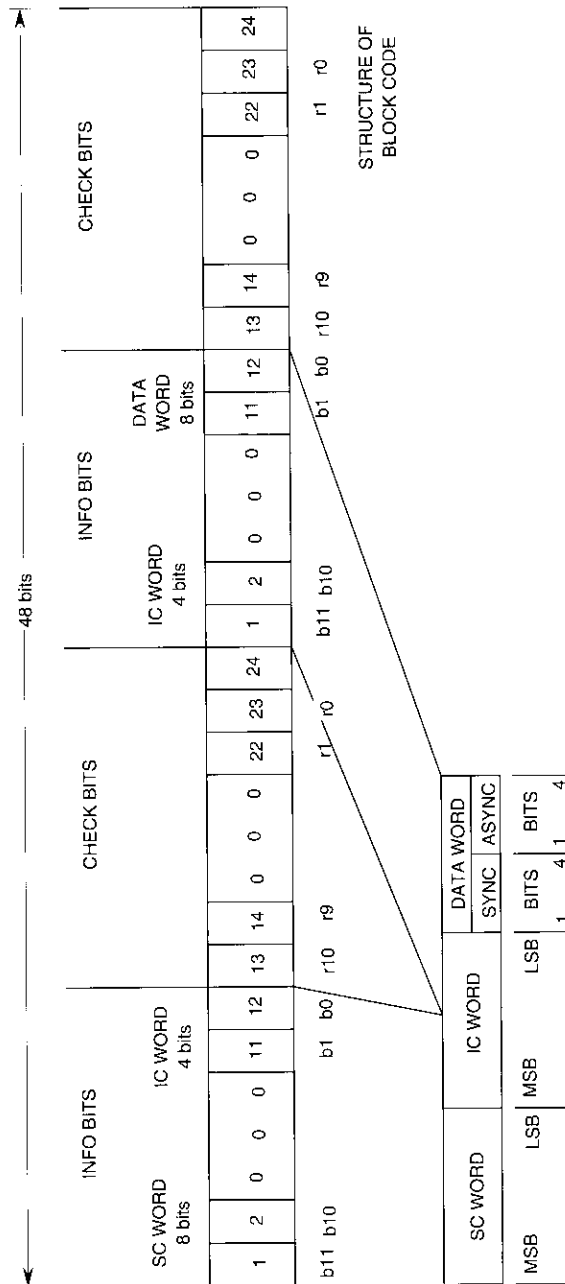


Figure 5. Assignment Message Format

**DCME structure**

The DCME structure, represented by the model shown in Figure 6, is divided into three main parts. The trunk interface and bearer interface perform the input/output function for the uncompressed traffic channels and bearer channels, respectively. The core functions encompass all aspects of the trunk and bearer processing performed by the DCME. These functions, described below, are separated into three components: the transmit-side structure, the receive-side structure, and the common elements. An additional function which

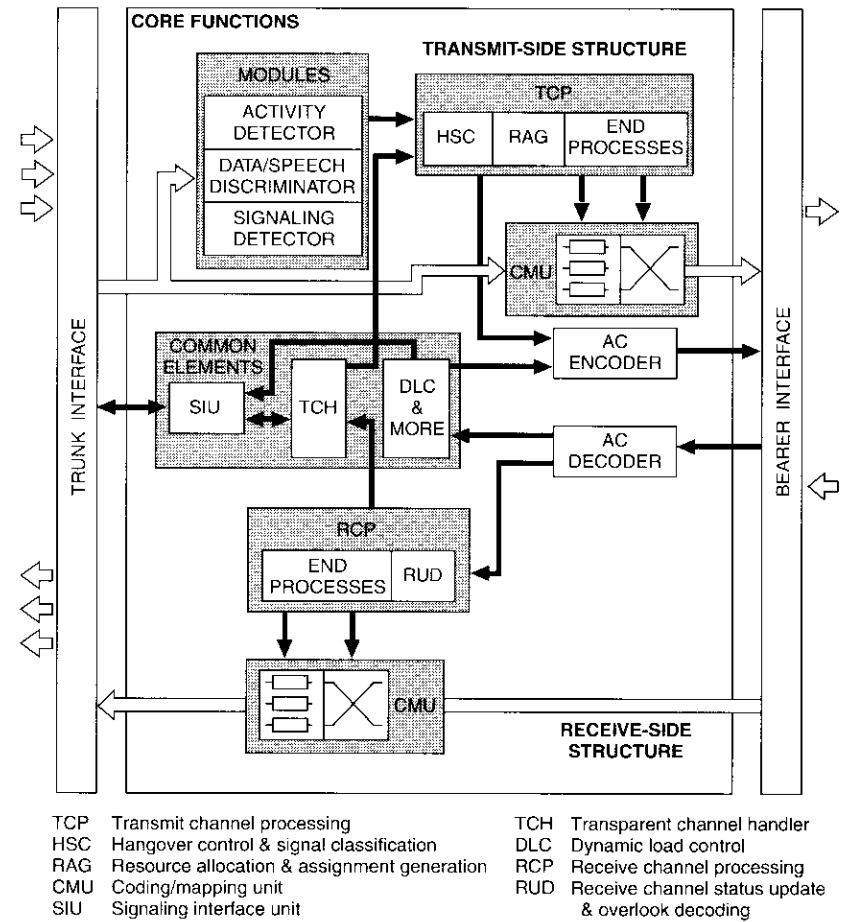


Figure 6. DCME Model

- TCP Transmit channel processing
- HSC Hangover control & signal classification
- RAG Resource allocation & assignment generation
- CMU Coding/mapping unit
- SIU Signaling interface unit
- TCH Transparent channel handler
- DLC Dynamic load control
- RCP Receive channel processing
- RUD Receive channel status update & overlook decoding

is common to all three components is the configuration control function (called the "map handler" in the specification), which permits initialization of all the components in accordance with the configuration selected for DCME operation.

#### Transmit-side structure

The transmit-side structure processes the input trunk signals and compresses them into the bearer channel. The structure consists of the input modules, the transmit channel processing function (TCP), the coding/mapping unit (CMU), and the AC encoder. In those cases where two cliques or pools are used (multiclique mode or mixed mode), the structure must be replicated twice.

The input modules perform first-level signal processing (consisting of trunk activity detection and determination of the signal type) on each connected trunk. The functional units used are the activity detector, the data/speech discriminator, and the signaling detector. The activity detector, incorporating an adaptive threshold, provides a real-time active/inactive indication that can significantly affect DCME performance. Different values of hangover time are specified, depending on the signal type, which is determined by a data/speech discriminator and a signaling detector. The outputs of these three modules are fed to the TCP, which performs the next level of signal processing. Control of hangover time is specified within the TCP.

The TCP is the most "intelligent" function of the DCME. It contains three main elements: the hangover control and signal classification (HSC) process, the resource allocation and assignment generation (RAG) process, and the end processes. In TESS-501, the TCP is entirely described by the CCITT-defined system description language (SDL) [14].

There is one HSC process for each connected IC. Inputs are received from the input modules, the common elements, and the receive-side structure. The HSC process generates output signals toward the RAG process. Control of the hangover time associated with activity detection is a part of the HSC process.

Table 1 lists the hangover times used for the different types of signals. The 25-ms speech hangover takes advantage of short intersyllabic pauses for interpolation among active channels, resulting in a higher gain. The 125-ms signaling hangover permits bridging over the time intervals between consecutive signaling tones to ensure the integrity of the signaling sequences. The 14-s initial data hangover (IDH) permits bridging of the time intervals between pages in the forward direction of a facsimile transmission. In the return direction, however, the time separation between the short facsimile acknowledg-

TABLE 1. HANGOVER TIMES FOR DIFFERENT SIGNAL TYPES

SIGNAL	HANGOVER TIME
Voice	25 ms
Signaling	125 ms
Data	IDH or SDH
IDH	14 s (typical)
SDH	<<14 s (typical)

ment messages is greater than 14 s; thus IDH will expire and second data hangover (SDH) will apply. Since SDH is short, the transmission channel will be seized for just slightly longer than the duration of the acknowledgment message itself, and the channel will be available for other uses. This feature is called "silence elimination."

The HSC processes produce an output which is sent to the RAG processor for each input trunk (IC). These outputs consist of either a request for capacity or a notification of terminated use. The RAG process generates resource assignment information, both for local use and for transmission to the remote DCME via the AC encoder. This information, which is logged in a resource map, includes the connection of each IC and SC, the type of connection (SC type), indication of terminated SC use, and the SCs reserved for preassigned channels. The SC types are voice, data, transparent, bank, and disconnected.

The messages received from the HSC processes constitute requests for an assignment action. Since the requests are randomly generated, but must be serviced at a regular rate (no faster than one per DCME frame), a queuing system is employed. The queue priorities are given in Table 2.

TABLE 2. QUEUE PRIORITIES

PRIORITY	REQUEST
0	Line signaling information
1	Transparent 64-kbit/s disconnect
2	Overload channel disconnect
3	Transparent 64-kbit/s connection
4	Data channel connection
5	Voice channel connection

The priority 0 queue is used in conjunction with an optional user signaling module (USM) to handle the transmission of line signaling information as required by Signaling System R2D or R1. The USM places a request in the priority 0 queue every  $n$ th DCME frame of the multiframe (typically,  $n = 8$ ).

At the start of every DCME frame (other than the  $n$ th frame defined above), the queues are scanned from priority 1 through 5 to determine whether there are any stored requests. If there are requests in a queue, the oldest request is serviced and then deleted. If the queue being examined is empty, or if it is not possible to service the request, the next lower priority queue is examined. When the lowest priority queue is examined and found empty, a refreshment procedure is invoked which generates an assignment message to refresh an old SC connection. The normal and overload SC ranges are alternately scanned, each in ascending numerical order. The minimum duration of the refreshment cycle is 244 ms.

Before servicing a request, the bit capacity of the bearer is checked. If it is sufficient, capacity is then allocated, an ADPCM encoder is selected, and the assignment message is generated. The encoder is selected from the pool of available encoders in the encoder bank (in the CMU). If the IC being assigned already has an encoder connected to it, the encoder in use is kept. When the IC is disconnected, the encoder is returned to the encoder pool.

Capacity allocation procedures vary as a function of traffic loading. Consider as an example a bearer configuration (Figure 7) in which there are 20 transparent channels, nine voice channels, nine data channels, and three bit banks.

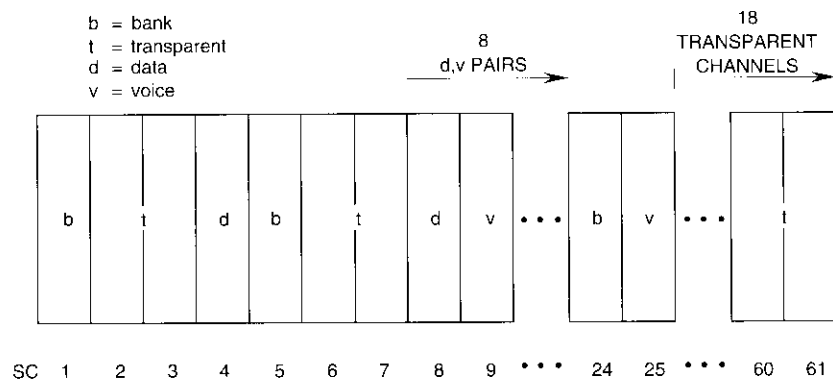


Figure 7. Bearer Configuration for Assignment Example

call. Since transparent channels require two contiguous, normal-range SCs starting with an even-numbered SC, the new transparent call can be accommodated only by reassigning one of the data/voice pairs (channels 8 and 9) and using the vacated SCs. The voice channel in SC 25 is reassigned to overload so that the data channel in SC 8 can take its place. The voice channel in SC 9 is then reassigned to overload so that the transparent call can be assigned to the SC pair 8,9. At this point SC 4, no longer occupied by a data channel, is disconnected. This causes the number of data channels to drop from nine to eight. As a result, the bit bank in SC 24 must be deleted (see the above specified criterion). The entire process requires four assignment messages to complete and results in a number of changes in the resource map.

The (internal) assignment messages generated by the RAG process are of the type (SC, IC, type, encoder) and go to the AC encoder and the end processes. The end processes receive information from the RAG process, combine it with the results of internal routines, and produce control information for the CMU. These processes perform the bit association between the banks and the data channels and create the overload channels from the normal SCs. Bank SCs created for preassigned channels can be used by interpolated data channels, if not fully occupied (see nibbles 1, 2, and 4 in Figure 3).

The end processes create both 3- and 4-bit overload channels. Each channel is obtained by taking 1 bit from three or four normal-range voice SCs, with the result that three or four voice channels will be operating in a 3-bit mode. The number of 4-bit overload channels ( $N_4$ ) is computed as follows:

$$N_4 = \text{Integer} \left( \frac{N_v \times 4 \times N_{ov}}{N_v + N_{ov}} + 0.5 \right) - N_{ov} \times 3 \quad (1)$$

where  $N_v$  is the number of normal-range voice SCs, and  $N_{ov}$  is the number of active overload channels. As a result, the available bits are allocated to the SCs of the two groups in proportion to the number of channels in each group.

The encoding rate among the voice channels is equalized by rapid rotation of channels in the 3-bit mode, using the IC number contained in the assignment message as a random pointer. The procedure is implemented in two phases. In the first phase, shown by example in Figure 8, the 4-bit overload channels are selected using the random pointer (the remaining overload channels are 3-bit). In the second phase, shown by example in Figure 9, the lowest numbered SC channel from which bits can be taken is selected randomly. The next higher normal SC channels also contribute to the generation of overload channels until all required overload channels are generated.

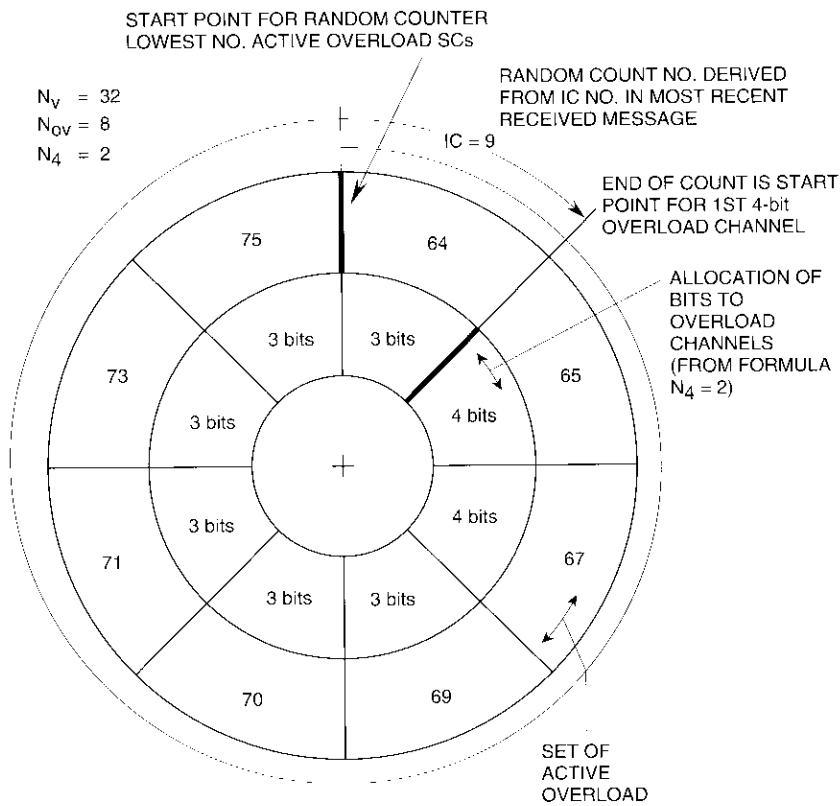


Figure 8. Selection of 3/4-bit Mode of Overload SCs

The creation/deletion of the bit bank channels is a special case. These channels are not created as a direct response to a request, but rather as the first step in assigning a data channel (when existing banks cannot be used). The criteria for creation/deletion of a bit bank are as follows:

1. Create bank if  $N_b < N_d/4$
2. Delete bank if  $N_b \geq N_d/4 + 1$

where  $N_b$  is the number of bit banks and  $N_d$  is the number of data channels. Note that creation of a bit bank requires an assignment message, while deletion of a bit bank is solely a map update operation. If there is more than one bit bank, the highest numbered bit bank channel is deleted.

The end processes receive the message (SC, IC, type, encoder) from the RAG process every 2 ms. The 3- or 4-bit mode of each voice channel is also known

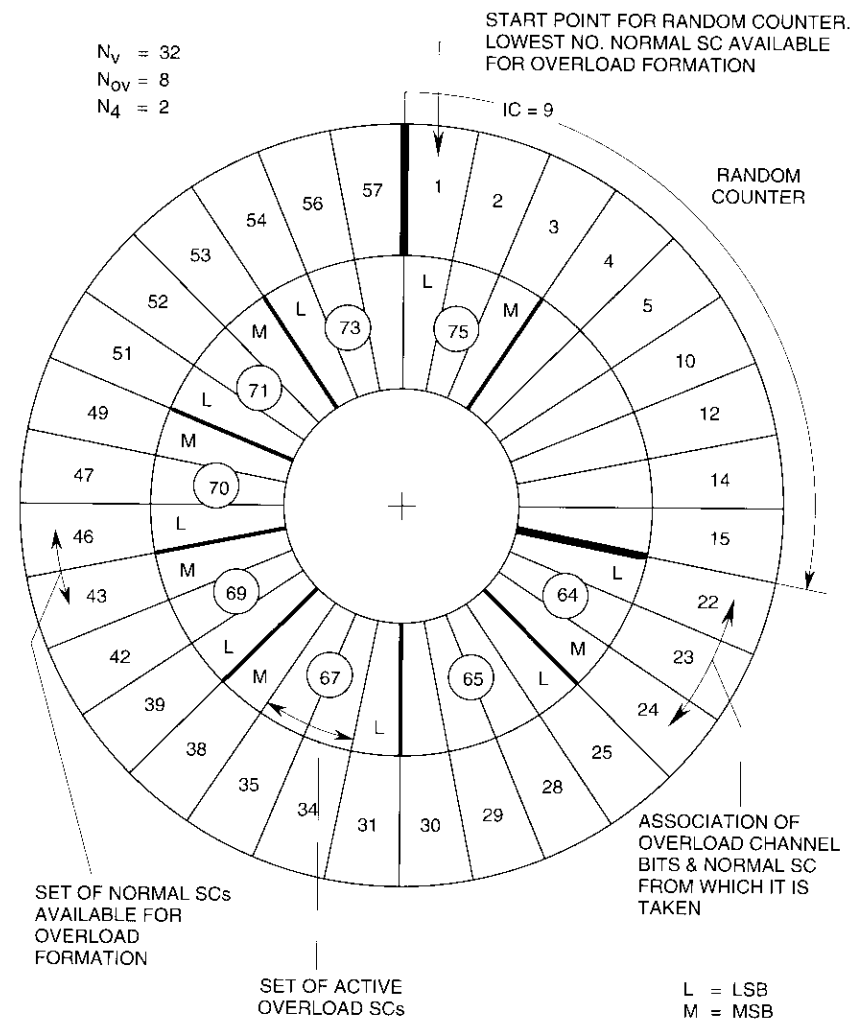


Figure 9. Selection of SCs for Bit Stealing

as a result of the internal task described above. Based on this information, a control message is assembled and sent to each encoder of the CMU, indicating the IC connection, the SC connection, the 3/4/5/8-bit mode of operation, and whether the encoder should be reset. Every control message is delayed by three DCME frames before being sent to the hardware, to provide a time margin for implementation at the remote DCME.

The CMU performs the actual compression of the  $N$  digital input trunks onto the bits of the bearer channel. This unit contains the ADPCM encoder bank and the SC mapping module. The mapping module places the bits of each SC in the appropriate bit locations of the bearer frame, in accordance with the map received from the end processes.

The AC encoder receives the assignment messages (SC, IC, type, coder) from the RAG process and encodes the first three information elements in the proper format for transmission. Additional information, received from the common elements, is encoded into the synchronous and asynchronous data words.

### Receive-side structure

The receive-side structure processes the bearer channel(s) for trunk channel regeneration. The structure must be replicated for each received bearer (only one is shown in Figure 6). The ADPCM decoder hardware can be shared among bearers of different origins. The receive-side structure consists of the AC decoder, the receive channel processing function (RCP), and the CMU.

The AC decoder extracts the assignment message information from the bits of the AC and forwards it to the RCP and to the common elements.

The RCP receives assignment information of the type (SC, IC, type) from the AC decoder and processes it to generate control messages directed to the receive side of the CMU. The RCP contains the receive channel status update and overload decoding (RUD) process and the end processes. This function is entirely described in SDL [14] in IESS-501.

The RUD process interprets the received assignment messages and generates information for the end processes. It also maintains an internal resource map, similar to the one described for the RAG process. Proper operation of a DCME system requires that the resource maps in the RAG and RUD processes of the transmit and receive DCME remain identical to each other while dynamically changing (as often as once every 2 ms).

The SC-decoder-IC connections are updated based on changes in the resource map. The rules for selecting and releasing decoders are the same as for the encoders on the transmit side. The RUD process also creates the overload channel and performs the bank/data channel bit association in the same way as on the transmit side. (On the transmit side, these two tasks are assigned to the end processes.)

The RUD process is designed to cope with transitions that are not the result of normal operation. The objective is to minimize the adverse impact of assignment message losses on DCME operation. However, if overload channels are in use, the loss of a single assignment message may disrupt communica-

tions in many or all channels. This is due to the loss of synchronization between the overload channel creation procedures in the transmit and receive DCME (caused, for example, by different values of  $N_{on}$ ). The disruption will continue until a refreshment message (or a new assignment) is received for the SC(s) affected by the lost assignment message(s). To minimize the duration of this service interruption, the overload SC range is refreshed more frequently than the normal SC range by alternate refreshment of the two ranges.

The RUD process possesses all the information necessary to control the hardware in the CMU. This information is forwarded to the CMU via the end processes, which drive the CMU hardware. Their only function is to insert a three-DCME frame delay (implementation delay).

The CMU regenerates the trunk channels from the bits of the bearer channel. This unit is similar to the corresponding unit on the transmit side, except that the ADPCM encoders are replaced by ADPCM decoders.

### Common elements

The common elements (see Figure 6) perform those functions that are not specific to the DCME transmit or receive sides. These include the end-to-end handling of transparent calls, DLC, and other functions such as the channel check procedure and the alarm function. Only the transparent channel handler (TCH) and the DLC facility are discussed here.

The TCH controls and supervises the setup and release processes for 64-kbit/s transparent circuits (duplex) between correspondent DCMEs, and initiates automatic recovery procedures in case of failure and double seizure. The TCH interfaces with the ISC through a functional signaling interface resident in the DCME, and through an implementation-dependent DCME-ISC out-of-band signaling link. The signaling message on this link is in accordance with CCITT Rec. Q.50 and covers the circuit setup/release request messages originated by the ISC, as well as acknowledgment messages returned by the DCME. Since the ISC messages are generated only in the forward direction of a call, the TCH and its peer at the opposite side of the DCME are responsible for establishing (and disestablishing) both the forward and return channels of 64-kbit/s transparent on-demand circuits between DCMEs.

The DLC facility reduces the probability of speech quality degradation (reduced average bits per sample or freeze-out percentage) due to excessive load conditions. It signals to the ISCs—via the signaling interface unit (SIU) and the ISC-DCME out-of-band signaling link—the onset of excessive loads. The ISCs receiving the DLC "ON" message are expected not to seize any more circuits on the DCME link for new incoming calls. Corresponding DCMEs exchange DLC information via the asynchronous data word of the assignment

message. Separate DLC information is provided to the ISC for 64-kbit/s transparent traffic and voice/voiceband data traffic.

Load measurements within each DCME are based on a double (ensemble and time) averaging of the number of encoding bits per voice sample. Then DLC conditions are entered or exited based on the crossing of preset thresholds of average bits per sample.

### Comparison of IESS-501 to proprietary DCME

DCME can be applied to both QPSK/TDMA and QPSK/FDMA (the latter commonly known as IDR) carriers. IDR presents a burst error environment which must be accommodated in the design of the DCME. In the following, the robustness of IESS-501 in a burst error environment is compared with other proprietary DCME.

#### Environment

For spectral energy dispersal, data are scrambled by a self-synchronizing scrambler conforming to CCITT Rec. V.35. The scrambler consists of a 20-stage feedback shift register in which the parity of the third and twentieth stages are added (modulo 2) to data which are then fed into the first stage of the scrambler register. IDR employs differential encoding for phase ambiguity resolution, and uses forward error correction (FEC) consisting of a punctured convolutional code of rate 3/4, constraint length 7. Whenever a bit error occurs in the transmission link, the concatenation of the inverse of these three operations in the IDR receiver creates a burst of errors in the recovered signal. The concatenation creates a memory window of 22 bits, which must be flushed before an error event can be considered terminated. It is the output of the V.35 descrambler that is presented to the DCME.

Additional information that characterizes burst errors is required prior to considering the performance of DCME in the burst error environment. There are three principal characteristics of interest:

- The distribution of the duration of error events.
- Given that an error event has occurred, the distribution of errors within the error event.
- The distribution of the error-free intervals.

All of these distributions are functions of the carrier signal-to-noise ratio.

A typical distribution of the duration of error events is shown in Figure 10 [15],[16]. This distribution is important in assessing the effectiveness of the interleaving used in the DCME to protect the vital control channel. A typical

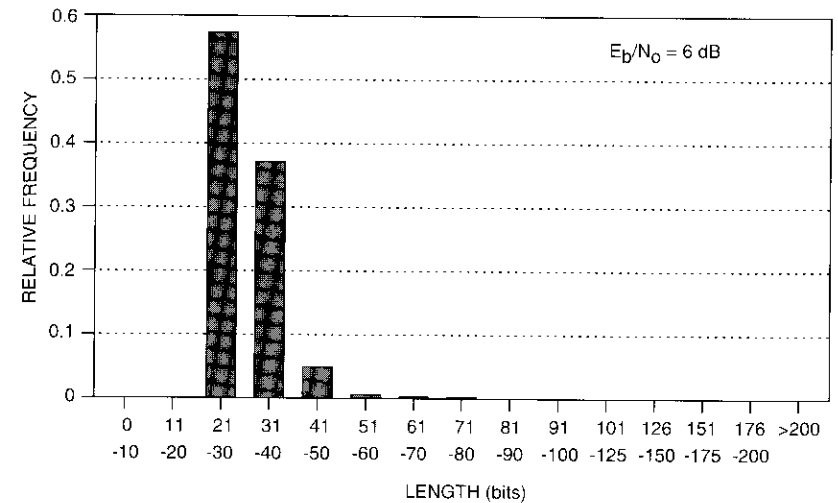


Figure 10. Relative Frequency of Length of Error Event (Burst)

distribution of errors within an error event is depicted in Figure 11. Figure 12 shows a typical distribution of the error-free interval. This information is necessary to assess the probability that a message in the control channel will be exposed to more than one error event.

#### Burst error vulnerability for various DCMEs

The relative performance of the INTELSAT IESS-501, the CIT ALCATEL CELTIC 3-G, and the ECI DTX-240 DCMEs in the IDR burst error environment will now be compared. These DCMEs all have fundamental limitations in their burst error performance as a consequence of their assignment message format and their unique bearer frame structures. The assignment message format and frame structure of each DCME are described below, along with the inherent sensitivity of these DCMEs to burst errors on the bearer facility.

##### INTELSAT IESS-501

The INTELSAT IESS-501 DCME uses a 2-ms bearer frame which carries one 24-bit assignment message. A rate 1/2 (24,12) Golay block code is applied to each of two 12-bit information blocks, thus generating two 24-bit coded blocks, or 48 bits. This 48-bit message is divided into 16 groups of 3 bits, which are interleaved into the bearer frame at 125- $\mu$ s intervals (Figure 13). Each 24-bit block is transmitted in 1 ms, and three bit errors can

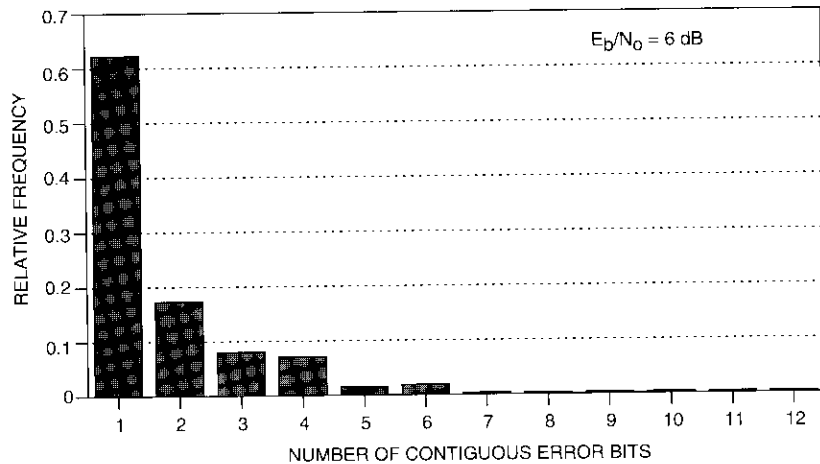


Figure 11. Relative Frequency of Contiguous Error Bits Within a Burst

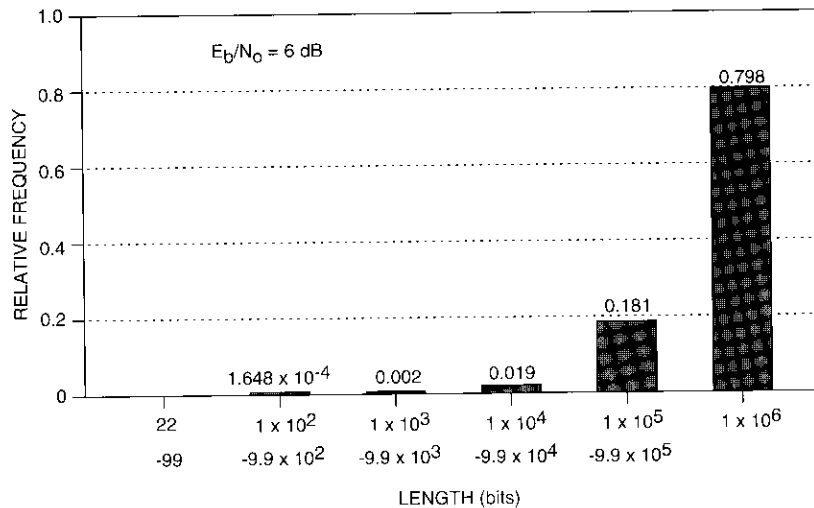


Figure 12. Relative Frequency of Length of Error-Free Interval

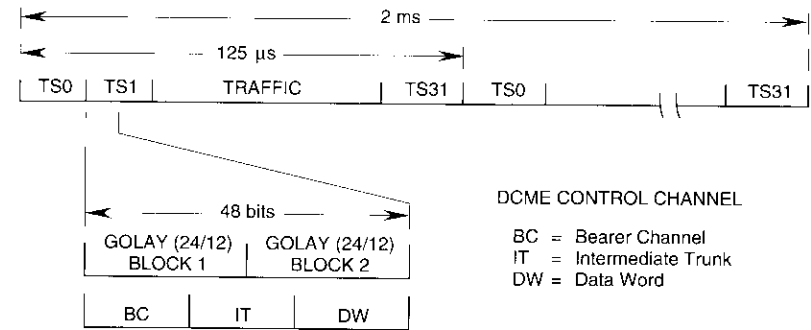


Figure 13. INTELSAT IESS-501 Frame Structure

be corrected within the block. This implies that the INTELSAT DCME bearer frame format can recover from burst errors lasting less than 256 bits on a 2.048-Mbit/s bearer, which occur at intervals of 1 ms or greater, and which affect fewer than 4 bits of the 24-bit encoded block.

ALCATEL CELTIC 3-G

The ALCATEL CELTIC 3-G DCME uses a 2-ms bearer frame which carries one 38-bit "long" assignment message or two 19-bit "short" assignment messages. A (63,39) Bose-Chaudhuri-Hocquenghem (BCH) code is applied to the 38 information bits and 1 supervision bit, thus generating a 63-bit code block. A synchronization bit is added to this block to complete the 64-bit assignment message channel. The 64-bit message is divided into 16 groups of 4 bits, which are interleaved into the bearer frame at 125-μs intervals (Figure 14). The complete 64-bit block is transmitted in 2 ms, and four bit errors can be corrected within the block. This implies that the ALCATEL DCME bearer frame format can recover from burst errors lasting less than 256 bits on a 2.048-Mbit/s bearer, which occur at intervals of 2 ms or greater, and which affect fewer than 5 bits of the 64-bit encoded block.

ECI DTX-240

The ECI DTX-240 DCME uses a distributed control channel (DCC) for transmitting assignment message information, and a dedicated variable-bit-rate control channel (VCC) to transmit overload and refresh messages. The ECI DTX-240 system was originally designed for the randomly distributed single-bit error environment. Both of the control channels have recently been reformatted to provide better performance in a high burst error rate environment.

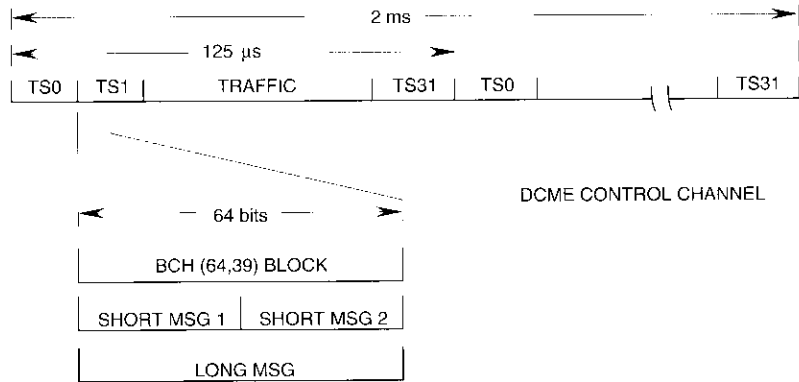


Figure 14. ALCATEL CELTIC-3G Frame Structure

The DCC (Figure 15) is carried as a header message at the beginning of each speech burst. The message consists of a unique-word field and an information field. The DCC message is 72 bits long and is transmitted using 3 bits in every 125- $\mu$ s PCM frame, thus 24 frames (or 3 ms) are needed to transmit the entire header message. The unique word uses 49 bits of the 72-bit message to carry a unique Barker code for synchronization, which has an error threshold of 2 in the present frame format. The header information field is 23 bits long and consists of 16 information bits and a 6-bit Hamming code, which can correct one bit error in the code block. This implies that the original DCC frame format (Figure 15a) can recover from bursts of errors lasting less than 256 bits on a 2.048-Mbit/s bearer, which occur at intervals of 3 ms or greater, and which affect fewer than 3 bits of the unique word or fewer than 2 bits of the coded information field. As indicated in Figure 11, three or more consecutive bit errors can occur within an error event. When such an event hits the unique word, it will not be recognized and the entire speech spurt of typically 400 to 700 ms will be lost. In addition, the header field is susceptible to either two out of three bits in error or two consecutive bits in error. This will also cause loss of the speech spurt.

The new interleaved DCC frame format (Figure 15b) can recover from bursts of errors lasting less than 256 bits on a 2.048-Mbit/s bearer and occurring at intervals of 3 ms or greater. Frame 24 of the DCC message is unique in that it carries three Barker code bits, and for that frame the error threshold is raised to 3 bits in order to maintain the same level of burst error tolerance in the unique word as in frames 1 through 23.

FRAME NUMBER	1	2	3	4	5	6	7	8	9	10	11	12	13	14	15	16	17	18	19	20	21	22	23	24
BIT 1	B	B	B	B	B	B	B	B	B	B	B	B	B	B	B	B	B	B	M	M	M	M	E	E
BIT 2	B	B	B	B	B	B	B	B	B	B	B	B	B	B	B	B	B	B	M	M	M	M	E	E
NR 3	B	B	B	B	B	B	B	B	B	B	B	B	B	B	B	B	B	B	M	M	M	M	E	S

(a) Present Format: Non-Interleaved

FRAME NUMBER	1	2	3	4	5	6	7	8	9	10	11	12	13	14	15	16	17	18	19	20	21	22	23	24
BIT 1	B	B	B	B	B	B	B	B	B	B	B	B	B	B	B	B	B	B	B	B	B	B	B	B
BIT 2	M	M	M	M	M	M	M	M	M	M	M	M	M	M	M	M	M	E	E	E	E	E	S	B
NR 3	B	B	B	B	B	B	B	B	B	B	B	B	B	B	B	B	B	B	B	B	B	B	B	B

(b) New Format: Interleaved

B = Barker Code  
S = Spare  
M = Message Data  
E = Error Correction

Figure 15. ECI DTX-240 Distributed Control Channel Message Format

The dedicated VCC (Figure 16) is 32 bits long and includes a 9-bit Barker code for frame synchronization and 16 information bits which are protected by a 6-bit parity word. The VCC is transmitted in bits 7 and 8 of TS 0 in alternating 125- $\mu$ s frames (that do not carry synchronization information), and thus requires 4 ms to transmit one message. The same Hamming code used for the DCC is used for the dedicated VCC. This implies that the present VCC frame format (Figure 16a) can recover from burst errors lasting less than 512 bits on a 2.048-Mbit/s bearer, which occur at intervals of 4 ms or greater, and which affect less than 2 bits of the 23-bit encoded block. Again, this channel is vulnerable to the occurrence of two consecutive bit errors. If the DCME is operating in the overload mode when one of these messages is corrupted by a burst error event, the consequences can be severe. This is because the information that may be affected carries the rapid rotation control, and its loss can affect all voice channels until recovery occurs.

The new interleaved VCC frame format (Figure 16b) consists of two independent encoded blocks, with one carried in bit 7 and one in bit 8 of TS 0 in alternating frames. The 12-bit encoded blocks include eight information bits and four error correction bits. The first encoded block consists of message bits  $M_0$  to  $M_6$  plus  $M_{15}$  and four error correction bits, which can correct one error in the encoded block. The second encoded block consists of message bits  $M_8$  to  $M_{14}$  plus one Barker code bit, and also can correct one error in the encoded block. The new interleaved frame format can recover from bursts of errors

FRAME NUMBER	1	3	5	7	9	11	13	15	17	19	21	23	25	27	29	31
TS0 BIT 7	B	B	B	B	B	M14	M12	M10	M8	M6	M4	M2	M0	E	E	E
TS0 BIT 8	B	B	B	B	M15	M13	M11	M9	M7	M5	M3	M1	E	E	E	S

(a) Present Format: Non-Interleaved

FRAME NUMBER	1	3	5	7	9	11	13	15	17	19	21	23	25	27	29	31
TS0 BIT 7	B	B	B	B	B	M14	M13	M12	M11	M10	M9	M8	E	E	E	E
TS0 BIT 8	B	B	B	B	M15	M6	M5	M4	M3	M2	M1	M0	E	E	E	E

B = Barker Code      M = Message Data  
S = Spare              E = Error Correction

(b) New Format: Interleaved

Figure 16. ECI DTX-240 VBR Control Channel Message Format

lasting less than 512 bits on a 2.048-Mbit/s bearer, which occur at intervals of 4 ms or greater.

The new interleaving in the ECI DTX-240 system now protects it against single burst error events to basically the same extent as the protection provided in the IESS-501 and CELTIC 3-G systems. The principal difference lies in the minimum error-free interval which can be tolerated by each system. For the IESS-501 system, loss of control channel information may occur for error events that are equal to or less than 1.0 ms apart (2,048 bits for a Conference of European Postal and Telecommunications Administrations [CEPT] carrier). For CELTIC 3-G, the control information loss may occur for error events that are separated by 2.0 ms or less. In the case of the ECI DTX-240, the DCC vulnerability begins at 3.0 ms, while the VCC threshold is equal to or less than 4.0 ms. It should be noted that two error events can occur within the specified times without any loss of control channel information. This can happen if the error event does not impact a nibble carrying control information, or if the total number of bit errors does not exceed the correcting power of the FEC codes. For example, two error events, each affecting 2 bits of the control message, are still correctable by the 4-bit error correcting code used in the CELTIC 3-G system. To put this in perspective, calculations predicting the performance for an IDR link BER of  $10^{-5}$  show that for the IESS-501 DCME one control message may be lost every 173 days, and for the CELTIC-3G one control message may be lost every 3.5 days. A similar estimate is under way for the ECI DTX-240.

Comparisons among DCMEs may be based on a variety of measures, which could include activity detector performance, voiceband data transmission error performance, control channel message loading, tandem DCME performance (voiceband data), bearer capacity efficiency during overload, and provisions for multidestination or multiclique operating modes. No single DCME will be rated best in all categories; however, the IESS-501 DCME would be highly rated for a majority of the measures.

### Future enhancements

A major milestone was reached with the approval of Revised Rec. G.763 by the CCITT under the accelerated approval procedures of Resolution 2 in December 1990. Future enhancements are expected to occur in DCME in the areas of facsimile compression, additional voiceband data compression, tandem DCME performance, and 16-kbit/s DCME.

The rapid growth of facsimile traffic surprised most users of DCME. Facsimile transmission is carried via DCME on a 40-kbit/s bearer channel. The

signal activity is 100 percent, compared to around 33 percent for speech. Thus, one facsimile call displaces four speech calls in the DCME bearer link. In a system consisting of five CEPT primary multiplex carriers applied to one DCME with a CEPT bearer, the total DCME bearer capacity would be utilized by 50 facsimile calls representing only 33 percent of the input channels. To combat this loading effect and retain circuit multiplication gain, a method known as facsimile compression or "demod/remod" is being developed. In this approach, the DCME is required to recognize that a particular circuit is carrying facsimile traffic and to route that call to a processor where the facsimile signal is demodulated and the digital bit stream applied to the facsimile transmit modem is recovered. The demodulated data are then time-division multiplexed onto a 32-kbit/s bearer and sent through the DCME, and the facsimile signal is regenerated at the remote DCME receive unit. This process is complicated by the fact that the facsimile signal must be demodulated in real time, the temporal relationships between the sequence of transmitted signals must be maintained, and the facsimile machines must believe they are still communicating with each other. In addition, the system must accommodate proprietary facsimile, as allowed by CCITT Rec. T.30.

The facsimile compression issue has been under study by INTELSAT, proprietary DCME manufacturers, and CCITT. In May 1992, a new CCITT Recommendation, G.766, "Facsimile Demodulation/Remodulation for DCME," was submitted for accelerated approval and was subsequently approved in October 1992. In November 1992, a working party of CCITT Study Group XV approved a revision to CCITT Rec. G.763 (1991) to harmonize it with new Rec. G.766. This revision must still be submitted to the next CCITT Study Group VX meeting in September 1993 for formal adoption. The results of the work of the Study Group XV working party were subsequently submitted to the INTELSAT Board of Governors Technical Committee at their meeting in November 1992, who concurred with the recommendation that the Board approve the document as INTELSAT Specification IESS-501 (Rev. 3). The INTELSAT Board of Governors approval is anticipated in December 1992.

A second major issue is a consequence of the success of DCME. Initially, DCME was envisaged to be applied only on expensive long-distance communications routes, with the (implied) expectation that only one DCME would occur in any given connection. The rapid growth of DCME, and its cost-effectiveness, have led to the increased probability of encountering tandem DCMEs. This has raised concerns about quality, since a number of degradation mechanisms may occur in a tandem DCME connection, including accumulated front-end clipping resulting from tandem speech detector activation, loss of the synchro-

nous tandem property of the ADPCM algorithm due to nonsynchronized speech detection, interactive D.L.C between the two DCMEs, and the accumulated quantization distortion that may occur if both systems are in the overload mode using 24-kbit/s (or optionally 16-kbit/s) encoding. Tandem DCME performance is under study in CCITT Study Group XV.

The CCITT is also working on standardizing an algorithm for use in special-purpose applications with an encoding rate of 16 kbit/s. One such application is DCME. It should be noted that the facsimile solution for 32-kbit/s DCME will be equally applicable, and of greater importance, to 16-kbit/s DCME. Voiceband data carried on a 40-kbit/s channel in a 16-kbit/s DCME will displace twice as many voice channels as in a 32-kbit/s DCME.

Other study groups within the CCITT are working on higher-speed voiceband data modems and faster facsimile transmission. These groups are examining how higher-bit-rate voiceband data modem signals will pass through DCME, and whether demodulation/remodulation will be applied to them, as well as to current facsimile signals. These concerns are encouraging increased cooperation among the various study groups, which it is hoped will lead to a standardized solution.

### **Conclusions**

DCME is a critical technology which has permitted satellite communications to remain competitive with other media through the INTELSAT V era and into the INTELSAT VI era. The leadership provided by COMSAT and INTELSAT has led to development of an international DCME standard that is being applied within INTELSAT VI systems. DCME built according to this standard not only provides a multideestination capability, but also has been shown to be more robust to bit errors than other proprietary DCMEs. Future challenges to be addressed include facsimile compression, other types of voiceband data compression, tandem performance, and 16-kbit/s DCME. The application of DCME will continue to be an important element in providing cost-effective communications and improving the efficiency of spectrum utilization by accommodating more simultaneous communications connections within a given limited-spectrum resource in the INTELSAT VI system.

### **Acknowledgments**

*The IESS-501 specification, and CCITT Recommendation G.763 which followed, resulted from the cooperative efforts of individuals from signatory/user administrations, manufacturers, and EUTELSAT, as well as COMSAT and INTELSAT. The authors wish to acknowledge the valued contributions of*

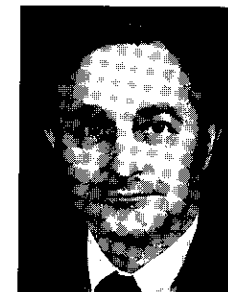
numerous colleagues without which the achievement of an internationally recognized standard would not have been possible. In particular, S. J. Campanella is acknowledged for his contribution to the history of the development of DCME presented in this paper, and for his early and continued contributions to the evolution of DCME technology.

## References

- [1] S. J. Campanella and J. A. Sciulli, "Speech Predictive Encoded Communications," 2nd International Conference on Digital Satellite Communications (ICDSC2), Paris, November 1972, *Proc.*, pp. 342-347.
- [2] I. Poretti, G. Monty, and A. Bagnoli, "Speech Interpolation Systems and Their Applications in TDM/TDMA Systems," 2nd International Conference on Digital Satellite Communications (ICDSC2), Paris, November 1972, *Proc.*, pp. 348-357.
- [3] S. J. Campanella, "Digital Speech Interpolation," *COMSAT Technical Review*, Vol. 6, No. 1, Spring 1976, pp. 127-158.
- [4] S. J. Campanella *et al.*, "The INTELSAT TDMA Field Trial," *COMSAT Technical Review*, Vol. 9, No. 2A, Fall 1979, pp. 293-340.
- [5] J. H. Rieser and M. Onufry, "Terrestrial Interface Architecture DSI/DNI," *COMSAT Technical Review*, Vol. 15, No. 2B, Fall 1985, pp. 483-509.
- [6] M. Onufry and S. J. Engelman, "Subjective Evaluation of the INTELSAT TDMA/DSI System," *COMSAT Technical Review*, Vol. 16, No. 1, Spring 1986, pp. 239-251.
- [7] S. Dimolitsas *et al.*, "Evaluation of ADPCM Coders for Digital Circuit Multiplication Equipment," *COMSAT Technical Review*, Vol. 17, No. 2, Fall 1987, pp. 323-345.
- [8] M. Onufry, "The New Challenge of DCME," *ITU Telecommunication Journal*, Special Issue on Speech Processing, Vol. 55, No. 12, December 1988, pp. 831-837.
- [9] INTELSAT Earth Station Standards, Document IESS-501, "Digital Circuit Multiplication Equipment Specification 32 kbit/s ADPCM with DSI Revision 2," March 14, 1989.
- [10] S. J. Campanella and J. H. Rieser, "Operating Aspects of New LRE/DSI DCME," 8th International Conference on Digital Satellite Communications (ICDSC8), Guadeloupe, FWI, April 1989, *Proc.*, pp. 803-811.
- [11] G. Forcina *et al.*, "INTELSAT Digital Circuit Multiplication Equipment," 8th International Conference on Digital Satellite Communications (ICDSC8), Guadeloupe, FWI, April 1989, *Proc.*, pp. 795-802.
- [12] G. Forcina and D. Kennedy, "32-kbit/s DSI System for INTELSAT," 7th International Conference on Digital Satellite Communications (ICDSC7), Munich, May 1986, *Proc.*, pp. 89-95.

- [13] P. K. Feher, ed., *Advanced Digital Communications Systems and Signal Processing Techniques*, New Jersey: Prentice-Hall, ISBN 0-13-011198-8 025, 1987, pp. 237-279.
- [14] CCITT, Rec. Z.100, IXth Plenary Assembly, Melbourne, November 1988, Vol. X, Fascicles X.1, X.2, X.3, X.4, and X.5.
- [15] F. Hemmati, COMSAT Laboratories Technical Note, CTD-89/022, "Burst Error Statistics of the INTELSAT IDR System," February 27, 1989.
- [16] T. Duong, COMSAT Laboratories Technical Note, CTD-90-005, "Burst Error Statistics of an INTELSAT IDR Type Carrier Occurring in a Thermal Noise Limited Linear Channel," January 11, 1990. COMSAT Data Catalog No. 90DC004.

Michael Onufry received a B.S. degree from Pennsylvania State University in 1962, and performed graduate work at both Northeastern University and George Washington University. He is currently Associate Director of the Communications Technology Division at COMSAT Laboratories. His experience includes echo canceller development, 64-kbit/s PCM and 32-kbit/s ADPCM, digital speech interpolation development, and encoding of speech. He has been active in planning and implementing international field trials in the INTELSAT network, and is responsible for subjectively assessing various speech processing devices. Since 1977, Mr. Onufry has been the COMSAT Representative to CCITT Study Group XV, where he has been a Special Rapporteur for questions concerning echo cancellers, syllabic companders, and digital circuit multiplication equipment. He is a member of IEEE, and past president of the Maryland Chapter of the ASSP.

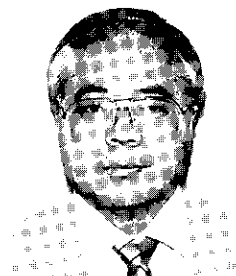




*GianPiero Forcina graduated in electrical engineering from the University of Rome, Italy, in 1965, and performed postgraduate work at the George Washington University, Washington, D.C. Since 1968, he has been involved in the design of satellite systems both in Italy, at Telespazio, and in the United States, at COMSAT Laboratories, Fairchild Space and Electronics Company, and COMSAT General, where he was Manager of Systems Development. In 1978 he joined INTELSAT, Washington, D.C., where he has been largely concerned with the development of the INTELSAT TDMA system.*

*W. Sian Oei received the Ingenieur Degree in electrical engineering from the Delft University of Technology, the Netherlands, in 1974. He joined INTELSAT, Washington, D.C., in February 1982, and is currently a Supervising Engineer in the Communications Engineering Section. He has had a number of responsibilities related to implementation of the INTELSAT TDMA system, such as TDMA reference and monitoring station (TRMS) technical evaluation, and the development of specialized test equipment and SSOG procedures. He also was active in developing specifications for digital circuit multiplication equipment (DCME).*

*Mr. Oei is currently involved in studies on the introduction of efficient ISDN-compatible networks and the new synchronous digital hierarchy (SDH) transmission technology in the INTELSAT system. He has represented INTELSAT in a number of CCITT Study Groups dealing with digital networks, ISDN, data communications, network switching and signaling, and digital transmission systems and equipment. In addition, he was active in the CCIR/CCITT 1990-92 Joint Ad Hoc Group on ISDN/satellite matters, which studied ISDN compatibility issues and other CCITT recommendations dealing with satellite network connection delay.*



*Tokuo Oishi received an M.Sc. in electronics engineering from Niigata University, Japan, in 1972; and a Ph.D. in electrophysics from George Washington University in 1988. He worked for Hamamatsu Corporation in Japan, Georgetown University, Online Computer Systems, and COMSAT World Systems. He joined INTELSAT in 1985, and has been involved in DCME, low-rate TDMA, and data communications protocol studies. He is currently Senior Engineer in the Communications System Engineering Section. Dr. Oishi also represents INTELSAT in CCITT Study Group VII and ISO SC 21. He is a Member of IEEE.*



*John F. Phiel, Jr. received B.S.E.E. and M.S.E.E. degrees from Drexel University in 1963 and 1965, respectively. From 1965 to 1967 he was with the U.S. Army SATCOM Agency, where he worked on the Initial Defense Communications Satellite Program. He joined COMSAT in 1967, where he was involved with transmission system engineering and earth station implementation. As a Senior Communications Engineer in the Space and Information System Office of COMSAT General Corporation, he was engaged in studies of new business activities and COMSTAR communications performance analysis.*

*In 1978, Mr. Phiel joined INTELSAT, where his activities have focused on the design and implementation of the 120-Mbit/s TDMA system and the development of the IESS-501 DCME specification. He is currently Department Manager of Communications Engineering at INTELSAT.*

*Jack H. Rieser received a B.S.E.E. from the University of Cincinnati in 1975 and an M.S.E.E. from the Johns Hopkins University in 1982. He is currently a Senior Scientist in the Voice Band Processing Department of the Communications Technology Division at COMSAT Laboratories. He was the Project Engineer responsible for the design and development of the INTELSAT BG-42-65 DSI terminal for use in the INTELSAT TDMA network, and the 32-kbit/s ADPCM/DSI system delivered to INTELSAT under contract INTEL-359. He served as lead engineer in the hardware and software development of a facsimile interface unit (FIU) for use in the Inmarsat network, and was chairman of a group which developed a DCME standard in the U.S. T1Y1 Standards Committee.*

*Since joining COMSAT in 1975, Mr. Rieser has had design and development responsibility for various DSI systems and voice switching pertaining to PCM and delta modulation. He has also performed several studies in data and facsimile transmission via delta modulation at 32 kbit/s, and was the senior member of the team responsible for developing the first commercial COMSAT echo canceller. He is a member of Eta Kappa Nu and a Senior Member of the IEEE. He is also the recipient of the ANSI T1 Outstanding Achievement Award for his work in DCME standardization, and the COMSAT Laboratories 1986 Research and Development Award for his pioneering work in DCME.*

## ***Video transmission and processing in the INTELSAT VI era***

L-N. LEE AND A. K. SINHA

(Manuscript received October 18, 1990)

### ***Abstract***

The performance of conventional and high-definition television (HDTV) transmission within the INTELSAT system during the INTELSAT VI era, using several video signal processing techniques, is examined. In addition, standard analog television transmission techniques within the INTELSAT system, including conventional full-transponder TV and half-transponder TV, are briefly reviewed. Efficient means of sending high-quality analog and digital television signals via satellites such as INTELSAT VI are discussed, including time-multiplexed television with its accompanying digital audio channels, conventional digital TV, compressed digital TV, and low-bit-rate teleconferencing TV. Potential techniques for distributing HDTV signals via INTELSAT VI are also presented.

### ***Introduction***

The volume of television transmission via the INTELSAT system has grown rapidly throughout the last decade. Video signal processing technology has progressed at a similar pace, as the global village becomes increasingly linked by international television. With the rapid advancement of digital video processing and satellite transmission technology, transmission techniques that can significantly enhance space segment efficiency have become practical to implement. TV services, particularly over leased transponders, enjoy the highest growth rate of all of INTELSAT's service offerings. This rapidly increasing demand competes for limited space segment resources. Thus, techniques

that provide high quality while making efficient use of the satellite are of ultimate importance as communications move into the INTELSAT VI era, and beyond.

As a consequence of major advances in solid-state integrated circuit technology in the last decade, the components required for digital video signal processing—such as high-speed analog-to-digital and digital-to-analog converters, high-speed memory and logic circuits, and digital filtering processors—are now available at reasonable cost. Thus it has become possible to apply digital signal processing to improve the efficiency of analog television transmission via INTELSAT. One example of a highly efficient transmission technique is time-multiplexed television (TMTV) [1],[2].

With efficient coding and modulation techniques that can be applied to reduce both the space and earth segment resources required to send digital signals, the prospect of using less transponder bandwidth and smaller earth stations constitutes a powerful economic incentive for digital TV. The important role digital TV is likely to play in the future development of telecommunications services is also evident in the continuing evolution of the integrated services digital network (ISDN), and particularly in the current emphasis on broadband ISDN (BISDN). High-definition television (HDTV), which promises far better picture quality than conventional television and offers the potential for many new services, is also expected to make the transition from experimental transmission to commercial service via the INTELSAT system in the 1991 to 1995 period.

This paper examines the impact of these new technologies in terms of improved efficiency and quality, as illustrated by examples using INTELSAT VI satellites. Following a brief review of the analog television transmission techniques currently used in the INTELSAT system, an efficient means of sending high-quality analog TV signals using time multiplexing is examined. Compressed conventional digital television, and potential techniques for distributing HDTV signals via INTELSAT, are also discussed.

### **Conventional analog TV/FM in the INTELSAT system**

Television signals have been transmitted in analog form with frequency modulation (FM) within the INTELSAT system for decades. This is typically done in two formats: full-transponder TV (FTTV) and half-transponder TV (HTTV) [3].

In general, a "studio-quality" signal is required for contributing raw program materials for electronic editing and special-effects composition. It has a weighted signal-to-noise ratio,  $S/N_w$ , of 56 dB or better, with full resolution

and virtually no distortion. A "broadcast-quality" signal, which is required for distribution prior to final broadcast to the viewer, has an  $S/N_w$  of 50 dB or better, with full resolution and minimum distortion (based on a set of quality measurements such as those specified by the Electronics Industry Association [EIA]). Prior to 1987, HTTV was also employed in 36-MHz global-beam occasional-use transponders.

FTTV typically occupies 30 MHz of bandwidth, providing a studio-quality signal for contribution-type services in both occasional-use and leased transponders, whereas HTTV typically uses 20 MHz in 41-MHz occasional-use TV transponders and may be suitable for distribution and broadcast-type services. Well-defined standards have been established within the INTELSAT community for the operation of FTTV and HTTV.

FTTV is generally used to achieve studio-quality transmission, while HTTV provides a less costly alternative for broadcast- or near-broadcast-quality transmission. FTTV is also used to provide sufficient link margin for small-station reception in domestic and international leases, where the quality can be much lower than established INTELSAT standards. The FTTV signal is typically operated at transponder saturation. Its deviation is set by Carson's rule so that no distortion caused by spectral truncation is generated, except in some cases where filter bandwidths less than 30 MHz are used to improve the received carrier-to-noise ratio,  $C/N$ .

HTTV is operated at 1.5- to 2.0-dB total output backoff to minimize crosstalk between the two TV carriers, or their sound program channels, carried by a single transponder with its attendant nonlinearity and AM-PM transfer characteristics. Its deviation is much greater than that allowed under Carson's rule, in order to maximize the  $S/N$  at the receive side. Recently, INTELSAT has also initiated leased-bandwidth services based on a mix of two 17.5-MHz TV carriers and one 20-MHz TV carrier in a 72-MHz hemi/beam transponder (3 TV/72 MHz). This is accomplished by carefully spacing the TV carriers and operating the transponder with sufficient backoff to minimize crosstalk and intermodulation products. Operation of both HTTV and 3 TV/72 MHz uses frequency-division multiple access (FDMA) so that different TV signals can be independently transmitted from separate up-link locations.

FTTV, HTTV, and 3 TV/72 MHz are expected to continue to be the most commonly used modes for TV transmission in the beginning of the INTELSAT VI era. They will enjoy the increase (of at least 2 dB) in effective isotropically radiated power (e.i.r.p.) provided by the INTELSAT VI spacecraft in some transponders (which generally can be translated into higher  $S/N_w$  and thus better quality, or the use of smaller earth stations). Consequently, increased use of HTTV is anticipated, particularly within the higher-power hemi,

zone, and Ku-band beams. Transmission parameters for the FTTV and HTTV modes are specified in *INTELSAT Earth Station Standards* Document IESS-306 [3] for open-network operation in global-beam C-band transponders. Recommendations for the 3 TV/72-MHz mode for Ku-band transponders have been introduced more recently. Table 1 shows the National Television System Committee (NTSC) 525/60 transmission parameters and the  $S/N_w$  that can be expected using these transmission techniques between original Standard A ( $G/T = 40.7$  dB/K) earth stations with  $10^\circ$  elevation angle. In the table,  $f_m$  is the maximum baseband frequency,  $\Delta f_p$  is the peak deviation, and  $Q$  is the combined weighting and emphasis gain. The International Radio Consultative Committee (CCIR) pre/deemphasis network with a  $Q$  value of 12.8 dB is assumed.

TABLE 1. TRANSMISSION PARAMETERS AND EXPECTED  $S/N_w$  FOR NTSC TV SIGNALS USING CONVENTIONAL FM TRANSMISSION

NO. OF TV CARRIERS/TRANSPONDER	RF BANDWIDTH (MHz)	C/N (dB)	$f_m$ (MHz)	$\Delta f_p$ (MHz)	$Q$ (dB)	$S/N_w$ (dB)
1 (FTTV)*	30.0	22.2	4.2	10.75	12.8	59.5
2 (HTTV)*	17.5 or 20	20.1 or 19.5	4.2	7.5 or 9.4	12.8	51.9 or 53.8
3 TV/72 MHz	17.5 or 20.0	12.0**	1.2	7.5 or 9.4	12.8	43.6 or 45.6**

\* Original Standard A earth station  $G/T = 40.7$  dB/K; INTELSAT VI global beam e.i.r.p. = 26.5 dBW

\*\*Minimum acceptable performance. May be higher with actual INTELSAT VI Ku-band transponder.

### Time-multiplexed analog television

As an alternative to the FTTV, HTTV, and 3 TV/72-MHz modes, the TMTV technique [1],[2] allows transmission of three near-broadcast-quality television signals, or two studio-quality television signals, in a single 36-MHz transponder. This is accomplished by removing information corresponding to diagonal resolution in the television signal (since human vision is relatively less sensitive to diagonal resolution than to horizontal and vertical resolution) and time-multiplexing each television signal in the component form. The bandwidth-reduction technique allows the high-frequency luminance informa-

tion and the chrominance-difference signals to be transmitted every other line within the same field. Thus, in a two-line period, four component signals are transmitted: a full-bandwidth luminance signal,  $Y$ ; a half-bandwidth luminance signal,  $Y_L$ ; and the two chrominance components,  $U$  and  $V$ . Time-multiplexing is accomplished by sampling each component at a rate appropriate for its bandwidth, writing the sampled data to separate buffer storage, and reading out the stored data at a higher speed at the appropriate time. Two or three television signals, each consisting of the four components, are then multiplexed in the two-line period, as shown in Figure 1. Since no temporal processing is involved, this technique generates no motion artifact. Using single-carrier-per-transponder time multiplexing, it is possible to operate the transponder at full saturation. By removing visually less-perceptible diagonal resolution information, the total transmitted baseband bandwidth is reduced, allowing more FM deviation for a given transponder bandwidth.

With component transmission, there is no color subcarrier or sound program channel(s) at the high end of the baseband. Thus, about 4-dB overdeviation is permitted. The transmission characteristics of the TMTV signal are outlined in Table 2. The  $S/N_w$  achieved by using this technique is comparable to FTTV for two TMTV signals per carrier, and to HTTV for three TMTV signals per carrier. The lower  $S/N_w$  of the three-per-carrier version is attributable to the greater baseband bandwidth of the time-multiplexed signal, which requires the use of a smaller deviation in the transponder and a wider post-detection filter in the receiver.

When a TMTV signal is transmitted in a 36- or 41-MHz transponder, the problem of intelligible crosstalk between adjacent channels within the same transponder (common to conventional HTTV in a frequency multiplexing scheme) does not exist in a time-multiplexing scheme. Similarly, NTSC artifacts such as cross-luminance and cross-chrominance are avoided. TMTV also uses a deemphasis network with an impulse response much shorter than that of the CCIR deemphasis commonly used for composite signals. Consequently, the impulse noise is also subjectively much less annoying than that encountered in conventional FTTV or HTTV when operating below the FM threshold. Thus, the NTSC signal reconstructed by the TMTV processor generally provides somewhat better subjective quality than conventional HTTV.

In TMTV, the synchronization signals are transmitted digitally using two-level amplitude shift keying. Because these two digital signal levels are within the standard peak-to-peak range for active video (e.g., 0.7 V into 75  $\Omega$ ), the combined TMTV signal has the same peak-to-peak range. Because this is about 70 percent of the peak-to-peak voltage range for the composite NTSC signal with standard analog sync-tip, a sync-removal gain of about 3 dB is achieved.

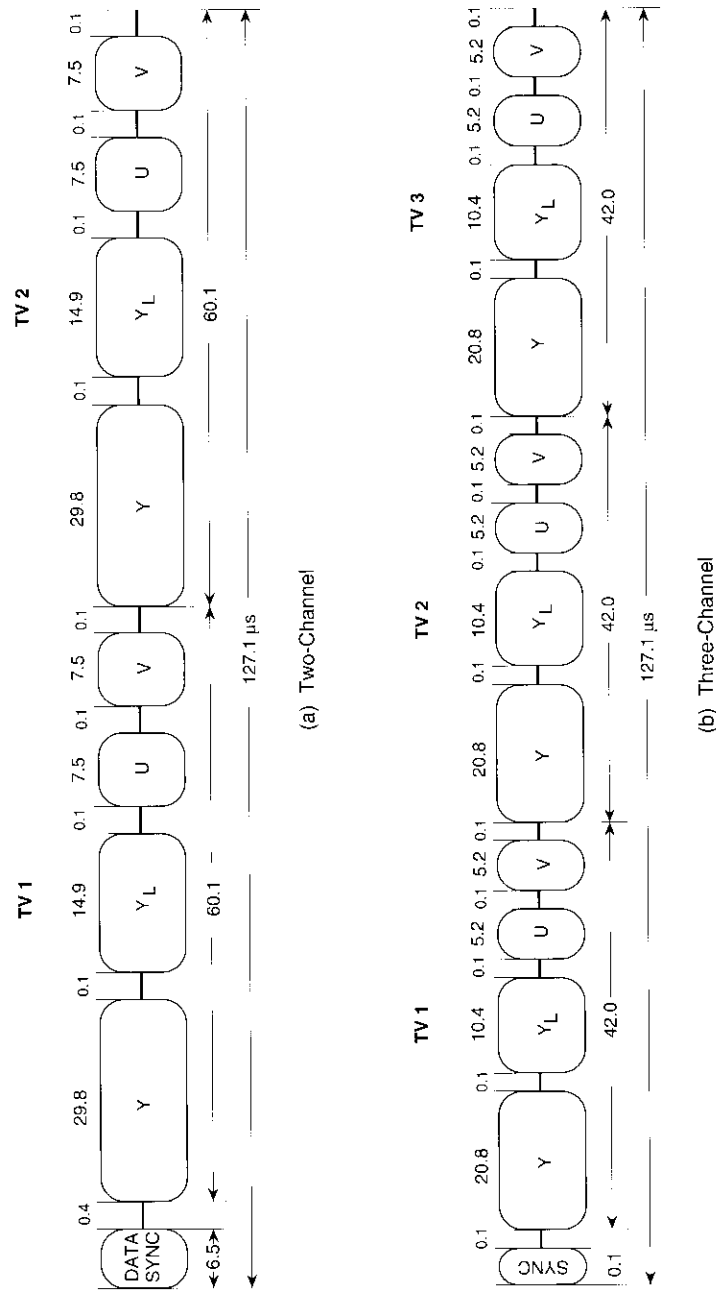


Figure 1. Time-Domain Signal Format for TMTV Transmission

TABLE 2. TRANSMISSION CHARACTERISTICS OF TMTV<sup>a</sup>

NO. OF TV SIGNALS/ CARRIER	RF BANDWIDTH (MHz)	C/N (dB)	$f_m$ (MHz)	$M_p$ (MHz) <sup>b</sup>	Q (dB) <sup>c</sup>	S/N <sub>w</sub> (dB)
2	36.0	21.5	7.4	16.8	15.0	55.5
3	36.0	21.5	10.5	9.0	15.0	50.5

<sup>a</sup> Original Standard A earth station  $G/T = 40.7$  dB; INTELSAT VI global beam e.i.r.p. = 26.5 dBW.

<sup>b</sup> Corresponding to 4 dB over Carson's rule.

<sup>c</sup> Includes 10-dB noise weighting gain, 2-dB emphasis gain, and 3-dB gain due to synchronization removal.

Extremely reliable synchronization can be maintained in very noisy channels, even for  $C/N < 0$  dB.

The sound program signal is encoded digitally. Digital audio data are transmitted in the horizontal blanking interval in the case of two television signals per 36-MHz transponder, or in the vertical blanking interval in the case of three television signals per 36-MHz transponder (for which horizontal blanking intervals are too small). Thus, no additional satellite capacity is needed to transmit sound program channels. TMTV is designed to accommodate at least one stereo pair of high-fidelity sound program channels for each video channel, with some additional digital channel capacity for ancillary data transmission.

With the higher e.i.r.p. available in the 72-MHz transponders on INTELSAT VI, it is possible to send two TMTV/FDMA carriers in a 72-MHz transponder with the transponder backed off by about 1.5 to 2.0 dB, thus allowing the transmission of four to six TMTV signals in a single 72-MHz transponder at broadcast or near-broadcast quality. Therefore, the TMTV technique provides a significant improvement in transmission efficiency for analog television transmission via satellite. In November 1990, this configuration was used in a successful demonstration of TMTV transmission, simulating six television signals per 72-MHz transponder between Goonhilly, U.K., and Staten Island, N.Y., U.S.A., using an INTELSAT VI satellite in the Atlantic Ocean Region (AOR) [4]. (A 30-MHz FTTV signal was used to emulate the second TMTV carrier in the same 72-MHz transponder.)

In practice, TMTV is implemented by means of a digital video processor which can be added to the existing FM link. Because this is an evolutionary change from existing FTTV or HTTV modes, transition from conventional transmission is not difficult. All existing earth station equipment (with the possible

exception of IF filters) can still be used; the TMTV processor is added before the FM modulator and after the FM demodulator. The initial version of the TMTV processor requires that all TV signals be routed through a single up-link. With additional buffers and controllers, television signals can be transmitted directly from more than one up-link station in a time-division multiple access (TDMA) mode.

### **Conventional digital television**

Due to the rapid advancement of digital integrated circuit technology and signal processing techniques, the quality of digital television has improved significantly in the last decade. A major step toward the implementation of digital TV service worldwide under an open-network concept will be the adoption of suitable standards for the compatibility of equipment and the interoperability of networks and systems. Such an international standard is currently being developed under CCIR and International Telephone and Telegraph Consultative Committee (CCITT) Joint Interim Working Party (JIWP) CMTT/2. A hybrid of two algorithms—one based on differential pulse-code modulation (DPCM) and motion compensation, and the other on discrete cosine transform (DCT)—is under test, and standards on coding algorithms for 34 and 45 Mbit/s are being finalized. Lower bit rates are also under consideration for secondary distribution service applications.

In recent years [5], 45-Mbit/s digital TV based on three-dimensional DPCM has been used regularly by U.S. broadcasters for certain programs between Washington and New York, over a fiber optic link. An eight-city field trial over fiber optic cables is currently being conducted by the regional Bell operating companies in the U.S., and eventual acceptance of 45-Mbit/s digital TV by U.S. broadcasters as an alternative to analog transmission is expected.

Combined with a rate 3/4 forward error correction (FEC) code, a 45-Mbit/s digital TV signal can be transmitted via INTELSAT's intermediate data rate (IDR), an ISDN-compatible digital service, in a 36-MHz transponder. Alternatively, two such signals can be transmitted in a 72-MHz transponder. With FEC coding, these signals require 4 to 7 dB less operating carrier-to-noise power density ratio,  $C/N_o$ , than FTTV, allowing the transmission of broadcast-quality television signals to smaller earth stations.

While the use of FEC improves satellite capacity for the power-limited case, the redundancy introduced by FEC increases the bandwidth requirement. The maximum capacity of a satellite channel can be reached by optimizing the FEC code rate selection for a given earth station type. Punctured convolutional codes with Viterbi decoding provide a powerful means for facilitating this

tradeoff between power and bandwidth. To illustrate the effectiveness of a combination of FEC and digital television coding using an INTELSAT VI satellite, the smallest earth stations that can be used for digital TV reception at 17, 34, and 45 Mbit/s were determined through a detailed link budget analysis and are summarized in Table 3 for three types of transponders with both low- and high-gain settings.

Currently, IDR service is available for transmission at bit rates up to 45 Mbit/s. Digital TV transmissions at all bit rates selected by the JIWP CCMT/2, as well as at any intermediate bit rate, could also be provided in the framework of IDR. Eventually, performance specifications at various bit rates, which are tailored to specific service applications ranging from video-teleconferencing to studio-quality contribution services, could be developed to achieve greater efficiency, flexibility, capacity, and economy. At this time, the cost of a 45-Mbit/s codec with the required quadrature phase shift keying (QPSK) modem and FEC codec to facilitate a 45-Mbit/s digital video link is significantly higher than that of a high-quality FM modem typically used for FTTV. However, this cost is rapidly decreasing as the technology for digital processing and storage advances. By the mid-1990s, it is expected that digital television will become very cost-effective, and the use of digital TV for various types of services will steadily increase.

An area of particular interest is the option of using enhanced bit-rate reduction techniques for certain service applications. With the rapid development of digital signal processing integrated circuits, sophisticated signal processing techniques such as DCT can now be implemented in a single chip. This has opened up opportunities for the digital coding of entertainment-quality\* television at data rates between 3 and 6 Mbit/s. With powerful FEC, these signals can be transmitted to small earth stations using IDR. Satellite news gathering (SNG) signals between 6 and 15 Mbit/s, allowing direct transmission of international news from a mobile up-link terminal via INTELSAT, are also likely to become popular. These reduced-bit-rate television codecs can also be incorporated into a "fly-away" terminal that can be transported to any part of the world on short notice to cover unfolding news events. (Antenna diameters smaller than 3.5 m are anticipated for such terminals.)

Substantial progress has also been made in the area of teleconferencing codecs operating at data rates between 56 kbit/s and 2.048 Mbit/s with limited motion. A  $p \times 64$ -kbit/s coding standard (where  $p$  represents an appropriate

\*Roughly defined as quality about the same as, or slightly better than, that of the present VHS videocassette recording (*i.e.*, reduced resolution and  $S/N$  of about 40 dB, with minor artifacts).

TABLE 3. SMALLEST EARTH STATIONS FOR DIGITAL TV RECEPTION FROM INTELSAT VI FOR VARIOUS TYPES OF CARRIERS AND TRANSPONDERS OPERATING AT HIGH AND LOW GAIN STEPS

NO. OF TV CHANNELS/ TRANSPONDER	CARRIER DATA RATE (Mbit/s)	FEC CODE RATE	TRANSPONDER TYPE					
			36-MHz GLOBAL		72-MHz HEMI OR ZONE		72-MHz SPOT	
			HIGH	LOW	HIGH	LOW	HIGH	LOW
1	45	1/2	-	-	F1	F1	E1	E1
1	45	3/4	F3	F3	F2	F2	E2	E2
2	45	3/4	-	-	F2	F2	E2	E2
1	34	3/4	F2	F2	F1	F1	E1	E1
2	34	3/4	-	-	F2	F2	E2	E2
1	17	1/2	F1	F1	F1	F1	E1	E1
1	17	3/4	F2	F2	F1	F1	E1	E1
2	17	3/4	F2	F2	F1	F1	E1	E1
3	17	1/2	-	-	F2	F2	E3	E3
3	17	3/4	-	-	F2	F2	-	E3
3	17	7/8	-	A <sub>n</sub>	B	F3	-	-
4	17	1/2	-	-	F2	F2	C	E3
4	17	3/4	-	-	F3	F3	-	C
4	17	7/8	-	-	A <sub>n</sub>	B	-	-
5	17	3/4	-	-	B	B	-	-
5	17	7/8	-	-	-	A <sub>n</sub>	-	-

Notes:

- The following  $G/T$  values (in dB/K) may be recalled for INTELSAT standard earth stations:
  - C-band (global/hemi/zone beams): A<sub>n</sub> (new A) = 35, B = 31.7, F3 = 29, F2 = 27, F1 = 22.7.
  - Ku-band (west and east spot beams): C = 37, E3 = 34, F2 = 29, E1 = 25.
- For a single TV channel, earth stations smaller than Standard E1 or F1 may be allowable (under Standard Z category) in some cases. For instance, an earth station with  $G/T = 22$  dB/K could receive a single 17-Mbit/s TV channel in the spot beam.
- Margins of at least 8.6 dB for the Ku-band down-links and 1.6 dB for the C-band down-links are assumed.
- Blanks indicate either power or bandwidth limitation.

integer) has been developed by the CCITT, and as a result the cost of teleconferencing codecs is expected to be reduced. This  $p \times 64$ -kbit/s digital television can be transmitted using both International Business Service (IBS) and IDR circuits, and also performs well with the INTELSAT TDMA network architecture. Furthermore, an important aspect of the emerging BISDN is its ability to provide one-way packet video and two-way video-teleconferencing to end users. Since INTELSAT TDMA, IBS, and IDR services are being used to interconnect various "ISDN islands" (regions having ISDN subnetworks), it is expected that transmission of  $p \times 64$ -kbit/s digital television signals will increase significantly throughout the INTELSAT VI era.

### HDTV transmission via the INTELSAT system

HDTV, which offers twice as much resolution in both the horizontal and vertical dimensions as conventional TV, is expected to transition from experimental transmission to revenue-bearing traffic in the INTELSAT VI era. However, HDTV signals must be considerably compressed in bandwidth before long-haul transmission becomes practical. Either analog or digital formats may be used. A format compatible with that of final distribution to the end users would be attractive, as no further conversion would be necessary.

Since a single worldwide HDTV standard is still far from a reality, it appears that as many as three different HDTV production formats may need to coexist during the INTELSAT VI era. As long as HDTV is handled on a leased-bandwidth basis, the closed-network operators will probably select the format most suitable for their audience. Thus, it is possible that cameras of all three standards may have to be used to produce the same international event for distribution to different countries, or that standards converters will be needed to convert from one format to another prior to transmission. "Live" satellite distribution of international events worldwide in HDTV form will be difficult without standards conversion. The availability of good HDTV standards converters can facilitate the use of INTELSAT for HDTV distribution.

The multiple subsampling encoding (MUSE) of the Japanese broadcasting company, NHK [6], and the high-definition multiplexed analog component (HD-MAC) [7] of western Europe's Eureka project are designed for FM transmission. Sophisticated noise-reduction signal processing techniques are used to significantly improve the  $S/N_{av}$  of the received signals. Table 4 summarizes the minimum-size INTELSAT earth stations required to receive MUSE signals using various INTELSAT VI 36-MHz C-band transponders [8]. The  $S/N_{av}$  values

TABLE 4. SMALLEST EARTH STATION FOR RECEPTION OF HDTV SIGNALS IN MUSE FORMAT USING 36-MHz BANDWIDTH WITHIN AN INTELSAT VI C-BAND TRANSPONDER.

TRANSPONDER TYPE	NO. OF HDTV SIGNALS/ TRANSPONDER	EARTH STATION	$S/N_w$ (dB)
Global 36-MHz	1	F3	52.5
Hemi/Zone 72-MHz	1	F2	55.0
Hemi/Zone 72-MHz	2	B	54.7

Notes:

1. Global and hemi/zone e.i.r.p. are 26.5 and 31 dBW, respectively.
2. Per-carrier output backoff of 5 dB is assumed for half-transponder HDTV.

in the table are obtained by numerical integration of the noise spectral density after noise reduction processing using the CCIR Rec. 451-2 noise weighting function. From the table, it appears that HDTV signals in these formats can be transmitted in an INTELSAT VI transponder using 36-MHz bandwidth, and received by appropriate standard INTELSAT earth stations with reasonable quality. If the final broadcast to the end user is in the same format, satellite transmission using these formats will be a logical choice.

With terrestrial telecommunications facilities rapidly being converted to digital transmission, an alternative to transmitting HDTV signals within the INTELSAT system in their final broadcast format is to transmit the HDTV signals digitally. While early development of digital HDTV has been concentrated at rates of 100 to 140 Mbit/s [9], a bit rate consistent with the local digital hierarchy in multiples of 34 or 45 Mbit/s may be more practical for many countries. In this range of data rates, the traffic received by the INTELSAT earth stations can easily be routed to its final destination for rebroadcast via terrestrial digital links. Direct on-premise reception using a fairly small antenna would also become possible for hemi- or zone-beam transponders, provided the coded HDTV signal has a reasonably low bit rate (45 Mbit/s, for example) [10]. Since the quality of a digitally encoded signal remains fairly constant until the bit error rate (BER) drops below a certain threshold, and since FEC can be used to maintain the BER performance above the threshold with an energy-per-bit to noise-power density ratio,  $E_b/N_o$ , as low as 5 to 6 dB, digital transmission will become increasingly attractive for HDTV.

In mid-1991, a 15-Mbit/s HDTV scheme was proposed by General Instruments as a possible candidate for terrestrial broadcast within the U.S. [11]. Other U.S. proponents also decided to change their original analog transmission formats to digital [12],[13]. While rate 3/4 FEC and 16- or 32-quadrature amplitude modulation (QAM) are used in these proposals for 6-MHz terrestrial broadcast, the same video information modulated with conventional QPSK can be transmitted via satellite using only a small fraction of an INTELSAT VI transponder. These proposals generally have an information bit rate in the range of 15 to 20 Mbit/s. For terrestrial broadcast, 16- to 32-QAM, in conjunction with FEC coding of about rate 3/4, were proposed. It is natural to expect that the same compressed information can be modulated by a QPSK modem, encoded with an appropriate FEC code, and transmitted through a small fraction of an INTELSAT VI transponder, based on the parameters given in Table 3.

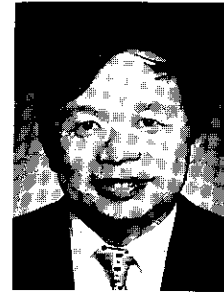
The U.S. Federal Communications Commission (FCC) is to make a final selection for the U.S. Advanced Television (ATV) format in the spring of 1993. Cost-effective receiver and digital ATV decoder hardware are expected to become available subsequently. Satellite distribution of highly compressed HDTV signals in the ATV format will then become a reality in the U.S.; however, the feasibility of concatenating MUSE or HD-MAC in tandem with the ATV compression has not been a consideration in the FCC selection process. Thus, it remains to be seen whether the highly compressed ATV format will be used for HDTV distribution within the INTELSAT system. Alternatively, a higher quality, less compressed HDTV format in the 34- to 45-Mbit/s range could become the choice. The intense development activities by HDTV proponents have also produced a "spillover" effect on the video compression technology for conventional television. Conventional television signals at 17 Mbit/s or lower may become quite acceptable for near-studio-quality applications by the end of the INTELSAT VI era.

## Conclusions

Significant improvements are being achieved in the efficiency of both digital and analog techniques for the international transmission of television signals. INTELSAT VI offers the additional advantage of higher e.i.r.p. in the hemi- and zone-beam transponders, which can make possible the use of smaller receiving earth stations or improved signal quality. The substantially greater capacity of INTELSAT VI may also help to usher the emerging HDTV technology into commercial reality. It is expected that many innovative video services will arise from the improved space segment technology of INTELSAT VI and further advances in video signal processing techniques.

## References

- [1] Y. S. Kao and L-N. Lee, "Time-Multiplexed Analog Transmission of Three Broadcast-Quality Television Channels Through One Satellite Transponder," *IEEE Journal on Selected Areas in Communications*, Vol. SAC-5, No. 4, May 1987, pp. 676-684.
- [2] L-N. Lee, T. L. Lin, and D. W. Power, "Studio-Quality Videomultiplexer for Satellite Transmission," *IEEE Global Telecommunications Conference*, San Diego, CA, December 1990, *Conf. Rec.*, Vol. 2, pp. 1139-1143.
- [3] "Performance Characteristics for Television/Frequency Modulation (TV/FM) Carriers With TV-Associated Sound Program Transmission (FM Subcarrier)," *INTELSAT Earth Station Standards Document IESS-306, Rev. 1*, International Telecommunications Satellite Organization (INTELSAT), Washington D.C., December 1986.
- [4] Private communication.
- [5] H. Meiseles, "ABC's Experience With Digital Television Transmission," DS3 Broadcast Television Multipoint Network, Technology Requirements Industry Forum, September 1987, Los Angeles, CA.
- [6] Y. Ninomiya *et al.*, "An HDTV Broadcasting System Utilizing a Bandwidth Compression Technique—MUSE," *IEEE Transactions on Broadcasting*, Vol. BC-33, No. 4, December 1987, pp. 130-160.
- [7] F. W. P. Vreeswijk, "HD-MAC Coding for MAC Compatible Broadcasting of HDTV," 3rd International Workshop on HDTV, Turin, Italy, August 1989.
- [8] Private communication.
- [9] S. Yamashita *et al.*, "Hardware Implementation of HDTV 120/140 Mbit/s Intra-Field DPCM System," 2nd International Workshop on HDTV, L'Aquila, Italy, 1988.
- [10] L. Lec, "Digital Coding of High-Definition Television (HDTV) Signals," *IEEE Military Communications Conference (MILCOM'90)*, September 1990, Monterey, CA, *Conf. Rec.*, pp. 1.5.1-1.5.5.
- [11] "DigiCipher HDTV System," General Instrument Corporation, VideoCipher Division, San Diego, California 92121, USA, June 8, 1990.
- [12] "Advanced Digital Television System Description," Submitted to the FCC Advisory Committee for Advanced Television Systems by the Advanced Television Research Consortium, David Saroff Research Center, NBC, North American Philips, Thomson Consumer Electronics, February 27, 1991.
- [13] "System Description, Digital Spectrum Compatible Advanced Television," Submitted to the FCC Advisory Committee for Advanced Television Systems by Zenith Electronics Corporation and AT&T, February 27, 1991.



*Lin-Nan Lee received a B.S.E.E. from National Taiwan University in 1970, and an M.S. and Ph.D. in electrical engineering from the University of Notre Dame in 1973 and 1976, respectively. In 1977, he joined COMSAT Laboratories, where he conducted research on forward error correcting (FEC) coding techniques and secure communications, and led development activities in digital signal processor (DSP)-based modems, video transmission, and high-definition television (HDTV). He held a number of technical and management positions at COMSAT Laboratories, and was Chief Scientist in COMSAT Systems Division. He is currently an Assistant Vice President of Engineering at Hughes Network Systems. Prior to his work at COMSAT, Dr. Lee was a Senior Scientist at Linkabit Corporation. He is a Fellow of IEEE.*

*Ashok K. Sinha received a B.Sc. and M.Sc. in physics from Patna University, India, and a Ph.D. in physics from the University of Maryland. In 1974 he joined COMSAT Laboratories, where he worked on modeling, optimization, performance analysis, and long-range planning methodology for communications satellite systems, including TDMA and ISL. Subsequently, he was involved in technical analysis and planning for several overseas (ARABSAT, SATCOL, and AUSSAT) and domestic (DBS) satellite systems with COMSAT's Systems Technology Division. He also participated in studies for NASA and others relating to the 30/20-GHz band, the space platform, the space shuttle, and the INTELSAT VI program.*

*Dr. Sinha was Manager of Systems Engineering for COMSAT's Inmarsat Division prior to joining INTELSAT in 1982, where he was initially responsible for service development as part of future planning activities. He has been active in many areas of INTELSAT, including R&D, communications systems analysis and evaluation, and CCIR/CCITT/CMTT. He is a member of the International Union of Radio Science, the International Association of Geomagnetism and Astronomy, the American Physical Society, and IEEE.*



## ***INTELSAT 603 “reboosted” to synchronous orbit***

S. B. BENNETT

(Manuscript received August 3, 1992)

### ***Abstract***

During the launch of the INTELSAT 603 satellite, the second stage of the TITAN launcher failed to separate and the satellite was left stranded in low earth orbit. A program was devised to rescue the satellite by bringing a new perigee kick motor to it using the Space Shuttle, and “reboosting” the satellite to synchronous orbit to fulfill its intended mission. Despite extensive preparations, unexpected problems were encountered in carrying out these plans, although complete success was ultimately achieved. This paper outlines the preparations, discusses the mission itself, and examines the lessons learned.

### ***Background***

On March 14, 1990, the INTELSAT 603 satellite was launched aboard a commercial TITAN launch vehicle. While the propulsion system of the launcher functioned properly, the second stage failed to separate from the satellite. To prevent the imminent reentry of the spent second stage with the attached satellite assembly, the launch team quickly acted on its only option—to release from the satellite the unused perigee kick motor (PKM), with the TITAN second stage attached. This left INTELSAT 603 in an initial orbit of  $193 \times 93$  nmi, with one major concern: the possibility that the silver interconnects between solar cells would be eroded by atomic oxygen at that low altitude. Of lesser concern was the effect of residual atmosphere in continuously perturbing the attitude or orientation of the satellite.

To minimize the effects of atomic oxygen on the solar cell interconnects, it was soon decided to raise the orbit of INTELSAT 603 using some of the limited

onboard propellants, thus reducing the eventual stationkeeping lifetime of the satellite. Orbit-raising was accomplished in two steps, as models for the erosion process were evaluated and refined. The orbit was first raised to  $215 \times 141$  nmi, and eventually to about 303-nmi circular.

To accurately assess the impact of atomic oxygen erosion, test panels were flown on National Aeronautics and Space Administration (NASA) Space Transportation System (Shuttle) mission 41 (STS-41) in October 1990. The results of these experiments, and the consequent refinement of the erosion model, provided confidence that the satellite would retain adequate silver thickness to survive the reboost mission and operate for 10 to 15 years in synchronous orbit, even after several years in low earth orbit (LEO) at 300 nmi. This effort is discussed by Dunnet and Kirkendall in Reference 1.

### **The power of teamwork**

The success of the reboost mission that positioned INTELSAT 603 in geosynchronous orbit can be attributed to teamwork, which involved literally hundreds of persons in a number of organizations: NASA, Hughes Aircraft Company (HAC), INTELSAT, COMSAT, Scitor, and others. Members of all these organizations worked together as one in the INTELSAT Launch Control Center (ILCC), which in turn worked as a team with personnel from these same organizations at Cape Canaveral during the launch phase and at the Johnson Space Center throughout the mission. While all cannot be listed here, some deserve special mention.

The NASA team included astronauts Dan Brandestein, commander; Kevin Chilton, pilot; Pierre Thuot, Rick Heib, and Tom Akers, extravehicular activity (EVA) team; Kathy Thornton, deployment; and Bruce Melnick, remote manipulator system (RMS) operator; as well as NASA flight director, Al Pennington. The HAC staff included Chuck Rubin, program manager; Jerry Salvatore, head of the rendezvous team; Loren Slafer, head of the attitude control and determination team; Len Dest, system engineering and alternate INTELSAT mission director; and Mark Altobelli, for the dynamic mission sequence of events. The COMSAT staff included Nelson Roth, propulsion; Keith Volkert, mechanisms; and Jeff Robinson, thermal. The INTELSAT team included Erland Magnusson, mission director; Lakh Virdec, systems engineering and INTELSAT Flight Operations team leader; Charlie Johnson, reboost program manager; and Ramu Potarazu, ILCC coordination—whose leadership was characterized by enthusiasm that was contagious! In addition, there were countless persons on the various teams, including those at the six INTELSAT tracking, telemetry, and command (TT&C) stations, who worked very long and well to bring about the eventual success of the mission.

### **Reboost mission planning**

As soon as the satellite was stabilized, INTELSAT approached NASA to explore the possibility of rescuing the satellite using the Shuttle. Preliminary investigations carried out by INTELSAT, HAC, and NASA were encouraging, and INTELSAT awarded contracts to HAC and NASA in July 1990. The reboost mission was planned to use STS-49, the maiden flight of the Shuttle *Endeavour*.

### **Reboost hardware**

The basic plan was to design and build a cradle, a grapple fixture (capture bar), and the associated hardware needed to support a fully loaded PKM to LEO. The astronauts would then grapple the satellite, secure it mechanically and electrically to the PKM, and release it from the Shuttle. To meet the initially projected launch schedule of April 1992, the hardware (Figure 1) was delivered, on schedule, 19 months after contract award. Details of the specially designed hardware built by HAC are presented in Figures 2 and 3 and discussed in Reference 2. HAC also supplied the PKM, which was originally intended for use by INTELSAT VI satellites with Shuttle launches prior to the *Challenger* disaster. This PKM was of the same design used for the TITAN launch, except that it was fully loaded with propellant [3]–[6].

Figure 4 depicts the capture bar assembly provided by NASA. The intent was for an astronaut, perched at the end of the Shuttle's RMS, to first attach the capture bar to the docking ring of the satellite. The RMS would then be "hard-docked" to the right-hand beam extension of the capture bar and would be used to place the satellite on top of the PKM for its final securing in the Shuttle payload bay. The first part of this procedure did not go according to script, although the last part did.

### **Maneuver plan**

A very complex series of maneuvers was planned to be executed before the satellite could be moved into the Shuttle bay. Because of the total payload mass of about 28,000 lb to be carried to orbit, the Shuttle could safely attain an orbit height of only 190 to 200 nmi, while the satellite was parked at about 303 nmi at the time of the mission. However, INTELSAT did not wish to lower the orbit of the satellite until it was assured that the Shuttle would be committed to orbit, since the satellite could not survive prolonged exposure to atomic oxygen at the orbit height of the Shuttle. In case of a Shuttle launch abort, the option of raising the orbit and lowering it once again for a later Shuttle mission would have been too costly in terms of satellite propellants.

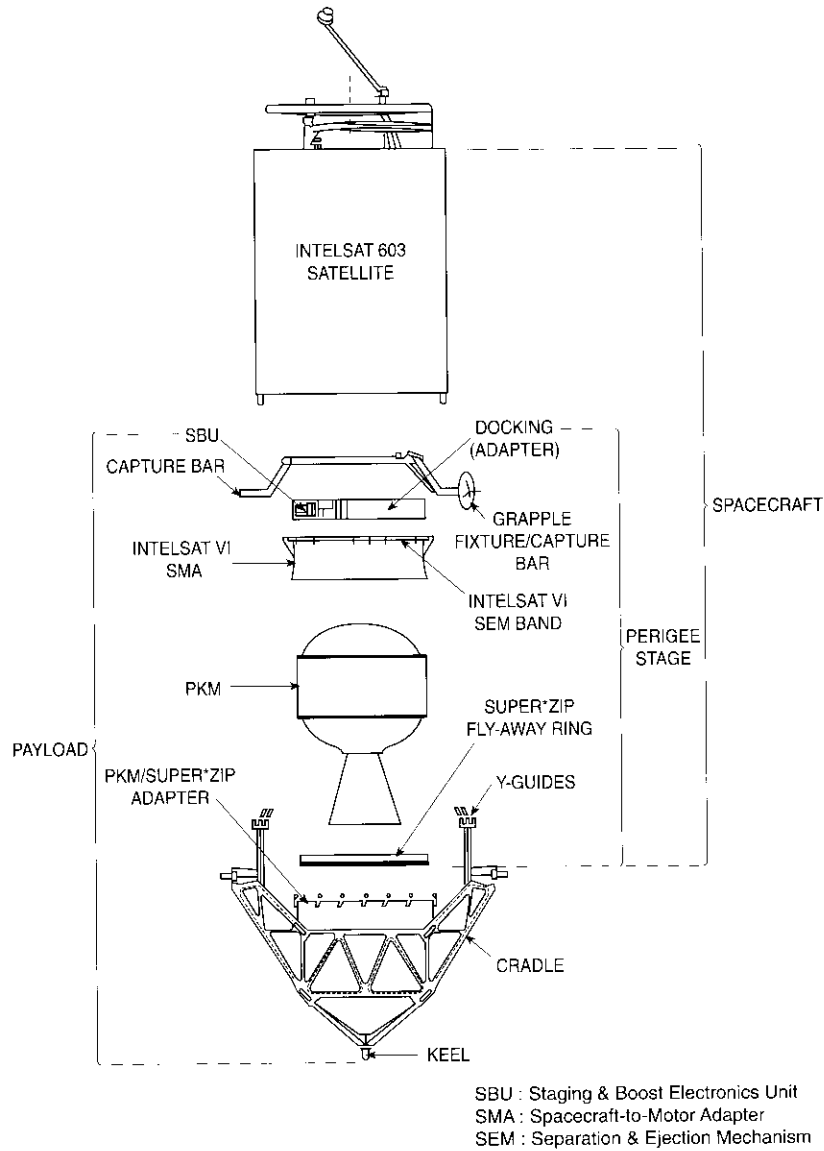


Figure 1. INTELSAT 603 Reboost Payload Assembly

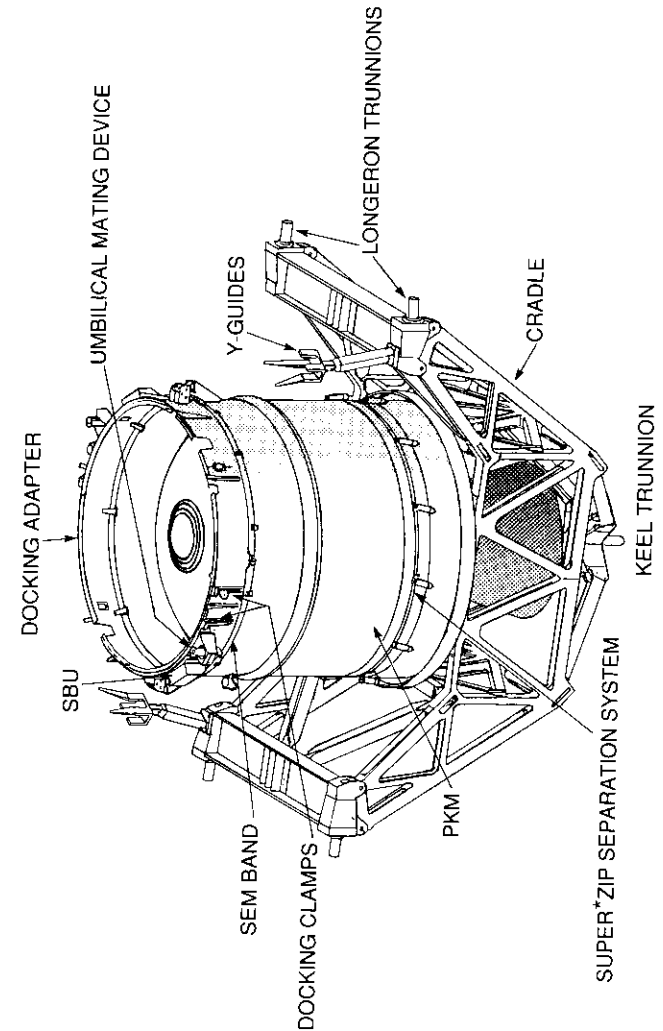


Figure 2. INTELSAT 603 Cradle

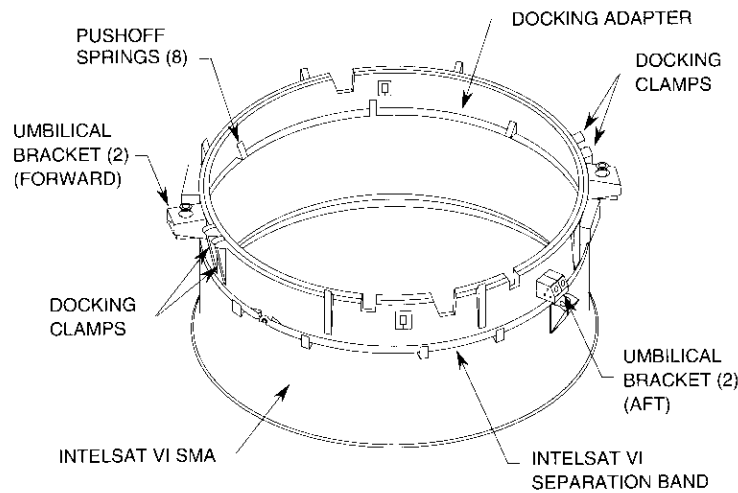


Figure 3. Docking Adapter

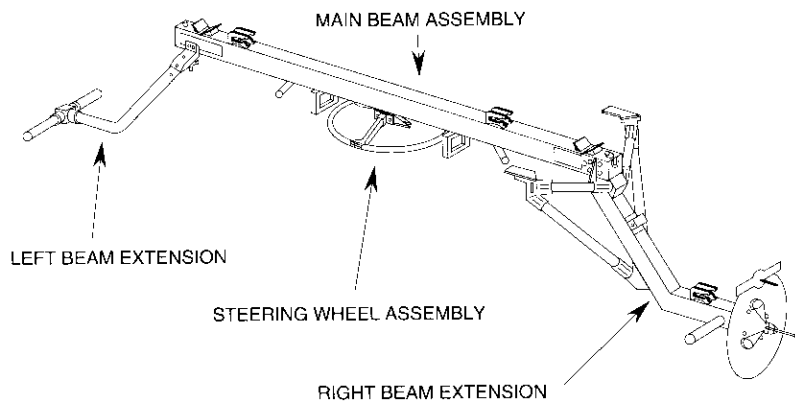


Figure 4. NASA Capture Bar

Based on these considerations, the reboost mission was planned on the basis of the first dual-active rendezvous since *Gemini*, and would entail the first in-orbit attachment of a large, solid-propellant rocket motor.

This unique mission required that INTELSAT 603 and *Endeavour* rendezvous within a "control box" at a control box start time (CBST) that occurred at a mission elapsed time (MET) of 46 hours. The control box is actually a volume in space whose exact location was to be defined by NASA approximately 5 hours after *Endeavour* liftoff. It would have the shape of a parallelogram whose boundaries define altitude and phase limits. The third boundary defines orbital planar limits. The control box extends over  $6^\circ$  of arc in a 190- to 200-nmi circular orbit, as depicted in Figure 5, with an inclination of  $28.35^\circ$ .

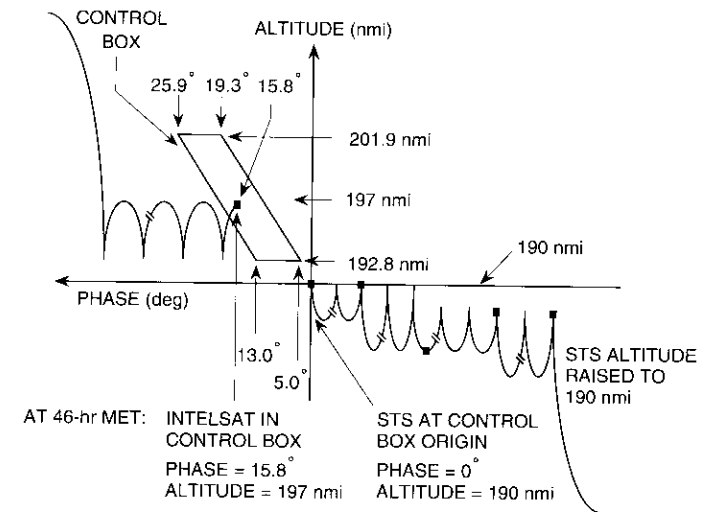
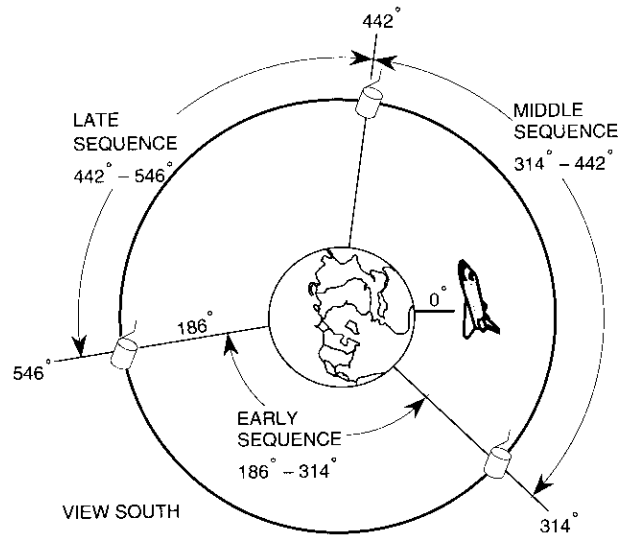


Figure 5. Rendezvous Profile: Liftoff to CBST

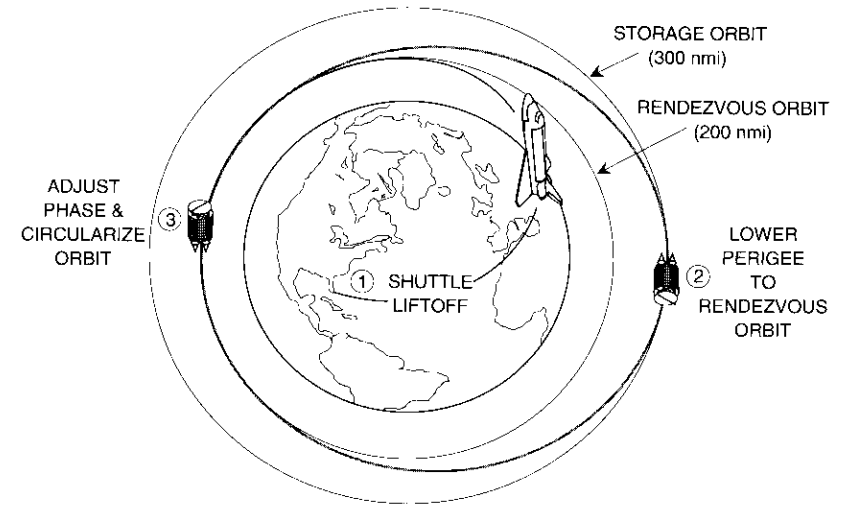
To rendezvous with INTELSAT 603, the Shuttle had to launch into a "phantom" orbital plane with the same inclination as the satellite and a right ascension of ascending node slightly offset from the INTELSAT 603 plane. This phantom plane is required because of the differential nodal regression of the two vehicles, which decreases to zero by the time of the rendezvous. Additionally, the phase angle between the vehicles must be brought to zero. The phase angle is defined as the angle measured from the position vector of the Shuttle (projected onto the orbital plane of the target) to the INTELSAT 603 position vector (Figure 6).



Note: Phase difference at STS liftoff determines baseline INTELSAT phasing allocation as early, middle, or late sequence.

Figure 6. *Phase Angle*

The need to achieve zero planar and phase difference between *Endeavour* and INTELSAT 603, along with various safety-related and other requirements, defined the launch windows of the Shuttle for each day [2]. Considering the maneuvering capabilities of the Shuttle, it was planned to limit INTELSAT 603's orbit-lowering maneuvers to four (OL1, OL2, OL3, and CIRC) at three predefined time sequences. The specific maneuver time sequence (early, middle, or late) was dependent on the time of launch within each day's launch window. The purpose of the OL1 maneuver was to lower one side of the satellite's orbit to establish perigee just below the control box altitude. OL2 was the first apogee-lowering maneuver, needed to bring the apogee to an intermediate altitude greater than the final rendezvous altitude. The OL3 maneuver was the second apogee-lowering maneuver, to bring the satellite's apogee to the final rendezvous altitude. The CIRC maneuver was carried out to raise the INTELSAT 603 perigee to the final rendezvous altitude and circularize the orbit. The final rendezvous altitude was planned for the center of the control box. The overall rendezvous phase is depicted in Figure 7.



#### DUAL-ACTIVE RENDEZVOUS

- 603 orbit-lowering begins 3 hr after liftoff.
- Satellite reaches final position at 46 hr.
- Rendezvous occurs at 69 hr.

Figure 7. *Rendezvous Phase*

In addition to lowering INTELSAT 603's orbit, it was also planned to reduce its spin speed from about 15 rpm to 0.65 rpm in preparation for capture by the astronauts. These maneuvers, along with any required attitude reorientations and nutation damping, were to take place after CBST, about 6 hours before *Endeavour's* final approach.

#### Extravehicular activity plan

During the final approach phase of the Shuttle, after all necessary INTELSAT 603 maneuvers were complete, INTELSAT was to make the satellite safe for the EVA phase. This involved closing the propellant latch valves and disabling the drivers for the latch valves and thruster solenoids, as well as deconfiguring all command links to the satellite. Once these and other steps were accomplished, two astronauts could begin the EVA and perform the tasks previously described. Once INTELSAT 603 was properly secured to the PKM and the electrical connections were verified, the astronauts were to return to the Shuttle's

air lock, signaling the end of the EVA, which was estimated to require about 4 hours.

### Post-deployment plan

Following the EVA, an astronaut in the cabin would activate deployment by using a standard switch panel interface to fire the Super\*Zip separation system, thus releasing the INTELSAT 603 and PKM combination from the cradle. After deployment, the Shuttle would need to perform only a minimal separation maneuver to allow commanding of INTELSAT 603 in order to prepare it for PKM firing, including spinup to 30 rpm.

### Transfer orbit plan

Figure 8 shows the transfer orbit operations required to transition INTELSAT 603 to geostationary orbit following PKM firing. Of particular interest is the use of a "supersynchronous" transfer orbit for the first time by INTELSAT to achieve a planned apogee of twice synchronous altitude.

In the original launch configuration, the PKM propellant had to be substantially off-loaded so that the PKM/satellite combination could be launched into the proper geostationary transfer orbit within the lift capability of the commercial TITAN III launcher. This constraint did not apply to the Shuttle, which was able to carry the fully loaded PKM and associated hardware. It was planned to take advantage of this situation to extend the stationkeeping lifetime of the satellite.

Because the velocity of the satellite is lower at supersynchronous apogee, the firing of the satellite's liquid apogee motors (LAMs) to raise perigee and remove the remaining orbit plane inclination consumed less onboard propellant than would be required at synchronous apogee. The propellant saved by employing the supersynchronous transfer orbit can be used to increase the satellite's on-orbit stationkeeping lifetime by about 1 year, thus offsetting some of the lifetime lost due to the expenditure of onboard propellant in raising the orbit to about 303 nmi, and then lowering it to meet the Shuttle at the control box.

### Mission execution

Liftoff of the Shuttle *Endeavour* took place on May 7, 1992, at 23:39:59 UTC (Universal Time Code), just 15 minutes before the closing of the 49-minute launch window for that day. This timing imposed the early orbit-lowering maneuver schedule for INTELSAT 603, and a CBST of 21:40 UTC on May 9, 1992.

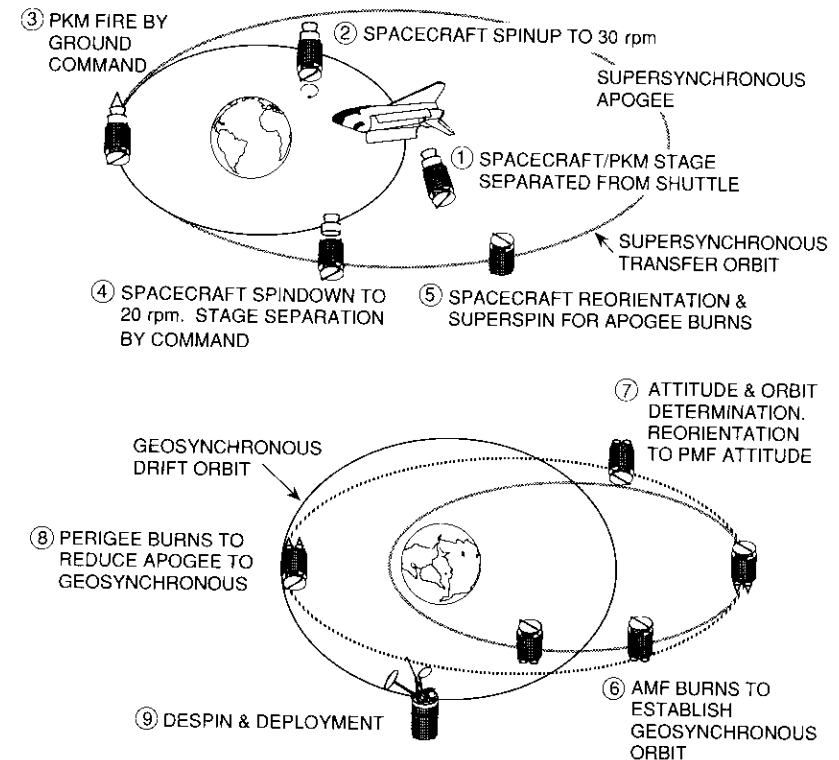


Figure 8. Transfer Orbit Phase

### Initial maneuvers

Maneuvers were carried out accurately by both *Endeavour* and INTELSAT 603. The last burn needed by INTELSAT 603 to reach the control box was executed at 01:05:59 UTC. The control box parameters achieved by the satellite are summarized in Table 1. It should be noted that the goal for phase was essentially achieved, while the mean altitude attained relative to the control box origin was adequate for mission purposes. The eccentricity and planar error were well within the targeted goals.

### First EVA, May 10

*Endeavour's* terminal initiation (TI) burn for the first EVA took place at 19:33 UTC on May 10. In spite of extensive pre-mission testing and practice at NASA's Johnson Space Center facilities, including practice in the Wet

TABLE 1. CONTROL BOX PARAMETERS

PARAMETER	GOAL	ACHIEVED	DISCREPANCY
Phase	15.8°	15.8355°	0.0335°
Mean Altitude Relative to Control Box Origin (nmi)	7.4	8.6	1.2
Eccentricity (nmi)	<8.0	3.83	0
Planar Error	<0.06°	0.01°	0

Environmental Test Facility (WETF) and with a dynamics simulator mounted on an air bearing table, three attempts to attach the capture bar to INTELSAT 603 failed. Each time the capture bar touched the satellite, it applied a small force that caused the satellite to translate and develop a nutation about its spin axis. The astronaut on the end of the RMS, P. Thout, was unable either to cause the satellite's rotation at 0.65 rpm to trigger the clamps on the capture bar (the primary mode of operation), or to manually trigger these clamps (the backup mode).

When further attempts were abandoned, the satellite was nutating with a period of 132 s and a cone angle (rotation of the spin axis about the velocity vector) of 52°. It had an average sun angle (spin axis to sun line) of 114° and a spin rate of 0.4 rpm. The INTELSAT mission team recovered the satellite by 23:46 UTC, leaving it with a spin rate of 2.3 rpm, nutation of 7°, and sun angle of 72° to 77°.

### Second EVA, May 11

A backup plan existed for a second EVA in case the work could not be completed the first day. In preparation for the second try, the Shuttle crew requested that the grapple take place in sunlight. The satellite was again spun down to about 0.65 rpm. The T1 burn for this EVA took place at 20:02 UTC on May 11. At the start of the EVA, Mr. Thuot practiced with the capture bar against a cable in the Shuttle's bay prior to attempting to capture the satellite at 23:04 UTC. On the first attempt, the capture bar appeared to be attached to the satellite for a few seconds, only to greatly disappoint everyone when Mr. Thuot pulled on it and it came away. The result was to again induce coning to the satellite.

Up to eight additional unsuccessful attempts were made to capture the satellite during this EVA. When the orbiter backed away from the satellite at 01:00 UTC on May 12, the satellite had a large coning angle of 50° to 60° and

a spin rate of less than 0.3 rpm. INTELSAT 603 was again recovered by the INTELSAT team in about 2 hours. The satellite was spun up to 2.6 rpm, and the sun angle was adjusted to  $100^\circ \pm 5^\circ$ .

### Third EVA, May 13

At the end of the second EVA, it was clear to everyone that grappling the satellite with the capture bar would be impossible. Various ideas were discussed, but the Shuttle's commander, D. Brandestein, suggested a three-person EVA to manually grapple the satellite. This concept was accepted as the baseline, despite the fact that a three-person EVA had never before been attempted. There was concern that the Shuttle air lock was only capable of providing air and cooling to resupply two space suits in an emergency, and it was not known if three persons could physically fit in the air lock. Manual grappling of INTELSAT 603 was potentially dangerous and had not been evaluated or practiced prior to liftoff, and there would only be 24 hours to work out all potential or real problems prior to making a final effort to capture the satellite.

It was decided not to attempt an EVA on May 12, but to use the time to prepare for the attempt on May 13. During this period, the Shuttle astronauts practiced placing the three selected astronauts in the air lock and proved that this was feasible. In parallel, other astronauts at the Johnson Space Center in Houston practiced capturing the satellite and attaching the capture bar in the WETF. Other teams of NASA, HAC, and INTELSAT personnel worked out the details required to ensure success.

For the EVA on the 13th, the Shuttle's T1 burn was planned at 17:55 UTC; however, still another potential disaster threatened when an onboard software problem occurred. Although the problem was soon recognized and the astronauts were able to work around it, NASA management did not feel that it could risk relying on the onboard software. Instead, in a courageous decision, management opted to target the burn using on-ground software. This too was a first. The T1 burn took place at 20:57 UTC on May 13.

In preparation for the manual capture, INTELSAT had achieved a satellite spin rate of 0.24 rpm, with a nutation of only 1°. The relatively slow motion of the satellite, coupled with the extremely precise and skilled maneuvering of the Shuttle by Commander Brandestein, enabled the manual capture of INTELSAT 603 on the first attempt at 00:00 UTC on May 14. A view of the satellite in the hands of three astronauts is shown in Figure 9. The astronauts handled the satellite with extreme care. They needed to rotate it about 120° to position it for attachment to the capture bar.

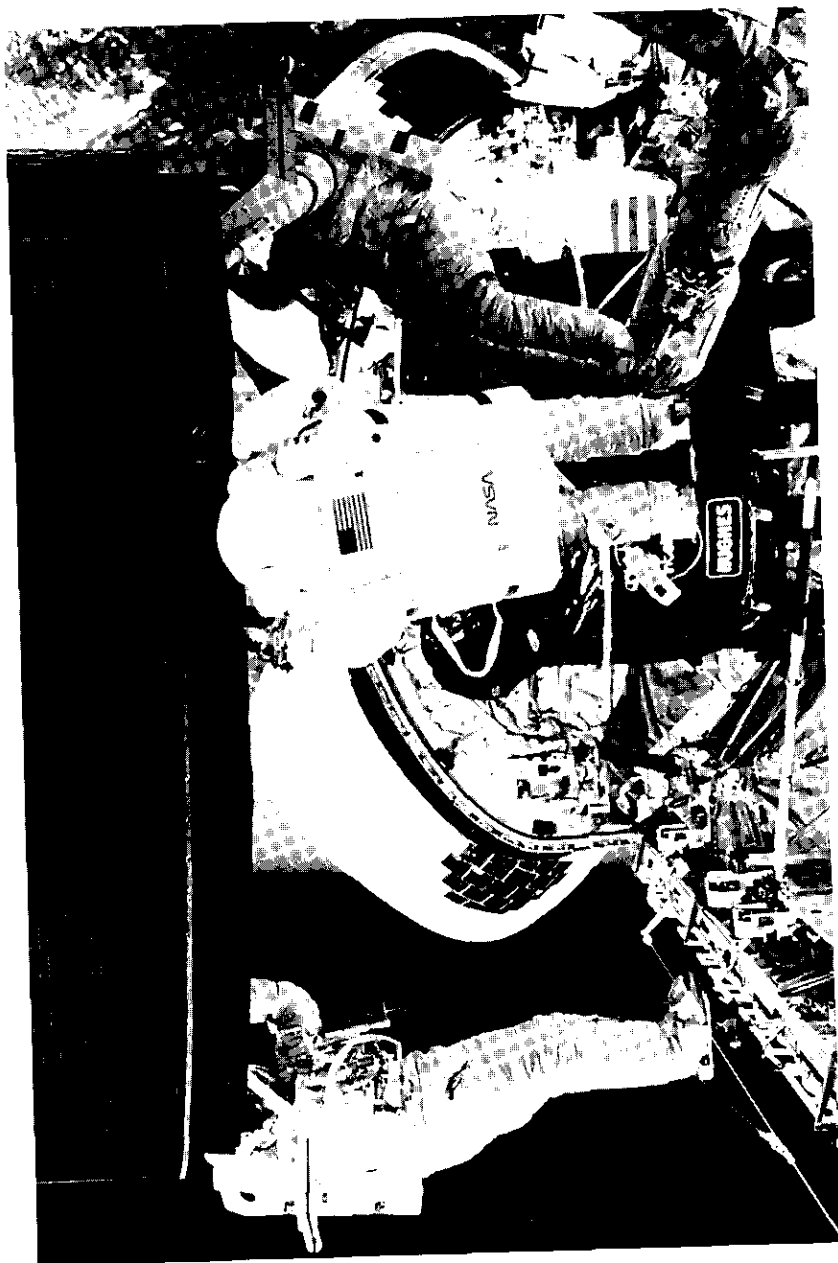


Figure 9. "Got It"

From that point, the remaining EVA activities went very well and more quickly than anticipated. The hard-docking of the capture bar to INTELSAT 603 was accomplished at 01:33 UTC, and the RMS grapple of the capture bar occurred at 01:48 UTC on May 14. The satellite's telemetered accelerometer signal for the RMS attachment is shown in Figure 10.

Satellite deployment from the Shuttle gave rise to another series of tense moments for this mission when, after the deployment hardware repeatedly failed to actuate, it was discovered that the Shuttle's power bus wiring to the deployment hardware was not the same as that shown on the astronauts' instructions. Once this problem had been resolved, the satellite was deployed at 04:56 UTC, as depicted in Figure 11.

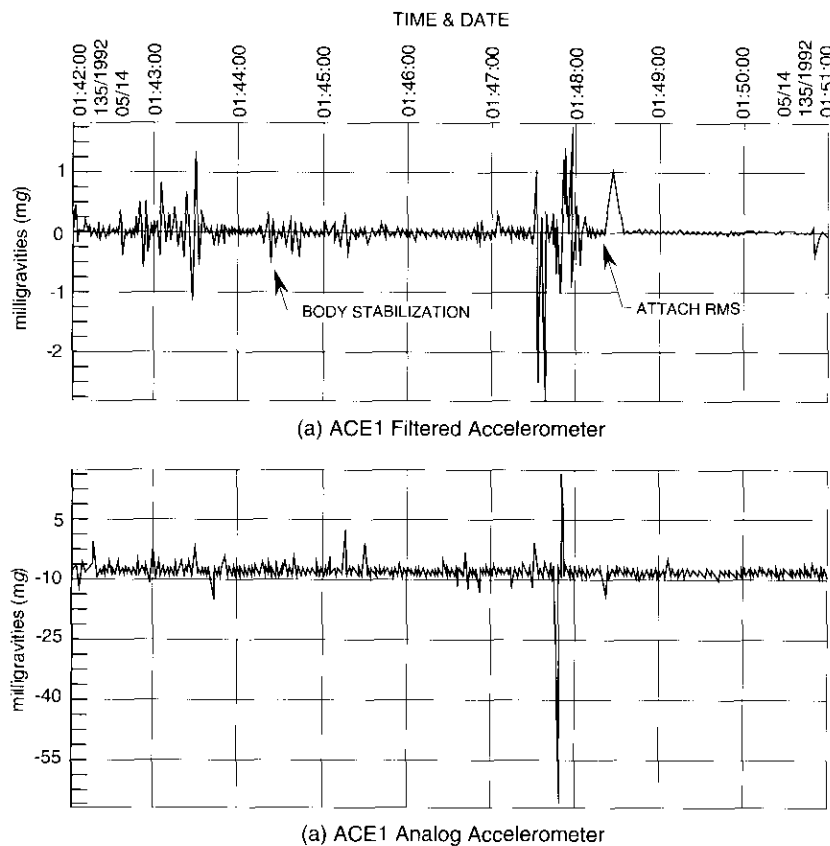


Figure 10. Accelerometer Signal: RMS Attachment

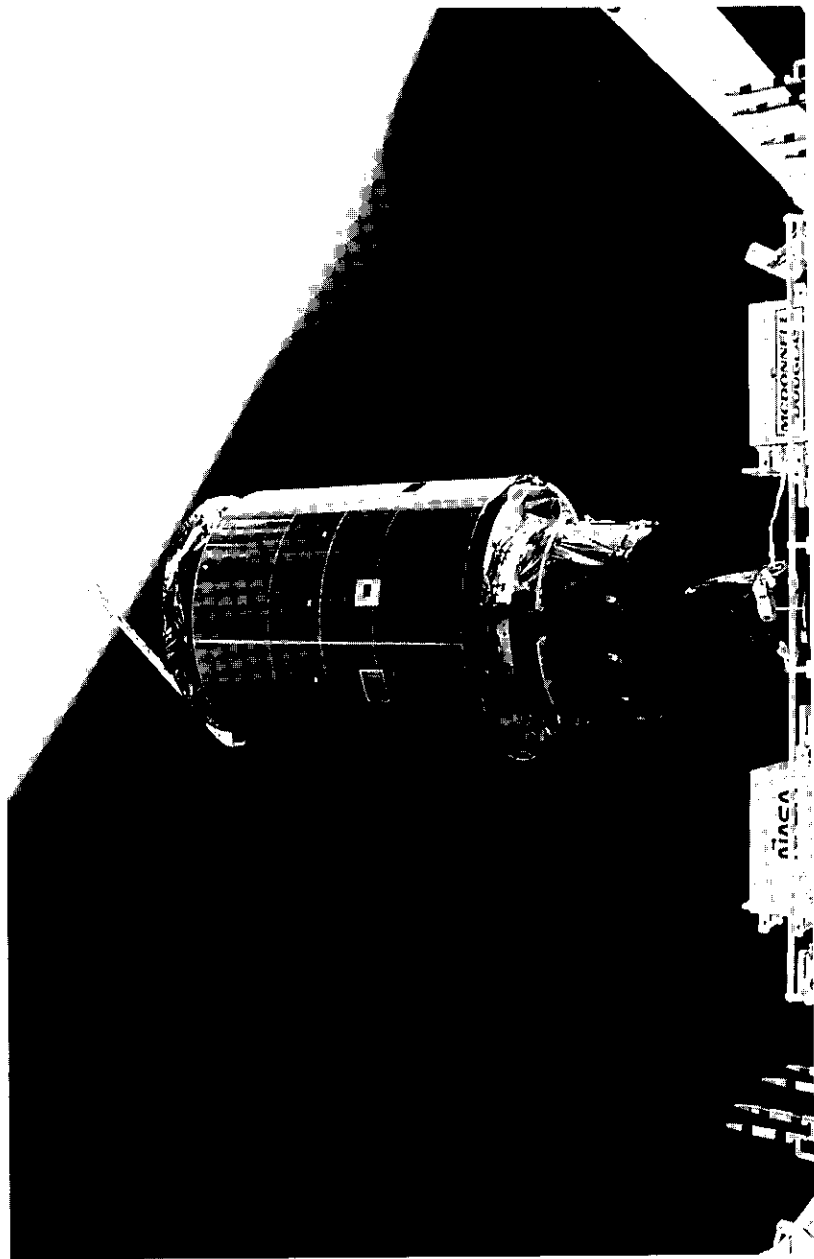


Figure 11. Deployment

### Final steps to orbit

Once the satellite was deployed from the Shuttle, INTELSAT again took over active control of INTELSAT 603. Prior to PKM firing, a number of key functions had to be carried out, including spinup to 15 rpm, attitude trim, gyro and perigee active nutation control checkout, reorientation to PKM attitude, spinup to 30 rpm, and attitude trim.

Due to the 2-day delay imposed by the capture on EVA 3, the last 3° of the reorientation of INTELSAT 603 to the correct attitude for PKM firing would be conducted in the blind, since the sun would not be in the field of view of both slits of the sun sensor for another 17 days. The risk of an attitude error due to conducting such a maneuver partly in the blind was judged much lower and preferable to the risk of remaining in LEO at about 190 nmi for the time necessary for the sun to be adequately within the field of view of the sun sensor at PKM attitude. Accordingly, the maneuvers were carried out and the PKM was fired at 17:25 UTC on May 14, less than 13 hours after deployment from *Endeavour*.

The principal remaining propulsion events involved six firings of the satellite LAMS. The orbits achieved, and other relevant parameters resulting from the PKM and LAM firings, are summarized in Table 2.

Activities subsequent to LAM 5 included all the deployments, which went exceptionally smoothly, followed by extensive in-orbit testing, as was done for prior INTELSAT VI satellites [7],[8]. With the exception of one redundant traveling wave tube amplifier (TWTA) in channel 1'-2' which failed to turn on, INTELSAT 603 was found to be the most trouble-free of all INTELSAT VI satellites.

INTELSAT 603 was placed in service on July 15, 1992, and is expected to serve INTELSAT for at least 11.5 years.

TABLE 2. TRANSFER ORBIT PARAMETERS ACHIEVED

ACTION	APOGEE (nmi)	PERIGEE (nmi)	PERIOD (nmi)	DELTA-V (ft/s)	FIRING		
					LENGTH (s)	DAY	UTC
PKM Fire	38,648	194	1,445	10,150	149	14	17:25
LAM 0	38,644	403	1,455	95	120	15	06:01
LAM 1	38,627	2,741	1,567	939	1,111	17	06:01
LAM 2	38,613	4,976	1,676	581	689	18	08:16
LAM 3	38,601	16,823	2,299	1,800	2,096	19	11:59
LAM 4	38,604	19,213	2,433	235	272	21	02:28
LAM 5	19,437	19,214	1,436	1,435	1,699	21	22:04

## Lessons learned

A number of important lessons were learned from the experience of operating and reboosting INTELSAT 603. The failure of the capture bar to function as originally expected illustrates that operations in zero-g follow rules that are still not well understood. It also shows the limitations of ground-based physical simulations. Clearly, very small forces can move very large masses in zero-g. Proper simulation of this procedure may only be possible analytically or in a zero-g environment.

Built-in redundancy and alternate modes of operation enabled INTELSAT 603 to operate in LEO for 2-1/2 years. Extensive testing and modeling predicted that INTELSAT 603 would survive its extended exposure to the LEO environment in good condition. This was subsequently borne out by geosynchronous in-orbit tests.

## Conclusions

It has been shown that satellites stranded in LEO can be recovered if they can be brought to altitudes compatible with the Shuttle. The INTELSAT 603 reboost mission required heroic efforts on the part of NASA, and the *Endeavour* astronauts in particular. The use of a three-man crew to manually grapple and stabilize the satellite during the longest (8-1/2 hour) EVA to date was an historic first. The option of even attempting a third EVA on May 13 was only available due to the very precise and propellant-conserving maneuvers performed by the crew on *Endeavour* and by INTELSAT in operating the satellite. Finally, the first use of a supersynchronous transfer orbit by INTELSAT for INTELSAT 603 recovered about 1 year of satellite stationkeeping lifetime, thus ensuring a service life of about 11.5 years.

## Acknowledgments

The author is indebted to L. Virdee and M. Seddon for compiling data for this paper, and to T. Rush for his helpful suggestions.

## References

- [1] A. Dunnet and T. D. Kirkendall, "Assessment of Atomic Oxygen Erosion of Silver Interconnects on INTELSAT VI, F3," European Space Power Conference, Florence, Italy, September 1991, *Proc.*, pp. 701-706. ESA Publication No. SP-320.

- [2] L. Virdee *et al.*, "INTELSAT VI (F3) Reboost Mission," AIAA 14th International Communication Satellite Systems Conference, Washington, DC, March 1992.
- [3] E. I. Podraczky and W. R. Schnicke, "The Process for Success—INTELSAT VI," *COMSAT Technical Review*, Vol. 20, No. 2, Fall 1990, pp. 231-246.
- [4] L. B. Perillan, W. R. Schnicke, and E. A. Faine, "INTELSAT VI System Planning," *COMSAT Technical Review*, Vol. 20, No. 2, Fall 1990, pp. 247-269.
- [5] G. P. Cantarella and G. Porcelli, "Specifying the Spacecraft Bus," *COMSAT Technical Review*, Vol. 20, No. 2, Fall 1990, pp. 309-333.
- [6] L. R. Dest *et al.*, "INTELSAT VI Spacecraft Bus Design," *COMSAT Technical Review*, Vol. 21, No. 1, Spring 1991, pp. 5-55.
- [7] L. S. Virdee *et al.*, "INTELSAT VI Launch Operations, Deployment, and Bus In-Orbit Testing," *COMSAT Technical Review*, Vol. 21, No. 2, Fall 1991, pp. 305-337.
- [8] G. E. G. Rosell *et al.*, "In-Orbit RF Test of an INTELSAT VI Spacecraft," *COMSAT Technical Review*, Vol. 21, No. 2, Fall 1991, pp. 339-390.



Simon B. Bennett received a B.E.E. from City College of New York in 1959 and an M.E.E. from New York University in 1961. His career, which spans the entire history of communications satellites, began with work on the first TELSTAR satellite program at Bell Telephone Laboratories from 1959 to 1963. He continued in this field from 1961 to 1974 at COMSAT, where he contributed to the success of satellite programs from *Early Bird* to INTELSAT IV.

In 1974, Mr. Bennett joined INTELSAT as Manager of Engineering, where he was engaged in the formulation and application of INTELSAT's intersystem coordination process. Subsequently, as Manager of Space Segment Programs, he was responsible for all technical and programmatic aspects of satellites and launch vehicles encompassing the INTELSAT V and VI series of satellites. This was followed by 1 year as Director of System Planning. From 1986 to 1990, he was in charge of the operation of INTELSAT's fleet of 15 to 18 satellites and associated tracking, telemetry, command, and monitoring facilities. From early 1990 until his retirement from INTELSAT in July 1992, he was assistant to the Vice President for Engineering and Research. He is currently President of Bennett Consultancy, Alexandria, Virginia.

## ***The IM Microscope: A new approach to nonlinear analysis of signals in satellite communications systems***

D. S. ARNSTEIN, X. T. VUONG, C. B. COTNER,  
AND H. M. DARYANANI

(Manuscript received August 6, 1992)

### ***Abstract***

This paper describes a new technique, called the IM Microscope, for studying the effects of nonlinearities in satellite transponders. The approach is to first derive a least-squares solution for equivalent gain on each signal as it passes through the nonlinearity, and then to subtract the signals one by one from the output to obtain a residual intermodulation (intermod) noise waveform. The algorithm is first derived, and examples are then given of its use in calculating power density spectra and power division.

The IM Microscope can handle routine problems such as determining the carrier-to-intermod ratio of signals in a frequency-division multiple access (FDMA) transponder, and out-of-band emission levels for earth stations. This new approach does not become computation-bound when solving for high-order harmonic distortion such as passive intermod, or in situations with a large number of input signals. It can handle difficult cases, such as the intermod generated in a spread spectrum transponder, in an arbitrary nonlinear function, with a large number of unequal signals, or in computation of distortion with a time-dependent nonlinear device.

### ***Introduction and background***

A new technique called the IM Microscope has been developed at COMSAT for computing intermodulation (intermod) power spectra and nonlinear power division in satellite transponders, high-power amplifiers (HPAs), and other

nonlinear devices. It provides capabilities beyond those of current intermod analysis techniques, which date back to the early 1970s [1],[2]. For example, the following problems are difficult to solve using current nonlinear analytical approaches:

- Finding the spectrum of intermod and power division with overlapping spectra—a case which occurs with code-division multiple access (CDMA) or overlapping frequency-hopping multiple access (FH) signals.
- Inclusion of high orders of intermod products, such as passively generated intermod (PIM), in high-power satellites.
- The case of arbitrary nonlinear characteristics (*e.g.*, discontinuous, piecewise linear, defined by an analytical expression, or time-varying).
- Computing intermod from large numbers of unequal carriers.

Unlike synthesis techniques which build a model for intermod noise component-by-component (*e.g.*, third order, fifth order, *etc.*), the new approach works directly on composite simulated signals stored as a computer file. It strips away the wanted signal components one by one until a small residual intermod noise remains (hence the term “microscope”).

Since its inception in 1990, the IM Microscope study at COMSAT has evolved through several stages. The software implementing the algorithm is designed to run on a 386-based personal computer (PC) with a math coprocessor. It is written in Lahey FORTRAN with DOS memory extension, and contains a variety of input signal models, including energy-dispersed carrier waves (ED/CWs), direct-sequence spread spectrum (DSSS) quadrature phase shift keying (QPSK) digital signals, bands of thermal noise, and unmodulated Cws. The IM Microscope played a key role in a Department of Defense-funded study [3],[4] testing the use of a voltage-controlled nonlinear function (time-varying nonlinearity) to enhance the antijam capability of a transponder.

This paper describes the new algorithm, discusses the rationale for development into its current form, and presents typical results.

### Theory of operation

The IM Microscope is a two-step analysis procedure. With reference to Figure 1 (showing input signals  $s_1, s_2, \dots, s_L$  and output signals with equivalent gains,  $\lambda_1, \lambda_2, \dots, \lambda_L$ ), the procedure is as follows:

*Step 1.* Compute equivalent (stochastic) gains of all signals passing through the nonlinearity.

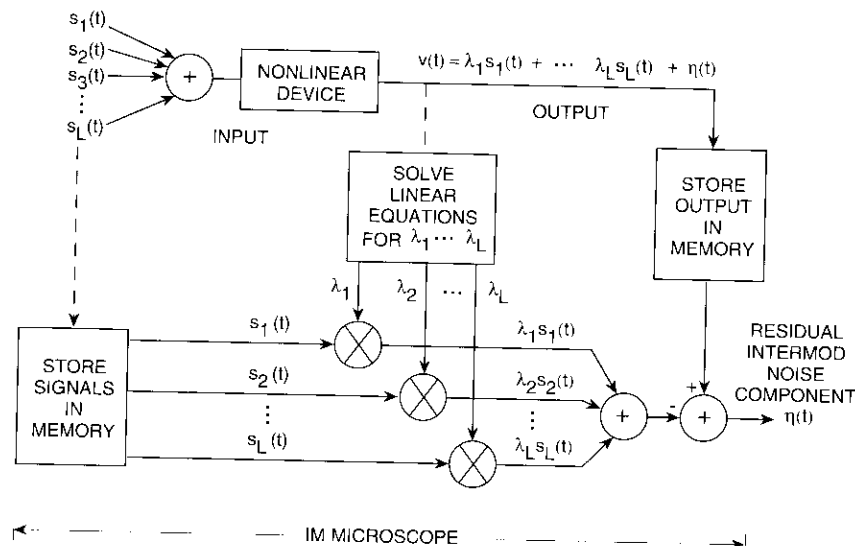


Figure 1. *Equivalent Gain and Residual Noise Model Forming the Basis of the IM Microscope*

*Step 2.* Subtract those signals from the output, leaving a residual which is the intermod noise.

Although this approach is intuitive, many problems had to be overcome to make it practical. A study program was initiated in 1990 by COMSAT World Systems (CWS) to test the feasibility of a software implementation of this procedure which was first suggested in 1979 [5].

The main problem encountered in carrying out step 1 is that, except for some simple nonlinearity problems with a few input signals, the closed-form analytical solution for equivalent gain produces intractable multidimensional integrals over the random variables that characterize the input signals. These integrals do not factor or otherwise simplify. For example, two independent signals in a transponder may be described in a vector space by a single random variable—the phase difference between the signals. Three signals could be characterized by two independent phase differences, and so on. Each time another independent signal is included, at least one more dimension is added to the integrals that must be solved to calculate a residual component. When

thermal noise and amplitude modulation signals are added to the collection of possible inputs, any hope of an analytical solution to steps 1 and 2 disappears.

A simulation approach which uses digital representations of the signals nicely sidesteps this dilemma, since a finite-time average can be computed directly from stored versions of computer-generated sample functions. Thus, a single variable (time) replaces the multitude of variables that would be needed to describe statistically independent signals, and a summation over the time variable replaces probability-based averaging. The IM Microscope, as realized in this study, is therefore a Monte Carlo-based approach that depends on accurately recreating digitally simulated versions of signals found in the transponder or other nonlinear device. The theoretical basis for the Monte Carlo approach is derived below, beginning with a narrowband representation of signals and associated bandpass nonlinearities.

### Representation of narrowband signals

All signals in the IM Microscope are simulated with complex envelope representations of bandpass signals [6]. A bandpass signal occupies a restricted region of the frequency domain and can be represented by its (narrowband) in-phase and quadrature components,  $x_i$  and  $x_q$ , as

$$x(t) = x_i(t) \cos(\omega_c t) - x_q(t) \sin(\omega_c t) \quad [\text{real signal}] \quad (1)$$

The real bandpass signal,  $x(t)$ , can be expressed as the real part of the product of the complex envelope component,  $[x_i(t) + jx_q(t)]$ , and the center frequency shift component,  $e^{j\omega_c t}$ . Calling  $s(t)$  this product, we have

$$\begin{aligned} s(t) &= [x_i(t) + jx_q(t)] e^{j\omega_c t} && [\text{complex signal}] \\ &= A(t) e^{jB(t)} e^{j\omega_c t} \end{aligned} \quad (2)$$

where

$$A(t) = \sqrt{x_i(t)^2 + x_q(t)^2}$$

and

$$B(t) = \arctan \left[ \frac{x_q(t)}{x_i(t)} \right] \quad [\text{four-quadrant arctan}]$$

Note that the original real signal can be recovered by taking the real part of the complex signal, as

$$x(t) = \text{Real} \{ \text{complex envelope} \cdot e^{j\omega_c t} \} = \text{Real} \{ s(t) \} \quad (3)$$

For purposes of calculation and computer representation, the complex envelope is better than the original signal because it consists entirely of low-pass functions,  $A(t)$  and  $B(t)$ , making it easy to go from complex to real, and vice versa.

The IM Microscope represents all signals as sampled complex envelope signals. The sampling frequency,  $f_s$ , establishes a sampling interval,  $\Delta t = 1/f_s$ , and signals are represented at their  $n$ th time sample as

$$s(t = n\Delta t) = s(n) = [x_i(t = n\Delta t) + jx_q(t = n\Delta t)] e^{j\omega_c n\Delta t} \quad (4)$$

It is possible to move back and forth between the time and frequency representations of the signals by using the discrete Fourier transform (DFT), which is performed on a block of data consisting of  $N$  samples [7]. The coefficients of the DFT are

$$X(k) = \sum_{n=0}^{N-1} s(n) W_N^{kn} \quad k = 0, 1, \dots, N-1 \quad (5)$$

where  $W_N = e^{j(2\pi/N)}$ .

The quantity  $X(k)$  represents the amplitude of a sinusoid at frequency  $f_k = (k/N)(1/\Delta t) = kf_s/N$ . From the  $N$  Fourier transform points, one then finds an approximate power spectral density function,

$$S(k) = X(k)X^*(k)/Nf_s = |X(k)|^2/(Nf_s) \quad k = 0, 1, \dots, N-1 \quad (6)$$

In the limit of large  $N$ , and after suitable normalization, the function  $S(k)$  approximates the power spectral density of the signal.

If the time samples are separated by  $1/f_s$  seconds, the frequency samples in a discrete complex Fourier transform are separated by  $f_s/N$  Hz. Thus, the width of the frequency window observed by the IM Microscope equals the sampling frequency,  $f_s$ , as sketched in Figure 2. The signals are placed within the window by the frequency-shifting function,  $e^{j\omega_c n\Delta t}$ . Signals are placed within the window to simulate carriers in a transponder.

Memory and run-time limitations caused by the DFT make it necessary to limit the block size,  $N$ . In the first working version of the IM Microscope program,  $N$  could be no larger than 2,048 samples. With a limit on block size, it then became necessary to average individual blocks of data to reduce the variance to an acceptable value, as follows:

$$\bar{S}(k) = \frac{1}{M} \sum_{m=1}^M S_m(k) \quad (7)$$

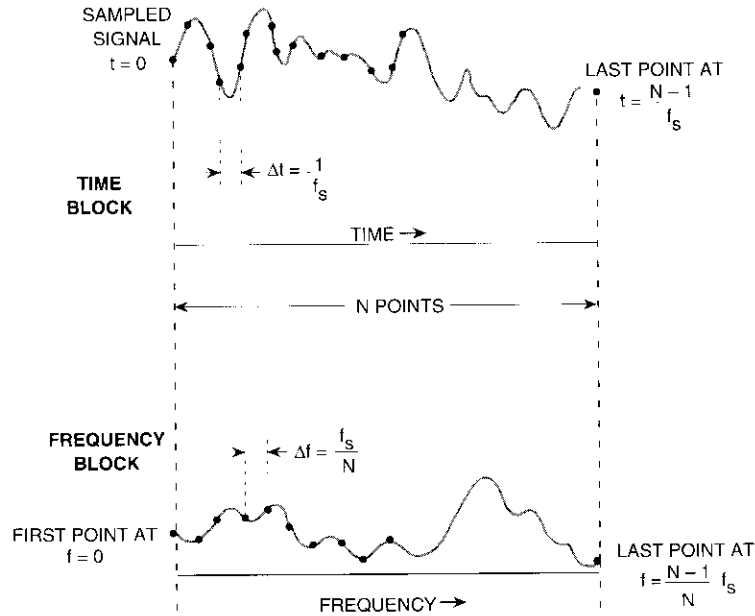


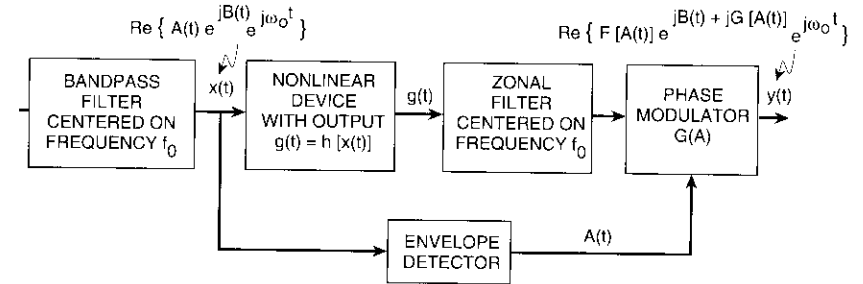
Figure 2. Time and Frequency Windows of Data Blocks With Discrete Fourier Transform

where  $M$  is the number of blocks of data, each with  $N$  points, and subscript  $m$  has been added to denote the spectrum from the  $m$ th block of data.

The spectrum of the complex samples of a bandpass signal "folds" or repeats with period  $f_s$ . With signal combinations near the middle of the window (i.e., near  $f_s/2$ ), folding takes place at the end-points,  $k = 0$  and  $N - 1$ . *Aliasing* is a phenomenon that occurs when components of the signal being analyzed exceed the window end-points, causing the adjacent spectrum replications to enter the analysis window. To avoid aliasing in the IM Microscope, the input signals must be confined to a small portion of the total sampling window.

### Representation of bandpass nonlinearities

A bandpass nonlinearity consists of three functional elements, as shown in Figure 3: a bandpass filter, a memoryless nonlinearity, and another bandpass (zonal) filter [8], [19]. In most satellite communications situations, signals are confined to a fairly narrow range of frequencies centered at  $f_0$ , so the first



Notes:

1.  $x(t)$  is defined using equations (1), (2), and (3).
2.  $y(t)$  is defined in equation (8).
3.  $h \leftrightarrow F$  is a first-order Chebychev transform pair.
4.  $F(A)$  is the AM/AM distortion.
5.  $G(A)$  is the AM/PM distortion.
6.  $\omega_0 = 2\pi f_0$ .

Figure 3. Representation of a Bandpass Nonlinearity With Phase Shift

bandpass filter is implicit. Similarly, because the output stage of a satellite (or earth terminal) amplifier is band-limited, the zonal filtering portion of the model is naturally present in most applications. This model is sufficient to explain so-called AM-to-AM types of nonlinear input/output characteristics. Because minor memory effects in high-power tubes or solid-state devices can have a major impact on the RF phase, a phase shifter is needed in the basic nonlinear model to account for these so-called AM-to-PM effects. The bandpass model, including phase shift, is described in References 1 and 10.

The IM Microscope combines the sampled data version of narrowband signals centered in the vicinity of  $f_0$  with the nonlinear model shown in Figure 3. The nonlinearity acts on the RF signal input to create components at DC,  $f_0$ ,  $2f_0$ ,  $3f_0$ , etc., while the final bandpass filter selects only the terms near frequency  $f_0$ . Calling  $y(t)$  the real output of the final bandpass filter,  $y(t)$  is given in terms of the input complex envelope variables  $A(t)$ ,  $B(t)$ , and  $\omega_0$  as

$$y(t) = \text{Re} \{ F[A(t)] e^{jB(t) + jG[A(t)]} e^{j\omega_0 t} \} \quad (8)$$

where  $F(\bullet)$  is the first-order Chebychev transform of the RF nonlinearity  $h(x)$ . Note that  $\omega_0 = 2\pi f_0$ . The function  $F(\bullet)$  is an envelope nonlinearity embodying AM/AM distortion effects. The phase function,  $G(\bullet)$ , in the exponent is the AM/PM distortion.

The basic theory relating the RF nonlinear function,  $h(\bullet)$ , to the first zone function,  $F(\bullet)$ , is given in Reference 9. The IM Microscope user can select any nonlinear function,  $F(\bullet)$ , although in practice the function is usually obtained as a laboratory measurement relating the single-carrier input and output. The same can be said for  $G(\bullet)$ , which is normally the measured relative phase between input carrier and output carrier as a function of the input amplitude.

### Equivalent gains and intermod noise

The basis for operation of the IM Microscope will be derived herein. With reference to Figures 1 and 3, the nonlinearity input can be written

$$s(t = n\Delta t) = s(n) = \sum_{i=1}^L s_i(n) \quad n = 0, 1, \dots, N-1 \quad (9)$$

This sum is in turn expressible as a composite complex envelope signal,

$$s(n) = A(n)e^{jB(n)} \quad n = 0, 1, \dots, N-1 \quad (10)$$

(Note that the frequency shift portion of the signal has been suppressed here for simplicity.) The post-nonlinearity complex bandpass envelope output,  $v(t = n\Delta t) = v(n)$ , with this input is given by

$$v(t = n\Delta t) = v(n) = F[A(n)]e^{jB(n) + jG[A(n)]} \quad (11)$$

An equivalent representation is that each individual input,  $s_i(n)$ , passes through the nonlinearity essentially unchanged except for a fixed (but presently unknown) gain and phase shift. This complex gain can be designated  $\lambda_i$ , and is known as the equivalent gain.

When these signals are added together, along with their associated gains and phase shifts, they will not necessarily yield the observed output signal. Therefore, a residual signal  $\eta(n)$  is needed as a correction. Thus, if  $L$  individual signals are summed, the output signal can be expressed as

$$v(n) = F[A(n)]e^{jB(n) + jG[A(n)]} = \sum_{i=1}^L \lambda_i s_i(n) + \eta(n) \quad (12)$$

As it stands, this representation is incomplete because any  $L$  arbitrary values for the  $\lambda_i$  can be inserted, with the equation being satisfied by adjusting  $\eta(n)$ . Consequently, additional constraints must be placed on the gains and the residual. If the  $\lambda_i$  are considered as unknowns, they may be adjusted individu-

ally to make the cross correlation of  $\eta(n)$  with each  $s_i(n)$  equal to zero over the signal block (*i.e.*, for  $t = n\Delta t$  from  $n = 1, 2, \dots, N$ ). The function  $\eta(n)$  takes on the meaning of a true uncorrelated residual function; that is, there is no part of  $\eta(n)$  which will contribute to a correlation receiver searching for  $s_i(n)$ . The function  $\eta(n)$  then becomes identical to intermod noise as defined in the literature—namely, a component orthogonal to all input signal components.

The above objective is achieved by taking the cross correlation of each signal,  $s_i(n)$ , with the noise waveform  $\eta(n)$  and equating them individually to zero. Begin by solving for  $\eta(n)$  in terms of the nonlinear output and input signals, using equation (12):

$$\eta(n) = v(n) - \sum_{i=1}^L \lambda_i s_i(n) \quad (13)$$

The cross correlation of  $\eta(n)$  with  $s_j(n)$  over a block of data is equal to the inner product of  $\eta(n)$  with  $s_j^*$  (complex conjugate), which is then set to zero. Carrying out the cross correlation yields a set of  $L$  simultaneous equations, as

$$\sum_{n=0}^{N-1} \eta(n)s_j^*(n) = \sum_{n=0}^{N-1} v(n)s_j^*(n) - \sum_{n=0}^{N-1} \sum_{i=1}^L \lambda_i s_i(n)s_j^*(n) = 0 \quad j = 1, \dots, L \quad (14)$$

After interchanging the order of summation, the set of  $L$  equations in the  $L$  unknowns  $\lambda_1, \lambda_2, \dots, \lambda_L$  can be written

$$\mathbf{H}\boldsymbol{\lambda} = \mathbf{w} \quad (15)$$

where  $\mathbf{H}$  is a positive definite Hermitian matrix of cross correlation values,

$$h_{ij} = \sum_{n=0}^{N-1} s_i(n)s_j^*(n) \quad (16)$$

$\mathbf{w}$  is the vector of output correlations

$$w_i = \sum_{n=0}^{N-1} v(n)s_i^*(n) \quad (17)$$

and  $\boldsymbol{\lambda}$  is the vector  $[\lambda_1 \dots \lambda_L]^T$ .

The solution to equation (17) is the set of desired equivalent gains. When a solution exists, it is unique. If a solution does not exist, it means that one or more of the original input signals is a linear combination of the others, so the

dimensionality needs to be reduced. In a practical communications setting, this condition should not occur.

Note that since the matrix  $\mathbf{H}$  is positive definite and Hermitian, the solution to equation (15) can most effectively be obtained by the Cholesky decomposition method [11], where  $\mathbf{H}$  is decomposed into a product of a lower triangular matrix,  $\mathbf{L}$ , and its conjugate transpose  $\mathbf{L}^{*T}$ , as

$$\mathbf{H} = \mathbf{L}\mathbf{L}^{*T} \quad (18)$$

and the solution to equation (15) can be obtained by solving the following two linear equations by substitution:

$$\mathbf{L}\mathbf{y} = \mathbf{w} \quad (19)$$

$$\mathbf{L}^{*T}\boldsymbol{\lambda} = \mathbf{y} \quad (20)$$

In the IM Microscope,  $\mathbf{H}$  has the additional property of being almost diagonal; that is, the off-diagonal terms are usually very small compared to the diagonal terms since the input signals will tend to have very low cross correlation. As the block size approaches infinity, the cross correlations will tend to zero as a fraction of the total; however, for any finite simulation block size, the residual cross correlations, while small, must be taken into account in order to accurately represent the phase and amplitudes of the equivalent gains. In solving equation (15) using equations (19) and (20), the IM Microscope takes into account off-diagonal terms.

The solution of equation (15) represents Step 1 referred to in the introduction to this section. Substitution of the solution for  $\boldsymbol{\lambda}$  into equation (13) represents Step 2.

The reason for using Monte Carlo or time-based averaging to derive  $\mathbf{H}$  and  $\mathbf{w}$  should now be clear. In a closed-form analytical solution of the simultaneous equations, having  $(L - 1)$  independent phase separations plus other statistical descriptors for each input signal, computation of each term in  $\mathbf{w}$  would require a minimum of an  $(L - 1)$  dimensional integration. However, the Monte Carlo approach requires only a one-dimensional summation over the time variable,  $n$ . This task is easily carried out in a computer simulation where the waveforms are generated and stored in files.

The introduction to Reference 5 gives some historical background on the use of equivalent gains in solving nonlinear problems, while Reference 12 presents a stochastic decomposition approach that was applied to frequency-division multiplex (FDM) signals. Others [13] have used equivalent gains to obtain closed-form expressions for signal-to-total-noise ratio after the nonlinearity. The use of equivalent gains presented here is novel in that it is

embedded in a purely Monte Carlo simulation, allowing a broad category of signal and nonlinearity types to be represented.

### Examples and applications

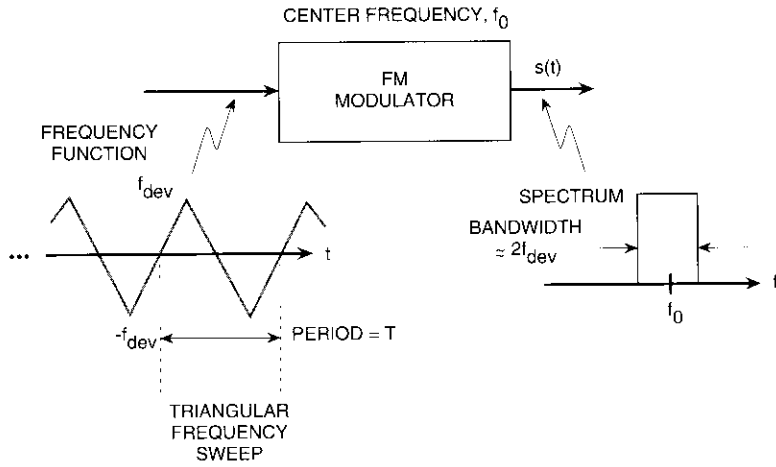
It was anticipated early in the study that most users of an intermod calculator would want to see a power spectrum plot. Hence, a significant effort was directed toward providing graphical output. This section describes the generation of a class of signals that can represent a transponder's frequency plan.

#### Rectangular spectrum inputs

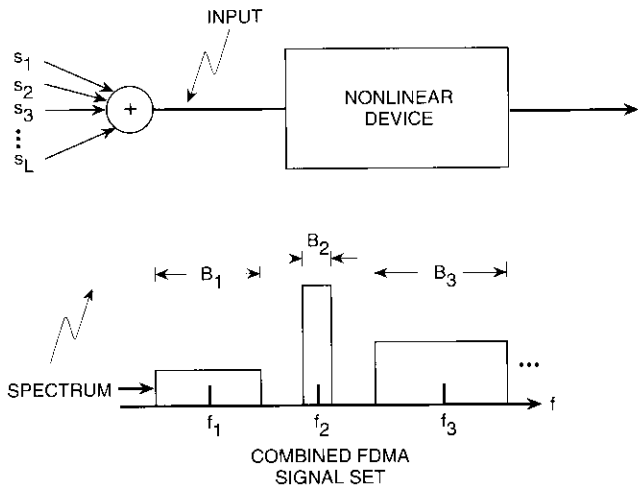
The first working version of the IM Microscope used FDM signals having rectangular signal spectra. This signal set is referred to as ED/CW. The IM Microscope generates a rectangular spectrum by frequency-modulating a carrier with a triangular waveform, as shown in Figure 4. The principle involved is that, for a sufficiently large modulation index, the spectrum of an FM signal approximates the probability density of the frequency modulation [14]. Thus in principle any spectrum shape can be created by properly frequency-modulating a carrier. The modulating frequencies are chosen to yield high modulation index FM, and the triangular start time and its frequency are randomized.

If the triangular frequency functions were not randomized, the intermod spectrum would be based on signals that were not statistically independent (even though they had close to zero cross correlation), and therefore would not contain all the spectral components normally found by analytical approaches. This fact, which was discovered early in the study, is important in applying a Monte Carlo approach. For example, if multiple QPSK DSSS signals are used, but they are all *in bit sync* (a situation that could exist in an earth station where all modems are synchronized to the same source), the intermod spectrum will appear very different than if the signals have a randomized bit sync. In the first case, the intermod products will themselves be QPSK, and hence the same bandwidth as the original signals. In the latter case, the products will be modulated by the out-of-sync condition of their respective components, thereby spreading the bandwidth. This is the same spreading that normally occurs via the convolution operation in analytical approaches. The discovery that intermod products do not necessarily convolve, or spread, if the input signals are not statistically independent necessitated efforts to ensure the randomizing of all input signals in the IM Microscope (see Figure 14).

The complex FM signal,  $s_i(t)$ , centered at frequency  $f_i$  [generated as shown in Figure 4 from a triangular sweep function,  $f(t)$ ], can be written



(a) Signal Generator Module for Energy-Dispersed CW



(b) Composite Input Signal Model

Figure 4. Rectangular Spectrum Signal Generation Module

$$s_i(t) = a_i e^{j\Phi(t)} e^{j2\pi f_i t} \quad (21)$$

where  $\Phi(t)$  is the integral of the instantaneous radian frequency function  $\omega(t) = 2\pi f(t)$ , with  $f(t)$  the triangular sweep function and  $a_i$  a constant that fixes the amplitude of the signal. Expanding the triangular function of Figure 4 in terms of a Fourier series gives

$$f(t) = 2f_{dev} \sum_{k \text{ odd}} (2/k\pi)^2 \cos(k2\pi f_r t) \quad (22)$$

where the repetition frequency,  $f_r$ , is equal to  $1/T$ , with  $T$  being the period. Thus, after integration of the frequency function, the phase function,  $\Phi(t)$ , is given by

$$\begin{aligned} \Phi(t) &= \int_0^t 2\pi f(t) dt \\ &= \frac{8}{\pi^2} \frac{f_{dev}}{f_r} \sum_{k \text{ odd}} \frac{1}{k^3} \sin(k2\pi f_r t) \end{aligned} \quad (23)$$

Representing the signal by its samples at  $t = n\Delta t$ , where, as before,  $\Delta t$  is equal to  $1/f_s$ , with  $f_s$  as the sampling rate [see also equation (14)], gives

$$s_i(n) = a_i e^{j\Phi(n\Delta t)} e^{j2\pi f_i n \Delta t} \quad (24)$$

The FM modulation index is the ratio  $f_{dev}/f_r$ , while the bandwidth of  $s(t)$ ,  $B$ , is given approximately by Carson's rule,

$$\begin{aligned} B &\cong 2(f_{dev} + f_r) \\ &\cong 2f_{dev} \quad \text{if } f_r \ll f_{dev} \end{aligned} \quad (25)$$

Then, the number of cycles of the sweep function in a data block of size  $N$  is given by

$$\begin{aligned} \text{No. cycles per block} &= \frac{\text{Total time in block}}{\text{Time per cycle of triangle}} \\ &= \frac{N}{f_s} \cdot \frac{1}{T} = \frac{f_r}{f_s} N \end{aligned} \quad (26)$$

Ideally,  $N$  should be very large, in order to make the number of cycles of the triangle in all signal blocks very large and thus obtain a good statistical averaging of the intermod. Since memory limitations have constrained the

block size (in an early version to  $N = 2,048$ ), a previously described block-averaging approach is used in which the number of cycles per block is purposely set low—on the order of one to two cycles per block, or less—and multiple blocks of computed intermod are averaged.

In the program that was implemented, randomized triangular start times and incommensurate repetition rates are used, with the triangular sweep functions continuing uninterrupted from one block to the next. It was found experimentally that block counts of 10 to 100 times the number needed for a complete triangular period (reciprocal number of cycles per block) are required to create good statistical estimates of an intermod spectrum. Approximately 50 triangular repetitions were found to yield a good tradeoff between spectrum smoothing and run time.

Subsequently, additional signal sets were added, including the following:

- *QPSK DSSS*. Digital signal modulated by a pseudorandom bit sequence.
- *Filtered QPSK DSSS*. The same as QPSK, but band-limited.
- *Bandpass Thermal Noise*. Bands of noise derived by filtering white noise (independent Gaussian-distributed samples).
- *Bandpass Hard-Limited Thermal Noise*. A single band of thermal noise that is hard-limited to create a broadband constant envelope signal.

Examples of intermod spectra with these various signal combinations are given below.

#### Intermod spectra examples

Figure 5 illustrates a typical satellite transponder in which intermods are generated in the HPA. The input is four FDM signals, each having a specific center frequency, bandwidth, and input backoff relative to HPA saturation. Note that these ED/CW signals were randomized as described above, and multiple block averages were used to find the spectrum. The spectral plots in Figure 5 show information that is readily available with any direct observation of the input/output signals, through simulation or direct laboratory measurement. However, the ratio of signal-to-intermod noise density, or  $C/IM$ , at the point in frequency where the input signal is located is not available in these two plots.

The IM Microscope can now be applied to obtain the intermod spectrum shown in Figure 6. The four signals are spaced with a frequency plan that was chosen to be free of third-order intermods at the points where the input signals

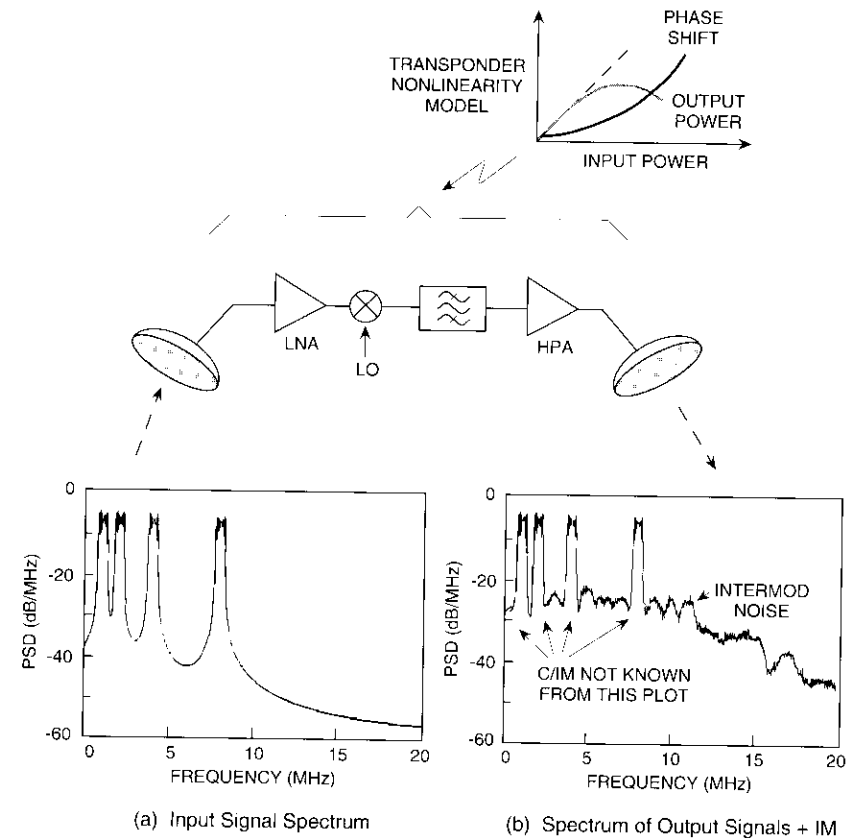


Figure 5. Example of Transponder Loading With Equal Amplitude Signals and 3rd-Order IM-Free Spacing

are located. (This is an example of a "1, 2, 4, 8" plan, where the number indicates the center frequency's location [here, in megahertz] relative to an arbitrary starting point of zero.) The design of plans that are free of third-order intermods is discussed in Reference 5. Since  $\eta(t)$  does not contain any intermods of the form  $2A - B$  or  $A + B - C$  (see Reference 15 for explanation), there are dips in the spectrum at the signal center frequency locations, hidden by the signals in Figure 5. Therefore, the intermod that appears at these locations in Figure 6 consists of all remaining products (fifth order, seventh order, etc.). Many approaches have been developed to design and analyze intermod-free or

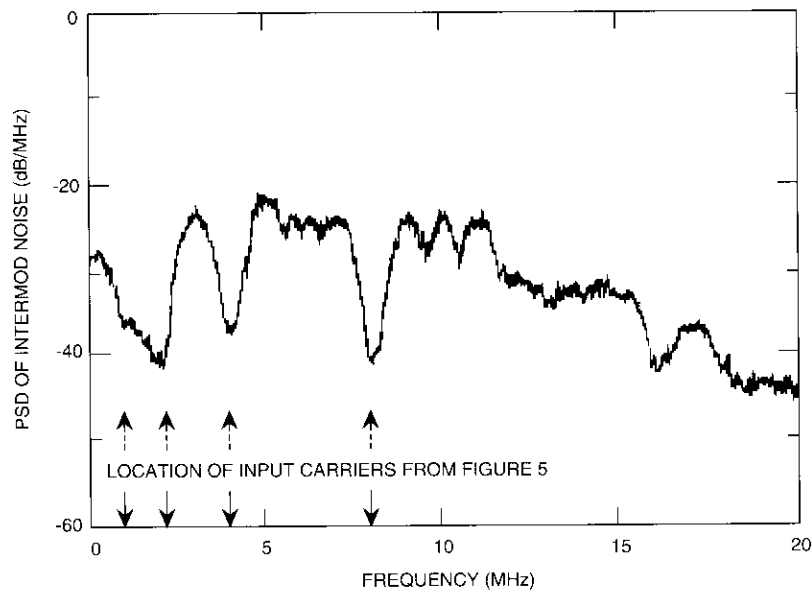


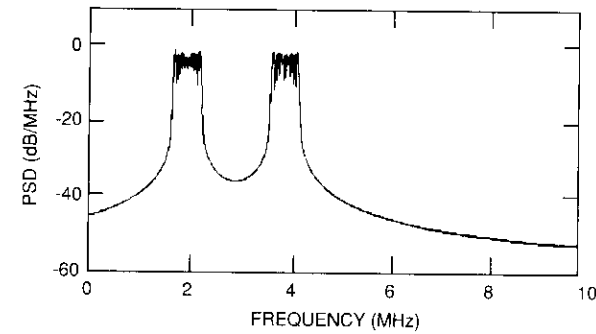
Figure 6. *IM-Only Spectrum With 3rd-Order IM-Free Carrier Plan*

low-intermod frequency plans [16], but all depend on the ability to compute the spectral level of intermod noise at the locations where the signals themselves are located.

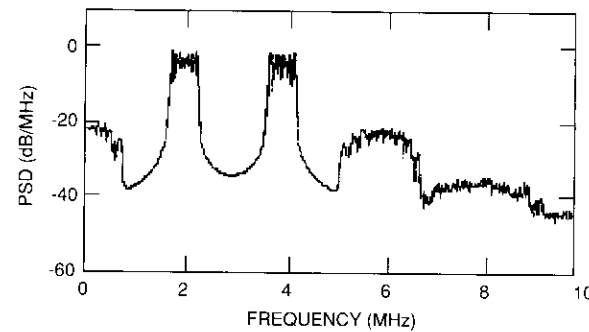
Figures 7 and 8 give other examples of input/output spectra and associated intermod based on use of the IM Microscope. The signal model used in these figures is ED/CW. The nonlinear characteristic used in Figures 5 through 8 was a measured traveling wave tube amplifier (TWTA) AM/AM and AM/PM curve.

The IM Microscope can handle a wide variety of nonlinear characteristics. Figure 9 shows a few representative types. Any piecewise continuous or analytically expressible curve can be employed; there is no need to represent the characteristic in terms of a polynomial expansion.

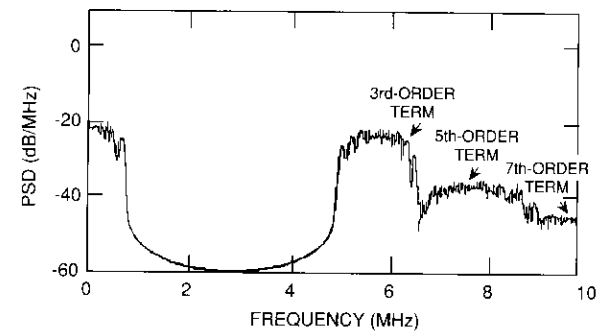
Another limitation of previous techniques has been the need to group intermod products by "order" (e.g., third order, fifth order, etc.). By computing the exact intermod waveform as a process of elimination, the IM Microscope is actually computing all harmonics of the intermod at once, to within the numerical accuracy permitted by the digital simulation. Figure 10 shows



(a) Spectrum of Input Signals

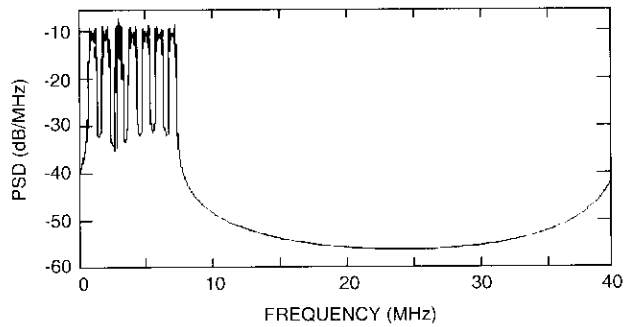


(b) Spectrum of Output Signals + IM

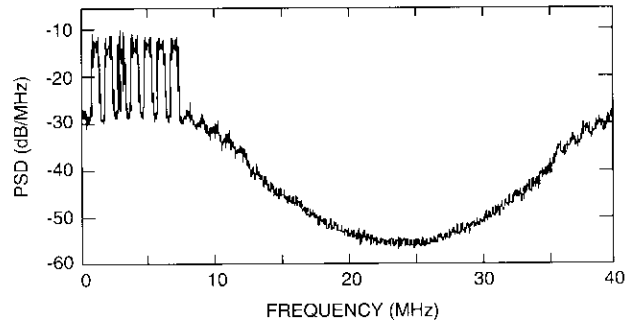


(c) Spectrum of IM Only

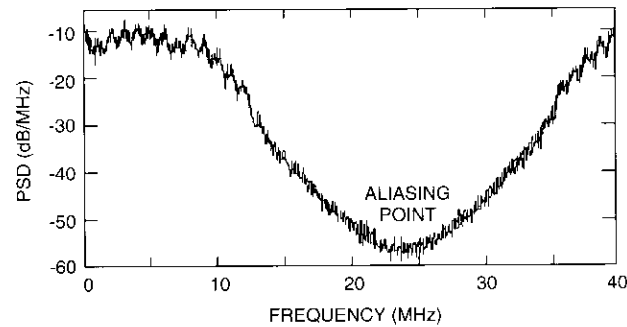
Figure 7. *Two-Carrier Frequency Plan Showing IM Generation Out-of-Band*



(a) Spectrum of Input Signals



(b) Spectrum of Output Signals + IM



(c) Spectrum of IM Only

Figure 8. Picket Fence Frequency Plan: Equal Size and Equal Spacing

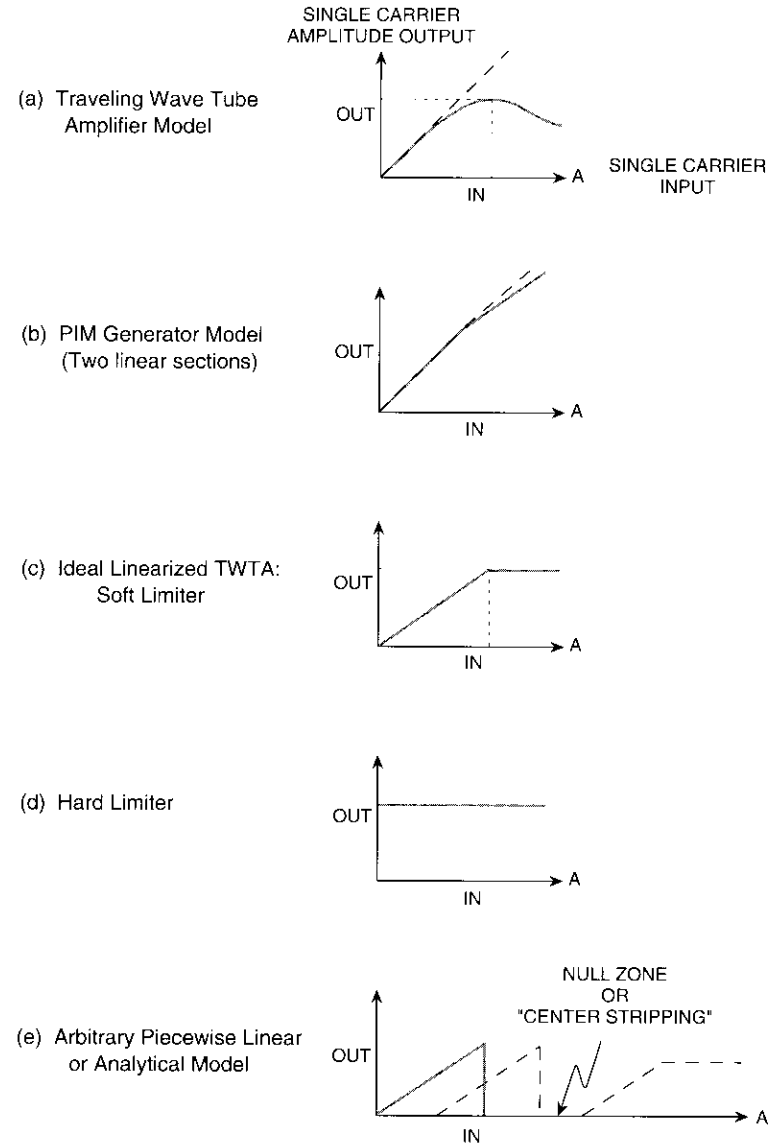


Figure 9. Examples of AM/AM Characteristics Allowed With the IM Microscope

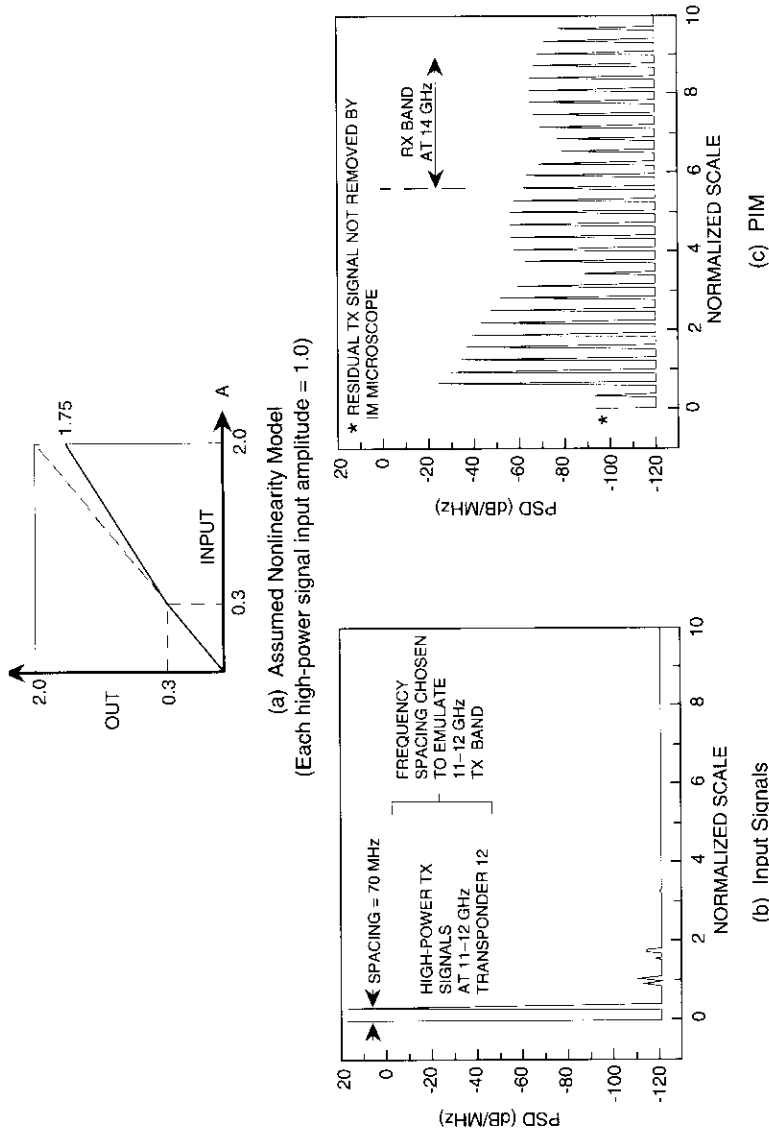


Figure 10. Example of Passive IM Calculation With Nonlinearity Model Consisting of Two Linear Sections

the spectrum for a hypothetical PIM nonlinearity model (given in the inset), showing the generation of very high orders of intermod originating from two CW signals. Two equal CW signals are illustrated being transmitted at the low end of the frequency scale through a hypothetical antenna system, with PIM components being generated in the receive band of the satellite's up-link at the upper end of the scale. As is usual in these cases, no filtering can take place once the signal leaves the antenna. Frequency spacings are chosen to simulate a Ku-band satellite. (It should be noted that an actual PIM nonlinearity would be much more subtle than that shown in Figure 10, and the frequency plan would be more complex than just two equal signals).

Note that by varying the breakpoint in the AM/AM characteristic, the PIM spectrum changes as shown in Figure 11. For the cases illustrated in Figures 10 and 11, where the intermod of interest is totally outside the transmit band, straight digital simulation could have been used as an alternative to the IM Microscope because subtraction of the input signals was not required. However, to see the effects of PIM in-band with wanted signals, or to see the actual time domain PIM waveform, the IM Microscope is necessary. Note that the IM Microscope could be used to find a nonlinearity that matches a given spectrum of a system under test. The nonlinearity shape might reveal the physical nature or source of the imperfection.

Figures 12 and 13 illustrate still other examples of the IM Microscope. In Figure 12, three bands of noise were chosen to simulate a network of spread spectrum users. Individual signals representing narrowband digital signals are added in the guard bands. The resulting intermod spectrum consists of discrete and continuous components. In Figure 13, a filtered QPSK signal is added to a large unmodulated CW signal (representing a jammer). The intermod spectrum is revealed as a series of discrete and continuous components.

**Nonlinear power division and the IM Microscope**

This discussion has thus far emphasized the spectrum of the intermod. In operations where there is a large disparity in input signal levels, the division of a nonlinearity's available RF power among those signals can be of primary interest. For example, in a transponder with one or two large FM/TV or QPSK/TDMA signals sharing the band with one or two small single-channel-per-carrier (SCPC) signals, both the division of power and the intermod spectrum are important. Another example is a military satellite with a single large hostile carrier attempting to jam a transponder filled with traffic.

In general, a large signal will capture power in an amplitude-limiting nonlinearity and suppress the smaller signals. For a center-stripping nonlinearity,

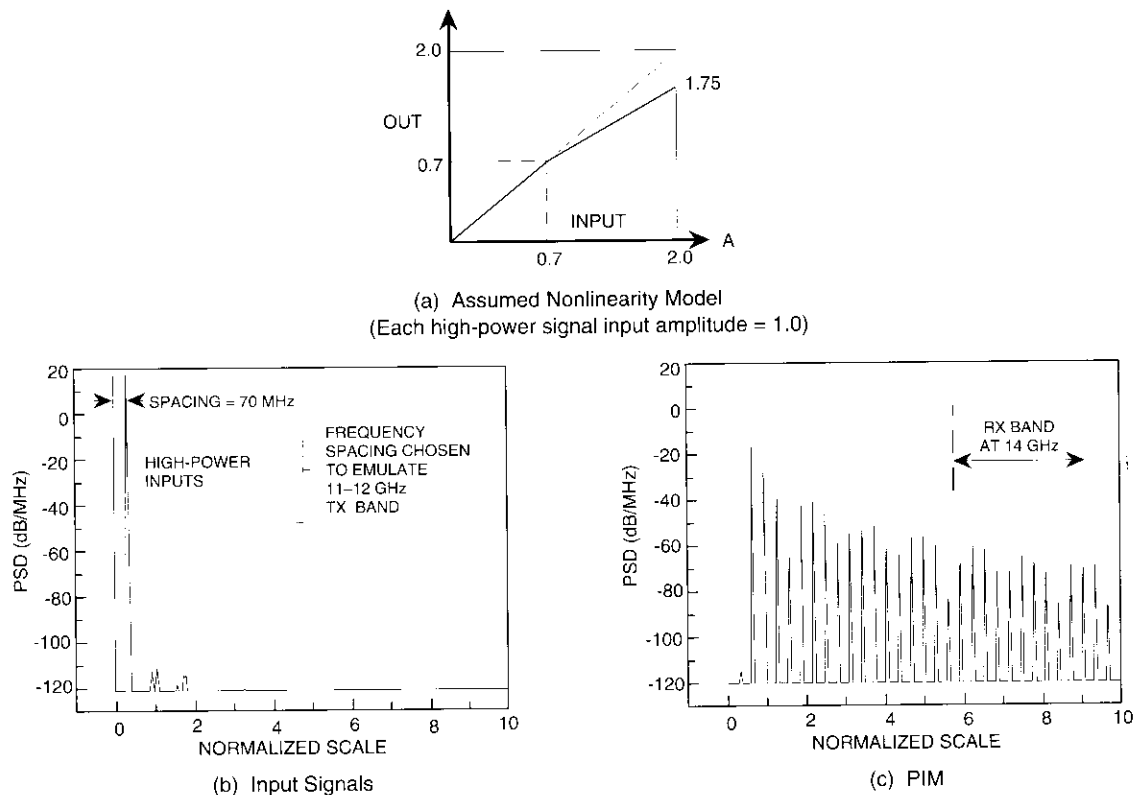


Figure 11. Effect of Varying Two-Section Nonlinearity Model (from Figure 10) to Observe Changes in PIM

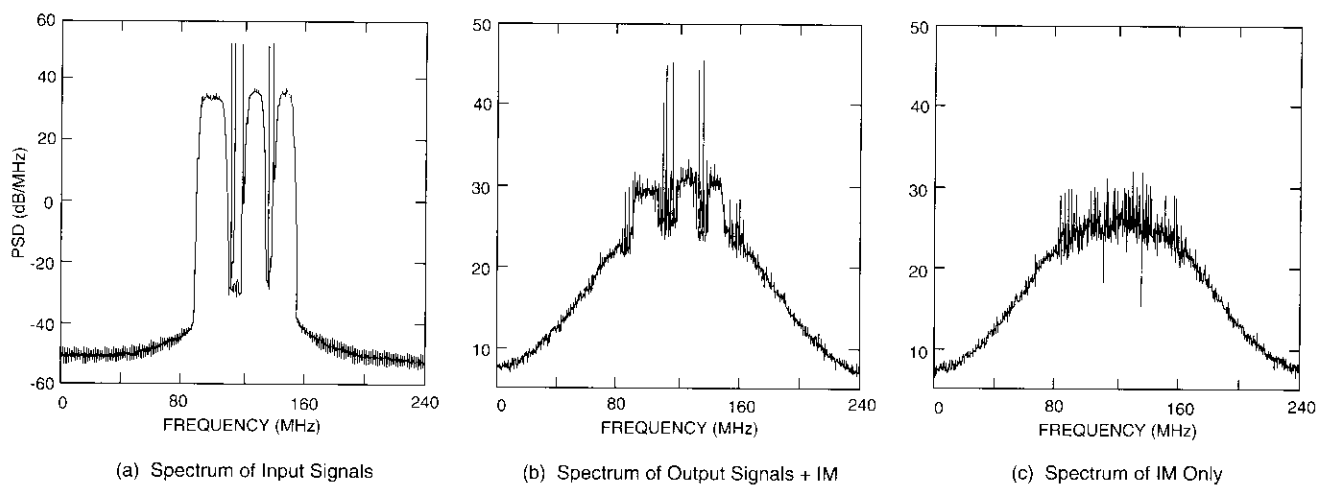


Figure 12. Simulation of Network of Spread Spectrum Users and Unspread Digital Carriers  
(Thermal noise bands and CWs)

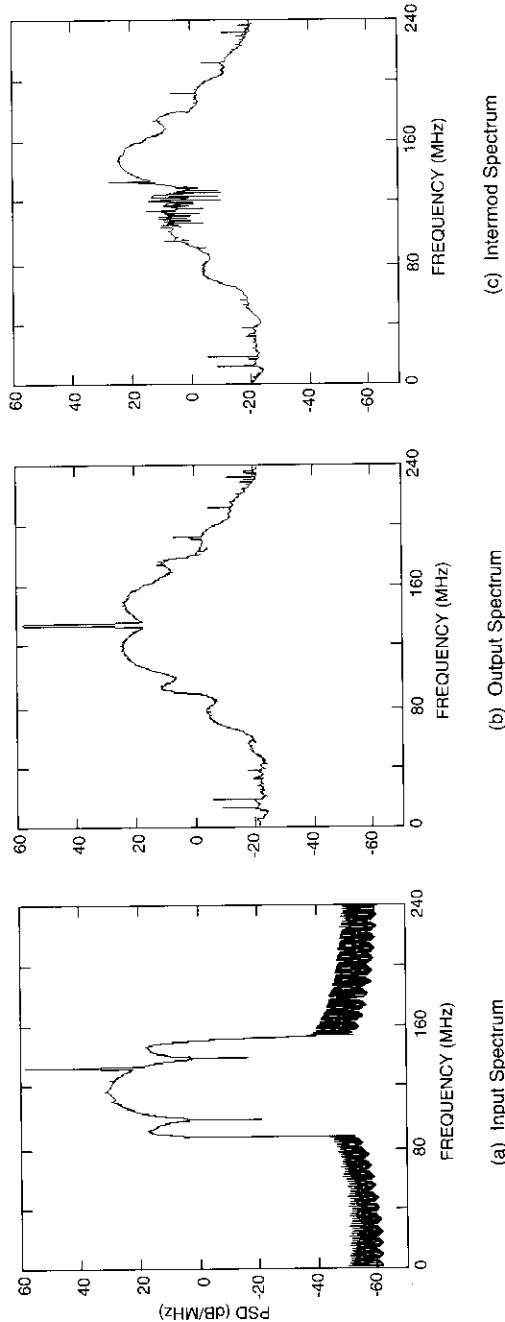


Figure 13. 40-Mbit/s QPSK DSSS Signal Plus CW Jammer in Hard Limiter (Input band-limited to 60 MHz)

as defined in References 3 and 4 and illustrated in Figure 9e, the situation is reversed and a small signal can emerge *enhanced* relative to a larger jamming signal.

Unequal power division among the signals transiting the nonlinearity may be computed by finding appropriate equivalent gains. By suppressing the total time variable in a block of samples, the total energy of the signal can be used in place of the average power for convenience of calculation, as shown below. The total energies in the signals and intermod components can be expressed as follows:

$$\text{Input total energy} = \sum_{n=0}^{N-1} |s(n)|^2 = \sum_{i=1}^L \sum_{j=1}^L \sum_{n=0}^{N-1} s_i(n) s_j^*(n) = \mathbf{u}^T \mathbf{H} \mathbf{u} \quad (27)$$

$$\text{Output total energy} = \sum_{n=0}^{N-1} |v(n)|^2 = \boldsymbol{\lambda}^T \mathbf{H} \boldsymbol{\lambda}^* + \text{IM energy} \quad (28)$$

$$\text{IM energy} = \sum_{n=0}^{N-1} |\eta(n)|^2 \quad (29)$$

where  $\mathbf{u}$  is the unit vector. Terms corresponding to the on-diagonal elements of matrix  $\mathbf{H}$  in equations (27) and (28) are the computed energies in the signals at the input and output, respectively, as

$$i\text{th signal input energy} = \sum_{n=0}^{N-1} |s_i(n)|^2 \quad (30)$$

$$i\text{th signal output energy} = |\lambda_i|^2 \cdot \sum_{n=0}^{N-1} |s_i(n)|^2 \quad (31)$$

In a simulation the terms associated with the off-diagonal elements of  $\mathbf{H}$  take negative and positive values that are small compared to those associated with the on-diagonal elements. For most practical applications, the power division can be accurately represented by equations (30) and (31), for  $i = 1, 2, \dots, L$ .

An important example of the use of power division involves a transponder containing a hard limiter in the presence of jamming. The input is characterized by a certain power ratio,  $J/S$ , while the output ratio,  $(J + \text{IM})/S$ , determines the ultimate performance of a receiver. In a hard-limiting transponder (see Figure 9d),  $(j + \text{IM})/S$  is usually a factor of four (or 6-dB) worse than the input  $J/S$ , when  $J$  is large compared to  $S$  and the jammer is a CW [17]. These types of standard analysis results are easily confirmed with the IM Microscope.

Note that if computations of power division can be run without the need for spectral plots (Fourier transforms), there will be a significant savings in run time and computer memory.

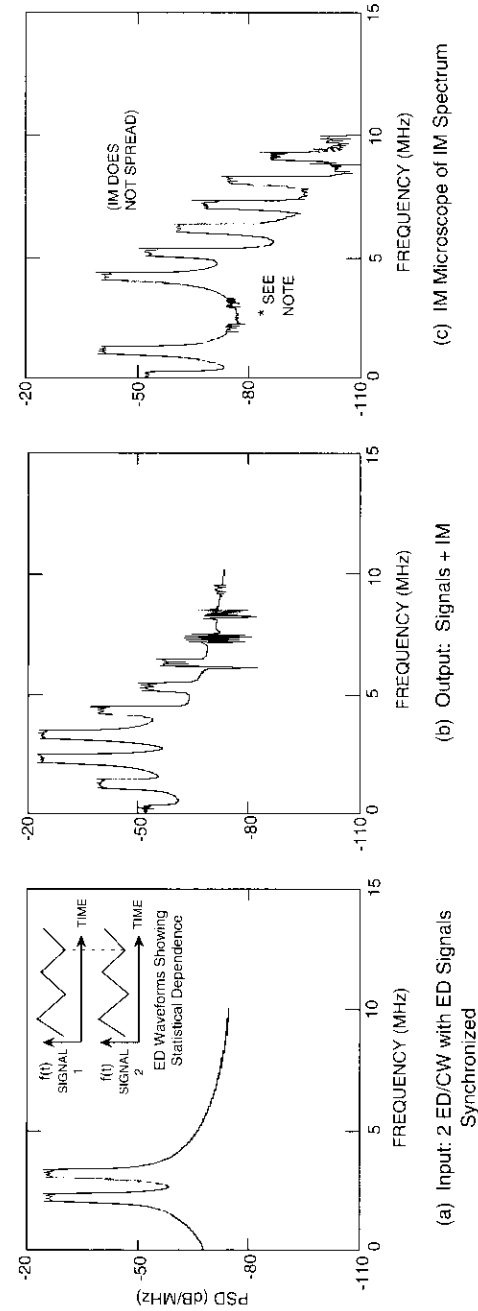
**IM Microscope results with nonrandomized input signals**

The simulation aspects of the new algorithm present many challenges which have not yet been thoroughly explored. While most commonly used signals in satellite systems are automatically orthogonal in the sense of frequency difference or information content, they are not necessarily statistically independent. Thus, two digital signals originating in the same earth station may be transmitted at different center frequencies but in bit sync. These signals will not have the same intermod spectrum as two digital signals whose bit streams are out of sync or that have incommensurate bit periods. Analytical approaches in the literature always assume that the signals are statistically independent. In this case, obtaining the spectrum of a harmonic involves the convolution of spectra from the fundamental components. The IM Microscope, on the other hand, always finds the spectrum that would be measured in a laboratory situation under rigorously identical input signal conditions, regardless of the statistical independence or non-independence of the inputs.

As an example of the spectrum obtained with nonrandomized signals, Figure 14 shows a two-carrier ED/CW input/output IM Microscope plot with a single signal block used in the computation. The triangular ED signals are synchronized and of equal amplitude. In contrast to Figure 7, where the triangular waveshapes are randomized and block averaging is used, none of the intermod spectrum components spread out, even at the higher harmonics. This result should not be interpreted as wrong, since it is the correct answer when the ED waveforms are synchronized, and would be observed in a laboratory measurement under identical conditions.

**Conclusions**

A new procedure for solving for intermod distortion in satellite systems has been developed at COMSAT and used in a number of applications. The IM Microscope has several attributes which set it apart from other methods—in particular its ability to solve for the intermod waveform directly, by a process of elimination. It can employ an arbitrary nonlinearity and, unlike previous approaches, does not depend on a series expansion. This procedure has been used to resolve practical satellite engineering problems that could not have been completed in any other way.



\*NOTE: These figures were created with a test version of the IM microscope that contained a minor error in calculation  $\lambda_1$  and  $\lambda_2$ , resulting in a small residual component of the original signals,  $S_1$  and  $S_2$ .

Figure 14. IM With Statistically Dependent Sawtooth ED Signals

## Acknowledgments

The authors would like to thank COMSAT World Systems for its support and funding of the work reported herein. S. J. Campanella's recommendations for revision of the original manuscript, and his careful proofreading, were very helpful. C. Pike, who used the IM Microscope in his work while at COMSAT [3], first demonstrated its use with filtered noise, tested various windowing functions, and contributed Figures 12 and 13. J. Lee used the IM Microscope while at COMSAT [4], and added to the memory capability of the original program by porting it to a new FORTRAN compiler, adding new graphics, and, with I. Brelian, adding the QPSK DSSS signal model.

## References

- [1] O. Shimbo, "Effects of Intermodulation, AM-PM Conversion and Additive Noise in Multicarrier TWT Systems," *Proc. IEEE*, Vol. 59, No. 2, February 1971, pp. 230-238.
- [2] J. C. Fuenzalida, O. Shimbo, and W. L. Cook, "Time-Domain Analysis of Intermodulation Effects Caused by Nonlinear Amplifiers," *COMSAT Technical Review*, Vol. 3, No. 1, Spring 1973, pp. 89-143.
- [3] D. Arnstein, C. Pike, and G. Estep, "On-Board AJ Enhancement Using Adaptive Nonlinear Processing: Practical Aspects of Smart AGC™ Implementation," IEEE Military Communications Conference (MILCOM '92), San Diego, CA, October 1992, *Conf. Rec.*, Vol. 1, pp. 7.5.1-7.5.7.
- [4] D. Arnstein and J. W. Lee, "AJ Performance of Smart AGC™ in MILSATCOM Networks: A Review of Space System Design Principles and Applications," AIAA 14th International Communications Satellite Systems Conference, Washington, D.C., March 1992, *Conf. Rec.*, pp. 23-31.
- [5] D. Arnstein, "Power Division on Spread Spectrum Systems with Limiting," *IEEE Transactions on Communications*, Vol. COM-27, No. 3, March 1979, pp. 574-582.
- [6] C. W. Helstrom, *Statistical Theory of Signal Detection*, Oxford, England: Pergamon Press, 1968, Ch. 2.
- [7] A. V. Oppenheim and R. W. Schaffer, *Digital Signal Processing*, Englewood Cliffs, New Jersey: Prentice-Hall, 1975, Ch. 3.
- [8] W. B. Davenport and W. L. Root, *An Introduction to the Theory of Random Signals and Noise*, New York: McGraw-Hill, 1958, Ch. 13, "Introduction to the Transform Method."
- [9] N. Blachman, "Detectors, Bandpass Nonlinearities, and Their Optimization: Inversion of the Chebyshev Transform," *IEEE Transactions on Information Theory*, Vol. IT-17, No. 4, July 1971, pp. 398-404.
- [10] A. Berman and C. Mahle, "Nonlinear Phase Shift in Traveling Wave Tubes as Applied to Multiple Access Communications Satellites," *IEEE Transactions on Communication Technology*, Vol. 18, No. 1, February 1970, pp. 37-48.
- [11] R. W. Hornbeck, *Numerical Methods*, New York: Quantum Publishers, 1975.
- [12] R. G. Lyons, "Stochastic Analysis of Signal Sharing in a Bandpass Nonlinearity," *IEEE Transactions on Communications*, Vol. COM-22, No. 11, November 1974, pp. 1778-1788.
- [13] N. M. Blachman, "The Signal X Signal, Noise X Noise, and Signal X Noise Output of a Nonlinearity," *IEEE Transactions on Information Theory*, Vol. IT-14, No. 1, January 1968, pp. 21-27.
- [14] D. Middleton, *An Introduction to Statistical Communication Theory*, Los Altos, California: Peninsula Publishing, 1987, p. 624.
- [15] R. J. F. Fang and W. A. Sandrin, "Carrier Frequency Assignment for Non-linear Repeaters," *COMSAT Technical Review*, Vol. 7, No. 1, Spring 1977, pp. 227-245.
- [16] X. T. Vuong *et al.*, "Some Practical Strategies for Reducing Intermodulation in Satellite Communications," *IEEE Transactions on Aerospace and Electronic Systems*, Vol. 24, No. 6, November 1988, pp. 755-765.
- [17] C. Cahn, "A Note on Signal to Noise in Band Pass Limiters," *IRE Transactions on Information Theory*, Vol. 7, No. 1, January 1961, pp. 39-43.



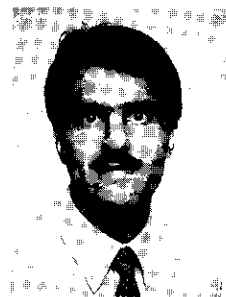
Donald S. Arnstein received a B.S.E.E. (*magna cum laude*) from City College of New York in 1962; Master's and Professional Engineer's degrees from the Massachusetts Institute of Technology in 1963 and 1967, respectively; and a Ph.D. from the University of California, Los Angeles, in 1972. He joined COMSAT in 1979 and is currently Manager of the Satellite Systems Department in the Microwave Technology and System Division at COMSAT Laboratories, where he provides systems analysis and design support for international, domestic, military, and mobile satellite systems. Dr. Arnstein is a Senior Member of IEEE; past Secretary of the Satellite and Space Communications Subcommittee of the IEEE Communications Society; past Chairman of the Washington, D.C., chapter of the IEEE Communications Society; and a member of Tau Beta Pi, Eta Kappa Nu, and Sigma Xi engineering honor societies.



*Xuyen T. Vuong obtained his B.S.E.E., M.Eng., and Ph.D. from California State University, Carleton University, and the University of Western Ontario, respectively. He received United States AID Scholarships during his undergraduate study, and Ontario Graduate Fellowships during his graduate study. He also taught and conducted research as a Postdoctoral Fellow and an Assistant Professor at the University of Ottawa and Concordia University.*

*Dr. Vuong has held various science, engineering, and management positions at COMSAT Laboratories and COMSAT Systems Division, GTE Spacenet, Telesat Canada, Canadian Astronautics and Spar Aerospace, and cofounded Syster Telecommunications. Currently, he is a Staff Engineer at Science Applications International Corporation (SAIC), performing systems engineering and analysis on future military satellite communications systems. He has published more than 40 journal and conference papers on satellite communications, optimization techniques, and state estimation and control, and is a Senior Member of IEEE.*

*Calvin B. Cotner received a B.S. in electrical engineering (cum laude) from Princeton University in 1962, and an M.S.E.E. from Cornell University in 1964. He has been with COMSAT since 1967 and is currently Director of Technical Liaison and Analysis with COMSAT World Systems. His primary technical interests are earth station design, transmission analysis, and high-power amplifiers. He has held several technical management positions in COMSAT Laboratories, COMSAT General, and COMSAT World Systems, including representing the U.S. Signatory on the INTELSAT Board of Governors' Technical Advisory Committee for 5 years. He is a colonel in the Signal Corps, U.S. Army Reserve, and a Commandant's List Graduate of the U.S. Army Command and General Staff College. He is a Senior Member of AIAA.*



*Haresh M. Daryanani received a B.S.E.E. with Honors from Old Dominion University in 1987. As a member of the Systems Analysis Department in COMSAT Systems Division (CSD), he provided systems engineering support for the design and integration of turnkey earth terminal systems, including earth terminal specifications and overall end-to-end network analyses. As a member of CSD's Firmware Engineering Department, he was responsible for developing and testing DSP and microprocessor code resident in Inmarsat-M/B maritime communications networks. Prior to joining COMSAT in 1988, he served as a research*

*assistant in the Instrument Research and Flight Electronics Divisions at NASA's Langley Research Center.*

*Mr. Daryanani is currently a Staff Engineer with the Defense Information Systems Agency in Reston, Virginia. He is a member of IEEE and the Eta Kappa Nu and Tau Beta Pi engineering honor societies.*

# ***Real-time transmission of group 3 facsimile over interconnected public switched digital mobile satellite networks***

S. DIMOLITSAS, J. H. RIESER, AND H. FELDMAN

(Manuscript received April 16, 1992)

## ***Abstract***

The importance of facsimile communication over public switched telephone networks (PSTNs) is evidenced by the rapid growth in the number of group 3 facsimile terminals in use. An approach is described whereby facsimile signals are demodulated and their associated protocols are converted, using a facsimile interface unit (FIU), to a format suitable for transmission over Inmarsat maritime and land-mobile digital channels. The FIU concept was developed to allow off-the-shelf facsimile terminals to be interconnected via the PSTN through Inmarsat's satellite networks, in order to permit the conversion of group 3 facsimile point-to-point protocols to point-to-multipoint operation; to compensate for the longer transmission delays encountered in mobile satellite systems; and to permit facsimile call recovery procedures to be successfully concatenated with satellite channel error detection mechanisms. To perform these functions, the FIUs comprise two protocols: a core protocol that permits the conversion of the group 3 facsimile protocols to meet mobile service requirements, and a satellite channel conversion protocol that is used to transport facsimile user data and control signals over Inmarsat's mobile data channels. This paper addresses the core protocols in detail.

## ***Introduction***

The rapid annual growth in the number of end user group 3 facsimile terminals demonstrates the importance of telecommunications employing facsimile transmission over public telephone networks. However, the

transmission of group 3 facsimile over digital mobile satellite networks presents a challenge because facsimile signals, which are transmitted as 9.6-kbit/s voiceband data over the public switched telephone network (PSTN), cannot be reliably encoded and transmitted using standard waveform coding techniques operating below 40 kbit/s [1]. Since the data channel transmission rate for Inmarsat's new digital services does not exceed 10.5 kbit/s, support of facsimile traffic requires the development of specialized, cost-effective solutions for interworking with terminals connected to the PSTN [2],[3]. Such solutions must reduce facsimile channel bit rate requirements and also convert facsimile protocols to a format that can be supported over digital mobile satellite networks.

These requirements can be met through waveform demodulation/remodulation methods whereby voiceband facsimile signals are converted into a digital bit stream prior to transmission over the satellite channel. There are essentially two approaches for carrying demodulated facsimile traffic over the network: real-time, and store-and-forward.

In real-time systems, facsimile messages are delivered to the destination before a call is cleared between the originating customer's facsimile terminal equipment (FTE) and the destination customer's facsimile terminal. Real-time facsimile service possesses important characteristics that contribute to its popularity, such as the assurance that the message has been received by the destination before a call is cleared, and the resulting simplification in customer billing if the receiving facsimile terminal happens to be incompatible or temporarily unavailable, or if the access network is unable to deliver the message to its destination.

In store-and-forward systems, a call is normally cleared between the originating facsimile terminal and the near-side facsimile interface or storage node before the message is delivered to the destination facsimile terminal. Such systems can improve the efficiency of facsimile message transmission over satellite links by eliminating some of the facsimile terminal handshaking signals. Conversely, the storage requirements at both earth stations can be substantial, and the call management requirements can curtail any benefits derived from additional reductions in transmission rate. Store-and-forward systems have typically found use in fixed thick-route, large-volume document transfer applications where economies of scale can be realized.

Since immediacy is essential in mobile communications systems, it is not surprising that real-time transmission is the preferred means of communication whenever it is economically and technically feasible. This paper describes the core characteristics of a real-time demodulation/remodulation ap-

proach in which voiceband facsimile signals are converted to a format suitable for transmission over Inmarsat-B and Inmarsat-M digital channels.

### **Network configuration**

As mentioned above, the transmission of group 3 facsimile over digital mobile satellite networks requires that voiceband facsimile signals be converted to a demodulated bit stream. Implementation of this approach requires that a channel-dedicated facsimile interface unit (FIU) be functionally placed between a customer's facsimile terminal and the satellite channel. That is, one FIU is required at each end of the communications channel.

For the fixed (PSTN)-based facsimile terminal customer, the FIU is normally part of the land earth station (LES) equipment, which is owned by the communications service provider. (See the simplified network configuration in Figure 1.) In this case, the FIU is remotely interconnected via the PSTN to the customer's facsimile terminal using a four-wire interface, with the two-wire conversion being provided elsewhere in the network, such as at a local telephone exchange. The LES must have an FIU available for each channel that may be simultaneously carrying facsimile traffic. It is envisioned that some calls will initially be set up in a voice mode (*i.e.*, a voice codec and a voice-grade satellite circuit will be assigned to the incoming call). However, in the case of automatic calling/answering, an FIU will be reassigned to the incoming facsimile circuit shortly after call initiation and prior to completion of phase A of the group 3 facsimile protocols [4]. The general principles behind the in-call service modification procedures will be addressed later.

For the mobile customer, the FIU is part of the mobile earth station (MES) equipment. In this case, the FIU is located close to the customer's facsimile terminal, and may be connected to the terminal via a two-wire interface. As with the LES FIU, one facsimile interface is required for each active channel carrying facsimile traffic. However, in this case one FIU will probably be permanently provided for each facsimile terminal associated with an MES.

### **Group 3 facsimile protocols**

Group 3 facsimile terminals employ protocols that are defined in International Telephone and Telegraph Consultative Committee (CCITT) Recommendation T.30 [4], which provides significant detail regarding the mandatory and optional features applicable to facsimile calls. However, to illustrate some of the interworking aspects addressed later in this paper, a simplified one-page protocol (which includes only mandatory capabilities) is presented

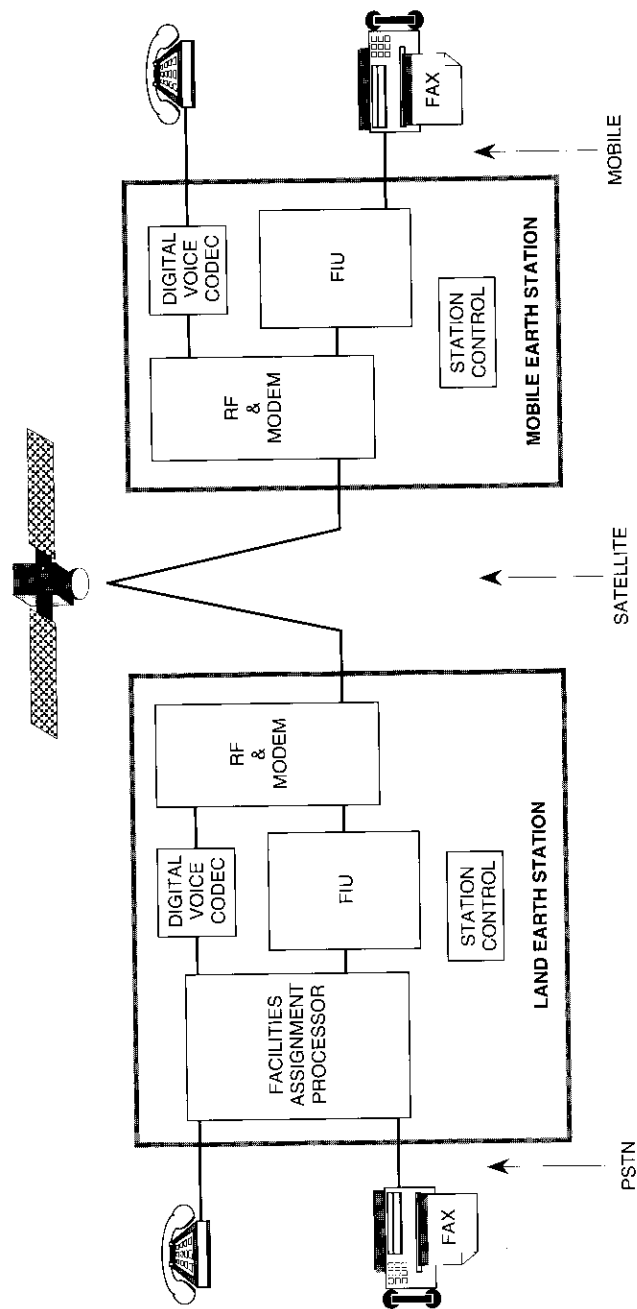


Figure 1. Network Configuration for Facsimile Transmission Over the Inmarsat Space Segment

in Figure 2. It can be seen that facsimile terminals employ several types of signals during a facsimile call, including the following:

- *CNG*. An 1,100-Hz interrupted "calling tone" which the calling terminal sends to the called terminal.
- *CED*. A 2,100-Hz echo control disabling, or called terminal identification, tone transmitted in the called-to-calling terminal direction.
- *NSF/CSI/DIS*. One or more of these signals are returned by the called terminal to indicate its capabilities (*e.g.*, the capability to receive at 9,600 bit/s). The most common signal is the digital identification signal (DIS), which is mandatory. The other signals are optional and relate to nonstandard facilities (NSF) and called subscriber identification (CSI).
- *DCS*. The calling terminal, having received the DIS, issues the digital command signal (DCS) to set up the signaling rate and other features to be used for the remainder of the facsimile call.
- *Training (TR)*. The training signal is used to condition the equalizing functions of the called terminal.
- *TCF*. This is a training check sequence which immediately follows the training signal and allows the called terminal to determine whether it has been trained satisfactorily.
- *CFR*. If training is acceptable (on the basis of TCF reception), a "confirmation to receive" signal is returned by the called terminal. Other possible signals returned include "failure to train" (FTT) or "retrain" (positive or negative). Reception of any of these other signals would indicate to the transmitting terminal that the called terminal is requesting to be retrained.
- *Message (MSG)*. This is the actual bit-encoded image of the page being transmitted. It is always preceded by training (TR), with no gap in signal energy.
- *EOP/MPS*. One of these signals will be sent following each page transmitted, to indicate an end-of-pages/procedure (EOP) or a multipage signal (MPS) transmission.
- *MCF*. The message confirmation signal (MCF) is sent from the receiver to the transmitter to acknowledge receipt of the EOP or MPS message.
- *DCN*. This signal is issued by the calling terminal to disconnect (DCN) and terminate the call.

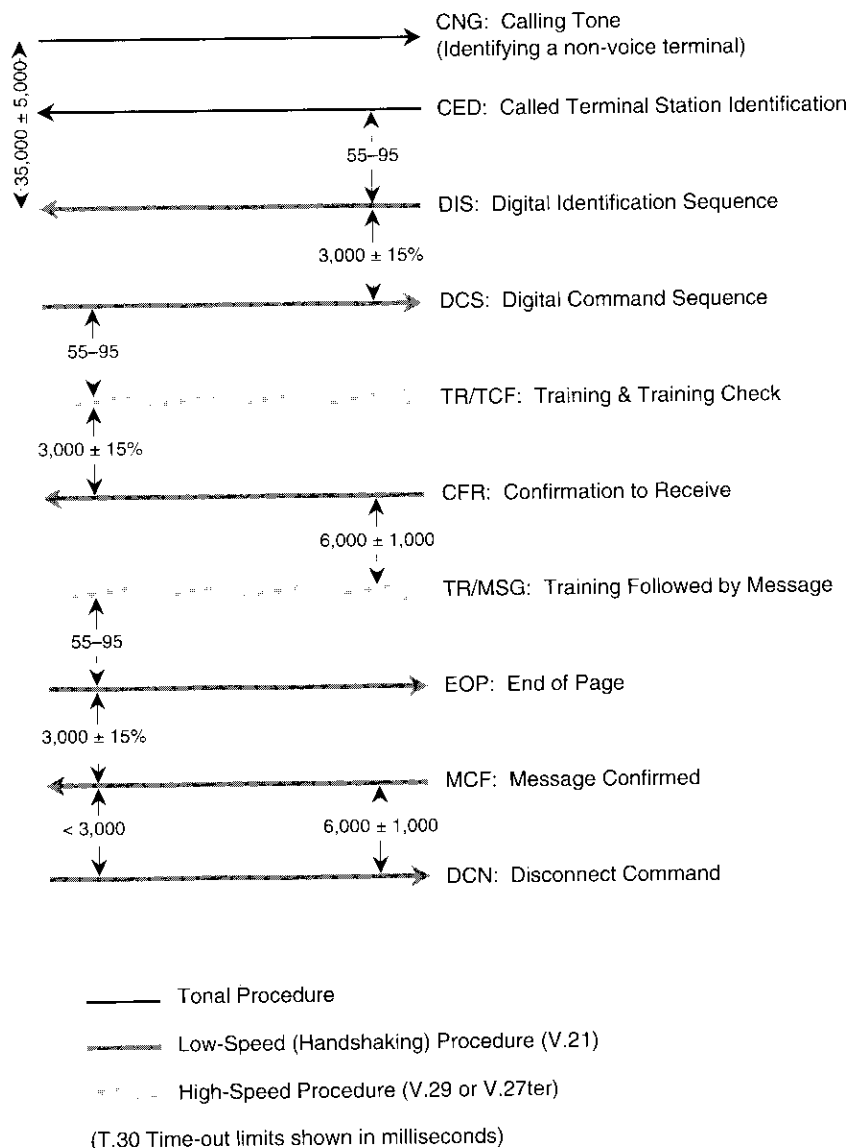


Figure 2. Typical Single-Page Group 3 Facsimile Document Transmission Protocol

### Basic functionality

The FIUS perform several basic functions. First, they intercept the incoming voiceband signal waveforms in the facsimile-terminal-to-satellite direction and demodulate them for transmission over the digital satellite channel. Subsequently, the FIUS remodulate the digital signals received over the satellite channel, converting them back to voiceband signals. They then transmit the voiceband signals to the customer terminal in the satellite-to-facsimile-terminal direction. Finally, the FIUS perform protocol conversions so that the group 3 facsimile protocols become compatible with the transport channel constraints of the mobile satellite service configurations.

To perform the signal waveform conversion functions, the FIUS comprise the following elements, as depicted in Figure 3:

- Telephone tone generators and detectors.
- A CCITT V.21-type modulator and demodulator [5], which is used to process handshaking signals.
- A bank of CCITT V.27ter and V.29-type modulators and demodulators [6],[7], which is used to process the page (image) signals.
- Logic for digital bit-stream formatting, facsimile process control, facsimile protocol conversion, call establishment, call control, and call clearing.

In performing the protocol conversions, the FIUS use a predetermined set of procedures that can be functionally partitioned into two types of protocols. The first is an Inmarsat service conversion, or *core*, protocol that permits the conversion of group 3 facsimile protocols for compatibility with Inmarsat's mobile service requirements. This protocol is generic to the different services provided (Inmarsat-B and Inmarsat-M). The second is a facsimile satellite channel conversion protocol, which permits facsimile user data and control signals to be placed on Inmarsat's facsimile data channels. This protocol differs significantly between the two services, as outlined later. These functional elements are illustrated in a protocol block diagram of an FIU (Figure 4). This paper addresses the core protocol in detail.

### Inmarsat service conversion (core) protocols

The Inmarsat service conversion (core) protocols provide the basic functionality that converts group 3 facsimile protocols for compatibility with the Inmarsat digital mobile satellite service requirements. The core protocols identify, demodulate, and interpret different types of facsimile-originated

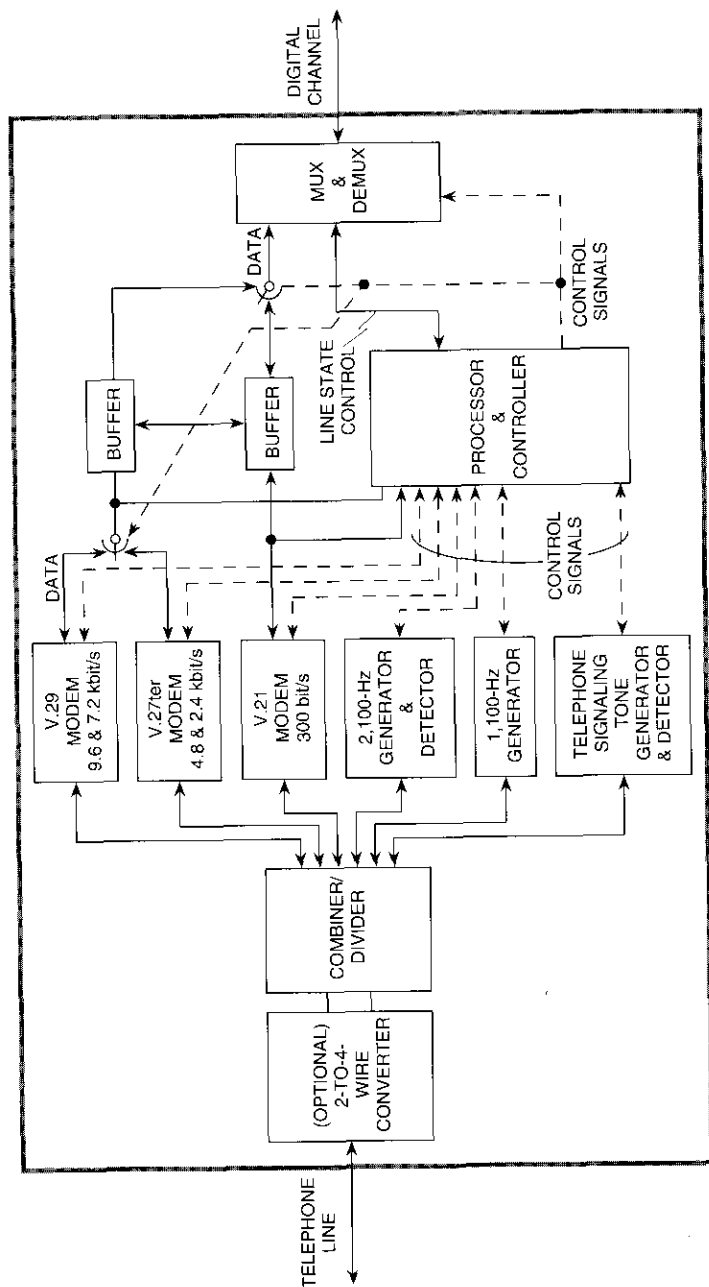


Figure 3. Functional Block Diagram of the Facsimile Interface Unit

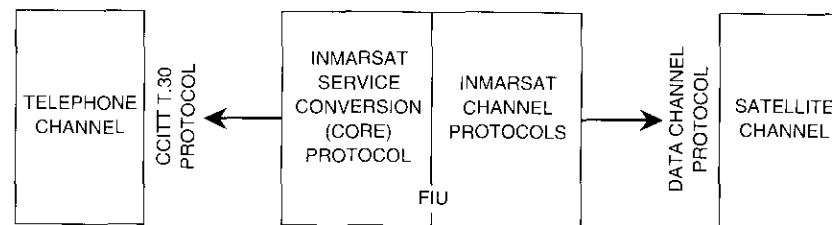


Figure 4. Block Diagram of FIU Protocol Partitioning

signals, and provide for their transmission over the satellite channel and association with line state signaling. Provisions are made to compensate for the longer access and transport link transmission delays encountered in the Inmarsat system, and a set of control functions is incorporated that permits the dynamic determination and introduction of signal-dependent transmission delays. Provision is also made for end user facsimile terminal call-recovery procedures to be employed and successfully concatenated with satellite channel error detection mechanisms. Finally, CCITT Rec. T.30 point-to-point protocol characteristics are converted to a point-to-multipoint (or broadcast) mode of operation.

#### Facsimile signal demodulation and transmission over baseband channels

The fundamental features of the facsimile interface function consist of the identification, demodulation, and interpretation of the various types of facsimile-terminal-originated signals; their subsequent treatment and transmission over the satellite channel; and their association with line state signaling. The FIUs detect all signals on the incoming telephone channel and demodulate them when mapping to the demodulated digital domain is possible. Such signals include all facsimile-terminal-to-facsimile-terminal control signals encoded according to the V.21 modulation scheme [5], as well as user image data encoded according to one of the four signaling rates addressed by the V.29 and V.27ter modulation schemes [6],[7].

The FIUs transmit over the satellite channel only the signals that are required for producing facsimile images (*i.e.*, the image data and information portions of the control signals). Demodulated signals, such as the V.21 signal preamble, that contain significant redundancy are instead regenerated by the receiving FIU in the satellite-to-facsimile-terminal direction. In addition, the FIUs will receive signals that are not modulated by a V.29, V.27ter, or V.21 scheme, such as call setup, echo control tones, and modem synchronizing/training sequences. These signals are also regenerated (by the remodulating

FIU) on the basis of appropriate line state signaling messages received over the satellite channel.

Line state signaling is a key characteristic of the FIU concept, since the different types of control and image signals cannot be generated solely on the basis of user data, without additional information pertaining to the telephone line state associated with these signals. For example, in order for the remodulating FIU to employ the correct modulation scheme for the transmission of 300-bit/s and 4,800-bit/s data (in the satellite-to-facsimile-terminal direction), a means of signaling is required which differentiates the signaling rate that was originally used by the transmitting facsimile terminal. This is because, when user data are transmitted over demodulated digital circuit-assigned connections, the bit rate information is lost and thus the signaling rate of the signals is no longer known. Furthermore, the different types of signals that cannot be mapped into a demodulated digital bit stream can be regenerated only if some type of signaling indicative of their nature and onset (or termination) is sent over the satellite channel.

Line state information can be conveyed between FIUs in a packetized or channel-associated format, depending on the type of service. Table 1 summarizes seven distinct line states that are used in the Inmarsat services.

#### Signaling rate control

Associated with the FIU signal detection capability is the ability to identify the correct scheme to be applied for the demodulation or remodulation of signals received from the facsimile terminal or over the satellite channel,

TABLE 1. LINE STATES FOR INMARSAT SERVICES

LINE STATE CONTROL INDICATION	TELEPHONE LINE STATE
• Idle	No signal
• CED Connection	2,100-Hz signal
• Binary-Coded Signal Connection	300-bit/s (non-preamble) binary-coded procedural signal
• Telephone Signaling Tones	Telephone signaling tones, such as ringing tone and busy tone
• Synchronizing Signal Connection	Modem synchronizing (or training) signal
• Preamble Connection	300-bit/s binary-coded preamble signal
• Message Connection	Facsimile message or training check signal

respectively. The FIU concept uses two approaches to accomplish such control. First, the remodulating FIU directly utilizes the line state control indication to differentiate between low-speed (V.21) and high-speed (V.27ter or V.29) data. If high-speed modulation is indicated, the remodulating FIU derives the appropriate signaling rate based on knowledge already obtained from the interception and interpretation of the DCS. As indicated previously, the DCS is issued by the transmitting terminal to convey to the receiver the signaling rate to be used for transmission of the facsimile message (page). If during a call a transmitter is forced to reduce its speed to accommodate degraded channel conditions, a new DCS is sent. The FIU continuously monitors such transmissions in order to adapt its signaling rate, if appropriate. Thus, the remodulating FIU employs a combination of line state information and prior signal/protocol knowledge.

The demodulating FIU, on the other hand, relies on a priori knowledge of the CCITT Rec. T.30 facsimile protocols to establish the nature of the signal received over the telephone circuit (low-speed V.21 or high-speed V.27ter/V.29). However, once the nature of the signal has been established, the demodulating FIU derives the appropriate signaling rate based on prior knowledge obtained from the interception and interpretation of the DCS.

#### Transmission and access delay compensation

To compensate for the long end-to-end delays encountered in the Inmarsat system, signal elements were developed specifically to extend the operating timing tolerances of group 3 facsimile terminals for compatibility with longer propagation delay circuits. The delays arise primarily from three factors: the long access and transport links encountered in the Inmarsat network topology; delays inherent in low-rate digital mobile transmission systems; and delays introduced by the FIU in demodulating, remodulating, buffering, interpreting, and controlling the processing of facsimile signals. Delay compensation is perhaps the second most critical function of the FIU concept, after the demodulation/remodulation process.

The signal elements consist of the transmission of a repeated series of 300-bit/s V.21 modulated high data link control (HDLC) flags, which are generated from the FIUs and transmitted to the facsimile terminals. The generation and termination of the flag sequence are the two key characteristics associated with correct usage of the sequence.

The flag sequence is generated by an FIU whenever an anticipated response to a command is not received within a prescribed time-out interval. The flag sequence is terminated when either the anticipated signal is received over the satellite channel, or the FIU-generated flag sequence has lasted for a prescribed

period of time. Subsequently, when the actual facsimile-terminal-generated signal is received over the satellite channel, it is concatenated with the FIU flags so as to appear as one signal to the receiving facsimile terminal. This process is illustrated in Figure 5. The flag sequence is invoked only in conjunction with signals that are expected to use the flag sequence as a preamble to their information fields.

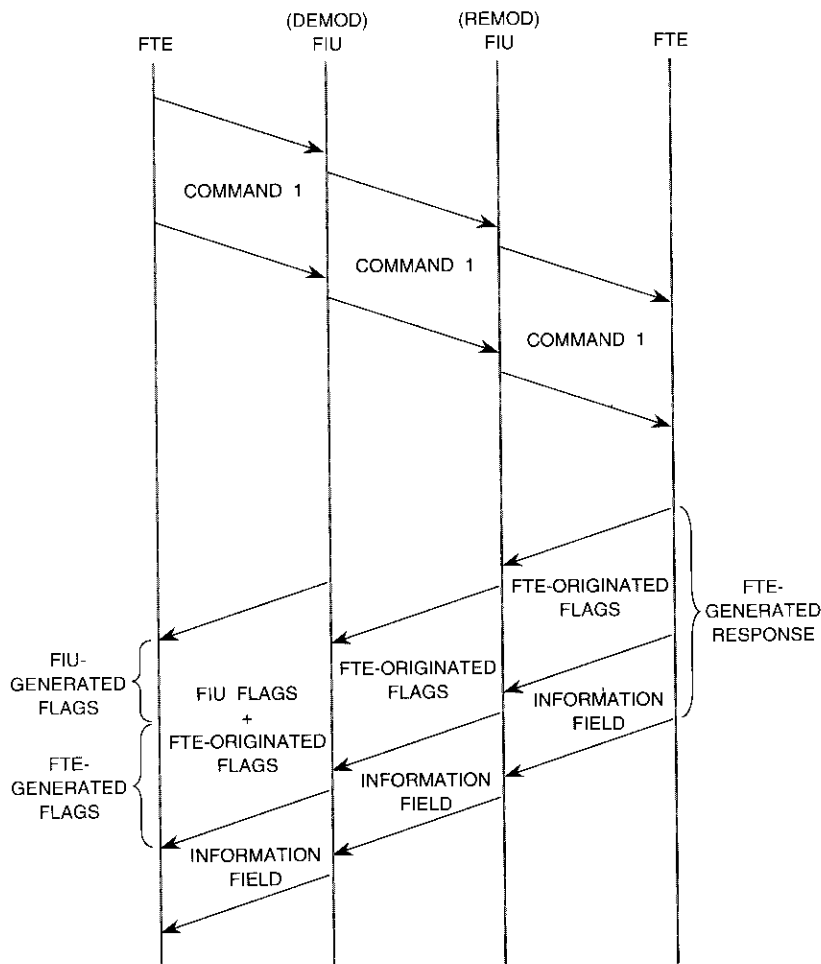


Figure 5. Example of Flag Sequence Usage

The prescribed flag sequence duration was determined in a manner that allows the continuation of call recovery (as initiated by the end user facsimile terminals), even under abnormal call conditions. If the flag sequence were terminated only in response to receipt of a valid signal over the satellite channel, an abnormal call condition could persist virtually indefinitely if no response was received, without any recovery action being initiated by either facsimile terminal.

The rules for the generation, termination, and duration of the flag sequence were derived on the basis of facsimile terminal time-out characteristics and estimated end-to-end transmission delays. Thus, the timer applicable to the generation of flags is derived by subtracting the estimated maximum round-trip delay between the PSTN-based facsimile terminal and the LES from the minimum time-out tolerance of facsimile terminals.

**Dynamic delay determination**

The FIU core protocol was designed to preserve the tight timing tolerances of facsimile protocols when consecutive signals encoded according to different modulation schemes are transmitted in the same direction. These tolerances are on the order to  $75 \pm 20$  ms. Of particular concern is the fact that detection times applicable to different modulation schemes (which generally fall in the range of 5 to 39 ms) are sufficiently different that two signals transmitted adjacent to one another can come significantly closer (or spread significantly farther apart) at the destination facsimile terminal, unless special precautions are taken.

Timing jitter can have a significant impact on facsimile performance for a number of reasons. First, exceeding the signal timing separations can void the echo control strategy adopted by the end user terminals [8]. Excessive violation of the timing specifications can also result in a time-out or adverse alteration of the receiving end user terminal behavior. Finally, violation of the timing specifications can lead to front-end clipping by other interconnected network equipment, resulting in even further degradation at the network termination points.

Conversely, if the separation of the two signals is significantly decreased while they are transported over the network, the receiving facsimile terminal could find it impossible to switch between different modulation schemes in time to receive the second signal without corruption. It should be noted that these types of problems are exclusively characteristic of mixed analog/digital networks and are expected to become more acute when interconnected processes are employed (e.g., an Inmarsat network interconnected with an

intercontinental network that uses circuit multiplication equipment employing facsimile demodulation/remodulation technology).

Figure 6 shows how two signals could spread farther apart at the receiving facsimile terminal. The two signals in this figure, which were initially separated by  $a$  milliseconds at the transmitting facsimile terminal, become farther apart,  $b$ , at the destination facsimile terminal as a result of demodulation, remodulation, and detection. This is because the detection/demodulation and remodulation times ( $p$  and  $q$ ) of signal 1 are shorter than the corresponding times ( $r$  and  $s$ ) of signal 2. It can be seen that, to maintain the proper separation at the destination facsimile terminal, the total minimum delays introduced by the FIUs for the termination of the first signal must be greater than the maximum total delays introduced by the FIUs (prior to the introduction of any further dynamically determined delay) for the processing of the onset of

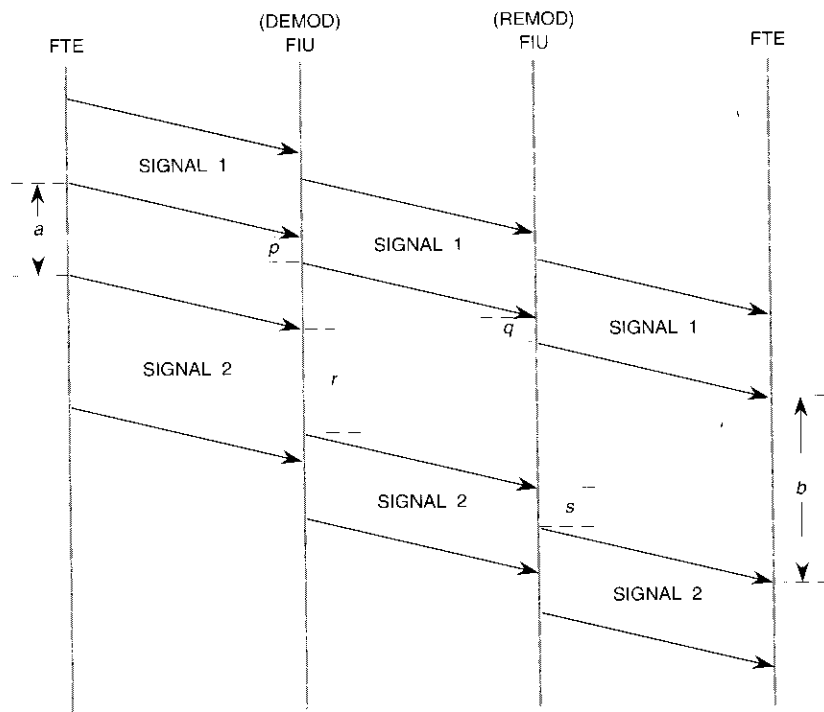


Figure 6. Example of Temporal Distortion at Destination FTE Caused by Detection, Demodulation, and Remodulation Processes

activity of the second signal. Otherwise, as shown in the figure, if signal separation  $a$  at the source facsimile unit is at its maximum allowable limit, then the temporal separation,  $b$ , of the two signals will exceed the timing tolerance of the receiving facsimile terminal. (Delay  $p$  here does not include any delay dynamically introduced by the FIU, which may be necessary in order to preserve the minimum signal 1/signal 2 temporal spacing at the destination facsimile terminal.)

The FIU concept overcomes this difficulty by artificially decreasing or increasing the delay applied to signals 1 and 2, based on the fact that the ranges of delays  $q$  and  $s$  are defined and thus known in advance. This principle assumes that the delays introduced by the remodulating FIU will be constant (although different) for each type of signal. On this basis, the demodulating FIU can determine in advance the temporal separation of a signal pair at the destination facsimile terminal, once the pair in question has been transmitted over the digital channel. Although the detection and generation times could be made the same (*i.e.*,  $p = r$  and  $q = s$ ), this would be undesirable since it could introduce significant additional transmission delay or degrade signal discrimination accuracy.

#### Efficient FTE capabilities negotiation

A further characteristic introduced into the FIU concept is the incorporation of capabilities that permit the in-band alteration of facsimile-terminal-to-facsimile-terminal control signaling so that the capabilities of the called facsimile terminal can be limited to the maximum supportable under the mobile channel constraints. (For example, attempts to negotiate at signaling rates in excess of 9.6 kbit/s in the Inmarsat-B system are blocked.) This is accomplished in two ways.

First, the demodulated data stream of the non-preamble portion of the 300-bit/s binary-coded procedural DIS is intercepted and analyzed. Then, if the signal is found to contain capabilities that are incompatible with those supportable by the mobile channel, its content is modified to achieve the desired facilities profile.

Second, any attempt to employ a proprietary mode of communication is intercepted and eliminated. Such modes can be established when a called facsimile terminal transmits the optional NSF frame, and the calling terminal recognizes this frame as belonging to the same manufacturer and thus adopts a different set of communications protocols. Upon selection of a proprietary mode of communication, the calling facsimile terminal transmits a nonstandard setup frame to the called terminal. To prevent the NSF mode from being

selected, the demodulating FIU intercepts any NSF frames transmitted in the called-to-calling facsimile terminal direction and substitutes a series of preamble line controls (flags) in their place. In this manner, the calling facsimile terminal never sees the NSF capabilities of the called terminal, and thus never issues a nonstandard setup command.

Although the capabilities alteration process does not affect the ability of the facsimile terminals to ultimately establish a successful communications path, it does expedite the negotiation of an acceptable profile of capabilities, thus reducing the overall call duration. For a single-page Inmarsat-M call, these savings can amount to approximately 15 percent of the call's duration.

#### **Concatenation of FTE error recovery with satellite channel protocols**

An additional characteristic of the core protocols is the special provisions made to ensure that error recovery procedures enacted by the end customer facsimile terminals can be used in the presence of a mobile satellite demodulation/remodulation transmission system. This is accomplished by forcing each FIU to check the integrity of the frame check sequence associated with each V.21 modulated binary-coded procedural signal transmission. If the frame check sequence field indicates an error condition in the address, control, or information fields, the check sequence is recomputed so that the regenerated sequence will result in detection of an error condition by the distant facsimile terminal, assuming subsequent error-free transmission. This recomputation is particularly important in instances where the information fields are subject to modification by the FIU system (such as the DIS mentioned above).

#### **Carrier activation**

The essentially half-duplex nature of facsimile protocols permits carrier activation procedures to be employed so that satellite power can be conserved in the satellite-to-mobile-terminal direction. Hence, when end-to-end communication is maintained in one direction of transmission for a significant amount of time—as during the mobile-originated image/message (or page) phase—the LES FIU core protocols permit the carrier in the satellite-to-MES direction to be deactivated. Once the message is completed, the LES FIU core protocols permit identification of the end of the message transmission phase, and a request is made for the carrier in the satellite-to-MES direction to be reactivated. These processes are accomplished through interpretation of the line state control received over the satellite channel, and through identification of the first and last scan lines of the page transmission.

#### **Facsimile call selection and clearing**

Facsimile calls are generally established in one of three ways: mobile-originated automatic calls, fixed-originated automatic calls, or manually established calls. For mobile-originated facsimile calls, the MES establishes a circuit in the facsimile data mode upon call initiation. In this case, call initiation is detected on the basis of the facsimile terminal "off-hook" indication, which is triggered by the customer's dialing of the destination service address and subsequent pressing of the "start" key available on most facsimile machines.

For fixed-originated automatic facsimile calls, the MES establishes a circuit in the facsimile data mode upon call initiation, similar to the above process. However, in this case facsimile (rather than voice) call detection is established on the basis of the mobile service address dialed, because a separate number is assigned to the facsimile-terminal-to-MES connection. Finally, in manually established (or switched) calls, the call is established by the MES or fixed user initially as a voice call. With respect to call clearing, once the main part of the call has been completed, the disconnect signal is received by the MES FIU. This signal, which can be interpreted by the FIU, may be used to initiate call-clearing procedures. Alternatively, the facsimile terminal "on-hook" condition can be used to initiate call-clearing.

#### **Broadcasting**

A common approach is defined so that point-to-point group 3 facsimile terminal protocols can be made to operate in a point-to-multipoint (broadcasting) mode. The two key features of these protocols are discussed here.

First, the CED, DIS, CFR, and MCF signals are locally generated by the LES FIU, rather than by the mobile facsimile terminal. In this process, it is assumed that high-speed message transmissions to the called mobile facsimile terminals are always successful. To increase the probability of successful communication with the widest range of mobile facsimile terminals, the DIS generated by the LES FIU only provides for minimal (*e.g.*, lowest signaling rate) capabilities. Consequently, the DCS issued by the calling (PSTN-based) facsimile terminal will request capabilities that are available at each mobile facsimile terminal.

Second, the timing response and duration of signals generated by the LES FIU are precisely controlled so that both the fastest and slowest mobile facsimile terminals can be synchronized with the calling (PSTN-based) facsimile terminal. This is accomplished by employing the longest possible duration and turnaround time for the LES FIU-generated signals (thus accommodating the slowest mobile facsimile terminals), and by relying on the mobile FIU flag sequence to keep the fastest mobile facsimile terminals on line.

Figure 7 shows an example of the protocol signal exchanges applicable to point-to-multipoint communications, once a call has been established. Note that the LES FIU incorporates a full set of CCITT Rec. T.30 protocols because it communicates directly, rather than transparently, with the FIU PSTN (or broadcasting) facsimile terminal.

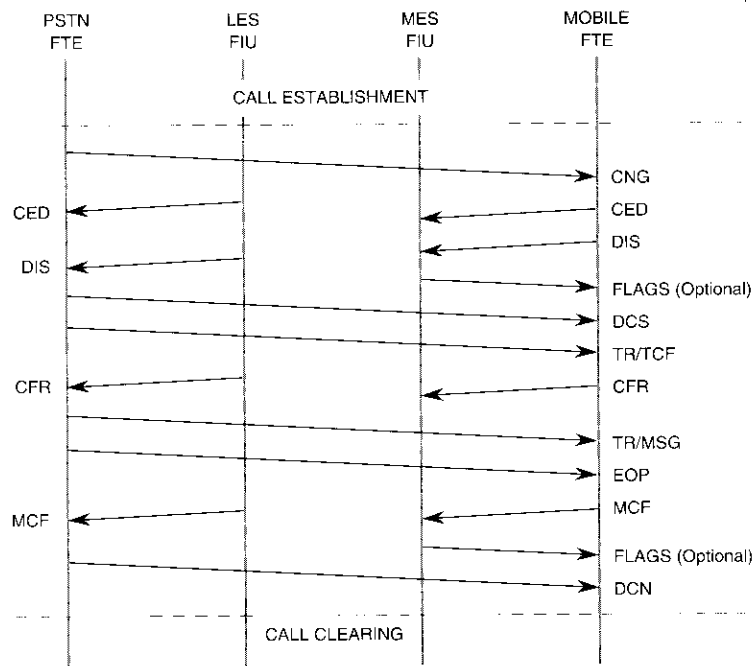


Figure 7. Example of Single-Page Broadcast Call

**Inmarsat facsimile channel protocols**

The Inmarsat service conversion or core protocols described above can be interfaced with a set of service-specific protocols—the Inmarsat channel protocols—to provide end-to-end facsimile connectivity in various modes of communication. The Inmarsat service conversion and the Inmarsat channel protocols interface with each other by exchanging user data, user data signaling rate information, indications when timing adjustments can be performed, and line state control. These concepts are illustrated in Figure 8.

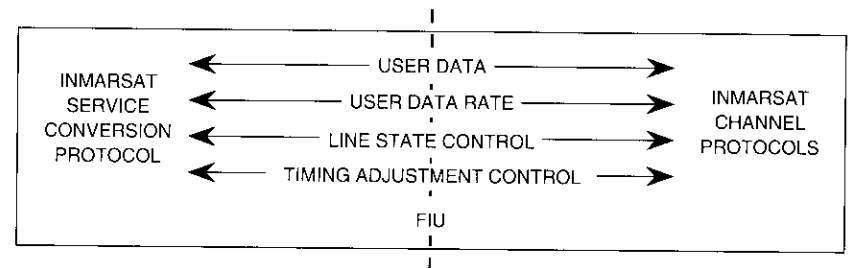


Figure 8. Interface Between Inmarsat Service Conversion and Inmarsat Channel Protocols

**Inmarsat-B facsimile service**

To provide adequate error performance, the Inmarsat-B channel employed for facsimile transmission consists of a 10.5-kbit/s single channel per carrier (SCPC) data channel, which is transmitted at 24 kbit/s after forward error correction (FEC) and framing coding. This channel is partitioned so that the bit rate available to the facsimile interface process comprises a 9.6-kbit/s channel (32-bit data field) and an associated 900-bit/s line control channel (3-bit field). As a consequence of this structure, the FIUs are able to transmit and receive digital signals to and from the satellite SCPC data channel in blocks of 35 bits, where 32 bits are employed for the transport of end user data and 3 bits for the transport of line state control [9].

**Inmarsat-M facsimile service**

To ensure adequate error performance, the Inmarsat-M channel employed for facsimile transmission consists of a 2.4-kbit/s SCPC data channel, which is transmitted at 8 kbit/s after FEC and framing coding. The Inmarsat-M data channel structure permits the FIUs to transmit and receive digital signals to and from the satellite's 2.4-kbit/s data channel in blocks of 72 bits. In the Inmarsat-M system, line state indications are carried as "line control packets," which are transmitted in-band over the 2.4-kbit/s data channel. Line control packets are generated whenever a line state transition occurs, and always precede the transmission of information (associated with the new line state) over the digital channel. The indication in the line control packet is then applied to all data bits of the satellite channel that immediately follow the packet, until a new line control packet is generated [10].

## Performance

The FIU concept enables facsimile signals to be transmitted via low data-rate channels, and can potentially improve the quality of service. Quality-of-service improvements are currently under investigation; however, three factors have already been identified as potential contributors to enhanced service quality. First, service quality may improve because of the special provisions incorporated to compensate for the long propagation delays and the long framing delay encountered in mobile communications systems. Quality may also improve because a substantial portion of the end-to-end link now comprises a demodulated data connection. Thus, the voiceband link lengths are reduced and any telephone channel equalization requirements are minimized. A third factor that can contribute to improved service quality is the enhanced robustness of demodulated data (as compared to voiceband) transmissions in the presence of digital transmission impairments. This robustness arises because a single error in voiceband transmission affects the integrity of multiple bits upon demodulation, unlike with demodulated transmissions where the correspondence is one-to-one [1].

These potential service improvement factors must obviously be weighed against potential service degradation factors, such as the introduction of additional end-to-end transmission delay arising from the FIU demodulation/remodulation process. It is known that facsimile communications can be adversely affected when transmission delay is significantly increased; however, any such degradation has to be investigated in light of the potential for improved service quality (including protocol and transmission aspects), as mentioned above.

Characterization studies of FIU performance in a laboratory environment are currently under way.

## Summary and conclusions

The FIU concepts described herein permit the transmission of facsimile signals via low-rate channels in real time, the conservation of satellite-to-mobile power, and the broadcasting of messages in a single call using off-the-shelf group 3 facsimile terminals. Quality-of-service issues are currently being investigated using a set of prototype FIU systems developed by COMSAT Laboratories, and the technology is now being integrated with mobile and fixed earth station equipment. The FIU protocols are designed so that the FIU can ultimately be implemented at a cost comparable to that of less expensive facsimile terminals.

## Acknowledgments

*This paper is based on work performed in part under the sponsorship of Inmarsat.*

## References

- [1] S. Dimolitsas *et al.*, "Evaluation of ADPCM Coders for Digital Circuit Multiplication Equipment," *COMSAT Technical Review*, Vol. 17, No. 2, Fall 1987, pp. 323-345.
- [2] Private communication.
- [3] S. Dimolitsas and J. Rieser, "Group 3 Facsimile Transmission Over Inmarsat's Digital Mobile Networks," 9th International Conference on Digital Satellite Communications (ICDSC9), Copenhagen, Denmark, May 1992, Session B, *Proc.*, pp. 25-29.
- [4] CCITT, "Procedures for Document Facsimile Transmission in the General Switched Telephone Network," VIIIth Plenary Assembly, Malaga-Torremolinos, October 1984, *Red Book*, Vol VIII.3, Rec. T.30, pp. 69-117.
- [5] CCITT, "300 Bits per Second Duplex Modem Standardized for Use in the General Switched Telephone Network," IXth Plenary Assembly, Melbourne, November 1988, *Blue Book*, Fascicle VIII.1, Rec. V.21, pp. 65-68.
- [6] CCITT, "4800/2400 Bits per Second Modem Standardized for Use in the General Switched Telephone Network," IXth Plenary Assembly, Melbourne, November 1988, *Blue Book*, Fascicle VIII.1, Rec. V.27ter, pp. 199-210.
- [7] CCITT, "9600 Bits per Second Modem Standardized for Use on Point-to-Point 4-Wire Leased Telephone-Type Circuits," IXth Plenary Assembly, Melbourne, November 1988, *Blue Book*, Fascicle VIII.1, Rec. V.29, pp. 215-227.
- [8] CCITT, "Interaction of Facsimile Protocols With Echo Control Devices," CCITT Study Group VIII, Geneva, Switzerland, September 1990, Contribution COM VIII-D.139.
- [9] S. Dimolitsas *et al.*, "Transmission of Group 3 Facsimile Over Inmarsat Maritime Digital Satellite Mobile Channels," to be published in *International Journal on Satellite Communications*.
- [10] S. Dimolitsas *et al.*, "Group 3 Facsimile Transmission Over Digital Satellite Mobile Networks," IEEE Vehicular Communications Conference, Denver, Colorado, May 1992, *Proc.*, Vol. 1, pp. 240-246.



*Spiros Dimolitsas received a B.Sc. (with Honors) in physics and mathematics from Sussex University, Great Britain, in 1977; an M.Sc. and Dipl. Eng. Q.M.C. in nuclear reactor engineering from London University in 1979; and a D.Phil. in computer engineering and digital signal processing from Sussex University in 1982. From 1982 to 1983, he worked for High Energy and Nuclear Equipment S.A. in Geneva, Switzerland, and later for the Mayo Clinic and for MOSTEK Corporation, where he was involved in digital image processing and voiceband modem design, respectively. He joined COMSAT Laboratories in 1986 and*

*has been involved in studies of linear and nonlinear voice processing systems, facsimile coding and transmission, and the quality evaluation of new digital processing technology. He is currently Manager of the Voiceband Processing Department.*

*Dr. Dimolitsas is Chairman of the CCITT Experts' Group on Speech Coding, and has represented COMSAT in the CCITT on telematic and network quality issues. He is a Senior Member of the IEEE, and Editor for Speech Processing of the IEEE Transactions on Communications, Associate Editor of the IEEE Transactions on Speech and Audio Processing, and Secretary of the Washington/Northern Virginia Chapter of the IEEE Communications Society.*

*Jack H. Rieser received a B.S.E.E. from the University of Cincinnati in 1975 and an M.S.E.E. from the Johns Hopkins University in 1982. He is currently a Senior Scientist in the Voiceband Processing Department of the Communications Technology Division at COMSAT Laboratories. He was the Project Engineer responsible for the design and development of the INTELSAT BG-42-65 DSI terminal for use in the INTELSAT TDMA network, and the 32-kbit/s ADPCM/DSI system delivered to INTELSAT under contract INTEL-359. He served as lead engineer in the hardware and software development of a facsimile interface unit (FIU) for use in the Inmarsat network, and was chairman of a group which developed a DCME standard in the U.S. TTY Standards Committee.*



*Since joining COMSAT in 1975, Mr. Rieser has had design and development responsibility for various DSI systems and voice switching pertaining to PCM and delta modulation. He has also performed several studies in data and facsimile transmission via delta modulation at 32 kbit/s, and was the senior member of the team responsible for developing the first commercial COMSAT echo canceller. He is a member of Eta Kappa Nu and a Senior Member of the IEEE. He is also the recipient of the ANSI T1 Outstanding Achievement Award for his work in DCME standardization, and the COMSAT Laboratories 1986 Research and Development Award for his pioneering work in DCME.*



*Howard Feldman received a B.S. in electrical engineering from the University of Michigan in 1979, and a Masters in electrical engineering from the University of Texas at Arlington in 1982. From 1979 to 1986, he worked for Motorola, Inc., as an RF engineer in Ft. Worth, Texas, and in Tel Aviv. He then joined Inmarsat in London, and initially worked on operations of existing mobile satellite systems. From 1988 to the present, he has been involved in the design and implementation of the new Inmarsat-M and Inmarsat-B digital services. His efforts in this area have focused on design and implementation of facsimile transmission and enhanced services, as well as on system design of mobile earth stations.*

## ***A digitally implemented modem: Theory and emulation results***

J. J. POKLEMB AND F. R. FARIS

(Manuscript received April 27, 1992)

### ***Abstract***

Theory and hardware emulation results are presented for a very flexible digitally implemented modem whose technology is useful over a broad class of satellite communications applications, both terrestrial and in-flight. The modem can be programmed for 2-, 4-, 8-, and 16-PSK (phase shift keying), 16-QAM (quadrature amplitude modulation), MSK (minimum shift keying), and Offset-QPSK (quaternary PSK) modulation schemes over a range of data rates from 2.34 to 300 Mbit/s, with programmable spectral occupancy from 1.2 to 1.8 times the symbol rate. These operational parameters are executable in burst or continuous mode. All critical processing in both the modulator and demodulator is performed at baseband using very-high-speed digital hardware (including application-specific integrated circuits [ASICs]) and memory. Analog front-ends in phase-quadrature are employed for translation between the IF and baseband, where the analog-to-digital conversion takes place.

The emulation results confirmed that the modem functioned over the entire range of operational parameters, and achieved and maintained synchronization at bit error rates (BERS) as high as  $2 \times 10^{-1}$ . The results also showed very good agreement with the tracking loop analysis, and validated the resolution apportionment of the various hardware elements in the tracking loops. The small degradation experienced in BER was attributed to an intentional mismatch of the transmit and receive data filters, which was introduced to minimize the hardware complexity for future spacecraft applications by restricting the demodulator's finite-impulse-response data filter to a two-symbol aperture.

### ***Introduction***

In 1977, a generic analog demodulator structure for digital data transmission was derived from multidimensional detection and estimation theory, and successfully implemented at COMSAT Laboratories [1]. Six years later, in

1983, a patent entitled "Concurrent Carrier and Clock Synchronization (CCCS) for Data Transmission Systems" was granted on the architecture; and the following year, the theoretical basis for the demodulator was described in a paper entitled "A Joint Estimator-Detector (JED) for QPSK Data Transmission" [2],[3].

In 1982, the development of a digital implementation of the JED was undertaken. Over the next few years, various improvements were made to the digital structure in an effort to provide as flexible a design as possible without the need for hardware changes. The emulation results presented herein are primarily taken from the programmable digital modem (PDM) version of the JED built for the National Aeronautics and Space Administration (NASA) Lewis Research Center (LeRC).

Because the JED structure is based on a mathematical representation of amplitude-modulated carriers in phase quadrature, it is applicable to many widely used, filtered signal constellations that can be represented in a two-dimensional space; for example,  $M$ -ary phase shift keying (PSK),  $M$ -ary quadrature amplitude modulation (QAM), minimum shift keying (MSK), and offset quaternary PSK (Offset-QPSK) [4]. The detection and estimation operations are interdependent, such that all of the post-detected values and estimates developed aid one another coherently. The benefits of this coherency include negligible degradation in bit error rate (BER) for nominal tracking loop bandwidths, as well as less output jitter and cycle skipping at a given signal-to-noise ratio,  $S/N$ , compared with other well-known techniques. This improved performance is largely due to the post-detected data feedback used to realize the estimator loop phase detectors. Another advantage is the ability to achieve and maintain synchronization at BERs in excess of  $10^{-1}$ .

Since 1977, numerous realizations of the JED approach, both analog and digital, have been built and tested at COMSAT Laboratories. They have primarily been QPSK structures at data rates ranging from 64 kbit/s to 20 Mbit/s. The current NASA version discussed here has been designed for 2-, 4-, 8-, and 16-PSK; 16-QAM; MSK; and Offset-QPSK schemes over a range of symbol rates from 2.34 to 75 Msymbol/s. Thus, the transmission rate for 16-ary modulation can be as high as 300 Mbit/s.

COMSAT's first table lookup modulator realization was designed and built in 1982. However, at that time high-speed memory sizes were so restrictive that only bipolar in-phase and quadrature ( $I, Q$ )-level modulation formats such as QPSK could be implemented. In the late 1980s, advances in high-speed static random-access memory (SRAM) made it possible to realize all of the useful modulation constellations for satellite communications mentioned above.

Patent applications for second-generation digital techniques such as "gear-shifting" and "pre-averaging" were filed in the mid-1980s, and are only now

being disclosed in the literature. These techniques allow the modem to operate over a very broad range of symbol rates (typically, a factor of 32) without any hardware changes. Hence, the modem is truly programmable.

An extensive analog and digital hardware modeling program was written on an Apollo DN-3000 workstation to emulate and evaluate the design. All of the performance results presented were taken from the emulations. The hardware is currently being fabricated, and measurements should soon be available.

### **Modem implementation**

The modulator and demodulator conceptual architectures, described in detail in References 3 and 5, are outlined herein to provide continuity in the analysis. Both architectures were chosen to provide the maximum practical flexibility and minimum hardware complexity consistent with the modulation techniques, data rates, operational modes, and spectral occupancies required.

#### **Modulator**

To achieve the greatest degree of programmability, the critical processing elements in the modulator architecture are digital. Because the modulation must ultimately be converted into the analog domain for transmission, one of the most important decisions to be made is whether this conversion should take place at baseband or IF.

#### BASEBAND VS IF DIGITAL-TO-ANALOG SAMPLE CONVERSION

A digital-to-analog (D/A) converter is inherently a sample-and-hold device that imposes a low-pass  $\sin(x)/x$  envelope on the replicated output spectral lobes at multiples of the sample rate clock. The first notch of the  $\sin(x)/x$  envelope occurs at the sample clock frequency  $NR_s$ , where  $R_s$  is the symbol rate ( $1/T_s$ ) and  $N$  is the number of samples per symbol ( $s/s$ ). Consequently, unless the sample rate is very high, the output spectrum should be compensated for D/A sample-and-hold aperture rolloff. To minimize the amount of compensation required, the center of the desired output spectral lobe can be located at DC. This effect is illustrated in Figure 1a for baseband sampling at a rate of 2  $s/s$  and 40-percent Nyquist rolloff filtering. Integer numbers of samples per symbol are preferred because they allow for simpler processing. Observe that the notches in the  $\sin(x)/x$  envelope conveniently provide some degree of replicated spectra removal. Also note that the gap between the baseband lobe and the first replicated lobe allows the use of a low-pass, finite-rolloff, replication-removal (RR) filter, whose asymptotes are sketched in the figure. Furthermore, as the Nyquist channel filtering rolloff increases to

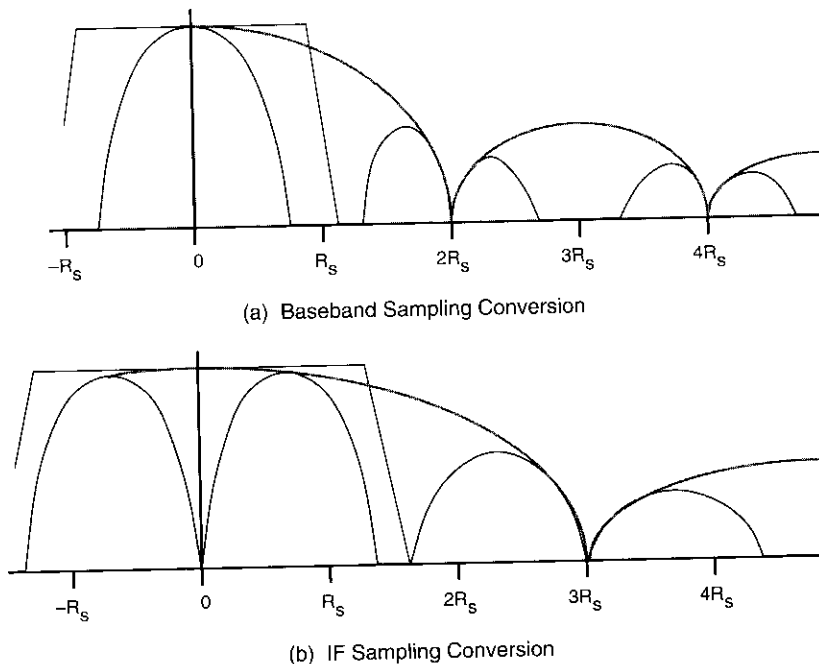


Figure 1. Modulator D/A Output Spectra

100 percent, the gap narrows to a notch, and the use of a finite-rolloff RR filter will alter the shape of the higher frequencies in the transition band of the transmit spectrum. From the figure, it is clear that 2 s/s is the lowest practical integer-multiple sample rate. This is important because, for a given hardware speed capability, the highest symbol rate of operation is achieved with the lowest number of samples per symbol. The disadvantage of baseband sample conversion is that it requires two D/A converters and quadrature mixing in order to convert to the desired IF, whereas IF sample conversion typically uses a single D/A and the frequency conversion is inherent.

An IF sample conversion technique is shown in Figure 1b for the case of 3 s/s, which represents about the lowest IF sampling rate for practical RR filtering at a single data rate of operation. Observe that the desired spectral lobe is centered at approximately  $0.7R_s$  for a 40-percent Nyquist channel. However, the narrower spectral gap is too small to support a transition band for replicated-spectra filtering for continuously-variable-rate operation. Hence, to widen the gap, the next higher integer multiple sample rate (4 s/s) would be required. This increased sample rate halves the maximum speed of operation

relative to baseband sampling. In addition, the IF sampling has greater amplitude skew across the passband to be compensated. This will cause more ringing in the transmit filter impulse response and require a wider aperture to represent. Thus, for very-high-speed, continuously-variable-rate operation, the baseband sample conversion approach is clearly more desirable.

#### MULTIRATE OPERATION

To provide for maximum rate flexibility without hardware changes, it is necessary to use a single analog RR filter over the broadest practical range of data rates. This implies that the first replicated spectral lobe of Figure 1a must always be above a given cutoff frequency, which is accomplished by keeping the sample rate sufficiently high that the first replica remains above the RR filter cutoff. To maintain this alignment as the data symbol rate is lowered, the number of samples per symbol must be increased proportionally. To preserve an integer number of samples per symbol, this technique is implemented in discrete sample-per-symbol steps rather than in a continuously variable fashion. A convenient and practical size for each step is an octave of data rate. Henceforth, this technique will be referred to as "gear-shifting." The data rate ranges for this particular design are detailed in Table 1. The table only addresses rates up to 32 s/s because of spectral shaping memory size limitations, which will be explained later.

The most difficult situation for replicated spectra removal occurs at both ends of the 2-s/s range. When operating at the maximum symbol rate,  $R_s = 75$  Msymbol/s, the RR filter must pass as much of the main lobe as possible. Consequently, it needs a passband somewhat wider than the Nyquist bandwidth,  $\sim 1.3R_s/2 = 48.75$  MHz. At the other extreme, for operation at the minimum symbol rate in the 2-s/s range ( $R_s = 37.5$  Msymbol/s), the RR filter must reject the low end of the first replicated lobe, at approximately  $1.6R_s = 60$  MHz. A good compromise, which was determined in conjunction

TABLE 1. MODULATOR GEAR-SHIFTING RATES

SYMBOL RATE RANGE (Msymbol/s)	SAMPLES/ SYMBOL
$37.5 < R_s < 75$	2
$18.75 < R_s < 37.5$	4
$9.375 < R_s < 18.75$	8
$4.6875 < R_s < 9.375$	16
$2.34375 < R_s < 4.6875$	32

with BER simulations, is an elliptic low-pass filter with a 0.2-dB equiripple passband extending from DC to 48 MHz, with a stopband beginning at 60 MHz of minimum attenuation greater than 30 dB. The sample-and-hold effect of the D/A provides additional filtering to suppress the sample clock replicated spectra below 40 dB. To avoid additional analog hardware, group delay dispersion in the RR filter is compensated for in the transmit spectral-shaping memory. This dispersion will be most pronounced at the highest symbol rates of operation.

TRANSMIT SPECTRAL SHAPING

The maximum number of  $M$ -ary signals is 16. To facilitate 16-ary 300-Mbit/s operation, the incoming data are received on four parallel lines designated  $A$ ,  $B$ ,  $C$ , and  $D$ , where  $A$  is the most significant bit (MSB) and  $D$  is the least significant bit (LSB). To properly represent the modulation techniques, a quadrature data mapping (QDM) between  $A$ ,  $B$ ,  $C$ ,  $D$  and  $I$ ,  $Q$  is necessary prior to spectral shaping. The mappings for the required modulation techniques are given in Table 2. A one's complement representation is used for the mappings because of the bipolar symmetry. The unity power-normalized signal constellation vectors  $(i, q)$  are also listed.

Nyquist band-limiting of the digital data spectrum is most easily realized on the modulator by means of a table lookup [5]–[7]. This is because the  $I$ ,  $Q$  signal input for band-limiting has only a few deterministic levels, and as a result the memory size is not unwieldy. Further, since the sample values are precomputed, the only impact on their precision is the output quantization of the memory. Alternatively, to be as accurate, a true finite impulse response (FIR) filter would require moderately high precision in all of its delays, multiplies, and adds, except for the very first input.

The table lookup approach is illustrated in Figure 2. Its operation is based on clocking-out a set of  $N$  precomputed sample values for a given input symbol pattern. Incoming  $A$ ,  $B$ ,  $C$ ,  $D$  data lines are mapped into an equivalent one's complement  $I$ ,  $Q$  representation by the QDM. The  $I$ ,  $Q$  symbol patterns are stored in shift registers of length  $L$ . The remainder of this discussion applies equally to either the  $I$  or  $Q$  channel. Different  $m$ -bit resolutions for  $I$  and  $Q$  are required in order to handle the various multilevel modulation techniques, as indicated in Table 2, where currently  $m = 1, 2, 3$ . Therefore, maximum length  $L$  shift registers must be reconfigurable into  $(m \times L/m)$  formats.  $L/m$  symbols of  $m$  bits are stored in the shift registers. The symbol patterns in a shift register are updated at the data symbol rate,  $R_s$ . Thus,  $L/m$  is the effective transmit filter impulse response aperture. The  $L$  bits constitute the MSBs of the precomputed memory lookup address, while synchronous sample clocks in octave multiples from  $NR/2$  down through  $R_s$  make up the

TABLE 2. MODULATION ENCODING MAPPING

MODULATION TECHNIQUE	NO.	A	B	C	D	NORMALIZED $(i, q)$	$I$	$Q$
BPSK	0	-	-	-	0	+0.7071, +0.7071	0	0
	1	-	-	-	1	-0.7071, -0.7071	1	1
MSK, QPSK	0	-	-	0	0	+0.7071, +0.7071	0	0
	1	-	-	0	1	+0.7071, -0.7071	0	1
	2	-	-	1	0	-0.7071, +0.7071	1	0
	3	-	-	1	1	-0.7071, -0.7071	1	1
8-PSK	0	-	0	0	0	+0.9239, +0.3827	01	00
	1	-	0	0	1	+0.3827, +0.9239	00	01
	2	-	0	1	0	-0.9239, +0.3827	10	00
	3	-	0	1	1	-0.3827, +0.9239	11	01
	4	-	1	0	0	+0.9239, -0.3827	01	11
	5	-	1	0	1	+0.3827, -0.9239	00	10
	6	-	1	1	0	-0.9239, -0.3827	10	11
7	-	1	1	1	-0.3827, -0.9239	11	10	
16-QAM	0	0	0	0	0	+0.9487, +0.3162	01	01
	1	0	0	0	1	+0.3162, +0.3162	01	00
	2	0	0	1	0	+0.9487, +0.9487	00	01
	3	0	0	1	1	+0.3162, +0.9487	00	00
	4	0	1	0	0	-0.9487, +0.3162	10	01
	5	0	1	0	1	-0.3162, +0.3162	10	00
	6	0	1	1	0	-0.9487, +0.9487	11	01
	7	0	1	1	1	-0.3162, +0.9487	11	00
	8	1	0	0	0	+0.9487, -0.3162	01	10
	9	1	0	0	1	+0.3162, -0.3162	01	11
	10	1	0	1	0	+0.9487, -0.9487	00	10
	11	1	0	1	1	+0.3162, -0.9487	00	11
	12	1	1	0	0	-0.9487, -0.3162	10	10
	13	1	1	0	1	-0.3162, -0.3162	10	11
	14	1	1	1	0	-0.9487, -0.9487	11	10
15	1	1	1	1	-0.3162, -0.9487	11	11	
16-PSK	0	0	0	0	0	+0.9808, +0.1951	011	000
	1	0	0	0	1	+0.8315, +0.5556	010	001
	2	0	0	1	0	+0.1951, +0.9808	000	011
	3	0	0	1	1	+0.5556, +0.8315	001	010
	4	0	1	0	0	-0.9808, +0.1951	100	000
	5	0	1	0	1	-0.8315, +0.5556	101	001
	6	0	1	1	0	-0.1951, +0.9808	111	011
	7	0	1	1	1	-0.5556, +0.8315	110	010
	8	1	0	0	0	+0.9808, -0.1951	011	111
	9	1	0	0	1	+0.8315, -0.5556	010	110
	10	1	0	1	0	+0.1951, -0.9808	000	100
	11	1	0	1	1	+0.5556, -0.8315	001	101
	12	1	1	0	0	-0.9808, -0.1951	100	111
	13	1	1	0	1	-0.8315, -0.5556	101	110
	14	1	1	1	0	-0.1951, -0.9808	111	100
15	1	1	1	1	-0.5556, -0.8315	110	101	

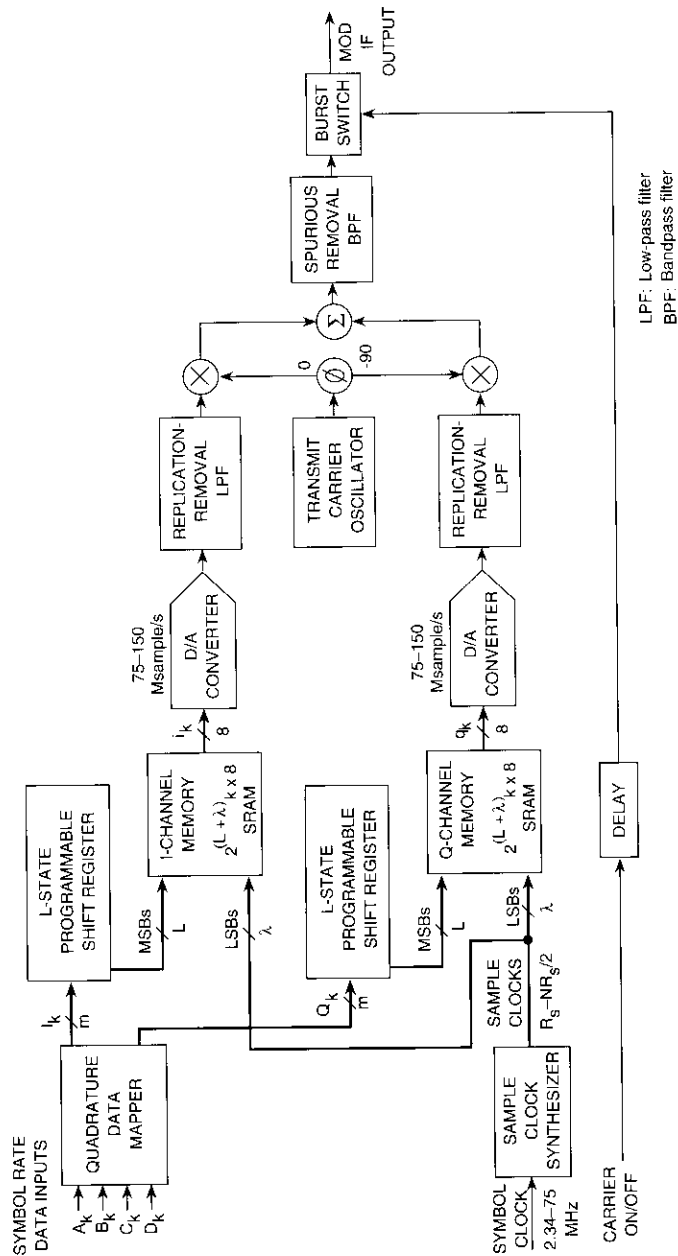


Figure 2. Modulator Spectral Shaping and IF Conversion

address LSBs. The memory MSBs correspond to a given input data sequence, and the LSBs select the samples within a symbol time, such that for each of the 2<sup>L</sup> possible bit patterns in the shift register, a set of N precomputed samples is clocked out. Altogether, there are a total of 2<sup>L</sup> • N samples or addressable memory locations. Moreover, the memory size increases linearly with the number of samples per symbol, but geometrically vs impulse response aperture length and the number of I or Q amplitude levels, (2<sup>m</sup>)<sup>L/m</sup>. This is evident in Table 3, where the maximum memory requirements for 32-s/s operation are listed vs impulse response aperture length and modulation technique. Also included are rough indications of the spectral occupancies in terms of their center-to-center carrier spacings.

TABLE 3. MAXIMUM I- OR Q-CHANNEL SPECTRAL SHAPING MEMORY REQUIREMENTS

MODULATION FORMAT	NO. OF SIGNAL LEVELS	APERTURE LENGTH (symbols)						
		2	3	4	5	6	8	12
BPSK, MSK, QPSK	2 (±a)	128	256	512	1K	2K	8.2K	<b>131K</b>
8-PSK, 16-QAM	4 (±b, ±c)	512	2K	8.2K	33K	<b>131K</b>	2.1M	-
16-PSK	8 (±x, ±y, ±w, ±z)	8.2K	16.4K	<b>131K</b>	1.0M	8.4M	-	-
Carrier Spacing (Symbol rate multiples)		2.0	1.9	1.8	1.6	1.4	1.3	1.2

The best compromise with the current state of the art in high-speed SRAM is to set L = 12. The resulting 131K × 8 memory configurations are shaded in the table. Only 16-PSK cannot be configured for the most commonly used 40-percent rolloff Nyquist channel (carrier spacing = 1.4R<sub>s</sub>). Finally, for all the modulation techniques listed, an 8-bit output resolution in the memory is sufficient to keep the transmit output spectral quantization noise better than 40 dB down.

PREDISTORTED TRANSMIT IMPULSE RESPONSE COMPUTATION

To obtain the best BER performance, it would be desirable to match the transmit and receive filters with a square-root Nyquist characteristic, assuming that the remaining filtering functions in the transmission link are transparent. However, in general the individual transmit and receive data filters cannot be

matched and must be predistorted to account for RR, IF, and anti-aliasing (AA) filtering, as well as transmission link impairments.

The primary filtering functions in the transmission path are illustrated in Figure 3. In addition to the digitally implemented transmit and receive Nyquist data-shaping filters, there are the previously discussed D/A aperture effect and analog RR filter, as well as the analog AA and analog-to-digital (A/D) input bandwidth filters of the demodulator. The predistorted transmit frequency response is obtained by subtracting the cascaded magnitude and phase of these other known filters, along with any measured dispersions in the transmission path, from the desired channel frequency response. The resultant predistorted transmit frequency response samples are converted into time domain impulse response samples by means of a fast Fourier transform (FFT). Superposition of the individual impulse responses is then used to obtain the aggregate impulse response for an  $L/m$  symbol sequence. The resultant sample values are preloaded into the  $I, Q$  transmit spectral shaping memories.

For illustration, two predistorted impulse responses have been computed over a 16-symbol interval for 50- and 75-Msymbol/s operation (as shown in Figures 4a and 4b, respectively). Observe that at the maximum symbol rate (75 Msymbol/s), the impulse response has considerable ringing on the leading edge. This is largely to compensate for the delay dispersion in the RR and AA filters when the main lobe of the transmit spectrum fills their bands. Also note that for this worst-case predistortion, the impulse response is not well-represented over a 6-symbol aperture; therefore, some degradation is expected for the higher-level modulation formats at 75 Msymbol/s. For 50-Msymbol/s operation, the bulk of the signal spectrum is well within the RR and AA filters, and the impulse response exhibits considerably better symmetry. Furthermore, for operation at progressively lower symbol rates, the effect of the D/A aperture becomes negligible, until eventually no predistortion is necessary.

**Demodulator**

The multiplier-accumulator (MAC) is a digital-signal-processing (DSP) hardware element that is used throughout the demodulator. To accommodate a design with reduced size and low power dissipation, a generic application-specific integrated circuit (ASIC) chip was developed for use in nine different locations in the demodulator. This ASIC consists of two MACs, which can be configured in several different ways. Its multipliers have 8-bit inputs and 16-bit outputs, and the accumulators have 24 bits of resolution and may be preloaded. As with the modulator, the greatest degree of programmability is achieved when the critical processing elements in the demodulator architecture are also digital. Again, one of the major concerns is whether to sample at baseband or IF in the demodulator.

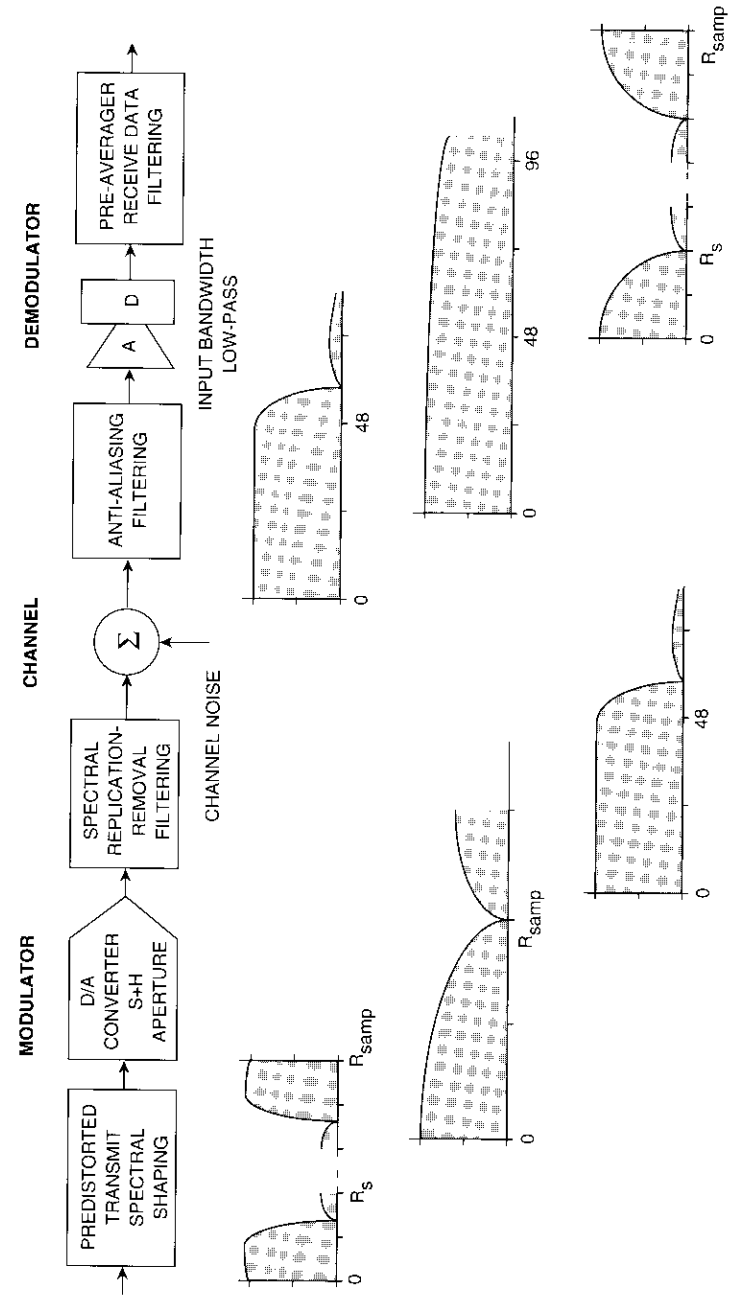


Figure 3. Significant Transmission Path Filtering Functions

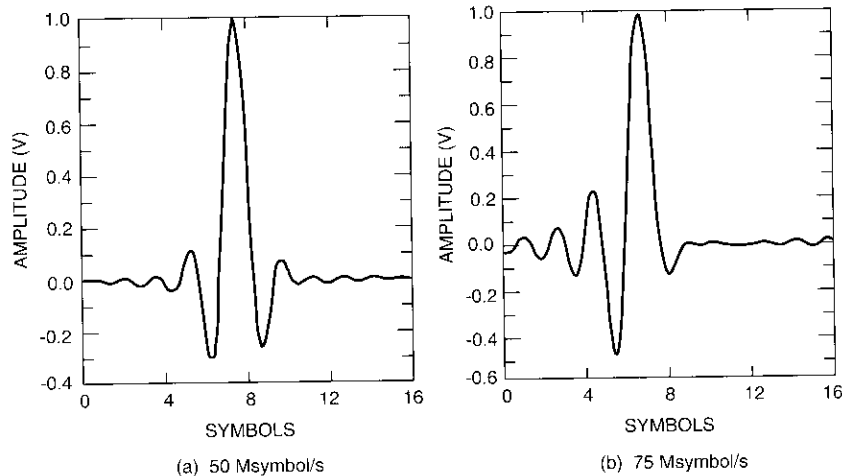


Figure 4. *Predistorted Transmit Impulse Responses for a 40-Percent Raised Cosine Channel*

#### BASEBAND VS IF A/D SAMPLE CONVERSION

In the demodulator, the first concern is whether to translate the incoming RF spectrum to a low IF or to baseband, for IF or baseband sampling, respectively. With IF sampling, the frequency can be set equal to the symbol rate and sampled at 4 s/s to greatly simplify the subsequent processing, because with a 4-s/s local oscillator (LO), every other  $I, Q$  sample is multiplied by zero [8]–[11]. The other reason for keeping the IF as low as possible is because of the effective sample aperture width of the A/D converter, which imposes a low-pass  $\sin(x)/x$  envelope on the incoming IF spectrum and requires progressively greater amplitude compensation for higher data rate operation.

The symbol-rate IF technique works well for applications where the data rate is high enough relative to the IF that its RF image can easily be filtered out. However, when operating at the low end of a broad range of continuously selectable rates, the desired band and its RF image can become very close, and difficult to separate. To provide adequate separation for continuously variable rate operation, the IF can be set at integer ratios greater than  $1 \times R_s$ . Thus, as  $R_s$  scales down from its maximum rate, the IF can be gear-shifted as  $4R_s/4$ ,  $6R_s/4$ ,  $8R_s/4$ , etc. Although this does not increase the highest absolute sampling frequency required, the front-end processing must run at 4, 6, and 8 s/s, respectively, and be averaged down to 2 s/s—the rate at which the remainder of the demodulator processing is most efficiently performed.

If the sample rate and symbol rate are not integer-related, an interpolating filter is needed to convert the non-integer number of samples per symbol to 2. Such interpolating filters are both hardware-intensive and speed-restrictive.

The minimum sample rate for the demodulator with bandpass sampling is 4 s/s, which makes 75-Msymbol/s transmission much more difficult to implement than with 2-s/s baseband sampling. Due to these restrictions, quadrature down-conversion and baseband sampling are used, as in the modulator.

The AA filter requirements for limiting the incoming bandwidth prior to A/D conversion are comparable to those for the RR filter in the modulator. Hence, for simplicity both the RR and AA filters will be designed with identical passband, transition-band, and stopband parameters.

#### DEMODULATOR IMPLEMENTATION ALTERNATIVES

As detailed in the introduction, the JED demodulator architecture is appropriate for this application because of its high degree of flexibility. However, several more specific implementation options remain to be decided upon, including acquisition techniques, the mechanism for carrier frequency conversion, and the receive data filtering realization. The rationale for choosing particular options is given below.

Figure 5 is a general block diagram of the demodulator. Fundamentally, it consists of  $I, Q$  detection paths with pre-averager (PA) receive data filtering and three estimation or tracking loops: automatic gain control (AGC), carrier phase, and symbol timing. As indicated in the figure, the detection and estimation operations are interdependent, such that all of the estimates developed aid one another coherently.

For burst mode operation, a parallel acquisition estimate processor is employed to develop initial tracking loop startup values in order to expedite synchronization and minimize the probability of phase-locked loop (PLL) hang-up [12],[13]. The acquisition processor's estimates are injected directly into the digital tracking loop accumulators. The specific algorithms used to compute these startup estimates are contained in Reference 5.

The demodulator analog front-end converts the incoming modulated RF signal (which is centered at 140 MHz) down to baseband with a fixed LO, such that a carrier offset beat frequency is superimposed on the baseband  $I, Q$  channels. Hence, after A/D conversion, the  $I, Q$  paths are passed through a carrier phase rotator to remove the beat, thereby simplifying subsequent processing. Since the A/D sample clock is always an integer multiple of the symbol clock, its phasing is properly aligned with the detection and transition sample points.

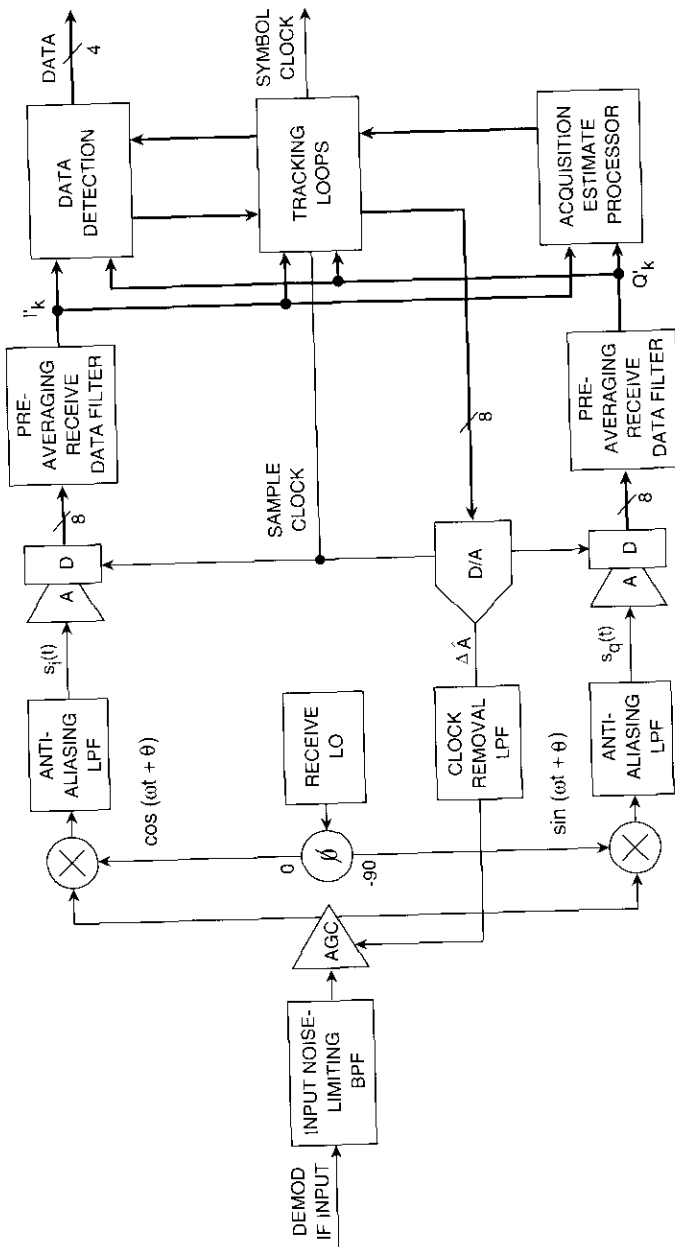


Figure 5. Demodulator Block Diagram

A voltage-controlled oscillator (VCO) could also be used for frequency translation. Although this would eliminate the carrier beat as well as the need for a carrier phase rotator, a moderate amount of additional analog hardware is required in order to step a VCO's output phase to avoid hang-up. A numerically controlled oscillator (NCO) whose phase accumulator could be preloaded or stepped would have been highly desirable, but was unavailable. Because of the 140-MHz IF, an NCO with a 350-MHz sample rate would be needed, as the maximum frequency that can typically be obtained from an NCO is its sample rate divided by 2.5 (due to practical Nyquist sampling limitations). Stepping-up or multiplying a lower-frequency NCO was ruled out because of the greater hardware complexity involved.

DETECTION PATH PROCESSING

There are three major processing blocks in the *I, Q* data detection paths: the PA receive data filter, the carrier phase rotator (CPR), and the quadrature channel detection mapper (QCDM). The detection paths are aided by the tracking loop estimates in the following ways. Since the arithmetic is fixed-point, the amplitude-level estimate is used to control the gain of the incoming signal, to avoid overflow. AGC is also essential for detection processing when the modulation technique has an amplitude-level dependency, such as QAM. The carrier phase estimate simply rotates out the carrier beat in the *I, Q* predetection samples. The symbol timing phase estimate is embedded in the sample clock at the A/D converter because the sample clock is actually tracked in the recovery loop and the symbol clock is obtained from it through integer division. Hence, the detection path samples are phase-coherent at their inception.

PA Receive Data Filter

The PA performs three important functions in the demodulator. First, it provides for a very broad range of data rate operation without any hardware changes (typically, a factor of 32). Second, the PA functions as a receive data filter and reduces the single-sided incoming noise bandwidth to  $R/2$ . Finally, the PA decimates the sample rate to 1 *s/s* for subsequent processing [14].

One patent has been granted on the basic conceptual implementation of the PA, and another is pending on an extension of its effective impulse response aperture [15]. Increasing the aperture of the PA filter provides more selective filtering for better adjacent channel suppression.

Figure 6 is a block diagram of the dual overlapping version of the PA used in this application, and Figure 7 illustrates its reuse of input samples for the case of 8 *s/s*. The effective impulse response aperture length of the PA is 2 symbols. Observe that the data detection samples are obtained by a weighted

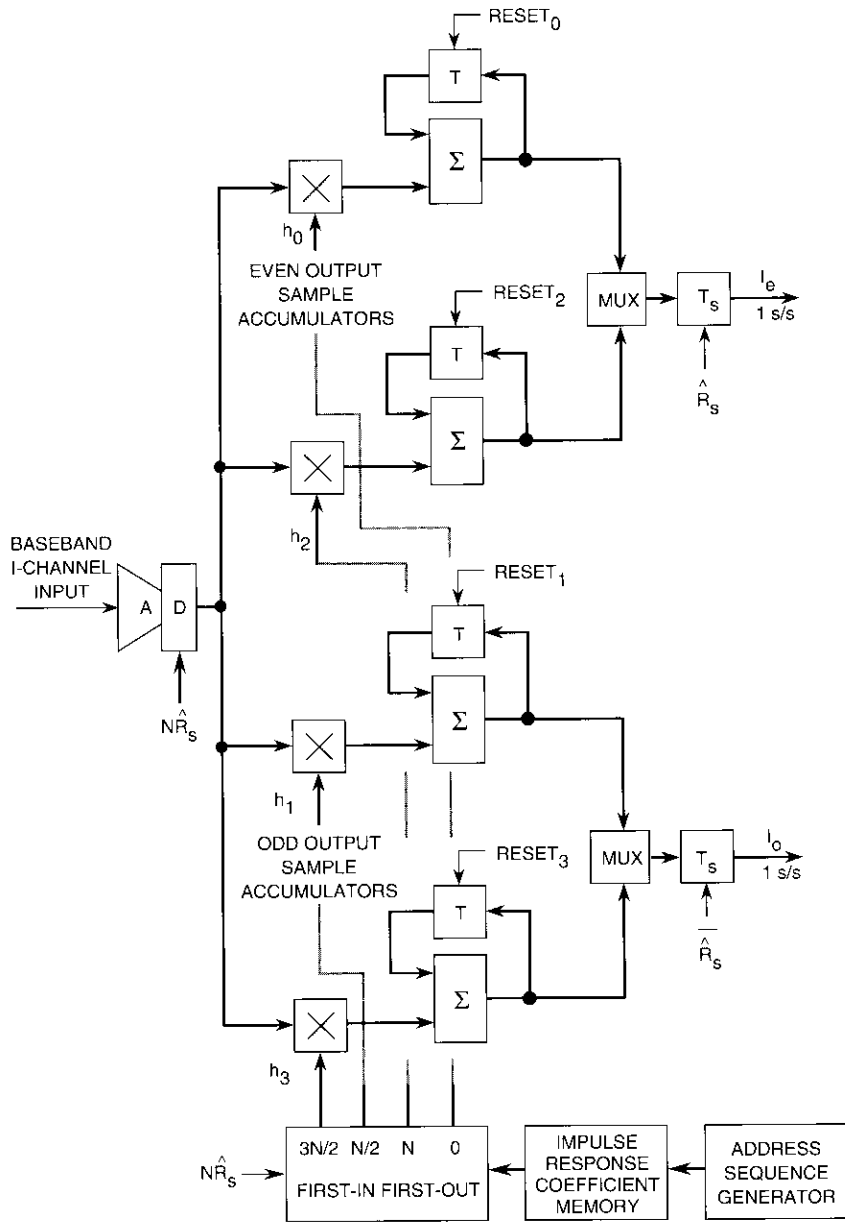


Figure 6. Dual Overlapping PA Receive Data Filter

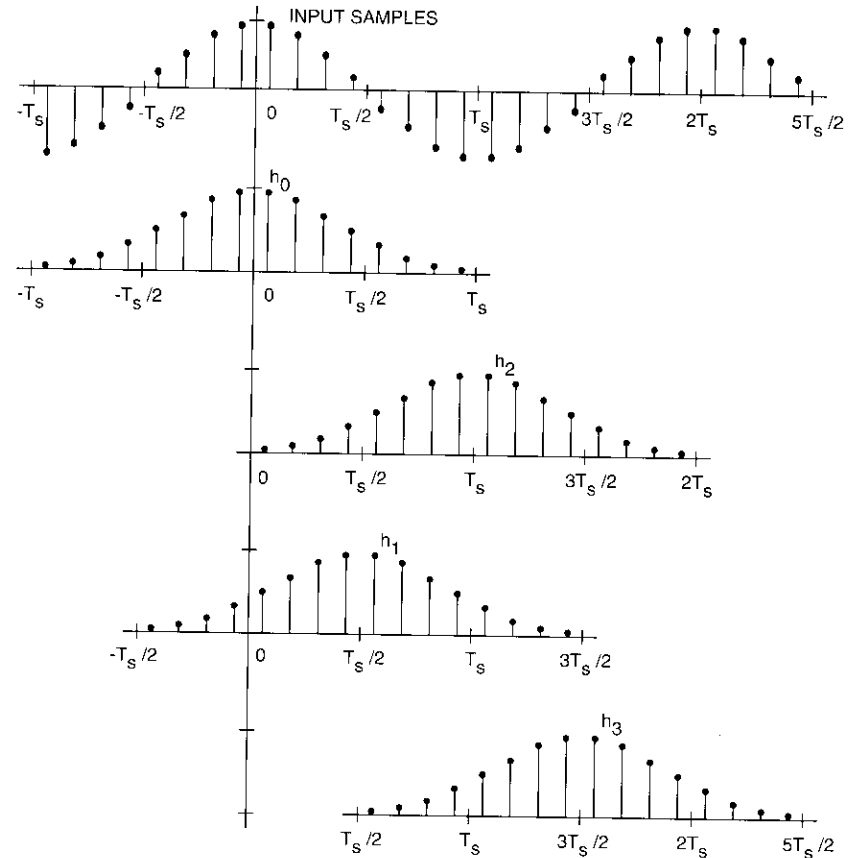


Figure 7. PA Sample Reuse

average of 16 incoming samples, which are evenly distributed about the desired point. The same is true for the data transition sample, except that its averaging intervals are staggered relative to the detection point intervals. To achieve a 2-symbol filter aperture with an output sample rate of 1 s/s, two overlapping PAs are needed for the data detection points and two others for the data transition points. The samples are weighted and averaged by MACS, which must operate at the incoming sample rate,  $NR_s$ . Moreover, all incoming samples are used twice to yield the two averages, and there are two parallel 1-s/s output streams for the data detection and transition sample paths in each I, Q channel.

The receive data filter impulse response is a raised cosine pulse, which was chosen as the best compromise between implementation complexity and adjacent channel rejection (ACR) [5]. The transition and stopband regions of the raised cosine pulse frequency response change vs the number of symbols per second used. This effect is illustrated in Figures 8a through 8d for sample rates of 2, 3, 4, and 32 s/s, respectively. Observe that the ACR improves as the number of symbols per second is increased.

The width of the frequency response window in each figure is equal to the sample rate, or  $\pm NR_s/2$ , which is  $\pm 75$  MHz at the maximum symbol rate. As a result of digital filtering, replicas of these receive filter passbands exist at integer multiples of the window interval,  $NR_s$ . Therefore, if the digital filter was acting alone, there would clearly be an adjacent channel aliasing problem with the 2-s/s case. Fortunately, at 2 s/s, the analog AA filter (whose passband range is  $\pm 48$  MHz) provides the bulk of the ACR. However, as the data rate is reduced, a range of operation with poor ACR would occur if the 3-s/s response were not included. Moreover, to avoid regions of poor ACR, the demodulator gear-shifting cannot be limited to powers of 2, as in the modulator, and must include factors of 3 as well. The resultant demodulator gear-shifting rates are listed in Table 4. Note that this technique also helps to avoid a reduction in S/N from noise aliasing.

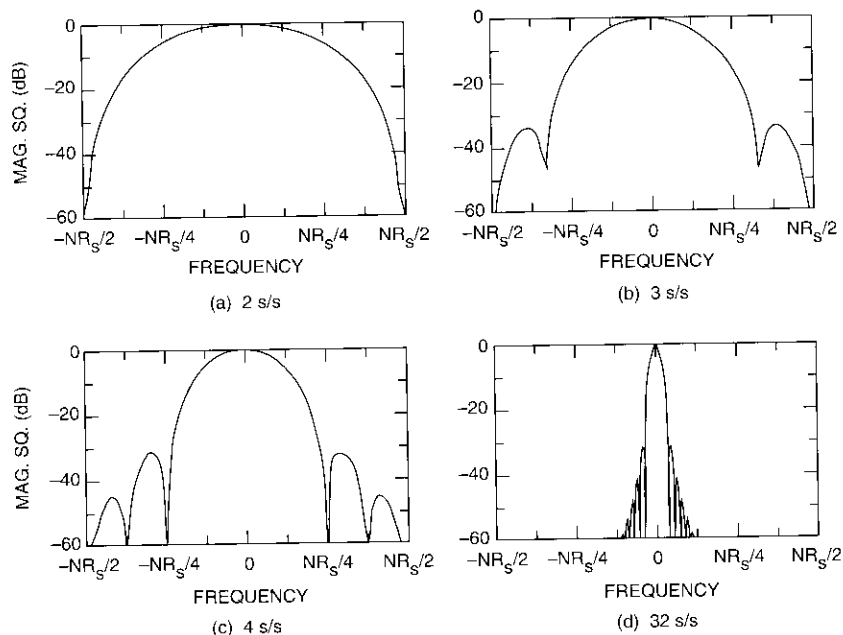


Figure 8. PA Receive Data Filter Frequency Response

TABLE 4. DEMODULATOR GEAR-SHIFTING RATES

SYMBOL RATE RANGE (Msymbol/s)	SAMPLES/ SYMBOL
$50 < R_s \leq 75$	2
$37.5 < R_s \leq 50$	3
$25 < R_s \leq 37.5$	4
$18.75 < R_s \leq 25$	6
$12.5 < R_s \leq 18.75$	8
$9.375 < R_s \leq 12.5$	12
$6.25 < R_s \leq 9.375$	16
$4.6875 < R_s \leq 6.25$	24
$2.34375 < R_s \leq 4.6875$	32

Notation

The notation used throughout the remainder of this paper is listed in Table 5. The  $2k$  and  $2k - 1$  (even and odd) subscripts denote sample values at the data detection and transition timing instants, respectively, while the  $k$  subscripts refer to all sample points. A caret over a variable denotes an estimated or detected value.

Carrier Phase Rotator

The CPR removes the frequency beat in the  $I, Q$  channels that results from the use of a fixed-carrier LO frequency translation. Prior to the CPR, the  $I, Q$  channels may be described by

$$I'_k = A_k [i_k \cos(\theta_k) + q_k \sin(\theta_k)] \tag{1a}$$

$$Q'_k = A_k [q_k \cos(\theta_k) - i_k \sin(\theta_k)] \tag{1b}$$

If the carrier phase tracking is accurate, the frequency beat is removed by performing the two matrix multiplications of the following equations:

$$\begin{aligned} I_k &= [\cos(\hat{\theta}_k), -\sin(\hat{\theta}_k)] [I'_k, Q'_k]^T \\ &= A_k [i_k \cos(\theta_k - \hat{\theta}_k) + q_k \sin(\theta_k - \hat{\theta}_k)] \sim A_k [i_k] \end{aligned} \tag{2a}$$

TABLE 5. NOTATION

NOTATION	DEFINITION
$i_k$	Unit power normalized transmit baseband in-phase samples
$q_k$	Unit power normalized transmit baseband quadrature samples
$I'_k$	Incoming baseband in-phase samples
$Q'_k$	Incoming baseband quadrature samples
$A_k$	Unknown incoming amplitude level
$\theta_k$	Random incoming carrier phase
$\tau_k$	Random incoming symbol time
$I_k$	Post-carrier phase rotated in-phase samples
$Q_k$	Post-carrier phase rotated quadrature samples
$\hat{I}_{2k}$	In-phase post-detected data feedback samples
$\hat{Q}_{2k}$	Quadrature post-detected data feedback samples
$\Delta\hat{I}_{2k-1}$	In-phase post-detected data feedback difference samples
$\Delta\hat{Q}_{2k-1}$	Quadrature post-detected data feedback difference samples
$\Delta\hat{A}_0$	Initial amplitude level offset estimate
$\hat{\theta}_0, \Delta\hat{\theta}_0$	Initial carrier phase and frequency estimates
$\hat{\tau}_0$	Initial symbol timing estimate
$\hat{A}$	Amplitude reference level
$\Delta A_{2k}$	Amplitude level error
$\Delta\theta_{2k}$	Carrier phase error
$\Delta\tau_{2k-1}$	Symbol timing error
$K_d$	Carrier and clock phase detector gain constant
$K_A, B_A$	AGC loop gain constant and single-sided noise bandwidth
$K_\theta, B_\theta$	Carrier loop phase gain constant and single-sided noise bandwidth
$K_{\Delta\theta}$	Carrier loop frequency gain constant
$K_\tau, B_\tau$	Symbol timing loop gain constant and single-sided noise bandwidth
$\Delta\hat{A}_{2k}$	Amplitude level offset output estimate
$\hat{\theta}_{2k}$	Carrier phase output estimate
$\Delta\hat{\theta}_{2k}$	Carrier frequency output estimate
$\hat{\tau}_{2k-1}$	Symbol timing output estimate

$$Q_k = [\sin(\hat{\theta}_k), \cos(\hat{\theta}_k)][I'_k, Q'_k]^T$$

$$= A_k[q_k \cos(\theta_k - \hat{\theta}_k) - i_k \sin(\theta_k - \hat{\theta}_k)] \sim A_k[q_k] \quad (2b)$$

The CPR can be implemented with two MACs that operate at  $4R_s$ , as indicated in equations (2a) and (2b), and whose accumulators are zeroed after every two samples; or equivalently, with four MACs at  $2R_s$  that operate on the detection and transition samples separately.

#### Quadrature Channel Detection Mapper

The QCDM performs the inverse operation of its counterpart in the modulator, the QDM, but at a much higher resolution because of the inclusion of noise in the demodulator. In general, the QCDM maps the post-CPR  $I, Q$  channels into as many as four parallel detected data streams  $\hat{A}, \hat{B}, \hat{C}, \hat{D}$  for 16-ary signaling. For PSK modulation techniques, the decision boundaries are radial lines that bisect the distance between adjacent signals in the constellation (assuming equally likely *a priori* signal probabilities), whereas for QAM, the boundaries form an amplitude-dependent grid pattern. The different mappings are most easily implemented as a table lookup.

To keep the QCDM memory from becoming too large, a second mapping is used to generate the data feedback waveforms, as indicated in Figure 9. Since these waveforms are noiseless and have few deterministic levels, they can be represented with relatively small output bit resolutions. Note that one symbol of delay is necessary to accommodate post-detection difference feedback for use in the symbol timing phase detector. Finally, for 16-QAM, the AGC reference amplitude must change as a function of the detected data.

#### TRACKING LOOP ANALYSIS

To enable coherent detection of the digital data, three tracking loops are typically necessary: amplitude level or AGC, carrier phase, and symbol timing. Each loop has a nominal operating setting (e.g., an amplitude reference level or NCO center frequency). In this implementation, an error signal is added to the nominal settings to make corrections for tracking. The error signals were derived in Reference 3 for QPSK modulation, but are readily extendable to most two-dimensional signaling formats, including such popular modulation techniques as 2-, 4-, 8-, and 16-PSK; MSK; Offset-QPSK; and 16-QAM.

The three digitally implemented, interdependent tracking loops will now be analyzed. Fundamentally, each loop consists of an error or phase detector and an equivalent linear filter that provides an output estimate. A generalized block diagram is shown in Figure 10, and the feedback signals required in the three different loops are given in Table 6.

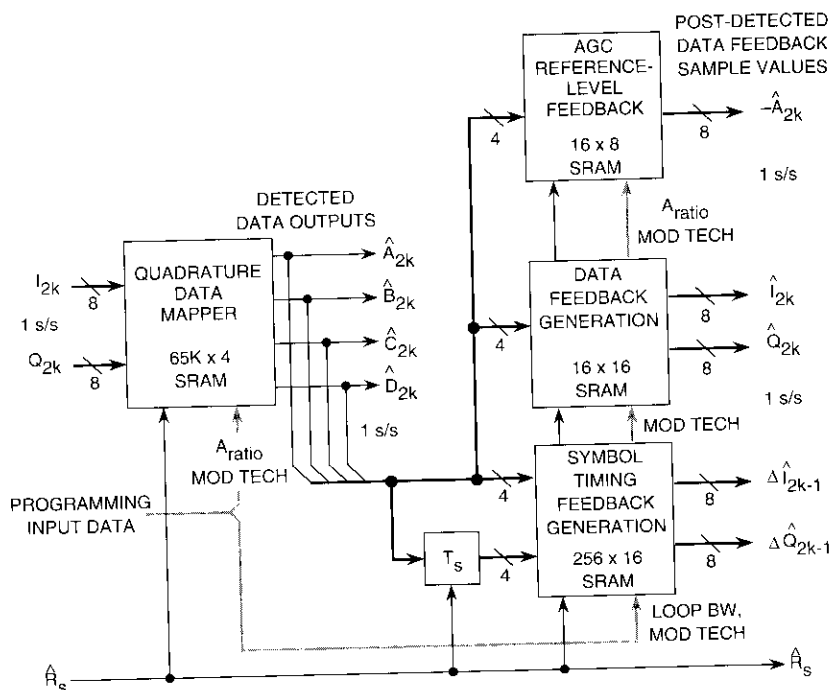


Figure 9. Quadrature Channel Detection and Data Feedback Mappings

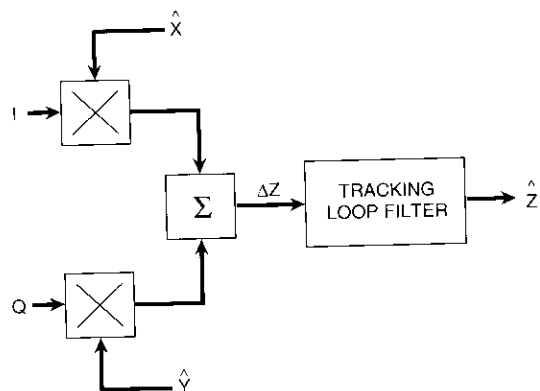


Figure 10. Generalized Tracking Loop Processing

TABLE 6. TRACKING LOOP ERROR DETECTOR FEEDBACK SIGNALS

FUNCTION	$\hat{X}$	$\hat{Y}$	$\Delta Z$	$\hat{Z}$
Amplitude Level	$\hat{I}_{2k}$	$\hat{Q}_{2k}$	$\Delta A_{2k}$	$\Delta \hat{A}_{2k}$
Carrier Phase	$\hat{Q}_{2k}$	$-\hat{I}_{2k}$	$\Delta \theta_{2k}$	$\hat{\theta}_{2k}$
Symbol Timing	$\Delta \hat{I}_{2k-1}$	$\Delta \hat{Q}_{2k-1}$	$\Delta \tau_{2k-1}$	$\hat{\tau}_{2k-1}$

AGC Tracking Loop

For signal constellations that can be placed on a common power circle, such as the PSK and MSK formats listed above, AGC is not explicitly necessary for the detection process because the decision boundaries are radial lines which are not amplitude-dependent. However, because the error signal detector gain in all three tracking loops scales with the incoming signal level, the incoming amplitude level affects their open-loop gains and closed-loop bandwidths. In addition, with a fixed-point arithmetic digital implementation, the maximum sample value excursions must be limited to prevent overflow.

Incoming gain or level fluctuations are generally extremely slow relative to the data rate. Hence, a first-order tracking loop is sufficient for most applications. For operation with relatively short bursts and a sufficiently accurate acquisition estimate, the estimate can be held for the duration of the burst and no AGC tracking is necessary [16].

Figure 11 is a block diagram for a gain parameter model of the AGC tracking loop. The model consists of a variable gain-controlled amplifier, an

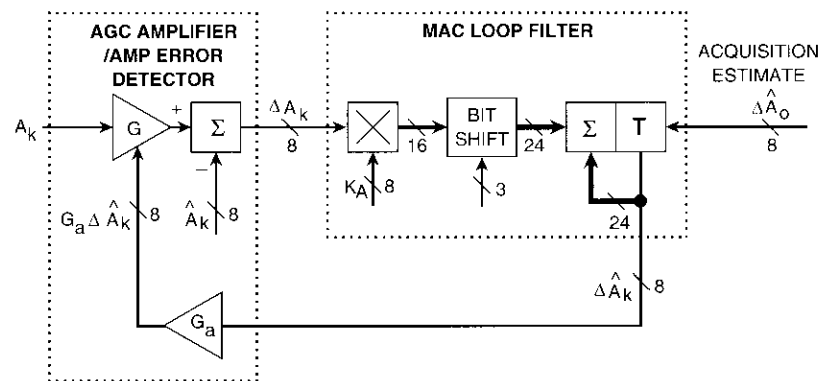


Figure 11. AGC Tracking Loop Model

amplitude-level error detector, and a multiplier-accumulator to provide filtering. Recall that the input data and error detector multiplier input resolutions are 8 bits, and the accumulator resolution is 24 bits. In this instance, the eight most significant accumulator bits are used to control the gain. The variable-gain amplifier is voltage-controlled and resides in the IF section of the demodulator prior to the A/D converters. Thus, the AGC error estimate output must pass through a D/A converter and back into the analog domain to control the gain. An initial estimate,  $\Delta\hat{A}_o$ , which is typically extracted from a parallel incoherent estimator, may be injected directly into the output accumulator to expedite acquisition.

**AGC Error Detector.** The AGC tracking error signal is defined as

$$\begin{aligned} \Delta A_{2k} &= (I_{2k}\hat{I}_{2k} + Q_{2k}\hat{Q}_{2k}) - \hat{A} \\ &= A_{2k}(i_{2k}I_{2k} + q_{2k}Q_{2k}) - \hat{A} \end{aligned} \quad (3)$$

with  $\hat{A} \triangleq (\hat{I}_{2k}\hat{I}_{2k} + \hat{Q}_{2k}\hat{Q}_{2k})$ . When the signals all reside on the same power circle, as with the PSK modulation family,  $\hat{A}$  is a constant from symbol to symbol. However, for constellations such as 16-QAM,  $\hat{A}$  takes on three values as a function of the post-detection data feedback.

**AGC Closed-Loop Transfer Function.** Dropping the subscripts for clarity, the amplifier gain may be expressed in terms of the amplitude level error output estimate as

$$G(\Delta\hat{A}) = G_{\text{nom}}\hat{A} / (\hat{A} + G_u\Delta\hat{A}), \text{ such that } G_u\Delta\hat{A} > -\hat{A} \quad (4)$$

Note that when the error signal  $\Delta\hat{A} = 0$ , the amplifier is set at its nominal gain. The parameter  $G_u$  is used to match this gain-controlled amplifier model to a specific implementation. It includes any amplification in the output error estimate feedback path after the D/A converter.

The MAC transfer function may be written in terms of its z-transform as

$$\Delta\hat{A} = K_A\Delta A / (z-1) \quad (5)$$

where  $\Delta A = G(\Delta\hat{A})A - \hat{A}$ . Substituting for  $\Delta A$  into equation (5) gives

$$\begin{aligned} \Delta\hat{A} &= K_A[G(\Delta\hat{A})A - \hat{A}] / (z-1) \\ &= K_A\hat{A}[G_{\text{nom}}A - (\hat{A} + G_u\Delta\hat{A})] / [(z-1)(\hat{A} + G_u\Delta\hat{A})] \end{aligned} \quad (6)$$

Equation (6) can be rewritten in standard second-order polynomial form as

$$\Delta\hat{A}^2[G_u(z-1)] + \Delta\hat{A}\{\hat{A}(z-1) + K_A G_u\} + K_A\hat{A}(\hat{A} - G_{\text{nom}}A) = 0 \quad (7a)$$

$$\Delta\hat{A}^2(a) + \Delta\hat{A}(b) + (c) = 0 \quad (7b)$$

The roots of equation (7) may be found from

$$\begin{aligned} \Delta\hat{A} &= -b(1 \pm \sqrt{1 - 4(ac/b^2)}) / 2a \\ &= -b\{1 \pm [1 - 2(ac/b^2) + \dots]\} / 2a \\ &\cong -c/b \end{aligned} \quad (8)$$

where only the first term in the expansion has been used, since  $b^2 \gg ac$ . The resultant transfer function is then

$$\Delta\hat{A} = K_A[G_{\text{nom}}A - \hat{A}] / [z + (K_A G_u - 1)] \quad (9)$$

A great deal is known about setting the closed-loop parameters for analog tracking loops to maintain stability and the desired transient response [17]. Hence, analog tracking parameters will be used, and the impulse invariance technique will map these into the corresponding roots of the digital loop. The impulse invariance conversion is related as

$$z_{\text{root}} = \exp(-\omega_A T_s) = -(K_A G_u - 1) \quad (10)$$

The multiplier gain constant is then determined by

$$\begin{aligned} K_A G_u &= 1 - \exp(-\omega_A T_s) \\ &\cong 1 - (1 - \omega_A T_s) \\ &= \omega_A T_s \\ &= 4(B_A / R_s) \end{aligned} \quad (11)$$

where  $\omega_A = 4B_A$  and  $T_s = 1/R_s$ . The AGC closed-loop time constant (in symbol time units) is then

$$(\tau_A / T_s) = (1/4)(R_s / B_A) \quad (12)$$

with  $\tau_A = 1/\omega_A$ .

*Symbol Timing Tracking Loop*

Like the AGC loop, the symbol timing loop is first-order and requires only a single phase accumulator. Since an NCO is used to reconstruct the clock, the oscillator's inherent phase accumulator serves as the loop filter. Figure 12 is a block diagram of the loop. Note that the loop also contains a multiplicative gain,  $M$ , before the NCO, as well as a divide-by- $N$  gain after the NCO. The multiplicative gain comes about because the independent sample clock that runs the NCO is much higher than the incoming sample rate. Therefore, incoming samples are typically added in the NCO phase accumulator on a greater than one-for-one basis. Also, since the NCO output is at the sample rate frequency,  $NR_s$ , it must be divided by  $N$  to obtain the symbol rate,  $R_s$ . If an initial estimate,  $\hat{\tau}_0$ , is employed to expedite acquisition, it must typically be modified as  $f(\hat{\tau}_0)$  to properly control both the output accumulator and divider in order to account for fine and coarse phase adjustments, respectively.

The timing phase accumulator resolution is 24 bits, of which the 10 most significant are mapped into sinusoidal sample values. After 8-bit D/A conversion and low-pass filtering (which are not shown in the timing parameter loop model), the sinusoidal samples are passed through a limiter to produce the properly phased sample clock waveform,  $N\hat{R}_s$ .

**Symbol Timing Phase Error Detector.** The symbol timing phase error signal is defined as

$$\begin{aligned} \Delta\tau_{2k-1} &= I_{2k-1} \Delta\hat{I}_{2k-1} + Q_{2k-1} \Delta\hat{Q}_{2k-1} \\ &= A_{2k-1} (i_{2k-1} \Delta\hat{I}_{2k-1} + q_{2k-1} \Delta\hat{Q}_{2k-1}) \end{aligned} \quad (13)$$

where  $\Delta\hat{I}_{2k-1} = (\hat{I}_{2k} - \hat{I}_{2k-2})$ . If no data transitions occur, the symbol timing phase detector output is zero. The loop gain and bandwidth are then effec-

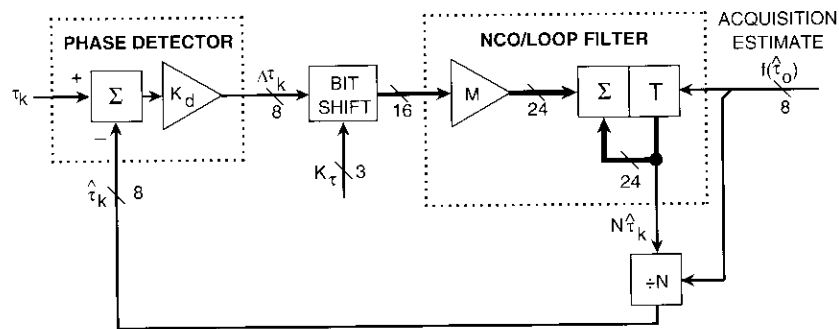


Figure 12. *Symbol Timing Tracking Loop Model*

tively zero, and the loop time constant is extremely long. Moreover, the best that the loop can accomplish in the absence of data transition information is to hold its last accumulated error value and coast. For multilevel modulation techniques, the error signal is weighted in proportion to the differential magnitude of the data transitions,  $\Delta\hat{I}_{2k-1}$ .

**Symbol Timing Closed-Loop Transfer Function.** The NCO transfer function may be written in terms of its  $z$ -transform as

$$\begin{aligned} \hat{\tau} &= (M/N)K_\tau \Delta\tau / (z-1) \\ &= (M/N)K_\tau K_d \sin(\tau - \hat{\tau}) / (z-1) \\ &\cong (M/N)K_\tau K_d (\tau - \hat{\tau}) / (z-1) \end{aligned} \quad (14)$$

where the final linearizing approximation results when the phase difference is sufficiently small. To avoid using an extra multiplier, the loop gain parameter,  $K_\tau$ , is incremented in powers of 2 by shifting the bits coming into the NCO up or down. The phase detector gain,  $K_d$ , is proportional to the incoming signal amplitude,  $A_{2k-1}$ , and to the number and magnitude of the transitions in the data pattern. For example, for QPSK with "10..." data patterns in both the  $I$  and  $Q$  channels,  $K_d$  is maximized, whereas with pseudorandom data,  $K_d$  would be half the maximum value.

Substituting for  $\Delta\tau$  in equation (14) gives

$$\hat{\tau} = (M/N)K_\tau K_d (\tau - \hat{\tau}) / (z-1) \quad (15)$$

Equation (15) may be written in standard transfer function form as

$$\hat{\tau} = (M/N)K_\tau K_d \tau / \{z + [(M/N)K_\tau K_d - 1]\} \quad (16)$$

Again, the impulse invariance conversion is related as

$$\exp(-\omega_\tau T_s) = -[(M/N)K_\tau K_d - 1] \quad (17)$$

and for the multiplier gain parameter this yields

$$K_\tau = (4/K_d)(N/M)(B_\tau/R_s) \quad (18)$$

with the symbol timing closed-loop time constant (in symbol time units) as

$$(\tau_\tau/T_s) = (1/4)(R_s/B_\tau) \quad (19)$$

Carrier Phase Tracking Loop

Since the carrier phase loop is second-order, it can track frequency as well as phase variations. Figure 13 is a block diagram of the loop, which consists of a phase detector, two MACs (one for phase and one for frequency), a quadrature component generator, and a CPR. As before, the input and multiplicative processing uses 8-bit resolution, whereas the phase and frequency accumulators employ 24 bits. The quadrature component generator table lookup uses the most significant 10 bits from the output phase estimate accumulator, which has a modulo-360° range. Initial incoherently derived phase and frequency estimates,  $\hat{\theta}_o$  and  $\Delta\hat{\theta}_o$ , may again be employed to expedite acquisition by injecting them directly into their respective output accumulators.

CARRIER PHASE ERROR DETECTOR

The carrier phase detector response is described by

$$\begin{aligned} \Delta\theta_{2k} &= I_{2k}\hat{Q}_{2k} - Q_{2k}\hat{I}_{2k} \\ &= A_{2k}(i_{2k}\hat{Q}_{2k} - q_{2k}\hat{I}_{2k}) \\ &= K_d \sin(\theta_{2k} - \hat{\theta}_{2k}) \end{aligned} \tag{20}$$

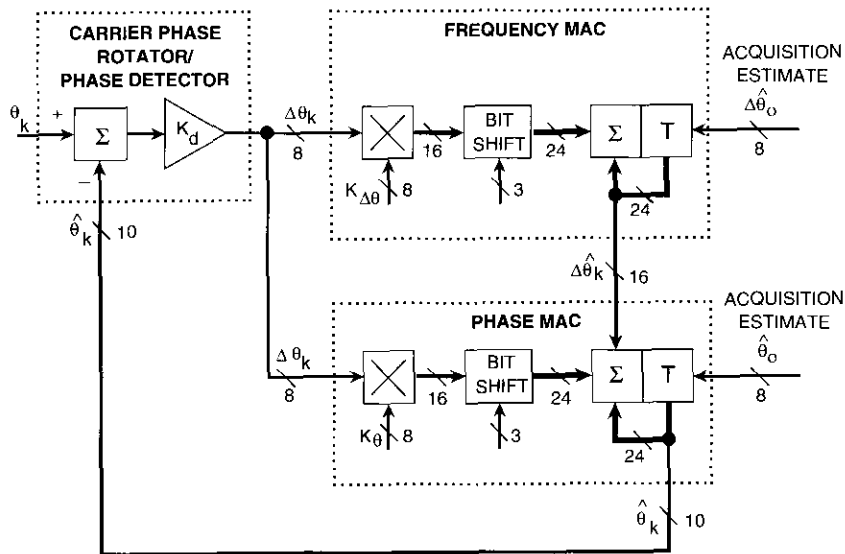


Figure 13. Carrier Phase Tracking Loop Model

When the phase difference is sufficiently small, linear tracking results, as

$$\Delta\theta_{2k} = K_d(\theta_{2k} - \hat{\theta}_{2k}) \tag{21}$$

**Carrier Phase Closed-Loop Transfer Function.** The z-transform for the two accumulators is

$$\hat{\theta} = [K_\theta \Delta\theta / (z-1) + K_{\Delta\theta} \Delta\theta / (z-1)^2] \tag{22}$$

Substituting in equation (21) gives

$$\hat{\theta} = [K_\theta K_d (\theta - \hat{\theta}) / (z-1) + K_{\Delta\theta} K_d (\theta - \hat{\theta}) / (z-1)^2] \tag{23}$$

Grouping terms and rewriting equation (23) into a transfer function format yields

$$\begin{aligned} \hat{\theta} / \theta &= [K_\theta K_d (z-1) + K_{\Delta\theta} K_d] / [(z-1)^2 + K_\theta K_d (z-1) + K_{\Delta\theta} K_d] \\ &= K_d [K_\theta (z-1) + K_{\Delta\theta}] / [z^2 + z(K_\theta K_d - 2) + K_d(K_{\Delta\theta} - K_\theta) + 1] \end{aligned} \tag{24}$$

The discrete-time response of equation (24) will be related to the analog transient response, as follows. In standard second-order notation, the complex roots in the analog s-domain are

$$s = -\omega_n (\zeta \pm j\sqrt{1-\zeta^2}) \tag{25}$$

To preserve the closed-loop phase stability predicted by the s-plane analysis, the impulse invariance transform of equation (10) is combined with equation (25) to give

$$z_{\text{roots}} = -\exp[-\omega_n T_s (\zeta \pm j\sqrt{1-\zeta^2})] \tag{26}$$

Expanding equation (26) and equating it with the denominator of equation (24) yields two simultaneous equations for setting the carrier tracking loop parameters:

$$K_d (K_{\Delta\theta} - K_\theta) + 1 = \exp(-2\zeta\omega_\theta T_s) \tag{27a}$$

$$K_{\theta}K_d - 2 = -2 \exp(\zeta\omega_{\theta}T_s) \cos\left[\omega_{\theta}T_s(\sqrt{1-\zeta^2})\right] \quad (27b)$$

These equations may be expanded in series form as

$$K_d(K_{\Delta\theta} - K_{\theta}) + 1 = 1 - (2\zeta\omega_{\theta}T_s) + (2\zeta\omega_{\theta}T_s)^2 / 2 - \dots \quad (28a)$$

$$K_{\theta}K_d - 2 = -2\left[1 - (\zeta\omega_{\theta}T_s) + (\zeta\omega_{\theta}T_s)^2 / 2 - \dots\right] \cdot \left[1 - (\omega_{\theta}T_s)^2(1 - \zeta^2) / 2 + \dots\right] \quad (28b)$$

Recall that the sampling rate of these loops is one sample per symbol, and the closed-loop bandwidths typically average sample values over hundreds of symbol times. Hence,  $2\zeta\omega_{\theta}T_s \ll 1$ , so equation (28) may be approximated with lower order terms as

$$K_dK_{\Delta\theta} \cong (\omega_{\theta}T_s)^2 \quad (29a)$$

$$K_dK_{\theta} \cong 2\zeta\omega_{\theta}T_s \quad (29b)$$

For a second-order tracking loop, the single-sided carrier noise equivalent bandwidth,  $B_{\theta}$ , is equated with the natural frequency,  $\omega_{\theta}$ , by

$$B_{\theta} = [\zeta + 1/(4\zeta)]\omega_{\theta} / 2 = 0.5303\omega_{\theta} \quad (30)$$

when the damping ratio  $\zeta = 1/\sqrt{2}$ . Equation (29) can be related in terms of the normalized ratio of symbol rate to bandwidth as

$$K_{\Delta\theta} = (3.556 / K_d)(B_{\theta} / R_s)^2 \quad (31a)$$

$$K_{\theta} = (2.667 / K_d)(B_{\theta} / R_s) \quad (31b)$$

**Hardware emulation results**

An extensive hardware emulation program was written at COMSAT Laboratories to validate the design and assess the modem's performance. This was particularly important because of the development of the critical ASIC chip, which is so widely used in the demodulator. Figure 14 is a functional block diagram of the emulation software. As indicated, it consists of a mix of analog

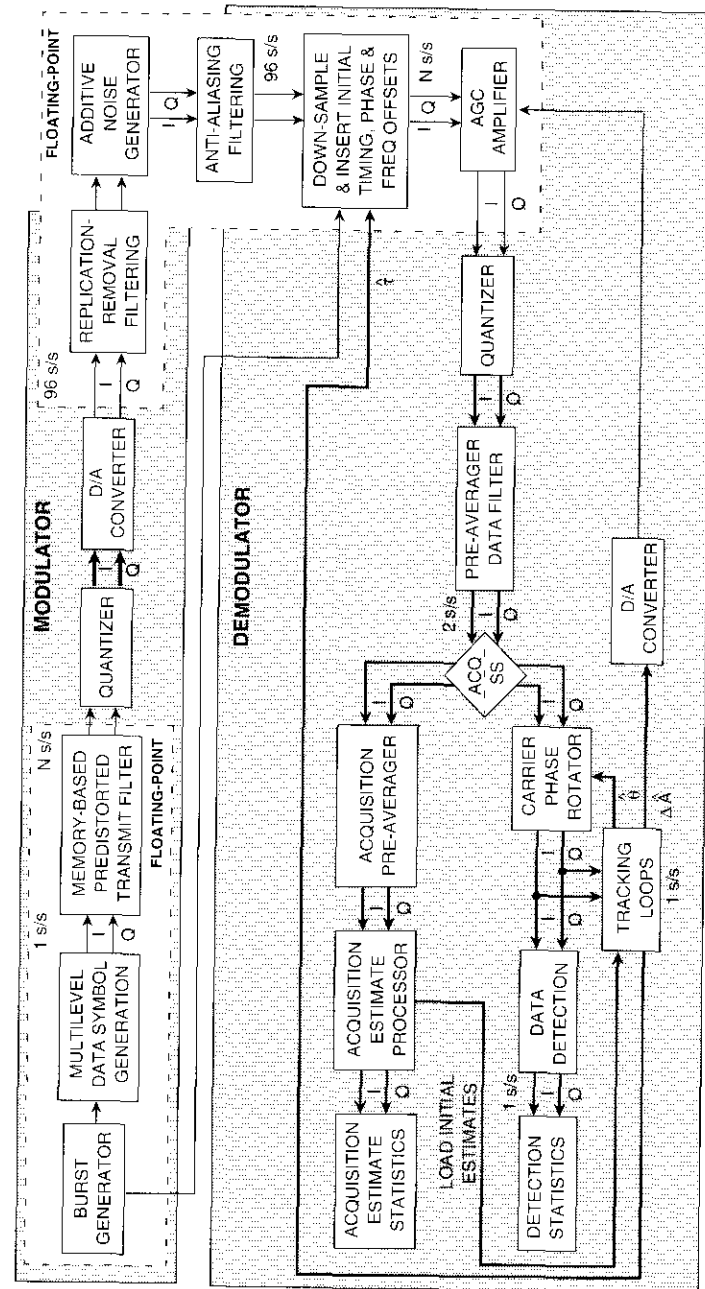


Figure 14. Hardware Emulation Block Diagram

and digitally implemented functions, fixed-point and floating-point arithmetic, and processing at variable numbers of samples per symbol. A Monte Carlo technique was used to simulate the effects of additive white Gaussian noise (AWGN). The emulations were performed on an Apollo DN-3000 workstation.

The results consist of both time and frequency domain responses. Unless stated otherwise, the plots represent a single data burst response with 2,048 information symbols, not including the preamble and unique-word sequences. Frequency domain plots were typically obtained by averaging the results from sixteen 128-point FFTs from the points in a time domain data burst. All of the modulation techniques previously mentioned were emulated; however, for brevity, only a representative group will be exhibited. These will typically be for QPSK because of its widespread applicability in satellite communications.

#### Modulator spectral purity

Transmit spectra were emulated to check the spectral fidelity of the modulator. Two sets of QPSK-modulated spectra with 8-bit D/A quantization are shown in Figures 15 and 16 before and after the transmit RR filter, for the extremes of symbol rate operation (2.34375 and 75 Msymbol/s [32 and 2 s/s]), respectively. Note the replicated lobes in Figure 15b, with their  $\sin(x)/x$  envelope from the D/A sample-and-hold aperture. The replicated lobes are not apparent in Figure 15a because the first pair occurs at  $\pm 75$  MHz. The spectral jaggedness is due to the relatively small sample set (2,048). Most significantly, the RR output spectra are monotonic and the quantization noise settles below 40 dB, the design goal.

#### EYE AND SCATTER DIAGRAMS

Eye and scatter diagrams were obtained at several locations in the data path to assess detection performance. Transmit and receive QPSK eye diagrams are illustrated in Figures 17 and 18, respectively, for 2.34375- and 75-Msymbol/s operation. To minimize the size of the data sets required, the transmit eyes are drawn with 8 s/s. The receive eyes are processed at 2 s/s, and consequently are triangular in appearance. As expected, the transmit eye is symmetrical at the lower symbol rate because the group delay predistortion required is negligible. The maximum peak-to-peak excursions of these eyes are important in making efficient use of the D/A and A/D reference level ranges. In particular, the signal levels were adjusted to occupy the full range in the modulator D/A, whereas they were typically backed off by approximately 6 dB in the demodulator A/D to allow room for amplitude level and carrier beat excursions, as well as noise overhead.

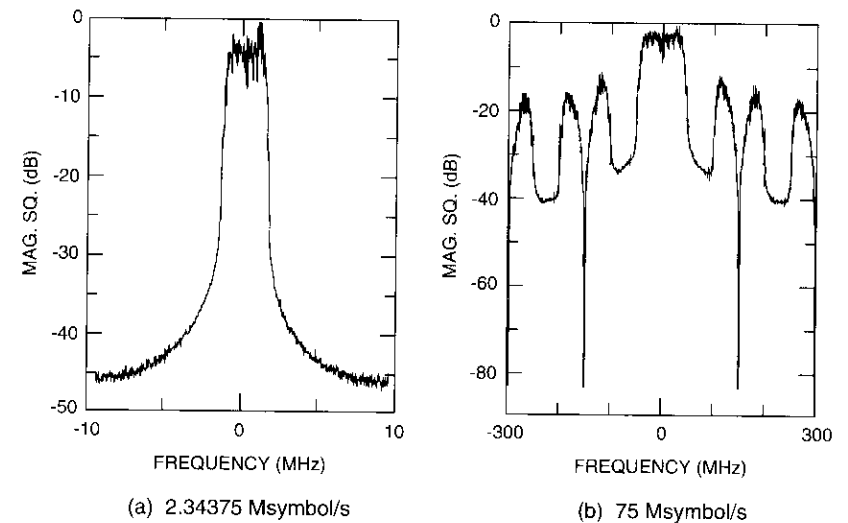


Figure 15. Pre-RR Filter QPSK Modulator Spectra

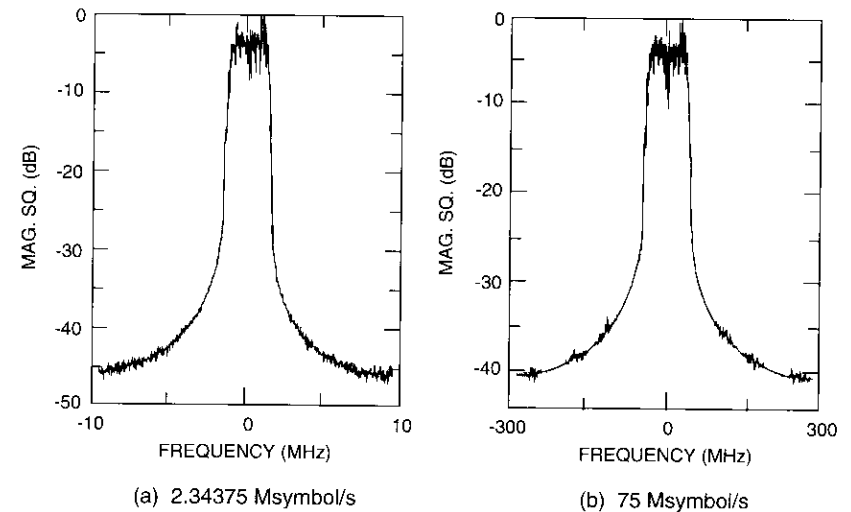
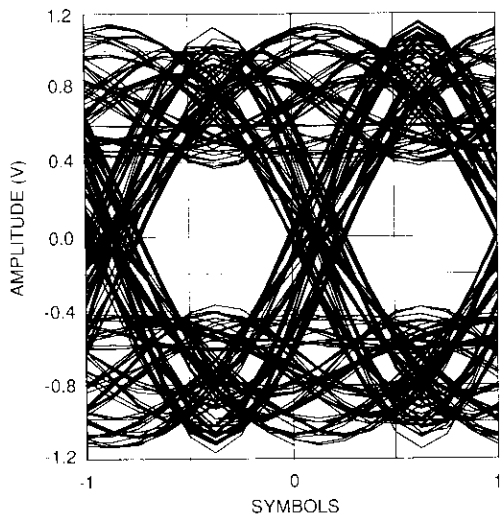
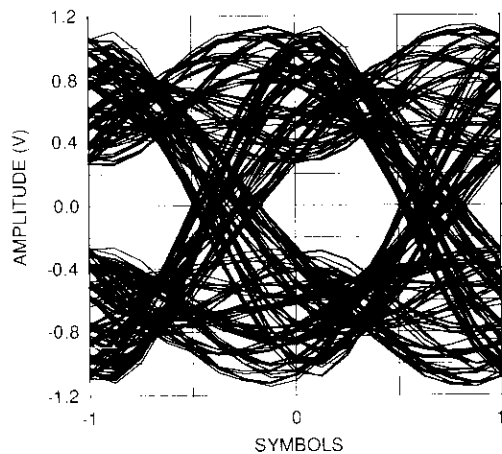


Figure 16. Post-RR Filter QPSK Modulator Spectra

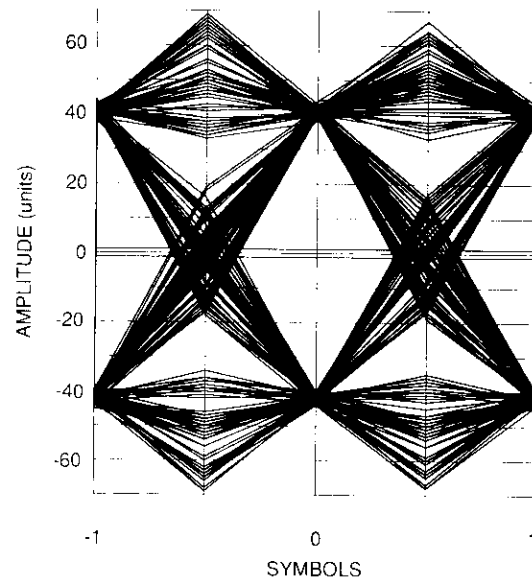


(a) 2.34375 Msymbol/s

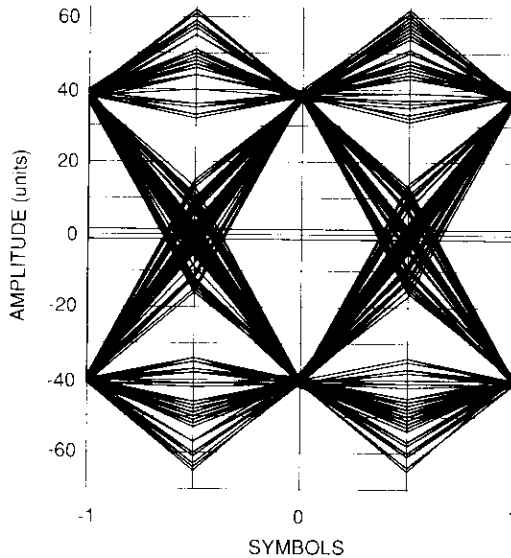


(b) 75 Msymbol/s

Figure 17. QPSK Modulator Eye Diagrams



(a) 2.34375 Msymbol/s



(b) 75 Msymbol/s

Figure 18. QPSK Demodulator Eye Diagrams

Demodulator QPSK and 16-QAM scatter diagrams are depicted in Figures 19 and 20, respectively, before and after the CPR, which removes the *I, Q* carrier beat. The scatter is indicative of the quantization effects due to the transmit and receive data filtering apertures and finite word length limitations in the entire modem, as well as the almost negligible effect of tracking loop jitter. With 8-bit quantization, the *I, Q* QPSK detection points were typically set around  $\pm 40$  units.

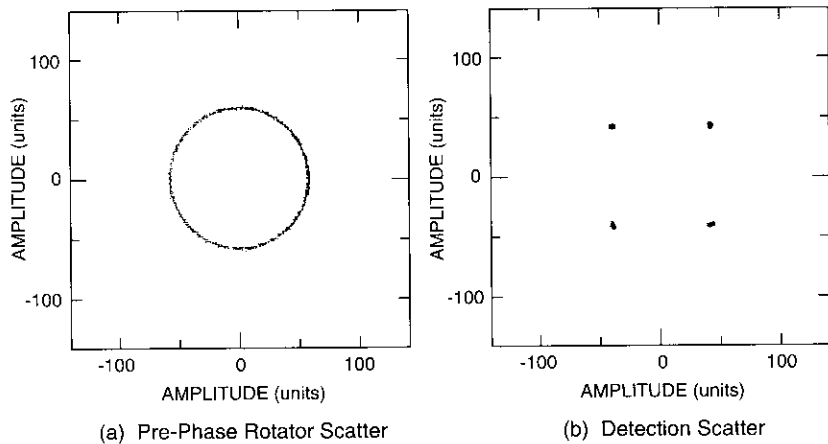


Figure 19. QPSK Demodulator Scatter Diagrams

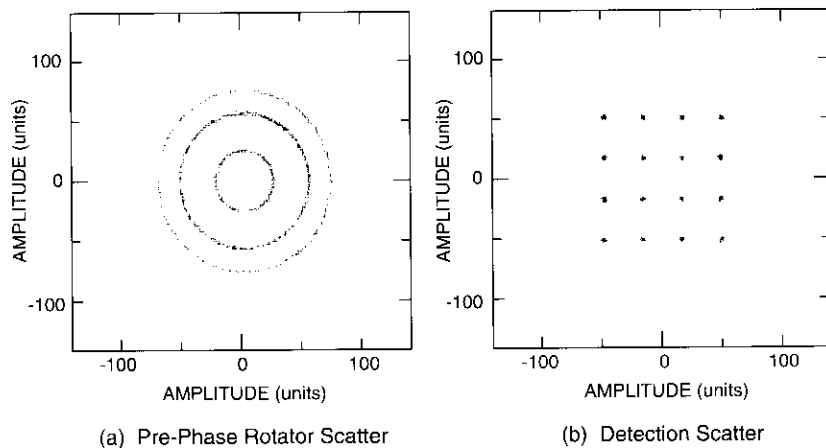


Figure 20. 16-QAM Demodulator Scatter Diagrams

For 16-QAM, the three concentric circles of signals with the same power are evident in the pre-rotated diagram. These require an AGC reference amplitude that changes on a symbol-by-symbol basis, rather than remaining at a constant level. This avoids an AGC tracking loop detector error buildup for moderately long strings of consecutive equal-power signals. Again, there is reasonable overhead to allow for initial AGC variations and carrier beating.

S/N PERFORMANCE

The BER was emulated at a single *S/N* point for all of the modulation techniques except MSK at  $R_s = 25$  Msymbol/s (6 s/s). The results are listed in Table 7. Complete curves were not obtainable due to the relatively lengthy Monte Carlo BER simulation times. About 0.55 dB of the degradation (delta) from ideal BER performance was due to the intentional mismatch of the transmit and receive data filters to minimize the demodulator hardware requirement. The increased degradation for the higher level modulation formats is primarily due to transmit and receive filter aperture limitations. All of the spectral occupancies were predistorted 40-percent raised cosine, except for 16-PSK, which was 80-percent raised cosine.

Tracking loop operation at low *S/N*'s was evaluated by including AWGN in the emulation channel. The minimum *S/N*, rounded up to the nearest half-dB at which the demodulator could consistently acquire and track in burst mode, is given in Table 8. Because of the complexity of the emulation and the relatively long period of time required to run a single data burst, these measurements were made on a burst-by-burst basis and thus cannot be directly related to a burst detection reliability. All of the preambles were binary, regardless of the modulation technique used. Likewise, the unique-word detection was binary to make maximum use of available *S/N* and to resolve the

TABLE 7. BER MEASUREMENT POINTS

MODULATION TECHNIQUE	$E_b/N_o$ (dB)	BER ( $\times 10^{-3}$ )	DELTA (dB)
BPSK	6.0	4.1	0.6
QPSK	6.0	4.7	0.7
Offset-QPSK	6.0	4.9	0.7
8-PSK	9.0	5.8	0.9
16-QAM	11.0	4.2	1.0
16-PSK	13.0	7.5	1.2

TABLE 8. MINIMUM S/N FOR ACQUISITION AND TRACKING

MODULATION TECHNIQUE	$E_b/N_o$ (dB)	BER ( $\times 10^{-1}$ )	PREAMBLE LENGTH
BPSK	0.0	1.0	32
QPSK	0.0	1.0	64
Offset-QPSK	1.5	1.2	64
8-PSK	4.0	1.3	96
16-QAM	2.5	1.6	112
16-PSK	5.0	2.2	144

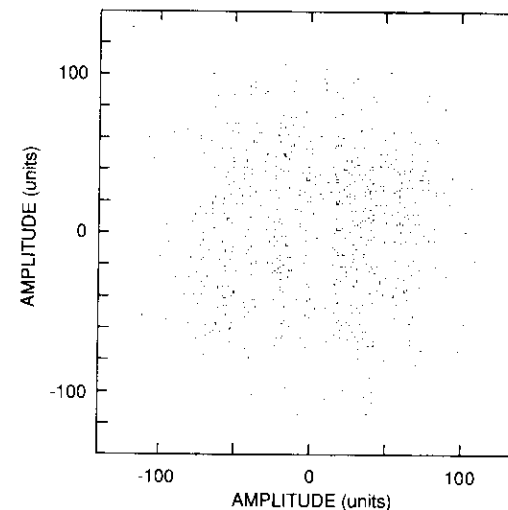
180° ambiguity resulting from the preamble modulation. Longer preambles were chosen for the higher modulation techniques to provide more accurate acquisition estimates. Because acquisition was binary, it is believed that the larger S/N's required for the higher-level modulation formats were necessary to maintain tracking.

Observe that the BERs are all on the order of  $10^{-1}$ . This is due to the effect of data feedback, where the tracking loop S/N drops by approximately 3 dB when the BER is  $1.5 \times 10^{-1}$ . That is, 85 percent of the feedback is correct, and 15 percent drives the loop in the wrong direction.

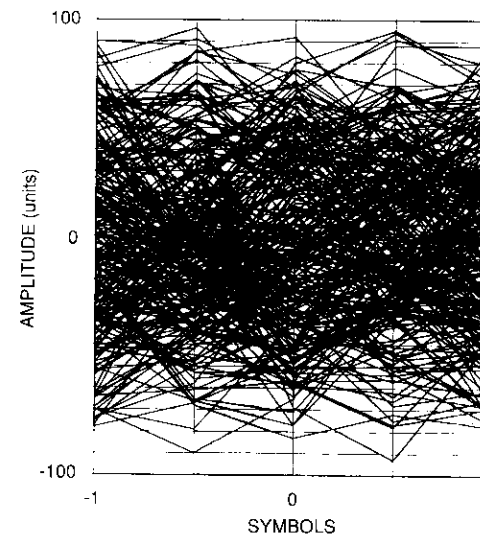
The detection scatter and eye diagrams, as well as the three time-domain tracking loop outputs for QPSK modulation at  $E_b/N_o = 0$  dB, are shown in Figures 21 and 22, respectively. From the scatter and eye diagrams of Figure 21, it is impossible to tell whether the demodulator is synchronized. However, the carrier tracking loop output (Figure 22b) clearly validates synchronization where the linear modulo-phase tracking of a frequency offset is evident. Also observe that there is little discernible noise on the tracking loop outputs, with the exception of the symbol timing (Figure 22c), which has been amplified by a factor of 1,024/96 relative to that of the actual hardware design due to limitations in the emulation run time.

TRANSIENT RESPONSE

The transient responses of the three tracking loops were emulated as a means of validating the analysis that defines the setting of their parameters. To generate a substantial transient response for evaluation, the acquisition estimate injection was disabled. From the analysis, the first-order AGC tracking loop has a normalized time constant of  $R_s/4B_A$  symbol times, and the



(a) Detection Scatter Diagram



(b) Eye Diagram

Figure 21. QPSK Detection Operation at  $E_b/N_o = 0$  dB

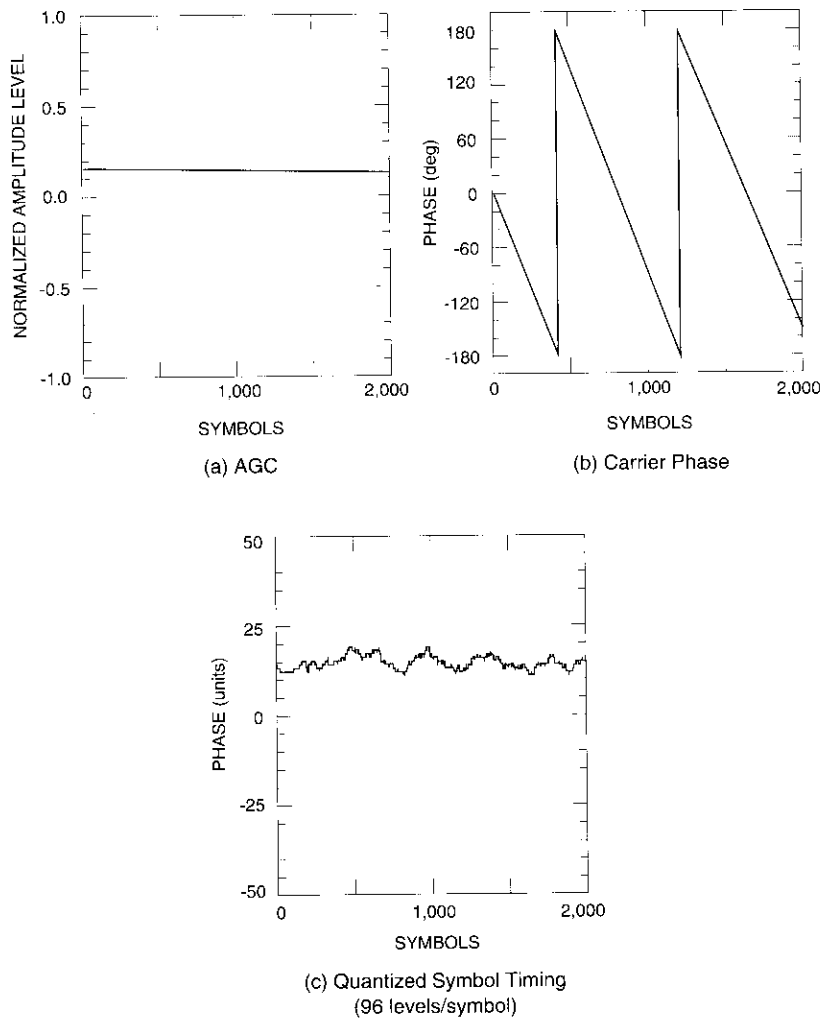


Figure 22. Tracking Loop Output Estimates at  $E_b/N_0 = 0$  dB

symbol timing loop is also  $R_s/4B_T$ . Their respective transient responses are shown in Figures 23 and 24 for normalized design time constraints of 75 and 150. In each figure, the transient response is given in two different locations in the loop. In the symbol timing loop, the output estimate was quantized into  $\pm 48$  levels to facilitate timing adjustment at the 96-s/s rate in the channel model. The AGC and symbol timing emulations indicate time constants of

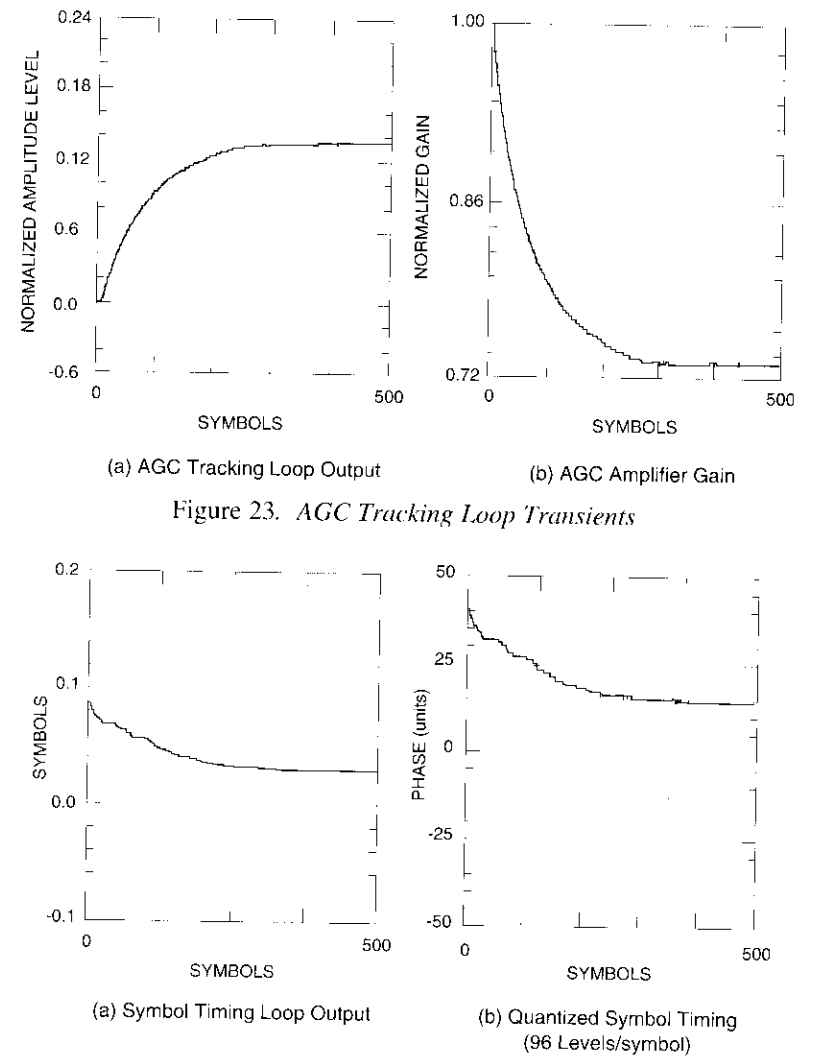


Figure 23. AGC Tracking Loop Transients

Figure 24. Symbol Timing Tracking Loop Transients

approximately 80 and 130 symbol times, respectively. The agreement is actually very close, considering that only 7 bits are available to quantize the loop gain coefficients,  $K_x$ , for relatively small ratios of  $B_T/R_s$ . In addition, the AGC loop analysis was nonlinear, and the symbol timing loop transient is pattern-dependent such that it is faster or slower depending on whether the probability of localized data transition groupings is greater or less than 0.5, respectively.

The second-order carrier tracking loop transients are depicted in Figure 25. With the damping ratio  $\zeta = 1/\sqrt{2}$  the analysis shows that the overshoot should be about 22 percent, or  $10^\circ$ , and the first zero-crossing of the transient should occur at  $0.583 (R_s/B_0) = 175$  symbol times. The values taken from the emulation agree precisely with these predictions. Also note that the data pattern noise jitter evident in the phase detector output is removed from the tracking loop output.

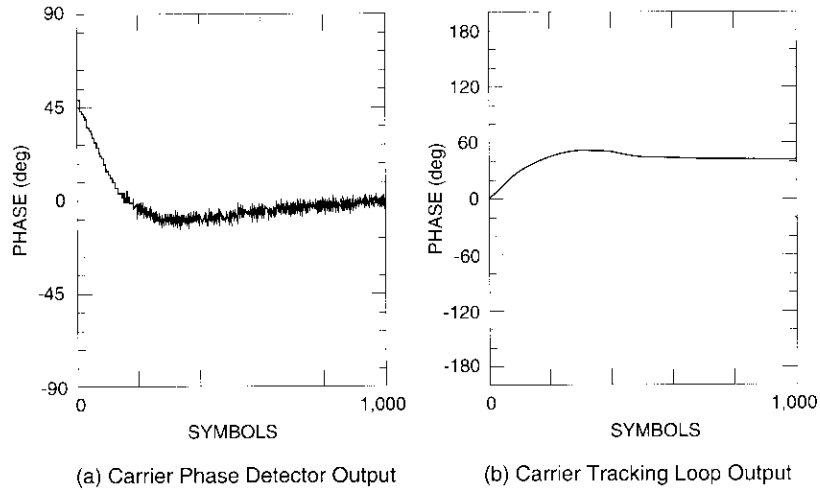


Figure 25. Carrier Phase Tracking Loop Transients

**Output estimate quantization noise**

The output estimate quantization noise is illustrated in Figures 26 through 28 for all three tracking loops operating at the two extremes of 2.34375 and 75 Msymbol/s (32 and 2 s/s). All of the outputs are exceptionally pure and exhibit quantization noise levels that are well below 40 dB, which should have negligible effect on the detection performance. It is not yet known why the lower symbol rate operation appears to show more quantization noise in the AGC and symbol timing loop outputs. Although the noise levels are so low that the differences may be insignificant, further investigation is warranted to obtain a better understanding of the quantization noise mechanisms in the loops.

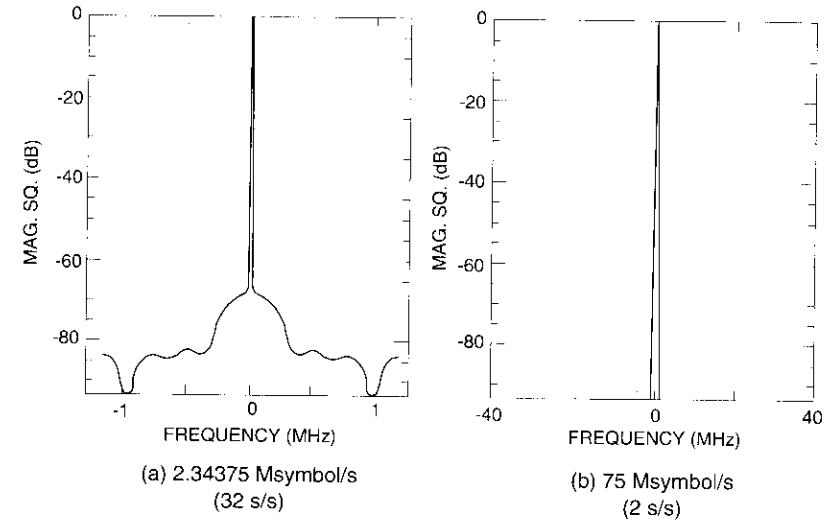


Figure 26. AGC Tracking Loop Output Phase Noise

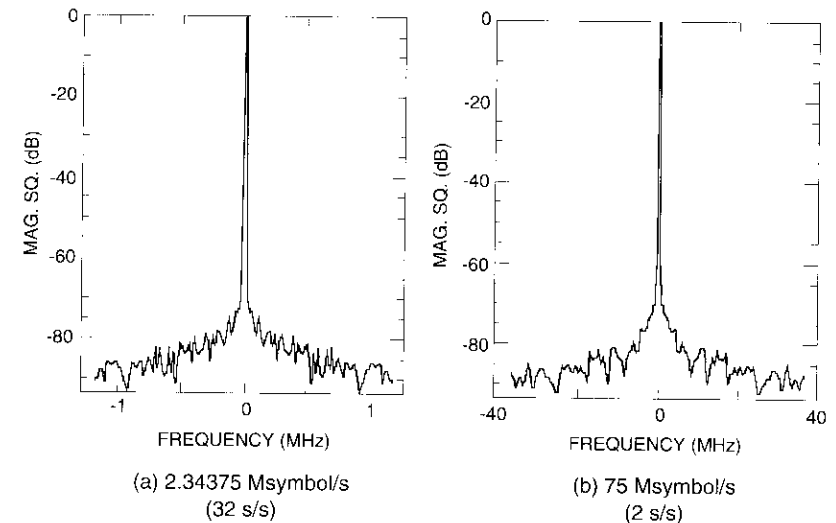


Figure 27. Carrier Phase Tracking Loop Output Phase Noise

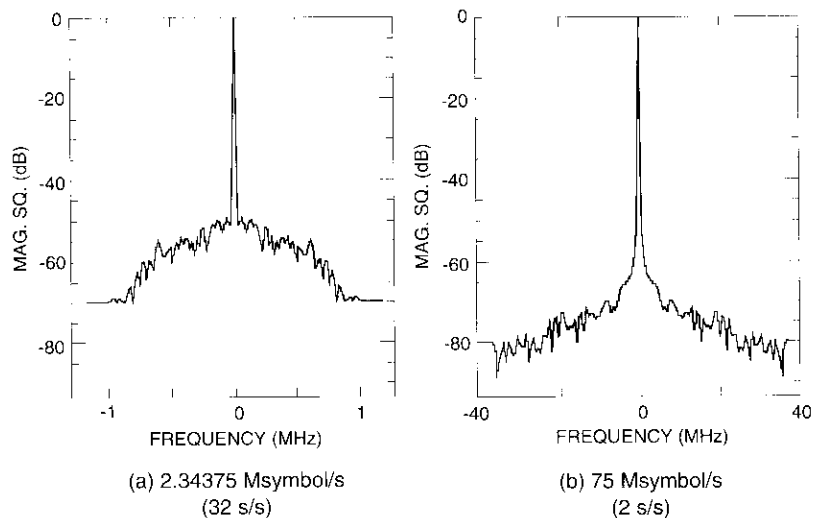


Figure 28. Symbol Timing Tracking Loop Output Phase Noise

## Conclusions

The interdependent detection and tracking loop architecture based on the JED approach has been shown to perform very well for a broad class of modulation techniques. The analysis is accurate in setting the loop parameters, as well as predicting their transient behavior. Both acquisition and tracking performance abruptly degrade at BERs on the order of  $10^{-1}$  as a result of an effective reduction in loop  $S/N$  through errors in the data feedback. It was not possible to run emulations over a large number of bursts to evaluate acquisition reliability because a single burst required on the order of 10 minutes to process. For non-hardware-restrictive applications, it is recommended to increase the demodulator PA aperture to 4 or more symbols. This will allow a close approximation to square root Nyquist filtering and minimize the BER implementation loss that was experienced. Further work is needed to evaluate the signal-to-quantization noise,  $S/Q$ , as well as the signal-to-thermal noise effects of PA filtering and the impact of the PAs on the tracking loops with regard to quantization.

This high-speed version of the JED has been fabricated in a rack-mount chassis which takes up about  $0.07 \text{ m}^3$  of space, including the power supplies

and fans, and uses approximately 200 W of power to achieve a 300-Mbit/s transmission capability. To minimize the space and power required, a general-purpose ASIC chip was devised for use in nine separate demodulator locations. Each chip primarily contains two MACs fabricated with emitter-coupled logic (ECL) bipolar technology. The chips are 5.1 cm on a side, have approximately 14K equivalent gates, 301 pins, and consume about 10 W of power. The current state of the art in complementary metal-oxide semiconductors (CMOS) could provide a 100-Mbit/s implementation with a much higher ASIC density (200K equivalent gates) and a considerable savings in power, which for CMOS would vary depending on the speed of operation. Moreover, except for the memories and the analog front-ends, the entire modem may well be fabricated in a single CMOS ASIC at speeds up to 100 Mbit/s for 16-ary signaling (25-MHz sample rate processing).

## Acknowledgments

This paper is based on work performed under the joint sponsorship of COMSAT and NASA. The authors would like to acknowledge J. Thomas, who built the original analog JED-based demodulator in 1977 and made major contributions to the design and development of its first-generation digital counterpart, the digitally implemented modem (DIM), in 1982–84. They would also like to recognize P. Chang for his significant contributions to the emulation program graphics and the noise performance.

## References

- [1] H. L. Van Trees, *Detection, Estimation, and Modulation Theory, Part I*, New York: John Wiley and Sons, 1968.
- [2] J. J. Poklemba, "Concurrent Carrier and Clock Synchronization for Data Transmission Systems," U.S. Patent No. 4, 419,759, December 6, 1983.
- [3] J. J. Poklemba, "A Joint Estimator-Detector for QPSK Data Transmission," *COMSAT Technical Review*, Vol. 14, No. 2, Fall 1984, pp. 211–259.
- [4] L. W. Couch, *Digital and Analog Communication Systems*, New York: Macmillan, 1983.
- [5] J. J. Poklemba, "Programmable Digital Modem," NASA 2nd Space Communications Technology Conference: On-Board Processing and Switching, Cleveland, OH, November 1991, *Proc.*, pp. 263–271. NASA Conference Publication No. 3132.
- [6] F. Snijders *et al.*, "Digital Generation of Linearly Modulated Data Waveforms," *IEEE Transactions on Communications*, Vol. COM-23, No. 11, November 1975, pp. 1259–1270.

- [7] M. Vanderaar *et al.*, "Flexible Digital Modulation and Coding Synthesis for Satellite Communications," NASA 2nd Space Communications Technology Conference: On-Board Processing and Switching, Cleveland, OH, November 1991, *Proc.*, pp. 295-303.
- [8] H. Samuelli and B. Wong, "A VLSI Architecture for a High-Speed All-Digital Quadrature Modulator and Demodulator for Digital Radio Applications," *IEEE Journal on Selected Areas in Communications*, Vol. 8, No. 8, October 1990, pp. 1512-1519.
- [9] G. Saulnier *et al.*, "A VLSI Demodulator for Digital RF Network Applications: Theory and Results," *IEEE Journal on Selected Areas in Communications*, Vol. 8, No. 8, October 1990, pp. 1500-1511.
- [10] C. M. Rader, "A Simple Method for Sampling In-Phase and Quadrature Components," *IEEE Transactions on Aerospace and Electronic Systems*, Vol. AES-20, No. 6, November 1984, pp. 821-824.
- [11] D. A. Linden, "A Discussion of Sampling Theorems," *Proc. IRE*, July 1959, pp. 1219-1226.
- [12] H. Meyr and L. Popken, "Phase Acquisition Statistics for Phase-Locked Loops," *IEEE Transactions on Communications*, Vol. COM-28, No. 8, August 1980, pp. 1365-1372.
- [13] S. A. Rhodes and S. I. Sayegh, "Digital On-Board Demodulator for Reception of an Up-Link Group of TDMA/QPSK Channels," 8th International Conference on Digital Satellite Communications, Guadeloupe, FWI, April 1989, *Proc.*, pp. 845-852.
- [14] R. E. Crochiere and L. R. Rabiner, *Multirate Digital Signal Processing*, Englewood Cliffs, NJ: Prentice-Hall, 1983.
- [15] J. J. Poklemba, C. Wolejsza, and J. Thomas, "Programmable Noise Bandwidth Reduction by Means of Digital Averaging," U.S. Patent No. 5,052,027, September 24, 1991.
- [16] C. Heegard *et al.*, "A Microprocessor-Based Modem for Packet Transmission Over Satellite Channels," *IEEE Transactions on Communications*, Vol. COM-26, No. 5, May 1978, pp. 552-564.
- [17] F. Gardner, *Phaselock Techniques*, 2nd ed., New York: John Wiley and Sons, 1979.



*John J. Poklemba received a B.S.E.E. from Drexel University in 1972, and the M.S.E.E. and E.E. degrees concurrently from the Massachusetts Institute of Technology in 1974. He is currently Associate Manager of the Transmission Processing Department at COMSAT Laboratories, where his principal interests comprise the application of detection and estimation theory to practical receiver structures, and the development of various types of filtering relevant to information transmission. At COMSAT, he originated the Concurrent Carrier and Clock Synchronization (CCCS) concept in 1978 and holds two patents on its implementation. In 1983, together with J. Thomas of COMSAT Laboratories, he developed the Digitally Implemented Modem (DIM), which is programmable in terms of data rate, spectral shaping, and modulation technique. Prior to joining COMSAT, Mr. Poklemba worked for 2 years with high-frequency receivers and high-resolution laser video signal processing. More recently he has been involved with the demodulator design and firmware development for the Onboard Multicarrier Demodulator Demultiplexer (MCDD), and has been the chief architect for NASA's Programmable Digital Modem.*

*Faris R. Faris received a B.E. in electrical engineering from the American University of Beirut in 1983, and an M.S.E.E. from the University of Virginia in 1988. He is currently a Senior Member of the Technical Staff in the Network Systems Department of the Network Technology Division at COMSAT Laboratories.*

*Since joining COMSAT in 1985, Mr. Faris has worked primarily in the areas of system studies and computer modeling. In the systems area, he has been involved with system architecture definitions, comprehensive transmission analysis/tradeoffs, and cost/benefit analyses for advanced network system concepts. In the area of computer modeling, he has been responsible for a number of computer simulation and analysis efforts ranging from low-level hardware emulation of specific communications subsystems, to high-level simulations of satellite-based communications networks.*



# **Translations of Abstracts**

## **Stations terriennes de la génération INTELSAT VI**

M. P. BROWN, JR., F. A. S. LOUREIRO ET M. STOJKOVIC

### **Sommaire**

Lorsqu'elle passe d'une génération de satellites à la suivante, INTELSAT fait tout son possible pour en limiter les effets sur le secteur terrien et pour réduire les frais au niveau des stations terriennes. Cet article décrit comment la transition à la génération INTELSAT VI s'est accomplie pour les stations terriennes compatibles avec les satellites INTELSAT V/V-A, compte tenu notamment des impératifs de poursuite par les stations terriennes et de l'utilisation de nouvelles fréquences en bande C avec le répéteur (1'-2'). Les auteurs examinent aussi le processus décisionnel qui a entouré la réduction du diamètre d'antenne des stations terriennes de classe A (bande C) de 30-32 m à 15-17 m, et celui des stations de classe C (bande Ku) de 15-18 m à 11-13 m.

## **Les EMCN à l'ère des INTELSAT VI**

M. ONUFRY, G-P. FORCINA, W. S. OEI, T. OISHI, J. F. PHIEL  
ET J. H. RIESER

### **Sommaire**

Cet article fait brièvement l'historique de la mise au point des équipements de multiplication des circuits numériques (EMCN) dans le système INTELSAT. Il rappelle le rôle important que joue dans ce système la multiplication des circuits et donne un aperçu des principaux éléments de la nouvelle spécification d'INTELSAT concernant les équipements de multiplication des circuits numériques (IESS-501). Il compare également la performance, pour les erreurs en salves, des équipements fabriqués conformément à la spécification IESS-501 et de ceux réalisés selon les normes d'autres fabricants. Enfin, il analyse les améliorations dont les EMCN pourraient bénéficier à l'avenir.